# Oscillatory signatures of neurodegeneration associated with Parkinson's Disease in the human brain.

Oliver Kohl

St. Catherine's College

University of Oxford

DPhil Thesis, Trinity Term 2024






# Oscillatory signatures of neurodegeneration associated with Parkinson's Disease in the human brain.

Oliver Kohl

St. Catherine's College

Submitted for the degree of DPhil in Psychiatry, Trinity Term 2024

## Abstract

Parkinson's disease (PD) is a progressive neurodegenerative disorder characterized by motor impairments and a range of non-motor symptoms. Its rapid increase in prevalence, disability, and mortality underscores the urgent need for early detection and intervention. Diagnostic classification typically relies on clinical symptoms evident at advanced disease stages, necessitating the identification of early markers to facilitate timely medical intervention and the development of disease-modifying treatments.

This thesis aimed to identify oscillatory brain activity signatures associated with PD using non-invasive electrophysiological recordings, with the potential to serve as markers for early disease stages. Three Magnetoencephalogram (MEG) studies are presented across three empirical chapters. Chapters 1 and 2 examined cortical oscillatory and network activity in PD compared to Healthy Controls (HCs) during

resting and task-related states. Resting-state MEG analyses revealed widespread alterations in cortical oscillatory activity and sensorimotor network dynamics in PD. Analysis of brain activity during sustained-gripping movements identified alterations in motor cortical beta power and sensorimotor network-specific oscillatory activity. In Chapter 3, individuals with REM Sleep Behaviour Disorder (RBD), a high-risk population for PD, were investigated, revealing changes in occipital, inferior temporal, and inferior frontal cortical oscillatory activity in RBD during resting-state recordings. These findings suggest promising cortical oscillatory signatures as markers of prodromal PD stages.

Overall, the findings of this thesis highlight various brain activity signatures capable of distinguishing individuals with PD or RBD from HCs, offering potential diagnostic utility for PD or its prodromal stages. Further replication of these findings in additional datasets is essential, and future MEG research on disease markers should aim to minimize ambiguities and inconsistencies across studies.

# Acknowledgements

Reflecting on the past 3.5 years, with all its struggles, achievements, and experiences, I am deeply grateful for the incredible support and guidance I have received along the way.

First and foremost, I would like to extend a heartfelt thank you to my supervisors, Mark Woolrich, Kia Nobre, and Andrew Quinn. Mark, thanks for your invaluable insights into data analyses and career guidance. I deeply appreciate the time and effort you have dedicated to our discussions. Kia, amidst your busy schedule, you always made time to meet with me. Your remarkable presence in meetings, coupled with your insightful feedback while always demonstrating that science is fun, has been truly inspiring. This, paired with your genuine interest in my development as both a researcher and a person, has been an invaluable source of motivation. I feel incredibly fortunate to have been supervised by you. Andrew, I owe a tremendous debt of gratitude to you for your unwavering support and mentorship. Your willingness to share your wealth of knowledge in signal processing and data analysis has been invaluable and has crucially shaped my understanding of brain functioning. Furthermore, I appreciate your openness to engaging in countless discussions about science and non-scientific topics, and your support during challenging times.

In addition to my supervisors, my co-workers and friends in the Brain and Cognition Lab and OHBA contributed largely to the great experience I had. Thanks to each one of you for making work feel like a community and for the camaraderie we shared. It was so much fun to work, travel to conferences, and go to the pub together with you! I

want to extend special thanks to Chet for his uncomplicated help in various projects, patiently explaining things that go beyond my understanding, and his occasional enthusiasm for the brain. To Nahid, for opening the doors to translational neurosciences for me by taking me on as an intern in 2019, and for entrusting me with the PD and RBD projects. And to Dani, I feel incredibly fortunate to have started my science journey with such a brilliant, supportive, and all-around great friend over the past 5 years.

On a different note, I want to thank my parents, Reinhard and Christiane, and my sister, Jasmin: Ich sage es viel zu selten, aber ich bin euch unendlich dankbar für eure bedingungslose Unterstützung. Ohne euch hätte ich diesen Meilenstein niemals erreicht – vielen Dank!

And of course, Helen! Thank you for guiding me through moments of doubt and celebrating with me in times of triumph. Thank you for your unwavering positivity, bravery, growing together with me, and for simply being my favourite human.

# Declarations

The work that will be presented within the doctoral thesis has greatly benefitted from the guidance provided by my DPhil supervisors: Kia Nobre, Mark Woolrich, and Andrew Quinn.

The analyses presented in the first two chapters were performed on data sets previously collected in our lab. The conceptualisation and analyses of these projects were led by me, with guidance from my supervisory team and collaborators.

The project presented in the third chapter was planned together with Nahid Zokaei and my supervisors. I collected the data for this project and led the data analysis.

The work in the first chapter has been submitted to a peer-reviewed journal and a preprint has been uploaded on medRxiv.org. I have generated the figures and authored the text, with guidance from my supervisory team and collaborators.

The preprint can be found here:

https://doi.org/10.1101/2024.01.22.24301617

Materials of this preprint will be reused in the first empirical chapter.

My supervisors and co-authors confirm that I have permission to include the submitted materials in the doctoral thesis.

In accordance with the guidelines, the body of this thesis does not exceed 50,000 words (excluding references, appendices, figures, and tables).

# Table of Contents

*Abstract* ..... *II*

*Acknowledgements* ..... *IV*

*Declarations* ..... *VI*

*List of abbreviations* ..... *XIII*

*Introduction* ..... *1*

**Parkinson's Disease** ..... **2**

Relevance ..... 2

Aetiology ..... 3

Pathology ..... 3

Diagnosis of Parkinson's Disease ..... 5

Treatment ..... 6

**Prodromal Phase of Parkinson's Disease** ..... **7**

Need for markers of prodromal phase of PD ..... 8

**REM Sleep Behaviour Disorder (RBD)** ..... **10**

Pathology ..... 10

RBD as prodromal marker for alpha-synucleinopathies ..... 11

**Magnetoencephalogram to identify electrophysiological markers of PD** ..... **13**

The potential of neuroimaging in uncovering markers of prodromal PD ..... 13

Magnetoencephalography (MEG) ..... 14

The potential of MEG in identifying electrophysiological markers of PD ..... 15

Different ways to describe the data ..... 17

**Overview of the Thesis** ..... **20**

*Chapter 1 – Changes in sensorimotor network dynamics in resting-state recordings in PD* ..... *22*

**Introduction** ..... **22**

Oscillatory changes in the basal ganglia-thalamocortical loop in PD ..... 23

Non-invasive studies on motor cortical beta oscillations in PD ..... 24

Large-scale network context to identify relevant motor cortical activations ..... 27

Chapter Overview ..... 27

**Materials and methods** ..... **29**

Software ..... 30

Pre-processing ..... 32
Static Power ..... 34
Burst Analysis ..... 34
Time-Delay Embedded Hidden Markov Model (TDE-HMM) ..... 35
Motor Beta Bursts in Large-scale Network Context ..... 39
Statistical Analyses ..... 41
**Results ..... 44**
Decreased static beta power in PD but no differences in conventional beta-burst analysis ..... 44
Hidden Markov Models describe fast, transient network dynamics ..... 45
Fast, transient network dynamics relate to individual differences in static spectral power ..... 49
Dynamics of sensorimotor network are associated with diagnostic group but not symptom severity ..... 49
Motor cortex beta bursts are associated with multiple large-scale networks ..... 54
Sensorimotor Network network-associated beta-burst (NABB) dynamics are sensitive to PD ..... 56
Different NAABs may relate to different processes ..... 61
**Discussion ..... 63**
Summary ..... 63
Static motor cortex-focused analysis reveals changes in oscillatory activity ..... 64
Sensorimotor large-scale network changes in PD group ..... 65
Network context identifies PD-related changes in cortical beta bursts ..... 67
Putative contributions of NABBs ..... 68
Limitations ..... 69
Conclusion ..... 70
***Chapter 2 – Large-scale network underpinnings of movements in Parkinson's Disease ..... 71***
**Introduction ..... 71**
Beta Oscillations in STN related to movement impairments ..... 71
Motor cortical beta oscillations are modulated by movements ..... 72
Movement-related modulations of beta oscillations are attenuated in PD ..... 73
Large-scale network context for a more fine-grained description of movement-related processes and PD-pathology ..... 74
Chapter Overview ..... 74
**Materials and Methods ..... 76**
Sample ..... 76
Sustained-Gripping Task ..... 76
Software ..... 77

Pre-processing ..... 79
Epoching ..... 80
Time-Frequency Representation (TFR) Analysis ..... 81
TDE-HMM Analysis ..... 82
Generalisability analysis ..... 86
Statistics ..... 90
Data availability ..... 93
**Results ..... 94**
Decreased beta power in the MRD period following grip-release in individuals with PD. ..... 94
Fast, transient network dynamics described by TDE-HMM. ..... 96
Sensorimotor networks show distinct spectral patterns ..... 98
Dynamics of sensorimotor networks are modulated by movements and gripping force. ..... 100
No significant differences in network dynamics between HCs and PD volunteers ..... 102
State-specific motor beta power is decreased in posterior sensorimotor network ..... 103
Replication of beta-power changes in sensorimotor networks, while probability time courses do not differ ..... 105
**Discussion ..... 110**
Summary ..... 110
Task-related oscillatory beta-power modulations are attenuated in PD ..... 110
Two distinct spatiotemporal networks underpin movement-related beta-power modulations ..... 112
Spatiotemporal patterns of sensorimotor and posterior sensorimotor networks hint at different functionalities ..... 113
Sensorimotor networks may underpin beta oscillations with varying peak frequencies ..... 116
Spectral properties of networks are significantly changed in PD whereas occurrence dynamics are maintained ..... 116
Potential underpinnings of alterations in state-specific spectra of sensorimotor networks ..... 118
Limitations ..... 120
Conclusion ..... 121
***Chapter 3 – Cortical electrophysiological markers of REM-Sleep Behaviour Disorder ..... 122***
**Introduction ..... 122**
RBD as a prodromal stage of alpha-synucleinopathies ..... 122
Non-invasive electrophysiological studies on RBD ..... 123
Slowing in PD ..... 124
Parametrisation of neural power spectra ..... 126
Chapter Overview ..... 127

**Materials and Methods ..... 129**
Sample ..... 129
Software ..... 131
Pre-processing ..... 131
Static Power Spectral Analysis ..... 134
Time-Delay Embedded Hidden Markov Model (TDE-HMM) ..... 135
Statistical Analysis ..... 135
**Results ..... 139**
Static oscillatory power is changed in PD and RBD volunteers ..... 139
Beta Oscillatory power in RBD is associated with cognitive performance ..... 141
Aperiodic Exponent significantly changed in PD and RBD ..... 143
Removing the aperiodic component diminishes beta-power group differences ..... 145
HMM Description ..... 148
Large-scale network occurrence probabilities are associated with static oscillatory power ..... 151
Large-scale network dynamics are not altered in RBD volunteers ..... 154
State 4-specific spectra do not underpin significant changes in static oscillatory power ..... 156
Mean across state spectra shows significant differences observed in static power spectral analysis ..... 158
Occipital theta power and 1/f Slopes, extracted from the mean across state spectra, are significantly associated with cognitive performance ..... 161
Repeating the analyses on solely the RBD dataset yields similar findings ..... 163
**Discussion ..... 167**
Summary ..... 167
Cortical oscillatory and aperiodic activity is altered in RBD ..... 168
Widespread alterations in cortical oscillatory activity in PD ..... 172
RBD and PD group show similar but not identical patterns of change ..... 174
Alterations of oscillatory activity occur at different timescales ..... 175
Limitations ..... 176
Conclusion ..... 178
***Discussion ..... 179***
**Electrophysiological Signatures of Parkinson's Disease ..... 180**
Static and dynamic alterations of cortical oscillatory power in PD ..... 180
Sensorimotor network as a marker for PD during rest and task performance ..... 182
**Electrophysiological markers of prodromal stages of Parkinson's Disease ..... 185**
**Implications for future research ..... 187**
Inconsistency in non-invasive electrophysiological research on PD ..... 188

Precise descriptions of PD-related electrophysiological alterations ..... 197
Disentangling simultaneously occurring pathological changes ..... 202
Embedding subcortical literature into cortical network context ..... 202
**Conclusion ..... 204**
***References ..... 206***
***Appendix ..... 261***
**A1 Chapter 1 ..... 262**
Literature referenced in introduction of Chapter 1 on beta oscillations in basal ganglia-thalamocortical loop ..... 263
Systematic sample differences between invasive and non-invasive literature on beta oscillations in basal ganglia-thalamocortical loop ..... 274
Detailed description of included PD samples ..... 279
Free energy of different TDE-HMM fits ..... 281
Robustness of NABB metric group contrast ..... 282
Robustness of NABB metric x UPDRS score associations ..... 283
**A2 Chapter 2 ..... 284**
Free Energy of all States ..... 285
Group contrast of motor cortical TFRs ..... 286
Good mixing of states ..... 287
Association between evoked response and state-probability time courses ..... 289
Group Contrasts of all network-probability time courses ..... 290
Group Contrasts of state-specific motor power spectra of all states ..... 291
Group Contrasts of state-specific motor power spectra peak frequencies ..... 293
GLM-Models for passive-movement task ..... 294
TFR Group Contrast for passive-movement task ..... 296
Sensorimotor networks exhibit distinct spectral profiles during passive movements ..... 298
Comparison of dynamics of sensorimotor networks in passive movement-task ..... 300
Group contrast of peak frequencies of sensorimotor-networks spectra ..... 301
**A3 Chapter 3 ..... 302**
Fooof fits across all participants and parcels ..... 303
Dynamic Metrics of large-scale networks ..... 304
Large-scale network occurrences are associated with static oscillatory power ..... 305
Power spectral alterations are not represented in state-specific power changes ..... 307
Power spectral alterations are present in majority of state spectra ..... 309
Large-scale networks extracted with TDE-HMM from only RBD data set ..... 311

**A4 Chapter 4 ..... 313**

Effect of power spectra normalisation on beta power ..... 314

# List of abbreviations

| | |
|---|---|
| ACE | Addenbrooke's Cognitive Examination |
| DBS | Deep Brain Stimulation |
| DLB | Dementia with Lewy Bodies |
| ECG | Electrocardiogram |
| EEG | Electroencephalography |
| EOG | Electrooculogram |
| FO | Fractional Occupancy |
| fMRI | Functional Magnetic Resonance Imaging |
| GLM | Generalised Linear Models |
| HC | Healthy Control |
| HMM | Hidden-Markov Model |
| ICA | Independent Component Analysis |
| IT | Interval Times |
| LCMV | Linearly Constrained Minimum Variance |
| LT | Lifetimes |
| MDS | Movement Disorder Society |
| MEG | Magnetoencephalography |
| MOCA | Montreal Cognitive Assessment |
| MRD | Movement-Related Desynchronisation |
| MRI | Magnetic Resonance Imaging |
| MSA | Multiple system atrophy |
| N | Number of Participants |

| | |
|---|---|
| NNMF | Non-Negativity Matrix Factorisation |
| OHBA | Oxford Centre for Human Brain Activity |
| OSL | OHBA Software Library |
| PCA | Principal Component Analysis |
| PC1 | First Principal Component |
| PD | Parkinson’s Disease |
| PET | Positron Emission Tomography |
| PMBR | Post-Movement Beta Rebound |
| REM Sleep | Rapid Eye Movement Sleep |
| RBD | REM Sleep Behaviour Disorder |
| RHINO | Registration of Headshapes Including Nose in OSL |
| SD | Standard Deviation |
| SMA | Supplementary Motor Area |
| SNpc | Substantia Nigra Pars Compacta |
| SPECT | Single-Photon Emission Computed Tomography |
| SQUID | Superconducting Quantum Inference Devices |
| SSP | Signal-Space Projection |
| STN | Subthalamic Nucleus |
| TDE-HMM | Time-delay embedded Hidden Markov Model |
| TFR | Time-Frequency Representation |
| UPDRS | Unified Parkinson's Disease Rating Scale |

# Introduction

Neurodegenerative diseases are characterized by neuropathological signatures of neuronal loss and misfolded proteins within the brain (Dugger & Dickson, 2017). As life spans increase in many countries, the prevalence of neurodegenerative diseases (Checkoway et al., 2011) and their associated economic costs are expected to rise (Yang et al., 2020). Among these conditions, Parkinson's Disease (PD) stands as the second most prevalent neurodegenerative disorder following Alzheimer's Disease (Willis, 2013). The diagnostic classification of neurodegenerative diseases typically relies on clinical symptoms evident at stages characterised by substantial degrees of irreversible neurodegeneration (DeMaagd & Philip, 2015; Dib, 2005). Thus, there exists a critical need for markers capable of detecting the disease before neurodegeneration reaches severe levels.

This thesis aims to identify oscillatory brain activity signatures of PD that have the potential to serve as markers for early stages of PD. Across three chapters, I will present my doctoral research intending to identify such markers. In the initial two chapters, I focus on identifying PD-related alterations in brain activity patterns using non-invasive brain activity recordings obtained from healthy controls (HCs) and PD volunteers during rest and task performance. In Chapter 3, I investigate whether PD-related changes identified in Chapter 1 are detectable in resting-state brain activity recordings of people at high risk of developing PD and, therefore, have the potential to serve as markers for prodromal stages of PD. Lastly, I will discuss the findings of my doctoral research and outline future directions for identifying non-invasive electrophysiological markers for prodromal stages of PD.

Before diving into the empirical analyses in Chapters 1 to 3, I will introduce Parkinson's Disease and its prodromal phase. Here, I will emphasize Rapid Eye Movement Sleep Behaviour Disorder (RBD) which is a promising marker for prodromal PD. Crucially, I will focus on features of PD and RBD that are important for the scope of this thesis but by no means are an exhaustive overview of the state-of-the-art research across all disciplines on these disorders. Lastly, I will set the stage by introducing Magnetoencephalography (MEG) and delineating the brain activity signals that can be captured through this method, laying the groundwork for analyses and discussions in the subsequent chapters.

## Parkinson's Disease

Parkinson's disease (PD) is a chronic, progressive neurodegenerative disorder that was first clinically described by James Parkinson in "An Essay on the Shaking Palsy" in 1817 (Parkinson, 2002). The hallmark of PD lies in its prominent impairments of motor functioning, alongside a spectrum of non-motor symptoms. In the following paragraphs, I will outline the relevance, pathology, diagnosis, and treatment of PD, before I discuss its prodromal stages and the importance of identifying markers indicative of these early phases.

### Relevance

In 2016, 6.1 million individuals were diagnosed with PD worldwide (Dorsey, Elbaz, et al., 2018), making it the second most common neurodegenerative disorder after

Alzheimer's Disease (Willis, 2013). PD has been reported to be the neurological disorder with the fastest growth in age-standardised rates of prevalence, disability, and death (Feigin et al., 2017). Projections indicate a strong increase in PD prevalence, with estimates suggesting that more than 17 million individuals will be affected by 2040 (Dorsey, Elbaz, et al., 2018; Rossi et al., 2018). Based on these observations it has been suggested that factors such as changes in global demographics and industrialisation have created and continue creating a "Parkinson Pandemic" (Bloem et al., 2021; Dorsey, Sherer, et al., 2018). In the USA alone, the total economic burden of PD was estimated to be $51.9 billion in 2017 (Yang et al., 2020), highlighting the immense financial consequences that globally increasing numbers of PD entail.

## Aetiology

The exact cause of PD is unknown, but a combination of genetic and environmental factors, as well as their interactions are believed to cause PD (Deng et al., 2018; Kalinderi et al., 2016; Tambasco et al., 2016).

## Pathology

The morphological hallmark of PD is the accelerated death of dopaminergic neurons in the substantia nigra pars compacta (SNpc), leading to compromised dopaminergic regulation of the basal ganglia (Hammond et al., 2007). This dysregulation manifests as abnormally synchronised oscillatory activity within the basal ganglia-cortical loop, indicating an over-inhibition of the loop (Hammond et al., 2007), which has been

linked to motor impairments such as Bradykinesia, Rigidity, Tremor, Postural Instability, and Dystonia (DeMaagd & Philip, 2015).

Another pathological hallmark of PD is the misfolding and aggregation of alpha-synuclein into Lewy bodies and Lewy Neuritis, which are hypothesised to be markers of PD-related neurodegeneration (Spillantini et al., 1997). Neuronal loss in PD, however, likely is the result of various processes and involves complex combinations of factors, including alpha-synuclein aggregation, dysfunction of mitochondria, impaired protein clearance, and neuroinflammation (Bloem et al., 2021; Kalia & Lang, 2015).

Given the strong association between loss of dopaminergic neurons in SNpc and the cardinal motor symptoms of PD, the majority of studies focused on SNpc neurodegeneration and its consequences. However, PD-related cell loss has been reported to extend beyond the SNpc encompassing other subcortical regions, i.e., Locus Coeruleus, nucleus basalis of Meynert, pedunculopontine nucleus, dorsal motor nucleus of the vagus, ventral tegmental area, raphe nuclei, and olfactory bulb (Braak et al., 2003; Giguère et al., 2018; Kouli et al., 2018). Crucially, PD-related degeneration in these areas likely affects the functioning of non-dopaminergic neurotransmitter systems such as the cholinergic, noradrenergic, serotonergic, GABAergic, glutamatergic, opioidergic, histaminergic, and adenosinergic system (Kalia et al., 2013). Alterations in these systems have been hypothesised to contribute to motor impairments described above (Kalia et al., 2013) as well as a heterogenous spectrum of non-motor symptoms (Aarsland et al., 2021; Chaudhuri et al., 2006; Schapira et al., 2017). In line with this, hyposomnia, sleep disorders, depression, constipation, and cognitive impairments, can be observed in addition to the cardinal motor symptoms,

as other brain systems are impacted as well (Aarsland et al., 2021; Schapira et al., 2017). Consequently, it is important to investigate PD-related alterations throughout the entire brain, in addition to focused analyses of the basal ganglia-thalamocortical loop, in order to comprehensively understand pathophysiological changes associated with PD.

## Diagnosis of Parkinson's Disease

The diagnosis of PD relies on neurological assessment and history taking (Bloem et al., 2021). The International Movement Disorder Society Clinical Diagnostic Criteria for PD (Postuma, Berg, et al., 2015), intended to guide clinical research, propose first to establish that a patient has parkinsonism, before determining whether the parkinsonism is caused by PD or atypical parkinsonian syndromes (e.g., Multiple System Atrophy, Cortico-Basal Degeneration, or Progressive Supranuclear Palsy).

The diagnosis of parkinsonism requires the presence of a combination of the three cardinal motor symptoms (Postuma, Berg, et al., 2015):

- Bradykinesia: Slowness of movements and decrease in speed and amplitude during continuous movements.
- Rigidity: Velocity-independent resistance to passive movements despite the patient is relaxing.
- Rest Tremor: 4 to 6-Hz tremor in resting limbs, which is attenuated during movement initiation.

A combination of Bradykinesia and either Rigidity or Rest Tremor or both indicates parkinsonism. The Unified Parkinson's Disease Rating Scale (UPDRS) Part III serves as a common clinical rating scale to evaluate these motor symptoms in PD (Fahn, 1987; Goetz et al., 2008; Ramaker et al., 2002).

Various studies further subdivided PD into tremor-dominant PD (tremor with no or weak motor symptoms), non-tremor-dominant (no-to-weak tremor while patients show akinetic-rigid syndrome or postural instability gait disorder), or a mixed phenotype with several equally pronounced motor impairments (Bloem et al., 2021).

## Treatment

Current treatment options for PD can alleviate symptoms, but no disease-modifying or neuroprotective options are available. Medications like levodopa, dopamine agonists, monoamine oxidase type-b inhibitors, and amantadine are commonly used to manage motor symptoms by either increasing intracerebral dopamine concentrations or stimulating dopamine receptors (Connolly & Lang, 2014; Fox et al., 2018). Levodopa is the mainstay for motor symptom management, particularly for bradykinesia and rigidity. It exhibits lower frequency of side effects and is better tolerated by the majority of PD patients compared to dopamine agonists (Armstrong & Okun, 2020; Bloem et al., 2021; Kalia & Lang, 2015).

At the beginning of the treatment, levodopa effectively eases motor symptoms but higher dosages and more frequent administration are often necessary in more progressed stages of PD (Armstrong & Okun, 2020). In addition to this, after several years of treatment, PD patients often develop fluctuations in their response to

dopaminergic treatment, commonly referred to as ‘wearing off effects’ of levodopa. These fluctuations manifest in the recurrence of PD symptoms and functional disability, typically occurring shortly before the next medication intake. These effects are often not alleviated by adjustment of medication. For patients experiencing ‘wearing-off effects’ or dyskinesia, deep brain stimulation (DBS) targeting the subthalamic nucleus (STN) or the globus pallidus internus can be considered (Armstrong & Okun, 2020; Bloem et al., 2021).

DBS is a neurosurgical procedure involving the chronic implantation of electrodes into specific regions of the brain relevant to the disease. In PD, these electrodes usually deliver pulsatile electrical stimulation to the STN or globus pallidus internus from an implanted battery, aiming to restore neurocircuit functioning (Lozano et al., 2019; Neumann et al., 2023). Typically, the mean disease duration prior to DBS surgery is 10 to 13 years. However, evidence from multi-centre randomised trials suggests that undergoing DBS surgery earlier, with a mean disease duration of 7.5 years, can lead to improvements in quality of life and secondary outcomes (Deuschl et al., 2013; Schuepbach et al., 2013).

## Prodromal Phase of Parkinson’s Disease

As described above, the diagnosis of PD depends on the manifestation of motor symptoms which in turn are the result of substantial degrees of neurodegeneration in the SNpc. It is estimated that these cardinal motor impairments manifest after 30% of the dopaminergic neurons in the substantia nigra or 50 to 60% of their axon terminals

are lost (Cheng et al., 2010). In line with this, there is evidence for a > 20-year-long prodromal phase in which non-motor symptoms occur. Especially constipation, olfactory loss, rapid eye movement sleep behaviour disorder (RBD), and depression have been proposed as prodromal markers of PD (Postuma et al., 2012; Postuma & Berg, 2019). For example, olfactory loss was observed >20 years (Fereshtehnejad et al., 2019), constipation >10 years (Adams-Carr et al., 2016), and RBD 12 to 14 years (Postuma et al., 2012) prior to the initial PD diagnosis. These symptoms are assumed to result from pathological processes outside the SNpc and hence, have been hypothesised to indicate that pathological processes in PD do not start in the SNpc but rather in other areas in the brain (Braak et al., 2003; Postuma et al., 2012) or even in the peripheral autonomic nervous system in specific PD-subtypes (Berg et al., 2021; Borghammer, 2021; Del Tredici & Braak, 2012; Horsager et al., 2020).

## Need for markers of prodromal phase of PD

While many of the above-described clinical markers for prodromal PD exhibit high sensitivity, their specificity for PD is low, with RBD being the only exception. This makes it difficult to use them as markers for diagnostic purposes (Postuma et al., 2012). As a result, motor impairments remain the first clinical symptoms resulting in a diagnosis of PD (DeMaagd & Philip, 2015). This is problematic, because substantial neurodegeneration precedes the onset of motor symptoms, impeding the evaluation and administration of potential treatments during earlier, possibly crucial, stages of the disease (Hu, 2020). The efficacy of disease-modifying drugs in individuals with established PD might be compromised due to advanced pathologies at the time of treatment (Dib, 2005; Mahlknecht et al., 2022; Poewe et al., 2020; Vijiaratnam et al.,

2021). Conducting trials with populations in prodromal stages of PD would enable testing interventions before (irreversible) severe neurodegeneration manifests, potentially improving the chances of success. Once disease-modifying or neuroprotective treatments have been established, prodromal markers could further aid in pinpointing optimal time windows in which the treatment is particularly effective in delaying or even preventing PD-related neurodegeneration (Mahlknecht et al., 2022).

The “Movement Disorder Society Research Criteria for Prodromal PD” (Berg et al., 2015; Heinzel et al., 2019) offer an evidence-based framework to estimate the probability of individuals to have prodromal PD. This comprehensive framework encompasses a variety of diagnostic markers, including motor and non-motor symptoms, clinical signs, and other supporting diagnostic tests (Berg et al., 2015). Notably, clearly abnormal results in Positron Emission Tomography (PET) and Single Photon Emission Computed Tomography (SPECT) that measure degeneration of dopaminergic projections from the SNpc to the striatum, are the only neuroimaging markers included in this framework. The reason for this is a lack of consensus on specific methods and analyses to extract other neuroimaging markers (Heinzel et al., 2019). Within this framework, RBD diagnosed via polysomnography stands out as the diagnostic marker with the highest likelihood ratio, indicating that individuals with this marker are 130 times more likely to develop PD than same-aged individuals without it. In comparison, dopaminergic PET and SPECT imaging, the second most robust diagnostic marker, only has a likelihood ratio of 43.3 (Heinzel et al., 2019).

# REM Sleep Behaviour Disorder (RBD)

REM Sleep Behaviour Disorder (RBD) is a sleep disorder in which inherent muscle atonia during REM sleep is decreased resulting in vocalisation and enactment of dreams (Hu, 2020; Postuma, Gagnon, et al., 2015; Roguski et al., 2020). Dreams often contain violent, unpleasant, or active scenes, such as being chased or attacked, which usually cannot be recalled unless the RBD patient wakes up during an episode (Hu, 2020). While elementary movements are usually performed during RBD episodes, they can contain violent behaviours on rare occasions (Frauscher et al., 2013). Examples of such violent behaviours are hitting, flailing, running, screaming, shouting, or swearing (Boeve, 2010).

## Pathology

Imbalances in excitation and inhibition in brainstem areas, such as the pontine sub-coeruleus nucleus and ventral medulla, have been proposed to dysregulate muscle tone during REM sleep, suggesting a crucial role in sleep-related motor dysfunction in RBD (Peever et al., 2014; Weber et al., 2015). Such dysfunction in brainstem activity may arise from an ascending spread of alpha-synuclein pathology, beginning in the peripheral autonomic nervous system and advancing to the brain, which results in pronounced alpha-synuclein pathology in brain stem areas (Borghammer, 2021).

Moreover, pathological changes have been implicated in affecting multiple neurotransmitter systems, including the cholinergic, noradrenergic, and dopaminergic neurotransmitter systems (Knudsen et al., 2018), as well as the pyramidal motor tract

(Roguski et al., 2020), and amygdala (Hu, 2020). These extensive alterations highlight the complexity of the neurodegenerative processes underpinning RBD.

## RBD as prodromal marker for alpha-synucleinopathies

Over the last few decades, increasing evidence has revealed a strong association between idiopathic RBD and prodromal stages of various neurodegenerative disorders. More specifically, 90% of RBD patients develop alpha-synuclein pathologies with 44% progressing to Parkinson's Disease and 25% advancing to dementia with Lewy Bodies (Galbiati et al., 2019; Iranzo et al., 2014). Importantly, RBD has been documented to manifest 12 to 14 years prior to the diagnosis of PD (Postuma et al., 2012), or 8 years prior to the onset of cognitive or motor symptoms leading to the clinical diagnosis of PD or dementia with Lewy Bodies (Postuma et al., 2019). Due to its high conversion rate and early onset, RBD is a very specific marker for alpha-synucleinopathies, including PD (Postuma et al., 2012) and it was even hypothesised that RBD marks an early prodromal phase of alpha-synuclein disorders (Hu, 2020).

However, a few caveats should be considered when utilising RBD as a marker for prodromal PD:

- **Current RBD patient samples may be biased towards severe cases.** As recognition of RBD increases, more cases with less pronounced loss of REM atonia during REM sleep may be identified and included in studies. Individuals with RBD exhibiting smaller loss of muscle atonia during REM sleep have been found to have a reduced risk of progressing to PD, potentially reducing the predictive power of RBD for PD (Postuma et al., 2010, 2019).

- **Not all RBD patients progress to PD**. As described above, a substantial number of individuals with RBD progresses to Lewy body dementia (Galbiati et al., 2019; Iranzo et al., 2014).
- **RBD may serve as a prodromal marker for a specific PD subtype.** Only 30 to 50% of all PD patients exhibit RBD (Postuma et al., 2012), and PD patients with RBD are more likely to have a diffuse/malignant (Fereshtehnejad et al., 2015) or body-first (Borghammer, 2021) PD subtype. This subtype demonstrates an increased probability of cognitive and autonomic impairments (Borghammer, 2021; Fereshtehnejad et al., 2015; Pasquini et al., 2021).

Despite these limitations, individuals with RBD present an unique opportunity to assess potential markers of prodromal PD in an enriched cohort with a substantially larger number of participants progressing to PD compared to the general population. Differences observed in individuals with RBD that predict their conversion to PD are very strong candidates for prodromal markers of PD. Moreover, identifying similarities between individuals with RBD and PD provides additional evidence, albeit slightly weaker, for prodromal markers. Such cross-sectional resemblances may facilitate the identification of markers that are already present in RBD and persist into PD.

# Magnetoencephalogram to identify electrophysiological markers of PD

In the present thesis, I aim to investigate electrophysiological markers of brain activity in PD. Since electrophysiological markers are promising candidates for prodromal markers of PD, the findings of this thesis hopefully hold the potential to inform future research aimed at identifying markers for prodromal stages of PD. In the following paragraphs, I will first outline why neurophysiological markers are very promising candidates for markers of early PD stages. Subsequently, I will introduce Magnetoencephalography (MEG), the method primarily utilised in this thesis and discuss the signal that it measures. Lastly, I will highlight the advantages of electrophysiological signatures in the context of prodromal disease markers and outline important perspectives for analysing the data.

## The potential of neuroimaging in uncovering markers of prodromal PD

Several clinical symptoms and signs have been identified as prodromal markers for PD with high sensitivity but low specificity (Heinzel et al., 2019; Postuma et al., 2012). This lack of specificity may be attributed to the fact that most of these markers reflect changes in behavioural or body functioning likely resulting from a cascade of processes triggered by underlying pathological changes. Neuroimaging markers aimed at assessing basal ganglia dopaminergic functioning (Brooks & Pavese, 2011), substantia nigra integrity (Castellanos et al., 2015; Cochrane & Ebmeier, 2013), brain structure (Laansma et al., 2021), or brain network functioning (Olde Dubbelink, Stoffers, Deijen, Twisk, Stam, Hillebrand, et al., 2013; Pan et al., 2017; Szewczyk-Krolikowski et al.,

2014; Tahmasian et al., 2017) target changes that are more closely related to PD pathology. This closer association with the underlying pathology may enable a more precise description of PD-related changes and is more likely to provide mechanistic insights into pathological alterations.

Among these neuroimaging markers, signatures of brain functioning are particularly promising. Unlike measures of structural integrity that serve as a proxy for the degree of (probably) irreversible neurodegeneration, these markers assess changes in brain activity as a response to pathological processes (Barber et al., 2017). Crucially, it Is hypothesised that brain activity markers can detect changes in synaptic functioning due to abnormal accumulation of alpha-synuclein even before significant neuronal loss has occurred (Barber et al., 2017). In line with this, the degree of abnormal alpha-synuclein accumulation in diagnosed PD patients has been linked to brain activity markers (Campbell et al., 2015; Caviness et al., 2016). Consequently, brain activity markers may offer a unique opportunity to identify prodromal disease stages with small degrees of neurodegeneration. A non-invasive neuroimaging method that is particularly promising to be sensitive to these prodromal changes is magnetoencephalography (MEG).

## Magnetoencephalography (MEG)

MEG is a non-invasive tool used to record the electrophysiological activity of the brain at the surface of the head. Utilizing superconducting quantum inference devices (SQUIDs), MEG captures tiny magnetic fields generated within the brain when larger numbers of neurons become active. Importantly, these magnetic signals are directly

produced by post-synaptic potentials flowing through apical dendrites of neurons oriented perpendicular to the brain's surface (Lopes da Silva, 2013). While the magnetic fields generated by a single neuron are too weak to be detected by SQUIDs, synchronous activations of tens of thousands of spatially-aligned pyramidal neurons produce detectable magnetic fields (Hämäläinen et al., 1993; Murakami & Okada, 2006). Consequently, MEG predominantly records synchronous fluctuations of membrane potentials across large neuronal populations that can be even below the spiking threshold (Gross, 2019).

Strikingly, the strength of these magnetic fields is 7 to 8 orders of magnitude lower than the Earth's magnetic field and 3 orders of magnitude smaller than those arising from heart activity. Thus, it is crucial to place the MEG scanner in a shielded room to remove interference from the Earth's magnetic field and nearby electrical devices (Gross, 2019). Additionally, the magnetic field strength diminishes significantly with distance from the signal origin, making it challenging to capture signals from deeper or subcortical structures (Pizzo et al., 2019).

## The potential of MEG in identifying electrophysiological markers of PD

The investigation of electrophysiological activity changes in PD using MEG is particularly promising for several reasons:

1. **MEG directly records brain activity in neuronal populations across the entire cortex with millisecond resolution.** This capability enables exploring the dynamics in local and large-scale brain activity, without relying on intermediate

processes such as neurovascular coupling (Gross, 2019) or intracranial electrode placement.

2. **MEG can be combined with structural MRI scans, resulting in brain activity recordings with high temporal and good spatial resolution.** While MEG may not match the spatial resolution of fMRI across the entire brain, studies have demonstrated that millimetre-range resolution can be achieved in cortical areas (Barnes et al., 2004). Moreover, MEG offers superior spatial resolution compared to EEG because magnetic fields are less affected by dura, skull, and scalp than their corresponding electrical currents (Hari, 2017).
3. **MEG is easy to record in elderly adults and patients.** The setup of MEG scans is quick and places less strain on volunteers compared to EEG. Additionally, unlike MRI, MEG does not require a strong magnetic field, reducing risks for participants and exclusion criteria. This is especially advantageous in older populations as many individuals have metal in their bodies. Furthermore, MEG enables the recording of brain activity of PD patients who underwent DBS surgery with minimal risk.
4. **Direct recordings of neuronal population activity with MEG might be sensitive to synaptic integrity and functioning in local and large-scale networks in prodromal disease stages.** Evidence from studies demonstrates that changes in oscillatory brain activity are associated with pathological protein aggregation in preclinical and prodromal stages of Alzheimer's disease (Nakamura et al., 2018), diagnosed Alzheimer's Disease (Ranasinghe et al., 2020, 2021; Smailovic et al., 2018), and diagnosed Parkinson's Disease (Caviness et al., 2016). Therefore, non-invasive electrophysiological methods likely have the potential

to identify disrupted neuronal dynamics in early stages of the disease before large numbers of cells die and strong behavioural markers of degeneration manifest (Barber et al., 2017; Lanskey et al., 2022).

## Different ways to describe the data

MEG provides information-rich recordings of cortical brain activity, offering insights into spatiotemporal activity patterns on a moment-by-moment basis. The data's complexity cannot be fully captured by a single analysis method, but various analysis approaches can be employed to highlight different aspects of the data. Importantly, these different levels of description offer complementary insights, emphasizing the importance of using multiple methods for a comprehensive understanding of neuronal activity.

In the following paragraphs, I will introduce neural oscillations and emphasize commonly used analysis approaches for investigating oscillatory activity in PD. Additionally, I will argue that employing dynamic large-scale network analyses provides a valuable complementary perspective that can enhance our understanding of oscillatory alterations in PD.

### Neural Oscillations

Fluctuations in the excitability of neuronal populations give rise to rhythmic activity known as neural oscillations. Electrophysiological recordings of the brain reveal the simultaneous presence of various rhythms with different characteristic frequencies. Signal-processing techniques, utilizing the Fast Fourier Transform, enable us to quantify the amount of energy within these oscillations (Cohen, 2014). Neural

oscillations are typically categorised into frequency bands based on underlying mechanisms related to synaptic current kinetics or signal-transmission dynamics (Buzsáki, 2006; Buzsáki & Draguhn, 2004). These frequency bands typically include delta (1-4 Hz), theta (4-8 Hz), alpha (8-12 Hz), and beta (13-30 Hz) oscillations.

### *Sustained Oscillations*

The most prevalent method to compare oscillatory power between conditions (e.g., PD volunteers vs HCs) is to calculate power spectra. This enables the quantification of oscillatory power in a specific region across a wide range of frequency bins for each participant. Subsequently, power averages across generic frequency bands are compared between the conditions. This approach permits investigating whether certain neural oscillations are stronger in the time series of one condition compared to another. However, it is important to note that power-spectrum approaches typically quantify oscillatory power over the entire duration of the measurement. As a result, neural oscillations are described as sustained activity, and dynamic fluctuations in the frequency content of the time series cannot be examined (e.g., fluctuations in the amplitude of neural oscillations) (Cohen, 2014).

### *Beta Bursts*

Beta oscillatory activity in the basal ganglia-thalamocortical loop occurs in transient events (=bursts), lasting approximately 90 to 115 ms, rather than as sustained activity (Feingold et al., 2015; Jones, 2016; Little et al., 2012; van Ede et al., 2018). Describing oscillatory activity in terms of these short transient events enables the investigation of their dynamic properties. Commonly used metrics to quantify burst dynamics include (Heideman et al., 2020; Quinn et al., 2019):

1. Fractional Occupancy: The proportion of the overall measurement time during which bursts are present.
2. Lifetimes: The average duration of burst occurrences.
3. Burst Rates: The rate of burst occurrences over a 1-second period.
4. Burst Amplitudes: The average beta power during burst occurrences.

Group differences in these finer-grained measures are likely more closely related to pathophysiological changes in PD. Consequently, they provide more sensitive markers for PD and PD progression (Feingold et al., 2015; Little et al., 2012; Tinkhauser, Pogosyan, Little, et al., 2017).

### *Dynamic Large-Scale Networks*

Both the power-spectrum and beta-burst approaches typically concentrate on the activity of a single region, neglecting the broader network context of these activations.

In neuropsychiatric disorders like PD, it has been proposed that individual pathological changes occur in heterogeneous regions but aggregate in common networks associated with clinical symptoms (Fox et al., 2018; Segal et al., 2023). Considering this, a dynamic network perspective may be essential to pinpoint neural activity changes that correspond to phenotypic similarities.

Furthermore, a network perspective could help identify motor cortical activations linked to PD pathology. In non-invasive recordings of cortical activity, various brain networks likely contribute to motor cortical activations. Understanding the network context of these motor cortical activations may be crucial to distinguish between different motor cortical activations that are not all affected by pathological changes in

PD. By segregating motor cortical activations based on their network context and pinpointing networks associated with PD pathology, we may obtain more precise markers of PD.

The introductions of the following empirical chapters will provide an overview of how electrophysiological activity is altered in PD. This will encompass key findings on changes in beta oscillations within the basal ganglia-thalamocortical loop and motor cortex during both rest (Chapter 1) and movements (Chapter 2). Additionally, research on widespread alterations in cortical oscillatory power, sometimes referred to as oscillatory slowing, in individuals with PD and RBD will be summarised (Chapter 3).

## Overview of the Thesis

In the present thesis, I aim to characterise electrophysiological signatures of Parkinson's Disease using non-invasive MEG recordings of neuronal activity. These findings will have the potential to inform future research aiming to identify electrophysiological biomarkers of prodromal stages of PD. In the following, I will give a brief overview of the contents of the three empirical chapters:

1. **Chapter 1** presents findings from analyses conducted on resting-state MEG data obtained from individuals with PD and HCs. The project's goal was to identify motor cortical electrophysiological signatures that are altered in PD. I investigated time-averaged motor cortical beta power and beta bursts, and explored whether adopting a large-scale network perspective yields novel insights into brain activity changes in PD.

2. **Chapter 2** presents findings from analyses of MEG recordings obtained from PD volunteers and HCs performing a sustained-gripping task. The main objective was to assess changes in motor cortical beta oscillations during movement performance in PD. I compared movement-related beta-power modulations between HCs and PD volunteers, explored electrophysiological activity during task performance from a large-scale network perspective, and assessed whether this refined description provides new insights into movement-related brain activity changes in PD.
3. **Chapter 3** analyses resting-state MEG recordings obtained from individuals with RBD, alongside the PD dataset from Chapter 1. The RBD dataset was collected as part of a larger MEG data collection project during my PhD. The aim was to investigate whether well-established patterns of cortical oscillatory alterations, known as oscillatory slowing, are present in individuals with RBD, and to test whether alterations in dynamic large-scale network properties observed in PD are also present in the RBD sample. Brain activity markers that are altered in both groups are exciting candidates for markers of prodromal stages of PD.

# Chapter 1 – Changes in sensorimotor network dynamics in resting-state recordings in PD

## Introduction

Parkinson's Disease (PD) is the fastest-growing cause of neurological-related disability worldwide (Dorsey, Sherer, et al., 2018). Its pathological hallmark is the progressive loss of dopaminergic neurons and accumulation of Lewy bodies within the substantia nigra pars compacta, compromising dopaminergic regulatory mechanisms of the basal ganglia (Hornykiewicz & Kish, 1987; Spillantini et al., 1997). This dysregulation has been linked to motor impairments such as Bradykinesia, Rigidity, Tremor, Postural Instability, and Dystonia (Hammond et al., 2007). A heterogeneous spectrum of non-motor symptoms, e.g., hyposomnia, sleep disorders, depression, constipation, and cognitive impairments, can be observed in addition to the cardinal motor symptoms, as other brain systems are impacted (Aarsland et al., 2021; Schapira et al., 2017).

An important effort is that of defining clear, sensitive, and selective non-invasive biomarkers of PD pathology that can be measured in a wide range of individuals. Magnetoencephalography (MEG) is a promising candidate, as it directly measures magnetic fields generated by postsynaptic potentials of thousands of simultaneously active pyramidal cells (Hämäläinen et al., 1993; Proudfoot et al., 2014). This may hold the potential for assessing synaptic integrity and function within both local circuits and large-scale networks (Lanskey et al., 2022). Such non-invasive biomarkers should prove useful for early disorder detection and may significantly contribute to treatment development and management strategies.

## Oscillatory changes in the basal ganglia-thalamocortical loop in PD

Experimental investigations using invasive methods in individuals with PD and animal models have advanced our understanding of the neurophysiological underpinnings of PD pathology. Excessive synchronisation of neural oscillations in the basal ganglia-thalamocortical loop, reflecting fluctuations in the excitability of neuronal populations, have been proposed to provide functional markers of PD (Hammond et al., 2007; Petersson et al., 2020; Singh, 2018). Invasive recordings taken from the subthalamic nucleus (STN) have revealed hypersynchronisation in low-beta frequencies in individuals with PD (Hammond et al., 2007), that is underpinned by prolonged periods of dynamically occurring low-beta synchronisation (=bursts) (Tinkhauser, Pogosyan, Little, et al., 2017; Tinkhauser, Pogosyan, Tan, et al., 2017). Both low-beta hypersynchronisation and prolonged beta-burst durations are suppressed by deep brain stimulation (Kühn et al., 2008; Oswal et al., 2016) and levodopa therapy (Brown et al., 2001; Eusebio et al., 2011; Lofredi et al., 2023; Tinkhauser, Pogosyan, Tan, et al., 2017) in a manner that scales with clinical improvement. Evidence from simultaneous STN and non-invasive cortical recordings further propose that projections from cortical motor areas drive STN hypersynchronisation (Oswal et al., 2016, 2021), and that STN bursts co-occur with motor cortical bursts (Tinkhauser et al., 2018). These observations, along with reports of exaggerated motor cortical beta power in animal models (Iskhakova et al., 2021; Sharott et al., 2005) and invasive motor cortical electrocorticography (ECoG) recordings in individuals with PD (Crowell et al., 2012; O'Keeffe et al., 2020) (but see also De Hemptinne et al. (2013)), pose the hypothesis that motor cortical beat power is exaggerated in individuals with PD.

## Non-invasive studies on motor cortical beta oscillations in PD

### Group Comparisons

The literature on non-invasive motor cortical M/EEG recordings is not as clear as the invasive literature outlined above, and it is a puzzling task to reconcile the literature of these two fields. Many non-invasive studies aim to access cortical nodes of the basal ganglia-thalamocortical circuit via recordings of motor cortical oscillatory power, implicitly hinging on the robust finding of beta oscillatory hypersynchronization throughout this circuit (Hammond et al., 2007; Petersson et al., 2020; Singh, 2018). However, M/EEG studies investigating oscillatory changes in the motor cortex have yielded mixed findings. Some studies reported no changes in motor cortical beta power (Shirahige et al., 2020; Swann et al., 2015), while others reported decreased (Heinrichs-Graham, Kurz, et al., 2014; Salenius et al., 2002; Vardy et al., 2011), or increased beta power (Hall et al., 2014; Pollok et al., 2012). Attempts to reconcile these discrepancies have suggested that motor cortical beta power may increase in early stages of PD but decrease in later stages (Boon et al., 2019). This hypothesis should be treated with caution because:

1. Studies investigating beta-power changes in central regions during early PD stages (notably with rather coarse spatial resolution) reported decreased beta power (Han et al., 2013; Olde Dubbelink, Stoffers, Deijen, Twisk, Stam, & Berendse, 2013; Stoffers et al., 2007).
2. Longitudinal research has indicated that beta power in sensorimotor areas remains largely unchanged over a period of 7 years, whereas it decreases in the majority of other brain regions (Boon et al., 2023).

Furthermore, the associations between changes in beta power in motor cortex and motor symptom severity are also inconsistent across studies (Boon et al., 2019; Geraedts et al., 2018; Pollok et al., 2012; Vardy et al., 2011).

### Effect of Dopaminergic Medication on Motor Cortical Beta Power

Various studies also investigated the effect of treatments on motor cortical beta power. Within-patient comparisons between dopaminergic medication on vs. off states suggested that dopaminergic medication intake decreases motor cortical beta power (Cao et al., 2020; Heinrichs-Graham, Kurz, et al., 2014; Melgari, 2014; Salenius et al., 2002). This decrease in beta power has been shown to normalise beta power decreases relative to HCs (Heinrichs-Graham, Kurz, et al., 2014) and scales with improvements in bradykinesia and rigidity scores (Cao et al., 2020; Melgari, 2014).

### Effect of Deep Brain Stimulation on motor cortical beta oscillations

In contrast to dopaminergic medication, the effect of DBS on motor cortical beta power is less clear. Studies reported conflicting results such as beta power increase (Cao et al., 2015), decrease (Abbasi et al., 2018; Luoma et al., 2018), no change (Cao et al., 2017; Swann et al., 2015), and mixed patterns of change (Boon et al., 2020) following DBS. Additionally, only one of these studies found a significant association between DBS-related motor cortical beta power modulations and improvements in bradykinesia and rigidity (Cao et al., 2017). This discrepancy led to the hypothesis that beta decrease induced by DBS may be attributed to antidromic propagation of action potentials along the hyperdirect pathway. However, it remains uncertain whether this pathway is mechanistically related to clinical improvement (Cao et al., 2020).

## Dynamic Burst Perspective

Adopting a dynamic, burst-based approach, has not proven sufficient to reconcile findings. Studies analysing motor beta bursts in non-invasive MEG recordings have produced inconsistent findings regarding patterns of changes in their dynamic properties: some report decreases in motor cortical beta-burst rates (Vinding et al., 2020), others find no group differences in burst rates but a steeper age-related decline in burst rates (Vinding et al., 2021), while another study observed increased burst durations and amplitudes in individuals with PD that normalised after deep brain stimulation (Pauls et al., 2022). Furthermore, changes in burst rates were suggested to scale with Bradykinesia symptom severity (Vinding et al., 2020, 2021), while burst amplitudes were associated with UPDRS hemi-body scores (Pauls et al., 2022). During a cued Go/NoGo task, beta-burst interval times were shown to underly decreases in beta power during movement preparation in individuals with PD (Heideman et al., 2020).

This puzzle of inconsistent findings among non-invasive studies, as well as between non-invasive and invasive studies, may be caused by many factors such as varying disease progression, symptomatology, assessment of intervention effects in contrast to HC vs. PD group contrasts, or different scale of measurements (see Discussion, Table A1 , and Figure A1.1). Given the large scale of M/EEG measurements, it is likely that activity in any single scalp region captures different types of activity, associated with distinct underlying brain networks.

## Large-scale network context to identify relevant motor cortical activations

I propose that considering the large-scale network context in which beta bursts occur is a fundamental factor to consider when investigating motor cortical activity non-invasively. Beta bursts recorded from motor sensors likely also include activity associated with brain networks beyond the sensorimotor areas. For instance, previous MEG studies demonstrated broad beta-power decreases that are linked to spectral slowing in central and posterior cortical areas in PD (Bosboom et al., 2006; Stoffers et al., 2007). Importantly, conventional spectral and burst analyses typically pre-select a sensor or region of interest, overlooking the network context of beta activations. However, this network context may be essential for dissecting relevant motor cortical activations and thereby pinpointing functionally relevant pathology. Considering the central role of motor symptoms in the diagnosis of PD, I hypothesize that focusing on motor beta activations occurring specifically within the sensorimotor network context may yield more reliable markers of PD.

## Chapter Overview

In this chapter, I investigate whether the large-scale network context of motor cortical activations, extracted with a time-delay embedded Hidden Markov Model (TDE-HMM) (Vidaurre, Hunt, et al., 2018), helps to identify pathophysiological changes in PD. Considering the previous literature, I hypothesise that sensorimotor network dynamics are altered in individuals with PD. Additionally, I propose that motor beta bursts may be associated with various large-scale networks, not all of which are closely linked to pathological changes in PD. By isolating motor cortical activations linked specifically to

the sensorimotor network, I aim to uncover processes more directly related to PD pathology.

I start by trying to replicate previously observed changes in static motor cortical oscillatory beta power and beta bursts identified through amplitude thresholding. Subsequently, I compare the dynamics of large-scale brain networks extracted using a TDE-HMM between Healthy Controls (HCs) and individuals with PD. This comparison aims to assess whether previously reported decreases in burst rates (Vinding et al., 2020) and increases in burst amplitudes and durations (O'Keeffe et al., 2020; Pauls et al., 2022) can be observed within the dynamics of a sensorimotor network. Finally, I investigate the co-occurrence patterns between large-scale networks and motor beta bursts to determine whether focusing on beta bursts associated with the sensorimotor network improves discrimination between individuals with PD and HCs.

## Materials and methods

MEG recordings from 8-minute resting-state scans with eyes open of 28 participants with PD and 36 HCs, matched in age and education, were analysed for this study. The resting-state scans were collected alongside task-based data in two previous studies by our lab (Heideman et al., 2020; Zokaei et al., 2021). The scanning protocol for the resting-state scans of both studies was matched. MEG recordings were acquired at a sampling rate of 1000 Hz using a VectorView scanner. Individuals with PD were asked to withdraw from their dopaminergic medication from 7 p.m. the night before the MEG scan. Cognitive scores, measured with the Addenbrooke's Cognitive Examination or Montreal Cognitive Assessment, did not differ significantly between the two groups. Demographics and clinical variables of included participants are presented in Table 1.1. PD volunteers were recruited via neurological clinics in Oxfordshire (UK) and the Dementias and Neurodegenerative Disease Research Network (DeNDRoN). An overview of the exclusion criteria of both studies can be found in Table A1 1. Both studies were approved by the NHS Oxford Research Ethics Committee and the Research Ethics Committee of the University of Oxford and followed the Declaration of Helsinki. All participants gave written informed consent before participating.

Table 1.1 Descriptive statistics and clinical variables of all included participants.

| Demographics | Healthy Controls | Parkinson's Disease |
|---|---|---|
| N | 36 | 28 |
| Sex (female/male) | 13/23 | 15/13 |

| | | |
|---|---|---|
| Handedness (right/left) | 34/2 | 25/3 |
| Age (years) (mean, range) | 68.36 (60-80) | 68.5 (54-83) |
| Education (years) (mean, range) | 15.36 (10-21) | 14.68 (10-24) |
| Years since Diagnosis (years) (mean, range) | N/A | 2.86 (1-7) |
| UPDRS III motor score (mean, range) | N/A | 30.36 (11-55) |
| Hoehn and Yahr scale (mean, range) | N/A | 1.77 (1-3) |
| Levodopa-equivalent daily dose (mg/day) (mean, range) | N/A | 393.94 (150-900) |

N = number of participants; UPDRS = Unified Parkinson Disease Rating Scale

## Software

All steps of the pre-processing were performed in Matlab R2020a using the Matlab version of the OHBA Software Library (OSL, https://github.com/OHBA-analysis/osl-core), Statistical Parametric mapping (SPM12; https://www.fil.ion.ucl.ac.uk/spm/) (Friston et al., 2007), or the HMM-MAR toolbox (https://github.com/OHBA-analysis/HMM-MAR) (Vidaurre et al., 2016), TDE-HMMs were run with the HMM-MAR toolbox.

Analyses of the TDE-HMM outputs were performed in Python 3.10. HMM state descriptions were estimated using OSL-Dynamics (https://github.com/OHBA-analysis/osl-dynamics). GLMs contrasting the two groups, while controlling for

confounds, were calculated with GLMTOOLs (https://pypi.org/project/glmtools/), and cluster-based permutation tests were calculated as implemented in MNE-Python (Gramfort, 2013). Analysis scripts used for the analyses can be found here: https://github.com/OHBA-analysis/Kohl2023_PD_HMM. A schematic of all the analyses performed in this paper can be found in Figure 1.1.

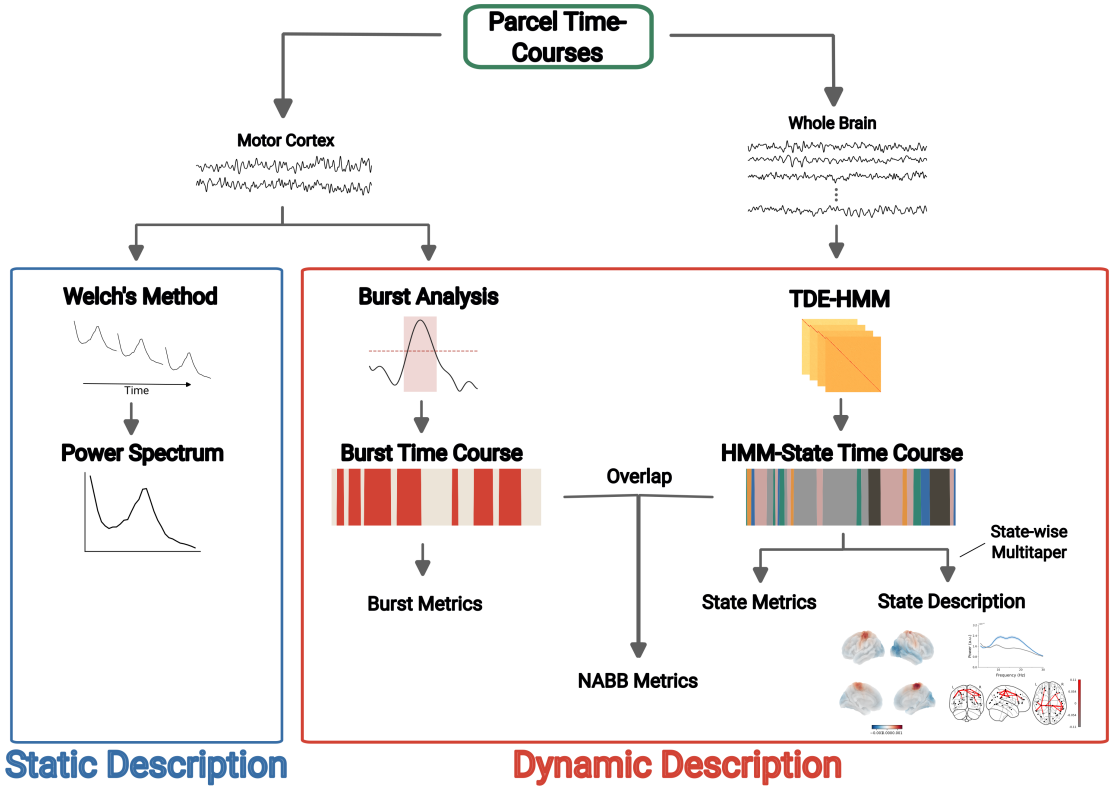


**Figure 1.1. Schematic of the different analyses reported in this paper.** All analyses were run on the parcellated and sign-flipped data. Welch's Method was applied to time-courses of the left and right motor cortex to obtain a static description of motor cortical oscillations. The same time courses were used for the conventional amplitude-thresholding burst analysis to extract motor cortical beta-burst time courses. From these burst time courses, burst metrics describing dynamic features of these events were calculated. A TDE-HMM was applied to

the time courses of all parcels to extract HMM-State time courses. Based on these state time courses; spectral state descriptions were calculated with a state-wise multitaper approach and state metrics were calculated to describe the dynamics of these states. Lastly, conventional beta bursts were subdivided according to the HMM-States with which they co-occurred, and metrics describing the dynamics of these co-occurrences were calculated.

## Pre-processing

The MEG data were maxfiltered (Maxfilter 2.2) with the temporal extension option (--tsss) to attenuate components in the MEG signal originating from outside the head. The data were further transformed to a reference head position (--trans) and corrected for movements during the scan (--movecomp.) The maxfiltered data were converted into SPM12 format in Matlab for further processing. The MEG recordings were registered to the participants' structural MRI scans with RHINO (Registration of Headshapes Including NOse). The data were downsampled to 400 Hz before applying a 0.1 to 125-Hz broadband filter and notch filters at 50 and 100 Hz using SPM12. Bad channels and bad segments were identified with osl_detect_artefacts. Across all participants, an average of 4 channels were rejected as bad channels and 5% of the recording duration was identified and removed as bad segments. To reject eye-movement and heartbeat artefacts in the data, OSL Independent Component Analysis (ICA) artefact removal was applied. ICA-Components highly correlated ($\geq$ .5) with the Electrooculogram or Electrocardiogram channels were rejected. In cases where no subcomponents were linked to the artefact channels or more than 4 channels were rejected, manual artefact detection was conducted on the ICA output. On average, 3

ICA components (SD = ±1) per participant were removed through this procedure. The MEG sensor data were then reconstructed without the 'artefactual' components and carried forward to the source analysis. These ICA-cleaned data have a reduced rank but are less affected by physiological noise sources.

Sensor normalization was applied to ensure equal contribution from magnetometer and planar-gradiometer channels to the source localisation (Woolrich et al., 2011). A Linearly Constrained Minimum Variance (LCMV) vector beamformer (Van Veen & Buckley, 1988; Woolrich et al., 2011), with a Principal Component Analysis (PCA) regularisation rank of 50, projected MEG sensor data onto an 8-mm MNI152 standard brain template. Parcel-wise time courses were calculated for a weighted parcellation with 39 cortical regions (Colclough et al., 2015). For each parcel, voxel contributions were weighted according to respective parcel weights and the first principal component across voxels was specified as the parcel's time course.

For the HMM analysis, the source reconstructed parcel time courses were broadband filtered to 1 to 45 Hz and downsampled to 250 Hz. I then performed symmetric multivariate leakage reduction, which corrects for both direct and inherited so-called ghost interactions (Palva et al., 2018) in spatial leakage (Colclough et al., 2015). Sign-flipping (Vidaurre et al., 2016) was applied next. Finally, the data were split into 10-second segments and generalized extreme Studentized deviate outlier detection (Rosner, 1983) was used to remove segments with exaggerated variance or kurtosis values. On average, 5% (SD = ± 3%) of the data were identified as bad segments. These pre-processing steps ensured that the time-delay embedded Hidden Markov Model

analysis could accurately identify brain states without being influenced by outlier events. The resulting data were used for all subsequent analyses.

## Static Power

To explore the signal power across a range of frequencies, I used Welch's method to compute power spectra. The algorithm was applied to each participant's individually z-standardized parcel time course using a window length of 500 samples and a window overlap of 250 samples to obtain relative power per frequency bin. After averaging relative power spectral values across the two superior motor parcels for each participant, average power at each frequency bin was contrasted between the PD and control group with a t-test and cluster-based permutations (Gramfort, 2013).

## Burst Analysis

I applied a conventional amplitude-thresholding burst analysis to the two superior motor parcels to explore the dynamics of individual beta-power events underpinning spectral power in the time domain. For each participant, the pre-processed data were filtered between 18 and 25 Hz, based on the significant cluster obtained from the static motor cortical power group contrast. Next, I calculated amplitude envelopes of the time courses using the Hilbert transform and thresholded them at the 75th percentile, separately for each participant. Finally, bursts were identified as instances in which the threshold was crossed for longer than 1 cycle of the lowest frequency (18 Hz) in the frequency range of interest (Cole et al., 2019). This resulted in binary on-versus-off time courses, with 1 indicating samples during bursts and 0 indicating

samples during burst-off periods. A bilateral motor cortical on-versus-off burst time course was created by assuming a burst occurrence at instances when a burst occurred in at least one of the motor parcels. The average burst overlap between motor cortical parcels was 69% (SD = ± 1%). Burst time courses of both motor cortical parcels were combined to enable fair comparisons with TDE-HMM states, which were predominantly bilateral. Using the combined burst on-versus-off time course, I extracted the fractional occupancy (fraction of total time with bursts present), burst lifetimes (duration of burst occurrences), and state rates (number of burst occurrences per second). Additionally, I estimated motor cortical beta-power changes during bursts using a multitaper approach, calculating power weighted by burst on- and off-sets (Vidaurre et al., 2016). After subtracting the mean power across burst-on and -off periods, motor cortical beta-power estimates were averaged across both motor parcels to obtain beta-power changes during burst events.

## Time-Delay Embedded Hidden Markov Model (TDE-HMM)

### TDE-HMM Description

I employed a time-delay embedded HMM to the data to investigate whether large-scale network information can improve differentiation between the HC and PD group. TDE-HMMs extract dynamic brain states in a data-driven manner, with each state representing a large-scale functional network characterised by distinct multi-region oscillatory activity, i.e., distinct power covariations and phase synchrony patterns (Vidaurre, Hunt, et al., 2018). Compared to conventional single-region beta-burst analyses, the HMM provides a richer description, by linking bursting activity in any

region to the associated large-scale, multi-region network activity. In other words, each time a large-scale network occurs, it can be thought of as a transient bursting event of a large-scale, oscillatory network. The data-driven (unsupervised learning) quality of TDE-HMMs further obviates the necessity of setting *a priori* assumptions (i.e., region of interest, filter range, or beta-amplitude threshold) thus reducing arbitrariness.

A detailed description of the inference process can be found elsewhere (Vidaurre, Hunt, et al., 2018). In short, the standardised time series are described as a sequence of a defined number of hidden states, in which only one state is active at any moment. Each state is defined by an observation model that captures a distinct auto- and cross-covariance pattern across regions. Autocovariance patterns are calculated for each sample by embedding it into a time window spanning ± 7 samples and subsequently reducing its dimensionality by selecting a subset of principal components (2 x number of parcels) inferred with a PCA. The dimensionality reduction reduces computational demands and prevents overfitting. To further reduce computational costs, I employed a stochastic variational inference approach (Vidaurre, Abeysuriya, et al., 2018). Importantly, the distinct auto- and cross-covariance patterns for each HMM state can capture different oscillatory activity, including distinct patterns of multi-region spectral power and phase-locking. Each time a state switches "on", it can be thought of as a transient bursting event of a large-scale, oscillatory network.

### State-Specific Power and Coherence

State-specific power and coherence were calculated for each participant post-hoc using the source reconstructed data and the a-posteriori probability time course of the

states inferred by the TDE-HMM. Following Vidaurre et al. (2016), a multitaper applying 7 Slepian tapers with a window length of 2 seconds was used to extract time-resolved power and coherence estimates between 1 and 45 Hz with a frequency resolution of 0.5 Hz. Time course data were weighted by the posterior state probabilities prior to applying the multitaper, resulting in state power spectra and cross-spectral densities. State-specific power spectra were calculated by subtracting the mean across all state spectra from the respective state power spectrum. To visualise large-scale network connectivity patterns, the mean coherence across states was subtracted from the state-specific coherence values. The resulting values were subsequently thresholded at the 97$^{th}$ percentile to highlight the most prominent connections in the respective figures.

## State Metrics

Temporal metrics were computed to compare large-scale network dynamics between the two groups. These metrics were calculated for each participant using the padded a-posteriori probability time courses of the states. The following state dynamics were extracted: fractional occupancy, lifetimes, interval times, state, and motor cortical beta-power change during state visits. State-specific motor cortical beta-power change was obtained by first subtracting the mean power across all states from state-specific power spectra and then averaging the 18 to 25-Hz power in the superior motor parcels.

## Robustness Check

The number of states extracted by the HMM is a parameter that must be specified before running the HMM and can yield varying results. Since the inference of the

algorithm is randomly initialised, different runs of an HMM with the same parameter settings on the same data can also yield slightly different results. However, the main state features such as state topologies and dynamics, as well as key findings of the analysis, should be robust across different HMM runs with the same parameter settings and varying numbers of states. To ensure that the obtained results were robust, I ran 10 HMMs inferring 8, 10, and 12 states respectively (Figure A1.1). The robustness of key findings was checked across all 30 HMMs. The representative results shown in the main figures come from the HMM with the lowest variational free energy (an approximation to the Bayesian model evidence) of all HMMs, which inferred 8 states.

### State matching across HMM runs

Analyses calculating TDE-HMM state metric group contrasts and state metric x UPDRS score associations were repeated across all the 30 HMMs to check whether key findings in the reported HMM fit generalise across different initialisations and number of states. Since the initialisation of the TDE-HMM is random, the order of inferred states is arbitrary, and states must be matched before assessing the robustness of the observed effects.

To match states across different runs inferring the same number of states, the HMM with the lowest free energy was identified as a reference. Then, states of all remaining HMMs were matched to it. This matching process involved extracting observation models for all states and calculating the correlation distance between all states of the two HMM runs, resulting in a distance matrix. The Hungarian algorithm (Munkres, 1957) was then applied to find an optimal state assignment between the states of the

two HMMs with minimal overall distance. This procedure was performed separately for all HMMs inferring 8, 10, or 12 states.

Additionally, to enable comparisons between runs with different numbers of states, states of the HMMs with 10 or 12 states were matched to the HMM with the lowest free energy inferring 8 states. Correlation distances were calculated between all states of the HMMs, resulting in a distance matrix that was zero-padded to a square shape for the Hungarian algorithm. States of the HMMs with 10 or 12 states that were allocated to one of the states of the 8-state HMM were retained for the robustness check, while states matched to zero-padded columns were discarded. States of the remaining HMMs inferring 10 or 12 states with higher free energy were matched first to the HMM with the lowest free energy inferring the same number of states, before being matched to the HMM with the lowest free energy inferring 8 states.

## Motor Beta Bursts in Large-scale Network Context

### TDE-HMM State and Burst Overlap

To investigate the temporal overlap between conventionally estimated motor beta bursts and the occurrence of TDE-HMM network states, I calculated the percentage of samples where HMM-state occurrences overlapped with motor beta-burst occurrences (Figure 1.10A). This was achieved by dividing the sum of overlapping samples by the total number of burst samples, allowing to interpret the overlap as the percentage of the overall motor cortex beta-burst occurrences. The significance of the overlap between TDE-HMM States and motor beta-burst occurrences was calculated with non-parametric permutation tests. Empirical TDE-HMM state time courses were

randomly shifted for each participant to generate null TDE-HMM state time courses that only differed in their temporal relationship to the empirical state time courses. Overlaps between the motor beta burst on-vs-off time courses and the shifted TDE-HMM state time courses were calculated as described above. Overlaps of motor beta bursts with the shifted TDE-HMM state time courses were contrasted against overlaps of bursts with the inferred TDE-HMM state time course with a directed t-test per TDE-HMM state. Bonferroni correction was applied to correct for multiple comparisons across states.

### Calculation of Network-Associated Beta-burst (NABB) Metrics

I segmented conventional motor beta bursts according to co-occurring large-scale networks derived in the TDE-HMM analysis, to investigate whether focusing on motor beta bursts associated with sensorimotor network activations recovered significant group differences in burst dynamics (Figure 1.10A). I refer to these segmented motor beta bursts as Network-Associated Beta Bursts (NABBs). Metrics describing NABB dynamics were calculated in a similar way as the TDE-HMM state metrics. To test whether group differences between individuals with PD and HCs only occurred for sensorimotor NABBs, I identified bursts overlapping with large-scale networks other than the sensorimotor network (other NABBs) and compared their fractional occupancies between the two groups. I further calculated NABB metrics for each large-scale network and compared them between the two groups.

## Statistical Analyses

Group contrasts for Burst, Network-State, and NABB metrics were assessed using GLMs with group constants, age, sex, education, and handedness as regressors to control for potential confounds (Figure 1.2). Significance was assessed using maximum t-statistic permutation tests by shuffling group labels before calculating the above-mentioned GLMs for 10,000 times. For group contrasts of large-scale network and NABB metrics, where a separate contrast is performed for each network, maximum t-statistic pooling across networks was used to determine significance while controlling for multiple comparisons (Nichols & Holmes, 2002): For each permutation, the largest t-statistic across all states was selected to construct a single null-distribution which was used to determine the significance of the metric's group contrast for each state. Observed t-statistics of state or NABB metrics were deemed to be significant if they exceeded the $p < .05$ threshold obtained from the null distribution.

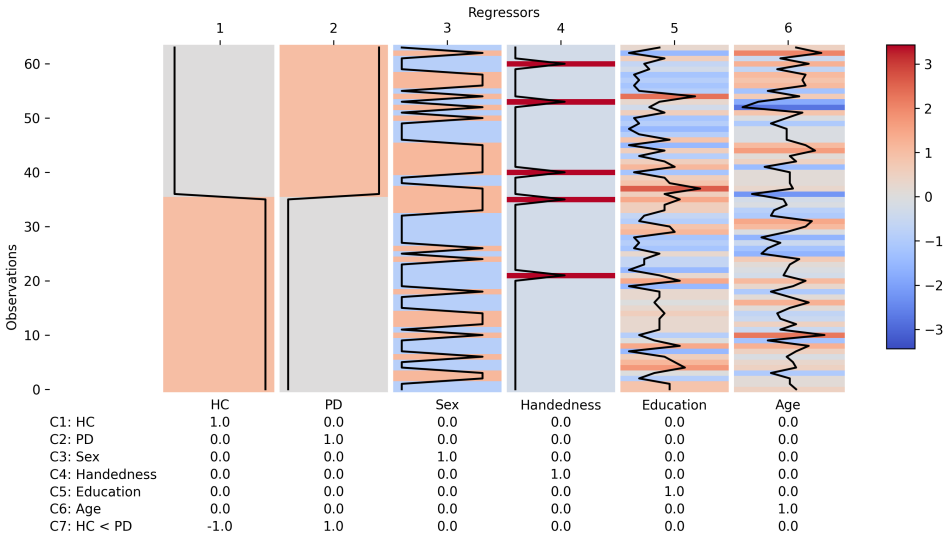


**Figure 1.2. Summary of GLMs used to compare variables between HCs and PD patients.** Regressors added to GLMs are represented as bars with each entry

representing the z-scored regressor value of a single participant. The contrast between the HC and PD groups is depicted below. Note that the contrast is specified in such a manner that positive t-statistics indicate larger values for PD and negative t-statistics larger values for HC.

UPDRS motor scale items were combined into Bradykinesia/Rigidity and Tremor scores (Hammond et al., 2007; Litvak et al., 2011). Relationships between metrics and UPDRS scores were assessed with GLMs, for all metrics that significantly differed between the two groups. In these models, metric scores were predicted from Bradykinesia/Rigidity and Tremor scores while controlling for the above-mentioned confounds (Figure 1.3). Maximum t-statistic permutation tests with 10,000 permutations were applied to determine the significance of the associations.

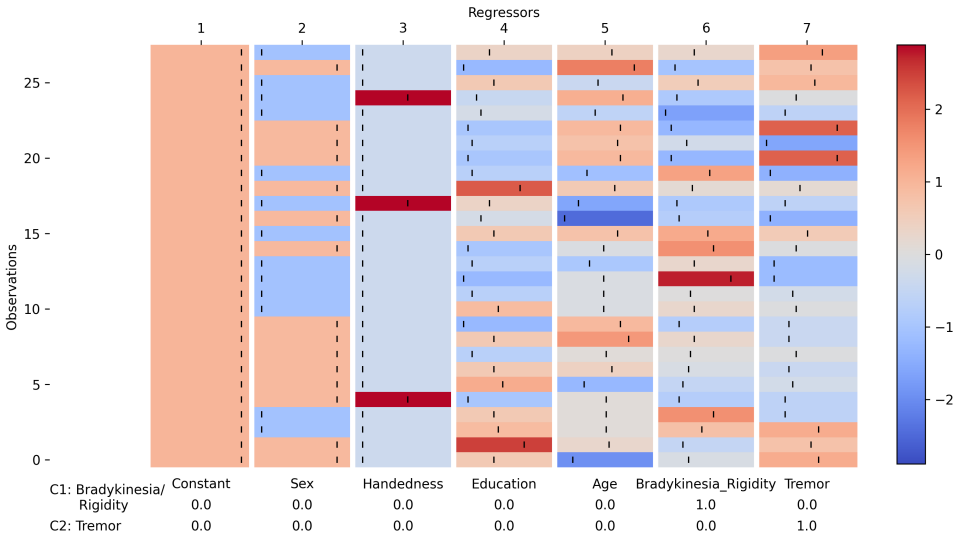


**Figure 1.3. Summary of GLMs used to calculate associations between variables and motor symptom severity scores.** Regressors added to GLMs are represented

as bars with each entry representing the z-scored regressor value of a single participant.

# Results

## Decreased static beta power in PD but no differences in conventional beta-burst analysis

The group comparison of motor cortical mean static power spectra (i.e., averaged over the whole resting-state scan) between the HC and PD group (Figure 1.4A) yielded a significant cluster in the beta range (18 to 25 Hz) with decreased power in the PD group ($p < .05$). Another non-significant 6 to 9-Hz cluster with increased power in individuals with PD was also found ($p = .09$). Beta power averaged across the range of the significant cluster was not associated with Bradykinesia/Rigidity ($t(14) = 0.35$, $p = .72$) or Tremor ($t(14) = 0.06$, $p = .95$) scores.

Comparisons of conventional motor cortical beta-burst metrics between the HC and PD group (Figure 1.4B) did not reveal significant changes in metrics describing the dynamic properties of bursts (all $p > .16$).

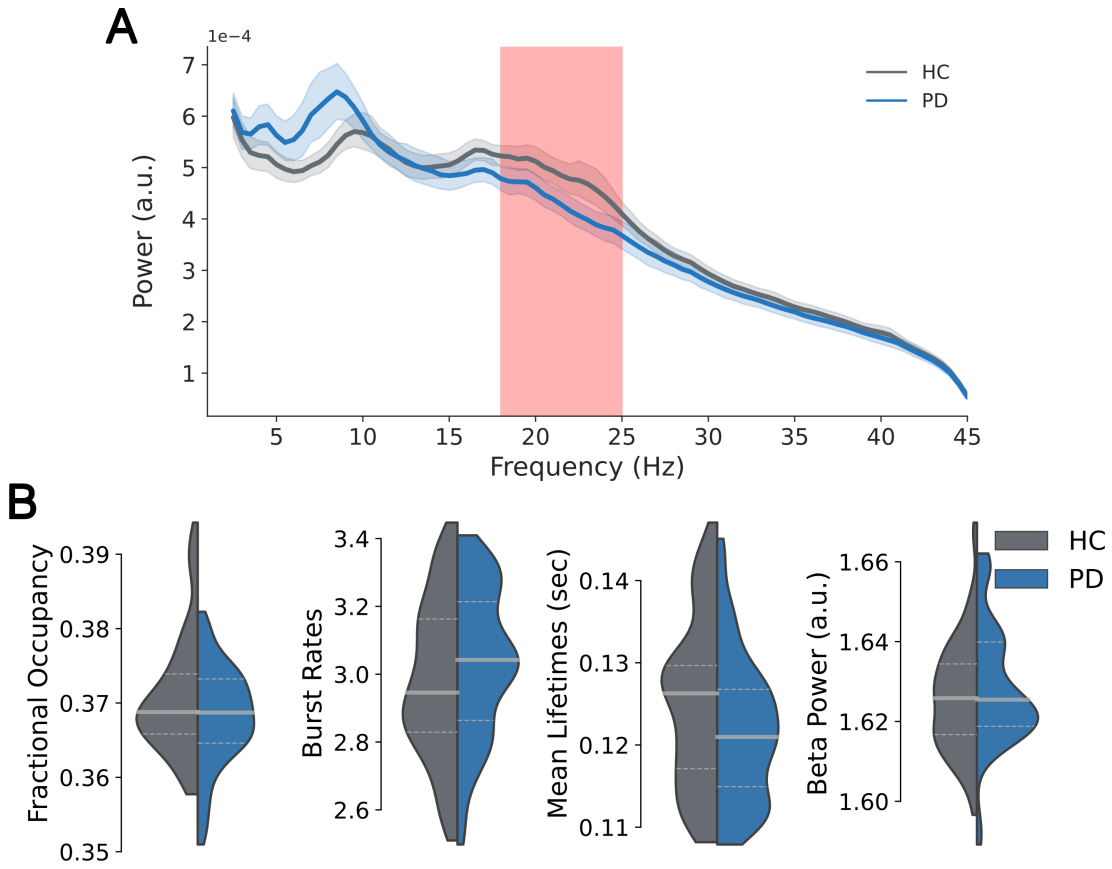


**Figure 1.4. Motor Cortical Beta Oscillatory power decreased in individuals with PD in the static power spectrum but there were no changes in conventional amplitude-thresholding beta-burst analysis. (A)** Motor Cortical average power spectra of HC and PD group. Cluster with significant power differences marked in red. **(B)** 18 to 25-Hz motor cortex beta-burst metric group comparison between the HC and PD group.

** indicates $p < .01$ and * $p < .05$.

## Hidden Markov Models describe fast, transient network dynamics

Descriptions of temporally and spectrally resolved large-scale networks inferred by the TDE-HMM are depicted in Figure 1.5. Each time a state switches “on”, it can be

thought of as a transient bursting event of distinct oscillatory network activity. These networks exhibited power covariance and phase connectivity patterns consistent with previous studies extracting large-scale networks from MEG resting-state data (Higgins et al., 2021; Vidaurre, Hunt, et al., 2018). Importantly, State 1 occurrences were linked to an increase in the wideband power and coherence in motor cortical areas. Therefore, from here on, I will refer to State 1 as the sensorimotor state. Since changes in motor cortical dynamics have been reported in PD (O'Keeffe et al., 2020; Pauls et al., 2022; Vinding et al., 2020), I will focus on the sensorimotor state in the following analyses.

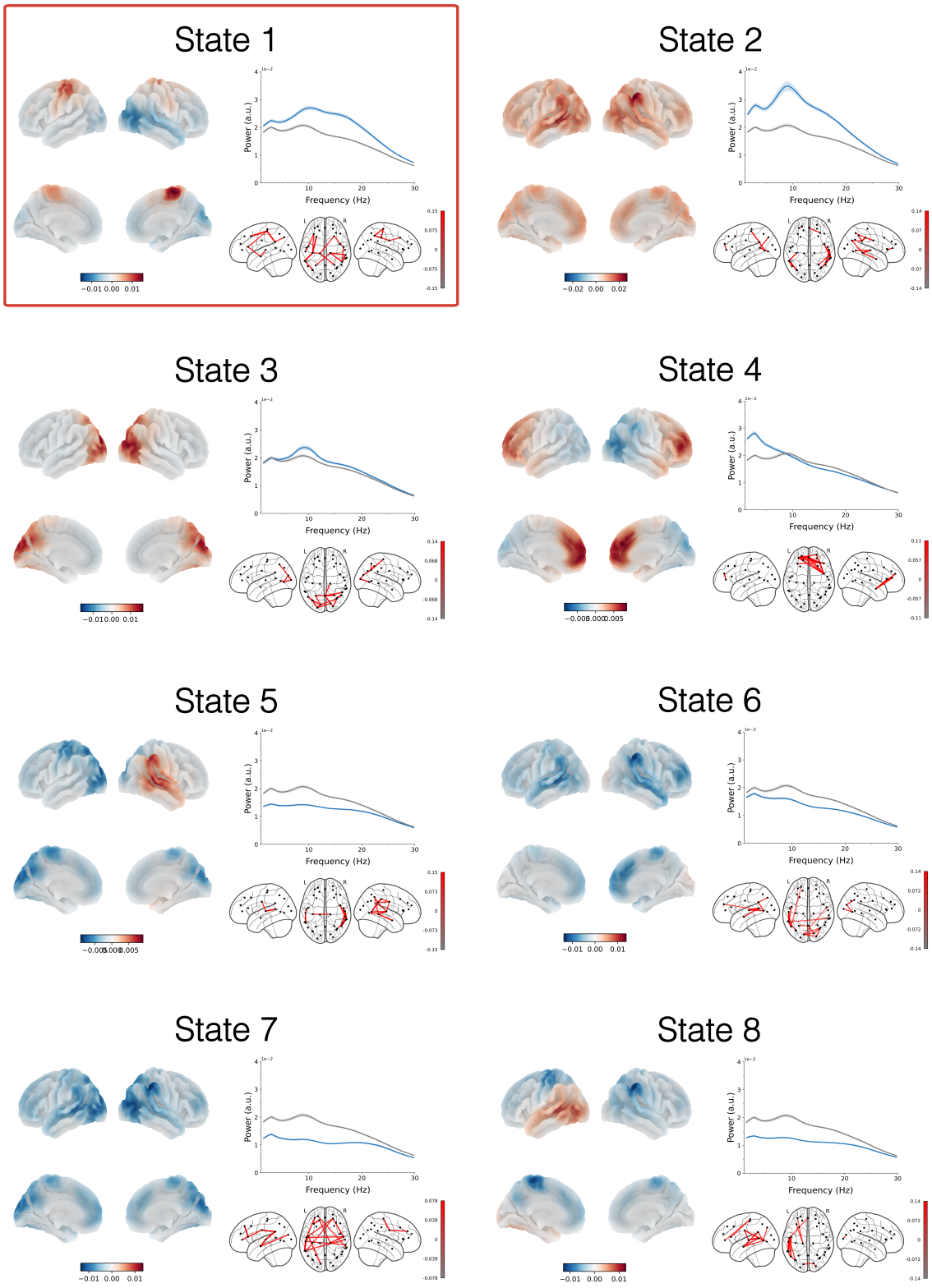


**Figure 1.5. Description of the dynamically switching large-scale networks inferred with TDE-HMM.** The red box highlights State 1 as the sensorimotor network state. States are sorted in descending order according to their 18 to 25-

Hz motor power. State-specific spatial maps of oscillatory power averaged over 2 to 30 Hz (relative to the average power across all states) are shown on cortical surfaces. Motor cortical state power spectra (blue line) are shown alongside state power spectra averaged across all states (grey line). State-specific coherence networks averaged over 2 to 20 Hz (relative to the mean coherence across all states) are shown below the state-specific motor power spectra.

The TDE-HMM state metrics (Figure 1.6) provide a summary of the temporal dynamics of the large-scale networks captured by the TDE-HMM. Extracted networks had similar mean fractional occupancies, ranging between 11 to 16%. Fractional occupancy values across all states and participants were smaller than 47% and larger than 3% indicating that the brain networks mix well within participants, i.e., all participants' data were not represented by a single state, and all networks were visited for each participant. Mean lifetimes varied between 50 and 90 ms and interval times between 460 and 778 ms, which is in line with previous studies (Higgins et al., 2021; Vidaurre, Hunt, et al., 2018).

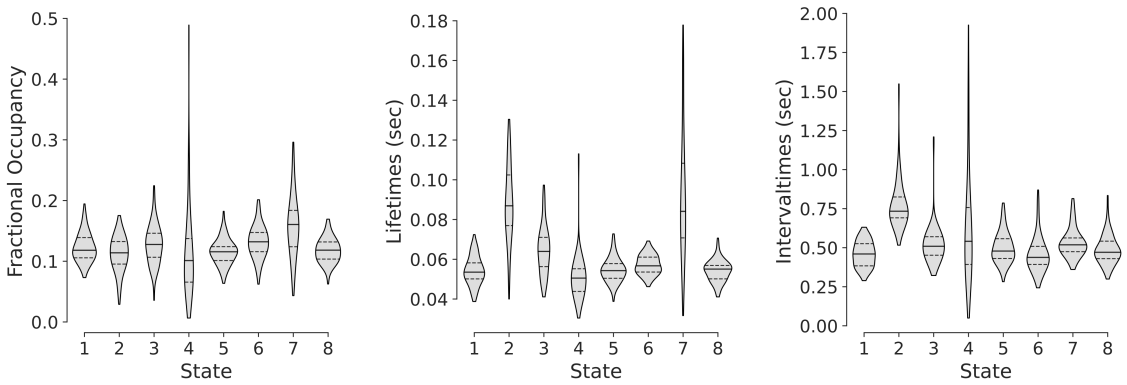


**Figure 1.6. State Metrics of TDE-HMM fit with lowest free energy extracting 8 states.** Fractional Occupancies of all States are below 0.5 and larger than 0

indicating that the extracted HMM-states mix well within and between participants.

## Fast, transient network dynamics relate to individual differences in static spectral power

I next assessed whether brain-network probabilities related to static spectral power by correlating fractional occupancies (FOs) of the sensorimotor network with motor cortical beta power across participants (Figure 1.7A). As expected, increased occurrence (i.e., FO) of the sensorimotor network was associated with increased beta power, indicating its contribution to the observed power variations across participants. To estimate how network occurrences influence power in a wide range of frequencies, GLMs predicting individual participants' power spectra from the sensorimotor network probabilities were fitted, and predictions of the obtained models for varying network fractional occupancies were extracted (Figure 1.7B). Note that a different GLM was fitted for each frequency. Predictions for fractional occupancies of the sensorimotor state indicated a pronounced increase in alpha and beta power in motor cortical areas.

## Dynamics of sensorimotor network are associated with diagnostic group but not symptom severity

Group comparisons of large-scale network dynamics revealed that the sensorimotor network occurred less frequently in individuals with PD. Contrasts between state metrics of the HC and PD groups (Figure 1.7C) indicated that the fractional occupancies

($t(58) = -3.77$, $p < .01$) and state rates ($t(58) = -3.47$, $p < .01$) of the sensorimotor state were significantly decreased, whereas interval times were significantly increased ($t(58) = 3.58$, $p < .01$), in the PD group. Additionally, increased lifetimes of a right temporal network (State 8) were observed in PD ($t(58) = 2.8$, $p = .04$). Group comparisons of all other state metric-x-brain state combinations did not reach significance (all $p > .13$). In all these analyses, I corrected for multiple comparisons across states for each metric separately with maximum t-statistic permutation tests. Repeating this analysis for 29 other HMMs extracting 8, 10, or 12 States, demonstrated that the observed group differences in the sensorimotor network were robust across different HMM inferences and number of states (Figure 1.7D).

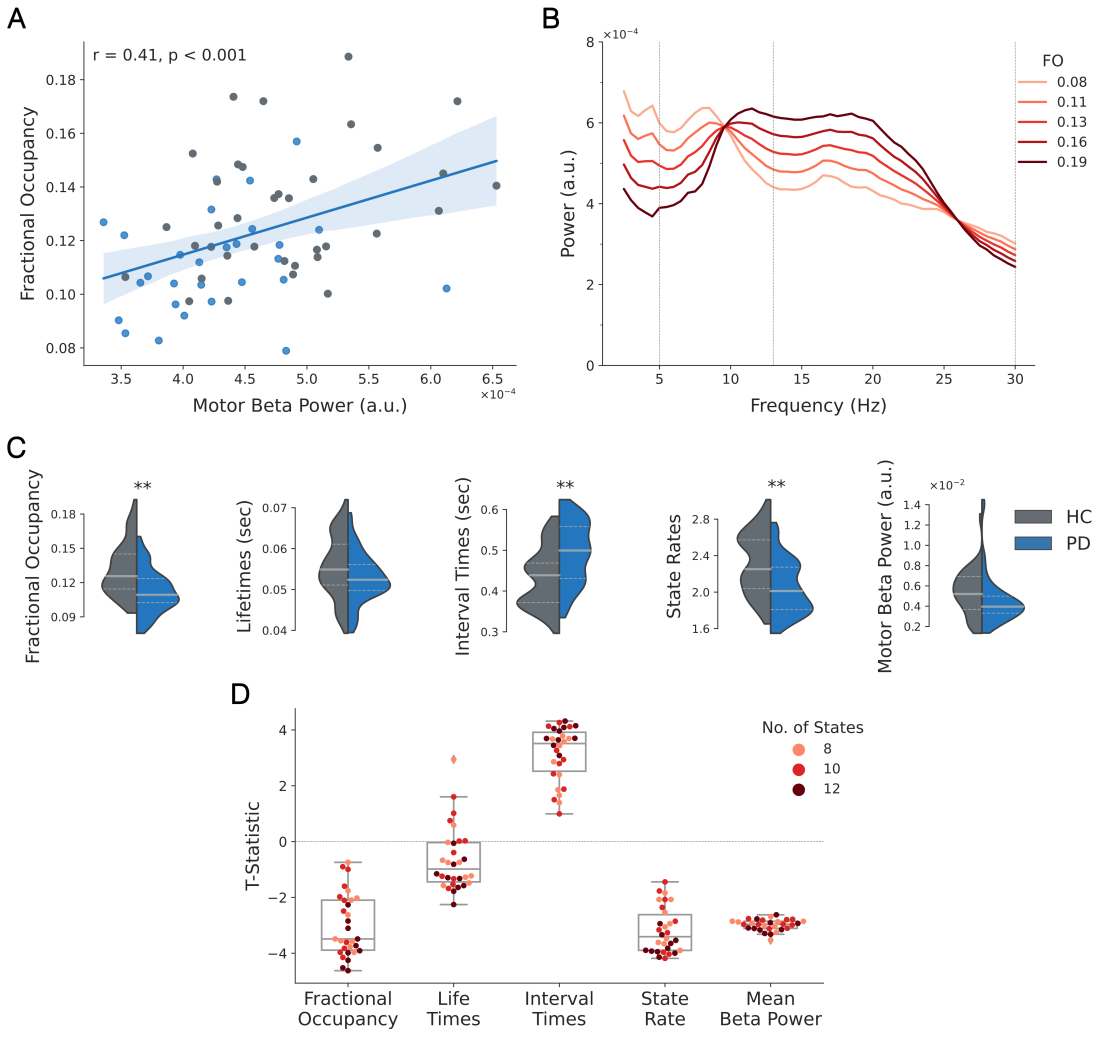


**Figure 1.7. Sensorimotor network dynamics are associated with motor cortical beta power and differ significantly between HC and PD group. (A)** The significant correlation between each participant's fractional occupancy of the sensorimotor state and motor cortical beta power confirms that brain state metrics related back to static oscillatory activity. Each dot represents the values of one participant and the colour indicates the participant's group with HCs coloured in grey and individuals with PD in blue. **(B)** Projections of a GLM that predicts how spectral power in motor cortex varies over subjects, using the fractional occupancy (FO) of the sensorimotor state for each participant as predictor. Note that a different GLM was fitted for each frequency. This indicates that as the fractional occurrence of the sensorimotor network increases, so does the alpha and beta power in motor areas. **(C)** Fractional occupancies, mean

lifetimes, mean interval times, state rates, and motor beta power of the sensorimotor network are presented for HCs (grey) and individuals with PD (blue). The significance of group differences is assessed with maximum t-statistic permutation tests controlling for multiple comparisons across states. T-statistics were calculated from GLMs accounting for confounds. **(D)** T-statistics of significant group differences in state metrics inferred with the TDE-HMM model with 8 States and lowest free energy are robust across 30 model fits extracting the 8, 10, or 12 states. Each dot represents the t-statistic of a group contrast from one of the fitted TDE-HMMs.
** indicates $p < .01$ and * $p < .05$.

More specifically, we repeated the state metric group contrasts of the sensorimotor state and the left temporal state across each of the 30 HMM fits to evaluate the robustness of group differences across different HMM fits. In the case of the sensorimotor state, most group contrasts involving fractional occupancies, interval times, and burst rates yielded t-statistics larger than 2 or smaller than -2 across various HMM fits. This suggests that these group differences are robust and consistent across different model iterations. However, for the group contrast of the left temporal state's lifetimes, many HMM fits resulted in t-statistics lower than 2. Based on this I concluded that the differences in lifetimes observed in the left temporal state are not robust across different HMM fits (Figure 1.8). In the following analyses, I focused solely on the sensorimotor network, because group differences were robust across different HMM inferences and parameter selections.

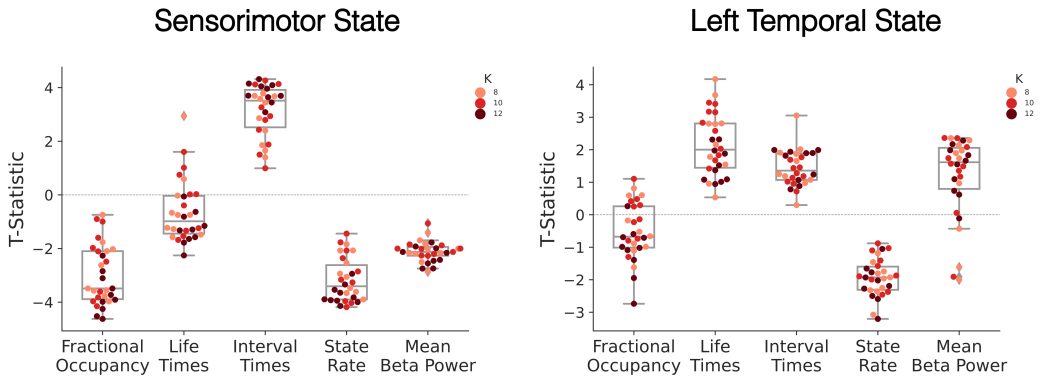


**Figure 1.8. Group differences of sensorimotor network metrics are robust across HMM inferences.** Each dot represents the t-statistic from the respective state metric's group contrast between HCs and PD volunteers for one of the 30 HMM inferences. The colours of the dots indicate how many states were inferred for the respective HMM inference. Negative t-statistic values indicate lower state metric values in the PD group, whereas positive t-values indicate increased state metric values in the PD group.

Correlations between sensorimotor state metrics, which differed significantly between the HC and PD groups, and motor symptom severity scores were assessed with GLMs accounting for potential confounds. No significant associations between sensorimotor state metrics of PD participants and Bradykinesia/Rigidity (all $p > .37$) or Tremor scores were observed (all $p > .17$). The lack of significant associations between sensorimotor state metrics and Bradykinesia/Rigidity scores (Figure 1.9) or Tremor scores was robust across different HMM inferences and parameter selections.

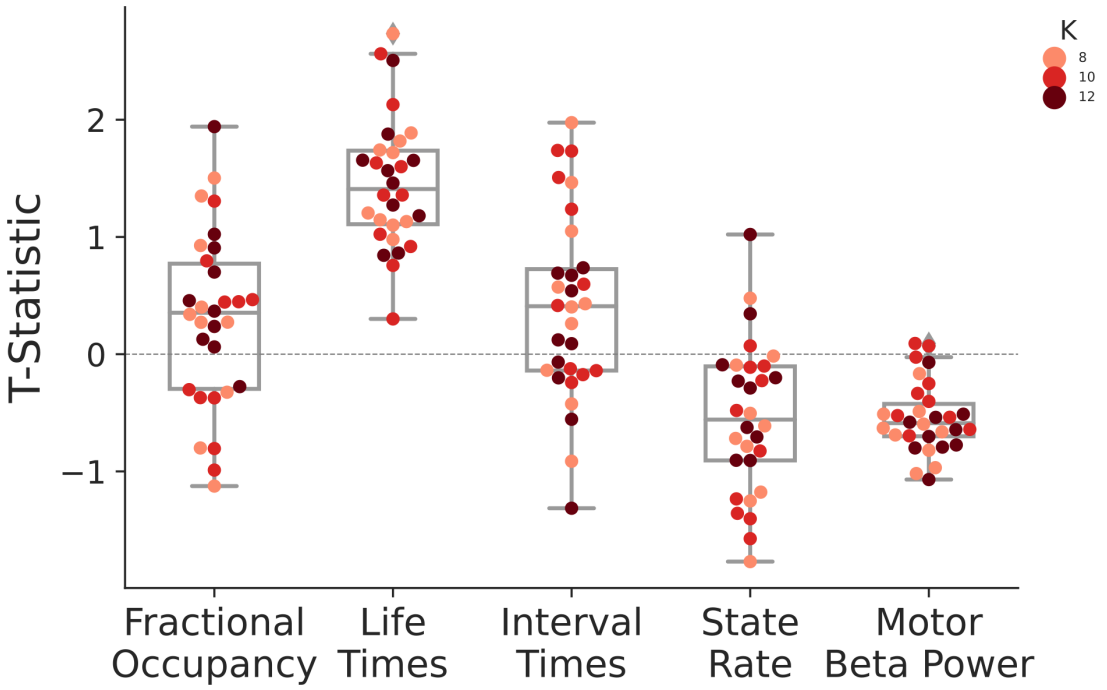


**Figure 1.9. Lack of associations between sensorimotor network metrics and Bradykinesia/Rigidity scores is robust across all HMM inferences.** Each dot represents the t-statistic from the respective state metric's correlation with Bradykinesia/Rigidity score for one of the 30 HMM inferences. The colours of the dots indicate how many states were inferred for the depicted HMM inference.

## Motor cortex beta bursts are associated with multiple large-scale networks

I next compared the TDE-HMM network state time courses and conventional motor beta burst on-vs-off time courses (Figure 1.10A). This revealed that the occurrence of beta bursts overlapped with visits to the sensorimotor state ($t(132) = 7.47$; $p < .001$). This indicated that both analyses were sensitive to similar events in the motor cortex. However, motor beta-burst occurrences also significantly overlapped with State 2 ($t(132) = 5.44$, $p < .001$) (Figure 1.10B), which is a state linked to widespread, increased

broadband power. This suggested that, while motor cortex beta bursts can be associated with the sensorimotor network, they can also be associated with other networks.

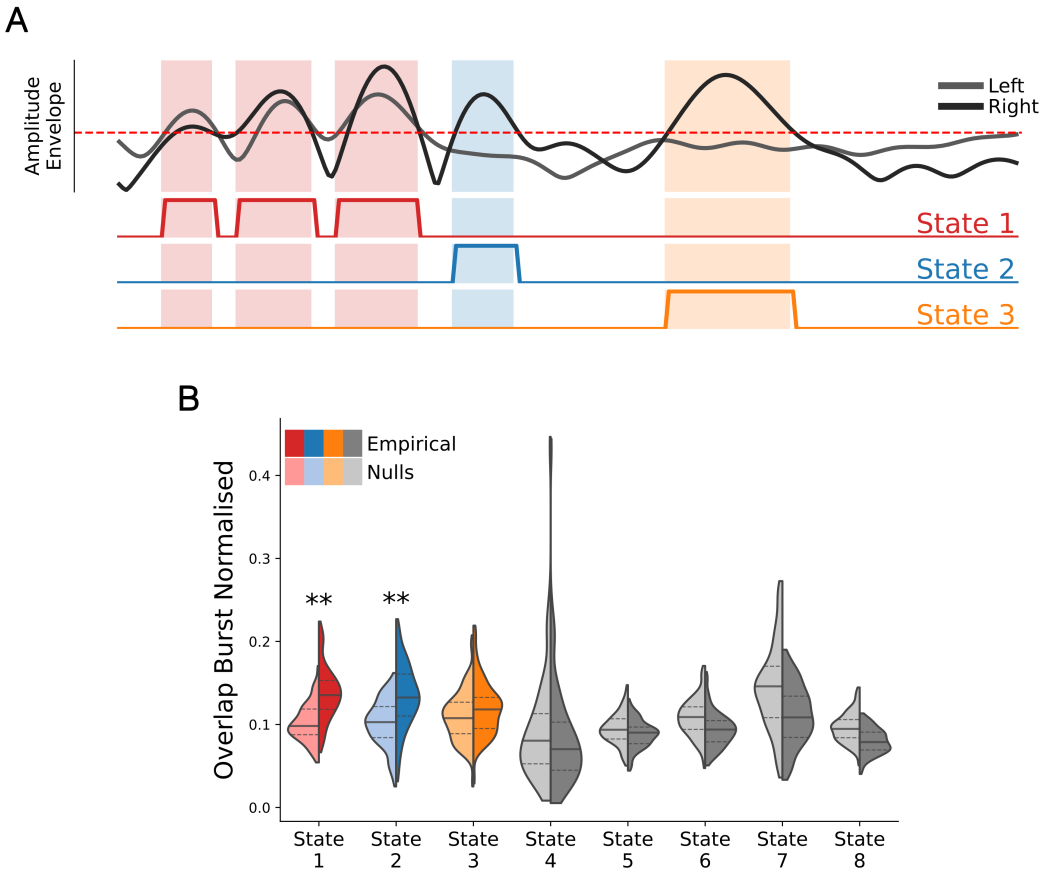


**Figure 1.10. Motor cortex beta bursts extracted with amplitude-envelope thresholding approach do not solely co-occur with sensorimotor network activations. (A)** Schematic depicting how overlap between the occurrence of conventional beta bursts and HMM-state visits is calculated. Amplitude envelopes of the left (grey) and right (black) motor cortex are thresholded using the 75$^{th}$ percentile (dashed red line). HMM-State on-vs-off time courses are depicted as red, blue, and yellow lines below. Shaded areas indicate periods in which amplitude envelopes cross the 75$^{th}$-percentile and HMM-state

occurrences overlap. **(B)** Empirically observed temporal overlap between the occurrence of conventional beta bursts and the different HMM states. The significance of the overlap was assessed with directed t-tests by contrasting the amount of empirically measured overlap (strong colours) with the amount of overlap obtained in the null case (where there is random overlap), obtained by shifting the HMM-state on-vs-off time courses by a random number of steps (shaded colours). Overlaps of beta bursts with HMM states that were associated with decreases in motor cortical beta power are depicted in grey colours. Bonferroni correction was applied to account for multiple comparisons across states.
** indicates $p < .05$ and * $p < .01$ after Bonferroni correction.

## Sensorimotor Network network-associated beta-burst (NABB) dynamics are sensitive to PD

I found that conventional beta bursts in the motor cortex were not predictive of PD. At the same time, I observed that beta bursts can be associated (through overlapping co-occurrence) with multiple networks and not just the sensorimotor network. To investigate whether focusing on motor beta bursts associated with sensorimotor network activations reveals significant group differences in burst dynamics, I segmented conventional motor beta bursts according to co-occurring HMM networks into NABBs. For example, in the schematic in Figure 1.10A the overlaps indicate that the first three beta bursts are State 1 NABBs, the next burst is a State 2 NABB, and the final burst is a State 3 NABB.

I found group differences (PD vs HCs) in fractional occupancy ($t(58) = -4.24$, $p = .001$), interval times ($t(58) = 4.77$, $p < .001$) and state rates ($t(58) = -4.70$, $p < .001$) for sensorimotor NABBs (Figure 1.11A). This is similar to what I found with the pure TDE-HMM analysis in Figure 1.7. In short, by titrating the conventional motor cortex beta bursts according to their co-occurrence with large-scale networks, I recovered the group differences observed in the pure TDE-HMM analysis.

To test further whether PD-related decreases in sensorimotor NABBs were specific for the sensorimotor network, I calculated the probability of bursts to overlap with any of the other networks (other NABBs) for the two groups. I observed that these other NABBs were significantly more likely to happen in the PD group ($t(58) = 3.18$, $p = .005$; Figure 1.11B). This suggests that the decrease in sensorimotor NABBs may be attenuated by activity in other NABBs in conventional burst analyses that ignore the network context of motor beta bursts.

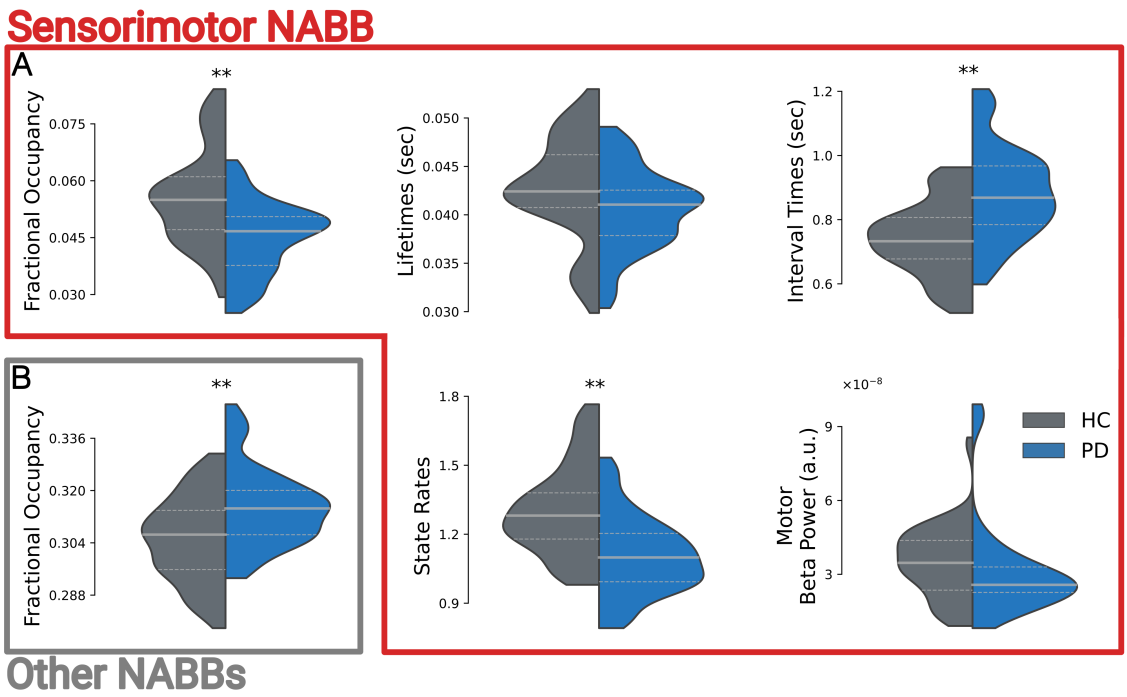


**Figure 1.11. State Metrics of sensorimotor network-associated beta-burst dynamics (NABBs) significantly differ between HC and PD group. (A)** Sensorimotor NABB fractional occupancies, mean lifetimes, mean interval times, state rates, and motor beta-power values of HCs (grey) and individuals with PD (blue) are depicted. **(B)** Fractional occupancies of all but the sensorimotor NABB occurrences per group. The significance of group differences is assessed with maximum t-statistic permutation tests controlling for multiple comparisons across states. T-statistics were calculated from GLMs accounting for confounds. ** indicate $p < .01$ and * $p < .05$.

I repeated the sensorimotor NABB group contrast for each of the 30 HMM inferences to make sure that the observed significant differences were not specific to the selected HMM inference. The group contrast t-statistics of the majority of HMM inferences were above 2 (Figure 1.12) because of what I conclude that the results of the NABB

metric group contrasts are robust across different HMM inferences and parameter selections.

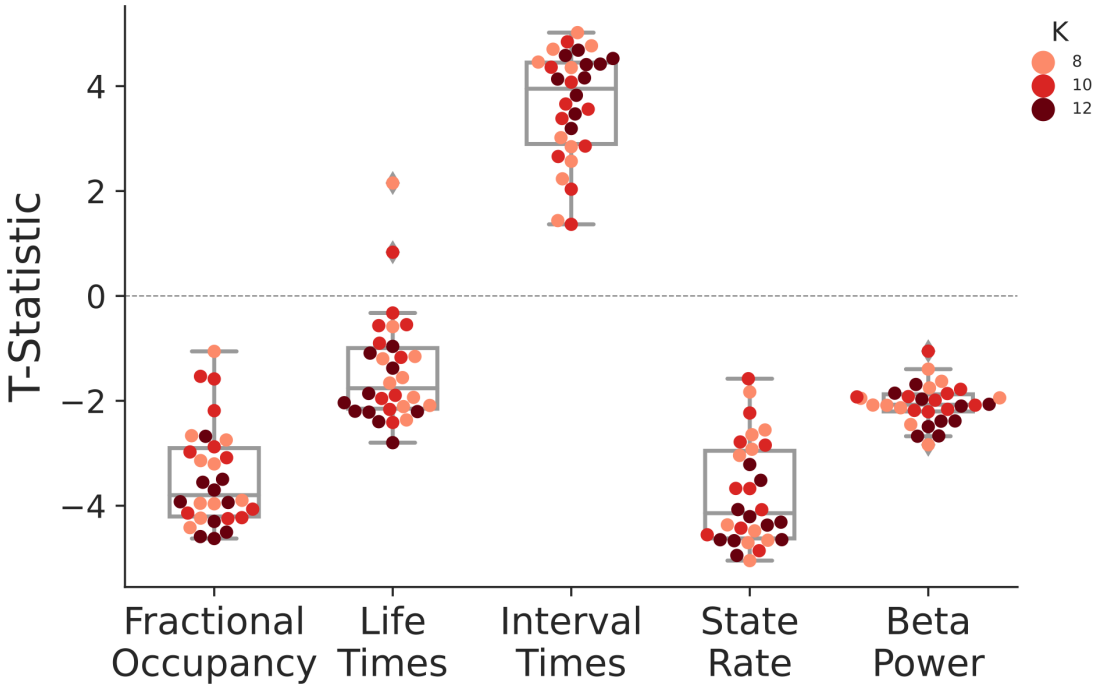


**Figure 1.12. HC vs. PD group differences of sensorimotor NABB metrics are robust across different HMM inferences and number of states.** Each dot represents the t-statistic from the respective sensorimotor NABB metric group contrast for one of the 30 HMM inferences. The colours of the dots indicate how many states were inferred for the depicted HMM inference.

In follow-up analyses investigating whether certain NABBs drive significant increases in the occurrences of other NABBs in PD, I found only State 7 NABBs to be significantly more likely ($t(58) = 3.01$, $p = .02$) and to show longer lifetimes in individuals with PD ($t(58) = -2.98$, $p = .03$) (Figure 1.13). The robustness analysis demonstrated that the

increased fractional occupancies of State 7 NABBs in PD were consistent across all 30 HMM inferences. However, the increase in lifetimes in PD did not yield t-statistics above 2 in the majority of cases, suggesting that this difference may not be robust across different model iterations. (Figure A1.3).

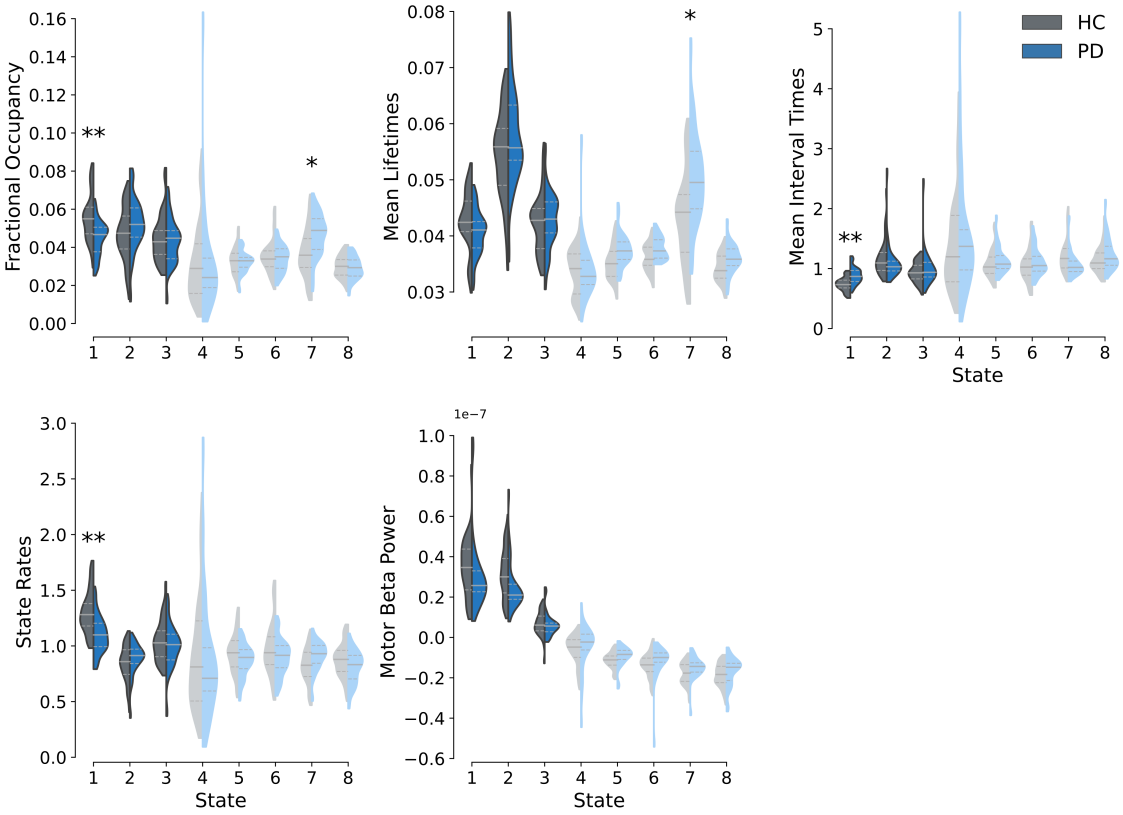


**Figure 1.13. Group comparison of network-associated beta burst dynamics (NABBs) between HCs and PD patients.** Fractional occupancies, mean lifetimes, mean interval times, state rates, and motor beta-power values of HCs (grey) and PD patients (blue) are depicted. The significance of group differences is assessed with maximum t-statistic permutation tests controlling for multiple comparisons across states. T-statistics were calculated from GLMs accounting for confounds. State metrics of NABBs of large-scale networks that have decreased motor

cortical beta power are plotted in shaded colours.
** indicate $p < .01$ and * $p < .05$.

## Different NAABs may relate to different processes

In an exploratory analysis, I investigated whether the extraction of NABBs could potentially differentiate beta events with distinct functionalities. I examined associations between NABB fractional occupancies and various variables such as Bradykinesia/Rigidity scores, motor cortical beta power, and coherence to discern any divergent patterns between sensorimotor and State 7 NABBs. Our analyses revealed significant associations between the fractional occupancies of sensorimotor NABBs and beta power, while no significant relationships were found with motor cortical beta coherence or Bradykinesia/Rigidity scores. Conversely, State 7 NABB fractional occupancies did not show significant associations with beta power but were significantly linked to motor cortical beta coherence and Bradykinesia/Rigidity scores (Figure 1.14). Notably, the significant association between Bradykinesia/ Rigidity scores and State 7 NABB fractional occupancies was robust across all 30 HMM inferences (Figure A1.4).

These distinct association patterns suggest differing functionalities of the State 7 and sensorimotor NABBs, with changes in State 7 NABBs potentially relevant to motor symptom severity in PD. The wideband power profiles of State 7 indicate a brain-wide decrease in 2 to 20-Hz Power from the mean power when State 7 occurs. However, given the unexpected nature of these findings and the complexity of their

interpretation in the existing literature, caution is advised, and further replication is necessary to confirm whether these associations are indeed meaningful or merely incidental.

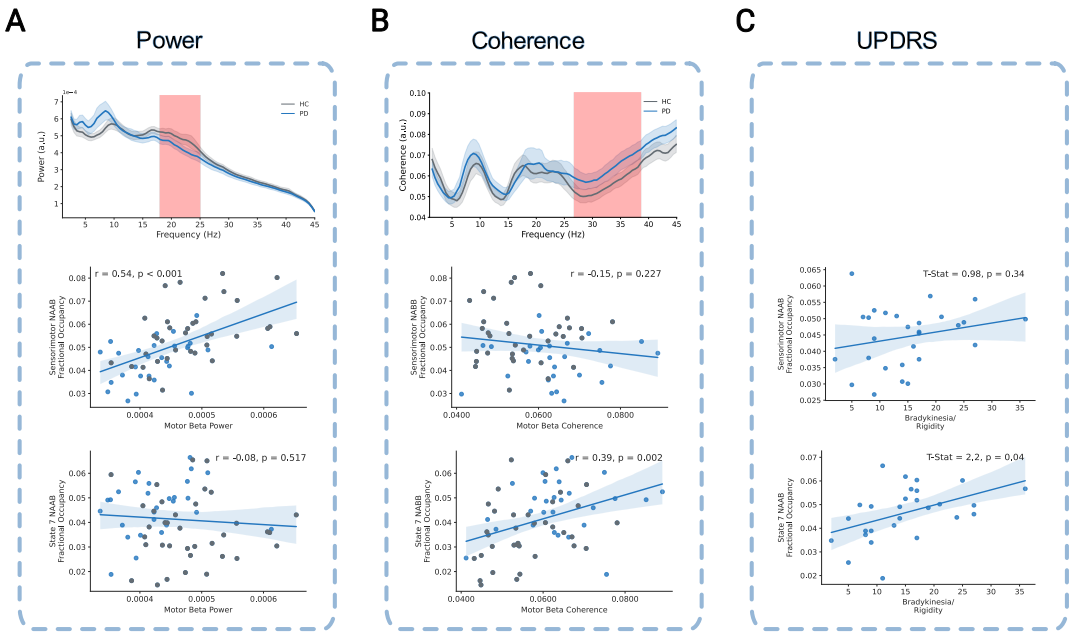


**Figure 1.14. Sensorimotor and State 7 NABBs show differing patterns of association with motor cortical beta power, beta coherence, and Bradykinesia/Rigidity scores. (A)** Motor Cortical average power spectra of HC and PD group. Cluster with significant power differences marked in red. Below correlations between beta power averaged across the significant cluster and sensorimotor and State 7 NABBs fractional occupancies are depicted. **(B)** Motor cortical average long-distance coherence of HC and PD group, calculated as the average coherence between the motor cortex and all other parcels. Cluster with significant coherence differences marked in red. Below correlations between coherence averaged across the significant cluster and sensorimotor and State 7 NABBs fractional occupancies are depicted. **(C)** Correlations between Bradykinesia/Rigidity scores and sensorimotor and State 7 NABB fractional occupancies are displayed.

# Discussion

## Summary

In this study, I explored whether examining motor cortical activations within their broader large-scale brain network contexts offers a more sensitive measure of oscillatory changes in individuals with PD. A comparison of static motor cortical beta power between HCs and PD volunteers revealed decreases in motor cortical beta power in the PD group. Conventionally estimated motor beta-burst dynamics did not differ between the two groups, while large-scale network dynamics obtained with a TDE-HMM revealed decreases in the occurrence probability of the sensorimotor network. I hypothesised that the differing findings may be due to different levels of network specificity of these two approaches. Accordingly, I found that conventional motor cortex beta bursts did not exclusively co-occur with activation of the sensorimotor network but also occurred alongside more widespread network activations. Separating motor cortex beta bursts that coincided with sensorimotor network activations from those coinciding with activations of other large-scale networks, enabled us to recover significant group differences between the HC and PD group, mirroring the observations from the pure large-scale network analysis. Importantly, the group differences observed between beta bursts coinciding with sensorimotor network visits and those coinciding with other large-scale networks exhibited opposing directions. Consequently, these contrasting changes may diminish group contrasts in conventional burst analyses that ignore the network context of motor cortical activations. Taken together, I replicated classical motor network results,

provided context about why they might be inconsistent in the non-invasive literature, and highlighted the importance of adopting a whole-brain perspective to accurately characterize changes in cortical oscillatory activity in PD.

## Static motor cortex-focused analysis reveals changes in oscillatory activity

The static power spectrum analysis revealed significant decreases in motor cortical beta power. In line with this, decreased motor cortical beta power in PD (Heinrichs-Graham, Kurz, et al., 2014; Vardy et al., 2011) and increased beta power after administration of dopaminergic medication (Cao et al., 2020; Heinrichs-Graham, Kurz, et al., 2014; Melgari, 2014) have been previously reported. However, it is important to stress that electrophysiological recordings of motor cortical beta oscillations have yielded varying findings (Boon et al., 2019; Underwood & Parr-Brownlie, 2021). Additionally, widespread beta-power decreases, potentially linked to spectral slowing, have previously been observed in central and posterior regions of the brain (Bosboom et al., 2006; Stoffers et al., 2007), which likely contribute to the observed beta-power decreases. It remains an open question what causes these varying findings on motor cortical beta changes in MEG recordings of individuals with PD. Methodological issues (O'Keeffe et al., 2020) or systematic differences in PD-sample properties across studies – such as differing medication status, PD subtypes, motor status, or disease progressions across studies (Boon et al., 2019) – might be potential reasons. Additionally, the spatial extent (Zich et al., 2020) and network context of motor cortical high-beta-power events need to be considered to dissect beta events that may be affected by PD in different ways.

## Sensorimotor large-scale network changes in PD group

The dynamics of the sensorimotor network, extracted with the TDE-HMM analysis, indicated a lower probability of this network to be present, reflecting decreases in the occurrences and longer intervals in-between visits. The observed reduction of sensorimotor network occurrences in individuals with PD replicates previous findings using static networks derived from ICA (Schneider et al., 2020), network-based statistics (Yassine et al., 2022), and motor cortical beta bursts (Vinding et al., 2020). Burst rate reductions were reported to be significantly associated with Bradykinesia scores (Vinding et al., 2020), whereas state-probability changes observed in our TDE-HMM analysis were not significantly associated with motor symptom severity scores. I linked variations in the fractional occupancies of the sensorimotor network to variations in static beta power, suggesting that these changes in large-scale network dynamics underpin static power spectrum measures. In sum, our findings indicate that large-scale network descriptions of brain activity enable distinguishing between individuals with PD and HCs and shed light onto the dynamic underpinnings of group differences in the static power spectrum.

Importantly, extrapolating results from studies investigating the role of beta activity in the basal ganglia-thalamocortical loop through invasive recordings of PD patients, suggests that motor cortical beta power is increased in individuals with PD. However, this hypothesis stands in contrast to the inconsistent findings regarding motor cortical beta-power changes reported in non-invasive (Boon et al., 2019), as well as to our observations of decreased beta power and sensorimotor network occurrence

probability. Several factors could account for this surface-level inconstancy between invasive and M/EEG studies:

1. Volunteers in invasive ECoG or DBS studies tend to have more severe disease progressions, symptomatology, exposure to and 'wearing off' of dopaminergic medication; and they may be less heterogenous due to surgery qualification criteria. (See Table A1.1 and Figure A1.1 for a detailed overview of disease durations, UPDRS-III on- and off-scores, and levodopa equivalent dose of PD samples in all papers on basal ganglia-thalamocortical beta oscillations referenced in the introduction of this chapter).
2. Comparisons of treatment effects, prevalent in invasive studies, are not equivalent to comparisons between PD and HC groups, prevalent in non-invasive studies.
3. Due to the larger scale of measurement, M/EEG may pick up changes in oscillatory power due to other pathological processes in PD, e.g., oscillatory slowing, which dilutes basal ganglia-thalamocortical loop-related motor cortical activity in MEG recordings.

Studies systematically investigating the effect of these factors on the inconsistencies between invasive and non-invasive studies may help to improve our understanding of how findings of these modalities relate to each other. This in turn would enable drawing better conclusions about PD-related pathologies that might underpin non-invasive electrophysiological biomarkers.

## Network context identifies PD-related changes in cortical beta bursts

In contrast to conventional amplitude-thresholding burst analyses, the spatiotemporal nature of large-scale networks allows for increased confidence about the spatial extent of network activation at each moment. I show that it is crucial to consider the underlying network distributions of transient, high-amplitude beta events when trying to identify sensorimotor network-specific markers of PD or other disorders. In contrast to previous reports (O'Keeffe et al., 2020; Pauls et al., 2022; Vinding et al., 2020, 2021), I did not initially observe changes in motor burst metrics in individuals with PD. Instead, our conventional amplitude-threshold beta-burst analysis revealed that bursts coincided not only with sensorimotor network activity but also with more widespread network activations. By separating motor beta bursts co-occurring with the sensorimotor network from motor beta bursts co-active with other large-scale networks, I revealed significantly decreased fractional occupancies and burst rates in motor beta bursts of individuals with PD, similar to what has been reported by Vinding et al. (2020). These findings suggest that a large-scale network perspective enables a more precise description of PD-related changes in sensorimotor network activity.

Interestingly, the group difference t-statistics obtained from the sensorimotor NABB metrics were larger than the t-statistics obtained from the sensorimotor network state metrics from the pure HMM analysis. This might indicate that targeting sensorimotor network visits with high motor cortical amplitudes can further refine the predictability of PD-related changes in motor cortical activity.

Motor beta bursts associated with different large-scale networks showed differing patterns of change in their occurrence probabilities. In contrast to sensorimotor

NABBs, the co-occurrence probabilities of beta bursts with all other large-scale networks (combined) were significantly increased in individuals with PD. This suggests that analysing the dynamics of all motor cortex beta bursts together, without subdividing them according to the networks with which they are most associated, diminishes group differences. Therefore, it may be crucial to extract sensorimotor networks or sensorimotor NABBs using a large-scale network perspective to differentiate between HCs and individuals with PD reliably.

## Putative contributions of NABBs

Further investigation into which of the non-sensorimotor NABBs drives the increases observed in the PD group revealed that State 7 NABBs played a significant role, being more likely to be present and having significantly longer lifetimes. Remarkably, the increase in lifetimes of the State 7 NABBs aligns with findings of increased burst lifetimes reported by Pauls et al. (2022), while the decrease in sensorimotor NABB rates is consistent with reports of decreased burst rates by Vinding et al. (2020). Thus, it is tempting to speculate that by embedding beta bursts in simultaneously occurring large-scale networks, different beta bursts can be disentangled. Differences in the activation of these NABBs in different PD subtypes may have the potential to reconcile differing findings in the literature.

Interestingly, increased State 7 NABB lifetimes match burst dynamics expected based on invasive studies of the basal ganglia-thalamocortical loop (Tinkhauser et al., 2018). Additionally, State 7 NABB fractional occupancy was significantly associated with Bradykinesia/Rigidity scores, and PD patients exhibited increased motor cortical long-

distance coherence in the high-beta-to-low gamma range during State 7 NABBs. Exaggerated high-beta coherence between the supplementary motor area and STN via the hyperdirect pathway has been discussed to drive STN beta hypersynchronisation (Oswal et al., 2021). Thus, State 7 NABBs may provide a dynamic window in which basal ganglia-thalamocortical loop-related activity can be picked up in M/EEG recordings of the motor cortex. If this hypothesis holds, basal ganglia-thalamocortical projections would not be associated with the sensorimotor network but rather with a state of decreased cortical oscillatory activity. This hypothesis should be treated carefully as this analysis was exploratory and requires replication in other datasets. Studies investigating the dynamics of STN-motor cortical connectivity and its cortical network context could test this hypothesis.

## Limitations

Our ability to associate neural changes with motor symptoms may have been compromised by utilising bilateral measures. All cortical metrics linked to PD motor symptom severity were aggregated across both hemispheres. Similarly, I employed Bradykinesia/Rigidity scores, derived from UPDRS-III item scores for both hemispheres, as a proxy for motor symptom severity in individuals with PD (Hammond et al., 2007; Litvak et al., 2011). In the context of PD, where motor symptom expression is frequently asymmetric, this approach might diminish sensitivity to unilateral associations between neural metrics and motor symptom severity scores.

The spatial resolution of the utilized parcellation is limited. All our analyses were conducted on source-localised data using a weighted parcellation with 39 cortical

regions (Colclough et al., 2015). Parcels within this parcellation stem from a group spatial ICA of fMRI recordings from the Human Connectome Project. Due to the grouping of several motor areas, such as the Supplementary Motor Area (SMA), pre-SMA, and motor cortex, into the same parcels, I cannot draw definitive conclusions about distinct processes within these areas. Refinement of the parcellation may enable a more precise delineation of the areas involved in the respective networks.

## Conclusion

In sum, the present study demonstrated that the spatiotemporal context of motor cortical activations is important for identifying PD-related changes in neuronal activity. I fitted a TDE-HMM to our data, providing a rich spatiotemporal description which can be linked back to the fundamental static power spectrum. The sensorimotor network dynamics distinguished between individuals with PD and HCs, whereas a conventional amplitude thresholding burst analysis failed to do so. The nature of the TDE-HMM approach provides greater confidence in identifying sensorimotor network beta activity because of the full network dynamics model. Finally, I provided evidence that relating conventionally estimated motor beta bursts to large-scale network activity may be crucial for exploring PD-related changes in the sensorimotor network and may help to clarify the contradicting findings in the literature. This work highlights the importance of taking a large-scale network perspective when attempting to identify non-invasive cortical biomarkers for PD.

# Chapter 2 – Large-scale network underpinnings of movements in Parkinson's Disease

## Introduction

The clinical hallmark of Parkinson's Disease (PD) are motor impairments (Postuma, Berg, et al., 2015), stemming from the dysregulation of the basal ganglia due to progressive deterioration of dopaminergic neurons (Hammond et al., 2007). These motor deficits include Bradykinesia, Rigidity, Tremor, Postural Instability, and Dystonia (Postuma, Berg, et al., 2015). Given the significance of motor impairments in PD, numerous studies have aimed to investigate the changes in brain activity underlying PD-related motor impairments.

### Beta Oscillations in STN related to movement impairments

Invasive recordings of subthalamic nucleus (STN) activity, which directly access the dysregulated basal ganglia, linked exaggerated oscillatory activity to motor impairments in PD (Hammond et al., 2007). Excessive synchronisation of low-beta oscillations in the basal ganglia-thalamocortical loop, characterised by prolonged low-beta bursts (Khawaldeh et al., 2022; Tinkhauser, Pogosyan, Little, et al., 2017; Tinkhauser, Pogosyan, Tan, et al., 2017), is a hallmark of PD (Hammond et al., 2007; Petersson et al., 2020; Singh, 2018) and is associated with clinical motor impairment scores (Kühn et al., 2006; Little et al., 2012; Oswal et al., 2016; Tinkhauser, Pogosyan, Little, et al., 2017; Tinkhauser, Pogosyan, Tan, et al., 2017), and reduced movement velocity, indicative of bradykinesia (Kühn et al., 2008; Lofredi et al., 2019; Torrecillos et

al., 2018). These excessive beta oscillations have been proposed to reduce the circuit's computational capacity, impairing the processing and initiation of new movements, and thus resulting in slower movements (Brittain et al., 2014). In line with this, hypersynchronisation is dampened by both deep brain stimulation (Eusebio et al., 2011; Kühn et al., 2008; Oswal et al., 2016) and Levodopa therapy (Brown et al., 2001; Kühn et al., 2009; Levy et al., 2002; Priori et al., 2004), demonstrating a correlation with clinical improvement (Kühn et al., 2008). Taken together, these findings suggest that exaggerated STN beta oscillatory activity likely underpins slowing of movements and motor symptom severity.

## Motor cortical beta oscillations are modulated by movements

Beta oscillations in non-invasive recordings of sensorimotor areas in healthy individuals exhibit a strong relationship with movements and movement outcome processing (Kilavik et al., 2013). Beta-power decreases during movements (movement-related desynchronisation; MRD), increases during static postural maintenance, and shows an increase after movement termination (post-movement beta rebound; PMBR) (Barone & Rossiter, 2021; Engel & Fries, 2010; Kilavik et al., 2013). Based on this, sensorimotor beta oscillations were initially proposed to reflect an idling rhythm indicative of a lack of movement (Pfurtscheller et al., 1996). However, it has been observed that processes such as signal expectancy, signal processing, and motor readiness modulate sensorimotor beta power in addition to movements (Kilavik et al., 2013). Different processes underlying task performance have been linked to beta oscillations with distinct beta frequencies, hypothesized to reflect the activation of different brain networks (Chandrasekaran et al., 2019; Kilavik et al., 2012; Schmidt et al., 2019).

Furthermore, studies suggested that beta oscillations promote the existing status of the motor system over changes to new movements (Androulidakis et al., 2006, 2007; Gilbertson et al., 2005) and especially that PMBR beta power indicates movement outcome processing (Alegre et al., 2002; Baker, 2007; Cassim et al., 2001; Tan et al., 2014, 2016). These findings led to the hypothesis that beta power does not solely reflect the absence of movements but rather serves as a marker for an active process promoting the maintenance and recalibration of the sensorimotor and cognitive status quo (Engel & Fries, 2010).

## Movement-related modulations of beta oscillations are attenuated in PD

Changes in sensorimotor beta power related to movement and movement outcome processing have been reported to be attenuated in individuals with PD. Decreased time-averaged beta power has been reported during rhythmically performed motor movements in PD, while alpha power was increased (Vardy et al., 2011). Time-frequency analyses, allowing for a time-resolved description of self-initiated movement-related beta-power modulations, revealed attenuated PMBR (Pfurtscheller et al., 1998), which is increased by levodopa and DBS administration (Devos et al., 2003), as well as reductions in MRD (Heinrichs-Graham, Wilson, et al., 2014). Notably, Vinding et al. (2019) observed attenuations in PMBR during passive index finger movements, that were unaffected by levodopa medication. This finding suggests that cortical processing of proprioceptive afferences may be impaired in individuals with PD, contributing to previously observed PD-related alterations in PMBR.

## Large-scale network context for a more fine-grained description of movement-related processes and PD-pathology

The large-scale network context of movement-related sensorimotor activations may provide a more nuanced understanding of PD-related changes by disentangling different motor processes. Beta power recorded from single regions of interest (ROIs) likely reflects activity from various underlying brain networks. The findings of Chapter 1 suggest that considering the network context of motor cortical activations can help to pinpoint functionally relevant pathology by dissecting sensorimotor beta activations relevant for PD. Especially in the context of movement-related sensorimotor beta power, which reflects multiple parallel processes (Kilavik et al., 2013) implemented by different beta oscillations (Chandrasekaran et al., 2019; Kilavik et al., 2012; Schmidt et al., 2019), the large-scale network context may facilitate the separation of functionally distinct processes. I hypothesize that this finer-grained description of movement-related network changes may enable to describe PD-related beta-power changes more precisely, potentially leading to the extraction of more reliable PD markers.

## Chapter Overview

In the present chapter, I investigate whether characterising movement-related beta-power changes in terms of dynamic, large-scale networks helps identify pathophysiological changes in PD. I start by trying to replicate PD-associated reductions in MRD and PMBR power during movements (Heinrichs-Graham, Wilson, et al., 2014; Pfurtscheller et al., 1998). Subsequently, I apply a time-delay embedded Hidden-Markov Model (TDE-HMM) (Vidaurre, Hunt, et al., 2018) to describe

movement-related sensorimotor beta-power modulations in terms of dynamic large-scale networks and demonstrate that network occurrences mirror modulation patterns observed for beta power during movements. Following this, I compare task-related network occurrence modulations and network-specific beta-power changes between healthy controls (HCs) and individuals with PD to assess if distinct sensorimotor networks exhibit unique alteration patterns in PD. Finally, I repeat key analyses in another dataset involving a passive movement task performed by HCs and PD volunteers. This additional analysis aims to demonstrate the robustness of observed sensorimotor networks and PD-related changes across different tasks and participant cohorts.

# Materials and Methods

## Sample

MEG recordings from a total of 14 individuals with PD and 16 age- and education-matched HCs were analysed in this project. The participants performed a sustained-gripping task previously collected by Zokaei et al. (2021). Magnetoencephalogram (MEG) recordings were acquired at a sampling rate of 1000 Hz using a Vectorview scanner, alongside forearm electromyogram (EMG) and grip force recordings. PD volunteers were instructed to refrain from taking their dopaminergic medication after 7 p.m. the night before the experiment. Inclusion criteria for the PD group were: 1) not currently enrolled in a drug trial; 2) not using any psychotropic, hypertensive, or vasoactive medication, as well as long-acting dopamine agonists; 3) absence of neurological or psychiatric disorders other than PD; and 4) ability to tolerate withdrawal from dopaminergic medication. Both groups showed no significant differences in cognitive scores, assessed using Addenbrooke's Cognitive Examination. Additional demographic and clinical variables are summarized in Table 2.1. The study received approval from the NHS Oxford Research Ethics Committee (Reference: 12/SC/0650) and adhered to the principles outlined in the Declaration of Helsinki. All participants provided written informed consent prior to participation.

## Sustained-Gripping Task

A schematic representation of the task is depicted in Figure 2.3C. During each trial, two bars were displayed on either side of the fixation cross, corresponding to each hand.

Within these bars, two red lines moved up and down, indicating the required bimanual gripping force to be exerted. The red lines on both bars ascended to either a high or low position and remained there for 3 seconds before descending to the bottom of the bars. The high position represented a gripping strength of ~17 Newtons, while the low position indicated a gripping strength of ~12 Newtons. Importantly, immediate visual feedback on the exerted force was provided via the height of a blue bar within each of the two bars. Each participant completed 60 trials per force condition, resulting in a total of 120 trials divided into 12 blocks of 10 trials each. Gripping strength was recorded using a MEG-compatible fibre-optic auxotonic force device (grippers) from Current Designs, USA. For further details regarding the task, refer to Zokaei et al. (2021).

## Software

All analyses were conducted using Python 3.10. Pre-processing was performed utilising the OHBA Software Library (OSL, https://github.com/OHBA-analysis/osl-core) and MNE-Python (Gramfort, 2013). TDE-HMMs and subsequent analyses on the HMM-outputs were run using OSL-Dynamics (https://github.com/OHBA-analysis/osl-dynamics) (Gohil, Huang, et al., 2024). Group comparisons between HCs and PD volunteers were performed with GLMTOOLs (https://pypi.org/project/glmtools/). A schematic illustrating the analyses performed in this chapter is provided in Figure 2.1.

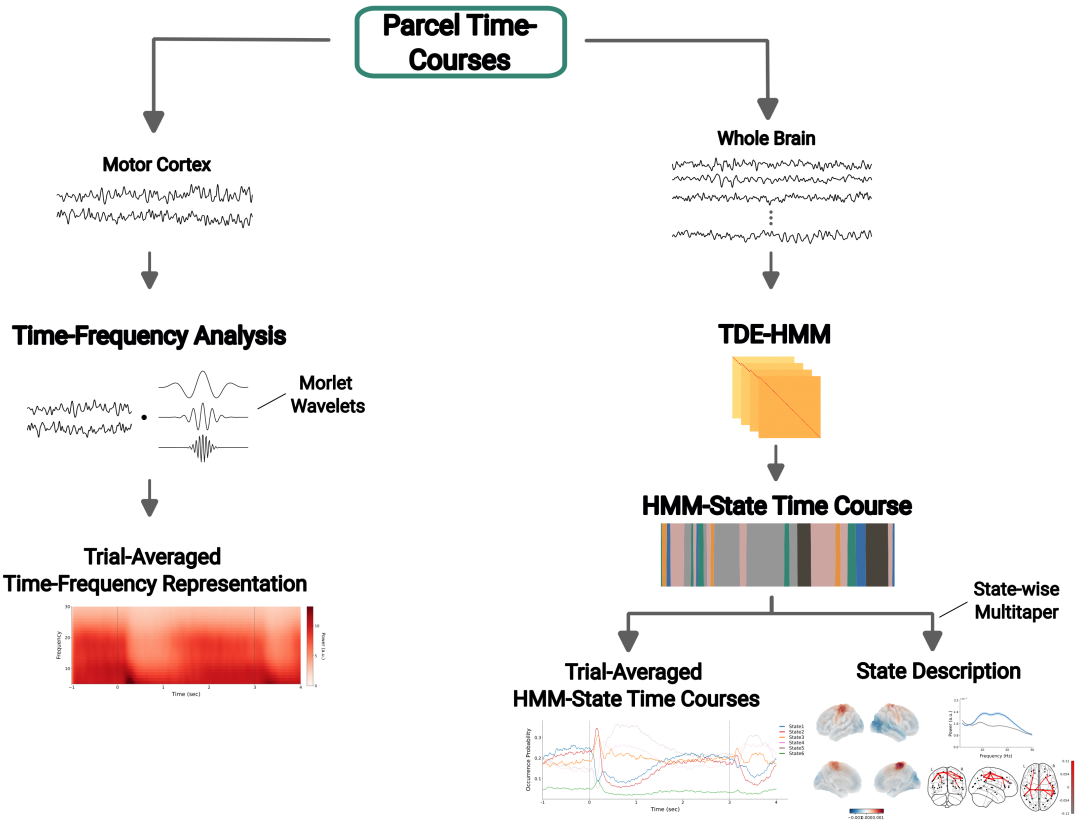


**Figure 2.1. Schematic of analyses reported in this paper.** All analyses were conducted using parcellated and sign-flipped data. A Morlet Wavelet analysis was applied to epoched time courses of the left and right motor cortex to extract trial-averaged beta-power time courses. A TDE-HMM was applied to the continuous time courses of all parcels to extract HMM-state time courses. Based on the obtained state time courses, spectral state descriptions were calculated with a state-wise multitaper approach. Furthermore, state metrics were computed to describe the dynamics of these states. Lastly, HMM-state time courses were epoched from -1 to 5 seconds around the gripping-stimulus onset, and trial-averaged HMM-state time courses were calculated. Trial-averaged HMM state time courses provide a moment-by-moment description of network activations during task performance.

## Pre-processing

The MEG data were maxfiltered (Maxfilter 2.2) with the "-tsss" option to remove signal components originating from sources outside the brain. Additionally, head movements during the scan were corrected (--headpos), and each scan was aligned to a reference scan (--trans). Notch filters were applied at 50, 100, 150, 200, and 250 Hz, followed by bandpass filtering from 1 to 45 Hz and downsampling to 250 Hz.

To mitigate eye movement and heartbeat artefacts, an automatic ICA data-cleaning procedure was applied. The data were divided into on average 49 (SD = $\pm$ 5) ICA components per participant, explaining a cumulative variance of 99% of the data. ICA components correlated ($r \geq 0.35$) with the electrooculogram (EOG) channel were rejected as EOG artefacts. Similarly, ICA components reflecting Electrocardiogram (ECG) artefacts were identified with cross-trial phase statistics (Dammers et al., 2008) and rejected. The automatic ICA data cleaning of each participant was visually inspected and refined if ICA components reflecting ECG or EOG activity were identified in the visual inspection. On average, 5 components (SD = $\pm$ 1.4) per participant were rejected.

To further clean the data by removing bad segments, each participant's Magnetometer and Gradiometer data were segmented into 1-second segments, and the standard deviation was calculated for each segment. Outlier segments were identified using generalized extreme Studentized deviate outlier detection (Rosner, 1983). The same procedure was repeated for the difference time series of the Magnetometer and Gradiometer data. On average 5% (SD = ± 3%) of the data were identified as bad segments.

The cleaned data were then co-registered to each participant's T1-MRI scan using Registration of Headshapes Including Nose in OSL (Rhino). Normalization of magnetometer and gradiometer data was performed to ensure equal contribution to the source localization (Woolrich et al., 2011). A Linearly Constrained Minimum Variance (LCMV) vector beamformer (Van Veen & Buckley, 1988; Woolrich et al., 2011), regularising the data to a Principal Component Analysis (PCA) rank of 60, was used to project MEG sensor data onto an 8-mm MN152 standard brain template. Parcel-wise time courses were then extracted for a weighted parcellation with 38 cortical regions (Colclough et al., 2015). Each parcel's time course was determined as the first principal component across voxels, with voxel contributions weighted according to respective parcel weights. Symmetric multivariate leakage reduction was applied to the parcel-wise time courses to reduce spatial leakage, including so-called ghost interactions (Colclough et al., 2015; Palva et al., 2018). Finally, the data were sign-flipped to remove ambiguities in the dipole orientations across participants (Vidaurre et al., 2016). The obtained continuous data was carried forward to the TDE-HMM analysis or was epoched for the time-frequency representation (TFR) analysis.

## Epoching

The pre-processed motor cortical parcel time courses and the HMM-state time courses were epoched to investigate task-related changes in motor cortical beta power and state occurrence probabilities. Data were epoched from -1 to 5 seconds after the grip stimulus occurred. Epochs containing segments identified as bad during pre-processing were rejected, with an average of 5.8 (SD = ± 4.69) trials rejected per participant. The choice of a long epoch duration from -1 to 5 seconds was made to visualize the full

shape of movement-related brain activity changes. However, this resulted in the period from -1 to 0 seconds and from 4 to 5 seconds showing almost identical data. Prior to calculating group comparisons, trial-averaged time courses were expressed as a percentage of the average value in the -1 to 0-second baseline window to focus on task-related modulations while accounting for interindividual differences. It is important to note that due to the short rest periods between grips, the selected baseline period contained post-movement beta rebound (PMBR)-related activity, which should be considered when interpreting the findings.

## Time-Frequency Representation (TFR) Analysis

I calculated time-frequency representations of the epoched time courses for the two superior medial motor parcels in each participant to investigate task-related modulations in motor cortical beta power. The signals were convolved with a set of complex Morlet wavelets spanning frequencies from 8 to 35 Hz in 1-Hz increments. The number of cycles for each wavelet was set to 0.3 times the wavelet's frequency. Trial-wise TFRs were averaged across trials to generate a trial-averaged TFR representation for each participant. Furthermore, to visualize the results of cluster-based permutation tests applied to the trial-averaged TFRs (see Statistics section), I averaged power values within 13 to 35-Hz frequency bins corresponding to the frequency range of the significant cluster identified from the permutation testing. This yielded trial-averaged power time courses for the cluster's frequency range. Finally, trial-average power time courses of the left and right superior medial motor parcels were average at each time point to obtain one bilateral trial-averaged motor cortical power time course.

# TDE-HMM Analysis

## Description

I applied a time-delay embedded Hidden Markov Model (TDE-HMM) to the data to explore the potential of utilizing large-scale network information to investigate PD-related changes in simultaneously happening processes during sustained gripping. TDE-HMMs describe continuous neuronal data as a set of dynamic, reoccurring brain states. Each state corresponds to a unique pattern of multi-region oscillatory activity, i.e., distinct power covariations and phase synchrony patterns, that are inferred in a data-driven manner (Vidaurre, Hunt, et al., 2018). A detailed description of the inference process is provided in Vidaurre, Abeysuriya, et al. (2018). In brief, the standardized time series are described as a sequence of a predefined number of hidden states, with only one state being active at any given time. Each state is defined by an observation model that captures specific auto- and cross-covariance patterns across brain regions. To compute autocovariance patterns for each data sample, it is embedded in a time window spanning ± 7 samples (i.e., 14 embeddings), resulting in a [parcels*embeddings x timepoints] 2D matrix. Subsequently, the dimensionality is reduced by selecting a subset of principal components (2 times the number of parcels) obtained through Principal Component Analysis (PCA), resulting in a [components x timepoints] 2D matrix. This dimensionality reduction serves to reduce computational demands. To further enhance computational efficiency, I adopted a stochastic variational inference approach (Vidaurre et al., 2017). Importantly, the states' dynamic nature, capturing changes between distinct patterns of multi-region spectral power and phase-locking at a moment-by-moment resolution, may enable the identification

of large-scale networks that are related to various processes underpinning sustained-gripping.

## Metrics describing Large-Scale Networks

### *State Dynamics*

Metrics quantifying the dynamics of large-scale networks were computed to compare large-scale network dynamics between HCs and individuals with PD. The padded a-posteriori probability time courses of the states, inferred by the TDE-HMM, were used to calculate several metrics. Fractional occupancy was determined for each participant, providing a measure of the fraction of the total time a state was present. Additionally, the average duration of state visits (lifetimes), intervals between state visits (interval times), and the rate of state visits per second (state rates) were quantified.

To obtain a more detailed description of state dynamics during task performance, I utilized the temporal structure of the task (Quinn et al., 2018, 2019). The padded a-posteriori probability state time courses of each participant were epoched from -1 to 5 seconds around the grip onset stimulus and averaged across trials. These trial-averaged state probability time courses provided a moment-by-moment description of the proportion of trials in which the respective state was present. Importantly, averaging state probabilities across trials provides a quasi-simultaneous description of state dynamics, despite the mutual exclusivity assumption of the model inference. This approach leverages the temporal structure of the task to average across moments in which similar processes are assumed to occur. Consequently, the trial-averaged state-probability time courses represent the probability of large-scale networks being present at specific time points during the performance of the sustained-gripping task.

To investigate the association between large-scale network dynamics and motor cortical beta-power modulations during the task, I assessed relationships between trial-average state probability time courses and trial-averaged beta-power time courses. I concatenated baseline-corrected average state probability time courses and average beta-power time courses of all participants and subsequently calculated the Pearson correlation coefficient between these two concatenated time courses. This tested whether moments with high occurrence probabilities of certain large-scale networks were associated with moments of high beta power, or vice versa.

Additionally, I compared network probability time courses between trials of the low gripping strength and high gripping strength conditions to demonstrate that large-scale network occurrences also scale with movement intensity. For each participant, a trial-averaged network probability time course was calculated for trials of each condition. I then determined the normalised differences between the high and low gripping strength conditions [i.e. ((high - low) / (high + low)) x 100]. Lastly, I tested whether the normalised differences were significantly different from 0 with GLMs and cluster-based permutation tests (see Statistics). Importantly, this approach obviated the need for baseline correction.

### *State-specific power and coherence*

State power and coherence were calculated for each participant post-hoc using the source reconstructed data alongside the a-posteriori probability time course of the states inferred by the TDE-HMM. Following Vidaurre et al. (2016), the source-reconstructed time courses were weighted using the a-posteriori state probability time

courses, before a multitaper analysis employing 7 Slepian tapers with a window length of 2 seconds was applied. This approach allowed for the extraction of power and coherence estimates across 1 and 45 Hz with a frequency resolution of 0.5 Hz. State-specific power spectra were calculated by subtracting the mean across all state spectra from the respective state power spectrum.

Next, Non-Negativity Matrix Factorisation (NNMF) was applied to the obtained coherence values to extract 2 spectral factorizations: one emphasizing frequencies below 25 Hz and the other focusing on frequencies above 25 Hz. By employing this factorization technique prior to averaging across frequency bins, wideband frequency-averaged coherence values were obtained without the need for arbitrary frequency band definitions. To visualize patterns of large-scale network connectivity, the spectral factorization emphasizing frequencies below 25 Hz was applied to the connectivity values, which were then averaged across frequencies and participants. Subsequently, the resulting coherence values were thresholded at the 98th percentile to highlight the most prominent connections within the respective network.

## Robustness Check

The inferred number of states is a crucial factor affecting the HMM's outcomes. Due to the stochastic initialization during the inference, multiple runs of the HMM with identical parameter settings may yield slightly different results on the same dataset. Nevertheless, key characteristics of the states, such as their topologies and dynamics, as well as the main findings of the analyses, should remain robust across different HMM runs inferring the same or varying numbers of states. To ascertain that our findings did not depend on a specific number of states or initialisation, I ran 30 HMMs

inferring 8, 10, and 12 states (Figure A2.1). The robustness of critical findings was assessed across the three HMM runs with the best fit to the data, as determined by the lowest free energy, for each number of states. The main figures present results derived from the HMM run with the lowest variational free energy, which serves as an approximation of Bayesian model evidence, among all HMM runs extracting 8 states.

### State Matching

Due to the algorithm's stochastic initialization, the order of the inferred states is arbitrary. Therefore, states obtained from different HMM runs need to be matched before they can be compared. To match states between HMM runs extracting the same number of states, I followed the procedure described in Chapter 1.

## Generalisability analysis

### Sample

Due to the small group sizes in the analysed task data, I aimed to demonstrate that observed key findings can be replicated in another, larger dataset. To achieve this, I repeated key analyses on passive movement task data contained in “The Swedish National Facility for Parkinson’s Disease Dataset” (Vinding et al., 2023; Vinding, Eriksson, et al., 2024). Demographics and clinical features of the 66 PD volunteers on medication (28 female; age = 41-80) and 68 HCs (30 female; age = 46-80) that were included in the replication analysis can be found in Table 2.1.

## Task Description

A detailed description of the passive movement task can be found in Vinding et al. (2023). In short, participants rested their right index finger on a pneumatic movement actuator while focusing on a red dot at the centre of the screen. In each trial, the red dot changed its colour to white after a random interval of 2.5 to 3.5 seconds. Following an additional random interval of 0.2 to 0.5 seconds, a passive movement lasting approximately 0.3 seconds was induced. There was a minimum interval of 2.25 or 2.75 seconds between movements. This procedure was repeated for 150 trials.

## Pre-processing

The data of the passive movement task underwent similar pre-processing procedures to those for the sustained-gripping task data. However, in this case, signal-space projection (SSP) was employed for cleaning the data from ECG and EOG artefacts, instead of manual ICA artefact rejection. Specifically, one EOG projection and an average of one (SD = ± 0.5) ECG projection were removed during the SSP cleaning process. Due to data sharing regulations, only individualised warped template MRI files (Vinding & Oostenveld, 2022) were provided for participants in the open dataset. MEG scans were registered to these warped MRI files without using the nose. For 13 participants, MRI files were not provided, so an 8-mm MNI152 standard brain template was used for co-registration. Co-registrations were carefully checked for all participants to ensure a good alignment between MEG data and MRI scans. Based on this, seven participants for whom good alignment could not be achieved were excluded. MEG data of the remaining 127 participants were beamformed, parcellated, and sign-flipped identical to the data of the sustained-gripping task.

## TFR- and TDE-HMM Analyses

TFRs, TDE-HMMs, and TDE-HMM metrics were computed following the identical procedures outlined for the sustained-gripping task analysis. However, for the passive movement task, parcel-specific TFRs and HMM-state spectra were calculated for the superior lateral sensorimotor parcel instead of the superior medial motor parcel.

The rationale behind this adjustment was to ensure that our analysis targets ROIs replicating findings of Vinding et al. (2019), who reported reduced PMBR in PD volunteers during the same task. Since the medial, superior motor parcels did not exhibit significant differences in beta power during the PMBR period, I closely followed the procedure described by Vinding et al. (2019) to identify a ROI. Specifically, ROIs demonstrating the strongest MRD 50 to 110 ms after movement onset were selected (Figure A2.10). This approach led to the identification of the superior lateral motor parcels as ROIs for our analysis.

## Epoching

To replicate analyses on epoched beta power and network probability time courses, I followed the protocol by Vinding et al. (2019).

Source reconstructed time courses and network-probability time courses were divided into epochs spanning from -1.5 to 3.5 seconds relative to passive movement onset. Subsequently, both trial-averaged beta power and network-probability time courses were normalized as percentage of the average value in the -1.25 to -0.2 second window.

Table 2.1 Descriptive statistics of included participants for both data sets.

| Demographics | Sustained-Gripping Task[a] | | Passive Movement Task[b] | |
|---|---|---|---|---|
| | Healthy Controls | Parkinson's Disease | Healthy Controls | Parkinson's Disease |
| N | 16 | 14 | 65 | 62 |
| Sex (female/male) | 6/10 | 10/4 | 28/37 | 25/37 |
| Handedness (right/left) | 15/1 | 14/0 | 62/3 | 65/6 |
| Age (years) (mean, range) | 68.73 (57-80) | 67 (54-78) | 61.22-65.38 (46-80) | 62.32-66.37 (41-80) |
| Education (years) (mean, range) | 16.13 (10-21) | 17.79 (10-40) | N/A | N/A |
| Years since Diagnosis (years) (mean, range) | N/A | 2.5 (1-5) | N/A | 3.94 (0-19) |
| UPDRS III motor score (mean, range) | N/A | 32.57 (20-55) | N/A | 19.35 (1-47) |
| Hoehn and Yahr scale (mean, range) | N/A | 1.93 (1-3) | N/A | 1.68 (0-3) |
| Levodopa-equivalent daily dose (mg/day) (mean, range) | N/A | 295.36 (150-540) | N/A | 520.43 (0 to 1130) |

N = number of participants; UPDRS = Unified Parkinson Disease Rating Scale;
In cases where values were not provided for all participants, values were calculated across the provided values.
For the passive movement dataset, no years of education and only age ranges were provided. For the latter, average age ranges are reported.
[a] Zokaei et al., (2021); [b] Vinding et al., 2023

## Statistics

Contrasts between HCs and PD volunteers were assessed using General Linear Models (GLM) incorporating group constants, age, and sex as regressors to control for potential confounds (Figure 2.2A).

For metrics not resolved over time (such as baseline beta power, state-specific beta power, fractional occupancy, lifetime, interval time, and state rates), group contrasts were compared using this GLM model. When metrics were compared across multiple states, separate GLM models were calculated for each state, and significance was assessed using maximum t-statistic permutation tests with maximum t-statistic pooling across states to correct for multiple comparisons (Nichols & Holmes, 2002). For each of the 1000 permutations group labels were shuffled before GLMs were applied to assess group differences of the respective metric. For each permutation, the largest t-statistic across all states was selected to construct a single null-distribution which was used to determine the significance of the empirically observed t-values. Empirical t-statistics exceeding the threshold of $p < .05$ obtained from the null distribution were deemed significant.

In the cases of trial-averaged large-scale network-probability time courses, a GLM was applied to each time point starting from the grip-onset stimulus or passive movement initiation. Significant clusters in the obtained t-statistic time courses were identified using cluster-based permutations with 1000 permutations. Cluster-forming thresholds were determined based on the significance threshold of parametric t-tests with appropriate degrees of freedom.

The identical procedure was also applied to group comparisons of power spectra, where a GLM was applied to each frequency bin, and significant clusters were identified using cluster-based permutation tests with 1000 permutations.

Group contrasts between TFRs of HCs and PD patients were conducted by applying the above-described GLM model to each frequency bin at each time point starting from the grip-onset stimulus or passive movement onset. Cluster-based permutation tests with 1000 permutations were performed to identify significant time-frequency clusters, with cluster-forming thresholds determined as described for network-probability time course group contrasts.

For comparisons of non-time-resolved metrics (such as peak frequency) between identified sensorimotor networks, GLMs without confound regressors were applied (Figure 2.2B)

Contrasts between beta-power or state-probability time courses of identified sensorimotor networks or conditions were calculated by testing whether their normalised difference time courses were significantly different from 0. A GLM containing only an intercept-regressor was applied at each moment to test whether the intercept differed from zero. Significant clusters were identified from the obtained t-statistics using cluster-based permutation tests as described above (Figure 2.2C).

**A**

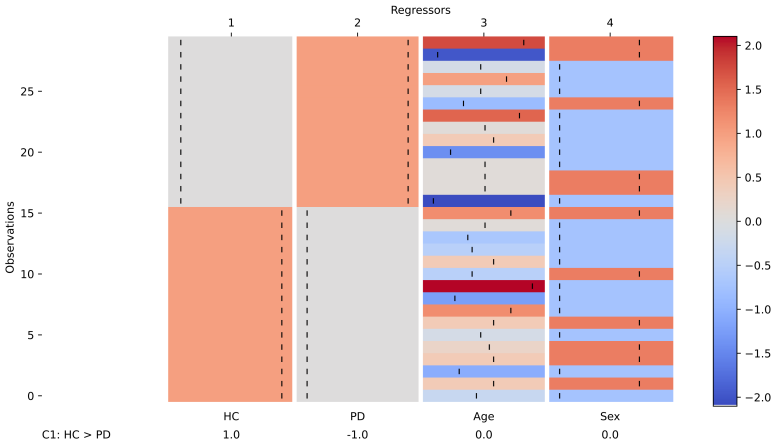
HC-vs.-PD Group Contrasts
Regressors
1
2
3
4
Observations
0
5
10
15
20
25
2.0
1.5
1.0
0.5
0.0
−0.5
−1.0
−1.5
−2.0
HC
PD
Age
Sex
C1: HC > PD
1.0
-1.0
0.0
0.0

**B**

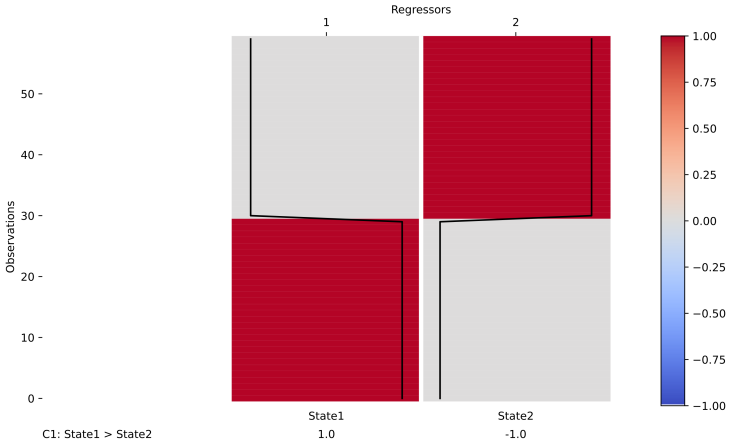
State1-vs.-State2 Contrasts
Regressors
1
2
Observations
0
10
20
30
40
50
1.00
0.75
0.50
0.25
0.00
−0.25
−0.50
−0.75
−1.00
State1
State2
C1: State1 > State2
1.0
-1.0

**C**

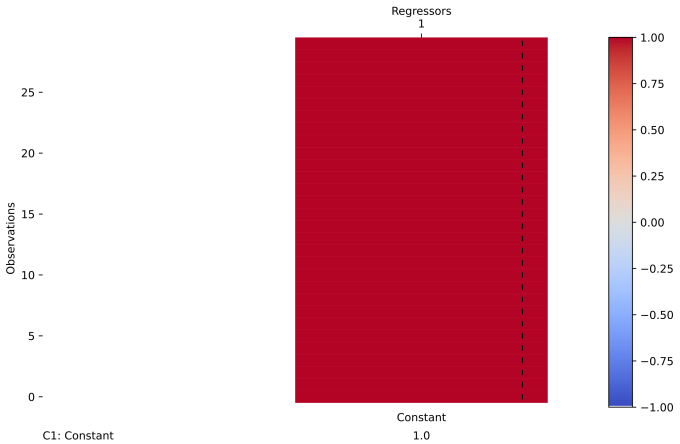
State Difference Contrasts
Regressors
1
Observations
0
5
10
15
20
25
1.00
0.75
0.50
0.25
0.00
−0.25
−0.50
−0.75
−1.00
Constant
C1: Constant
1.0

**Figure 2.2. Summary of GLMs used to compare variables between HCs and PD volunteers or HMM States for the sustained-gripping task.** Regressors added to GLMs are represented as bars with each entry representing the z-scored regressor value of a single participant. Applied contrasts are depicted below the respective models. **(A)** Model for GLMs comparing metrics between HCs and PD volunteers. Note that the contrast is specified in such a manner that positive t-statistics indicate larger values for PD patients and negative t-statistics larger values for HCs. **(B)** State 1 and State 2 corresponded to distinct sensorimotor networks. To describe differences between identified sensorimotor networks, GLM models depicted in (B) were applied for comparisons between State 1 and State 2 metrics. **(C)** Similarly, GLMs comparing State 1 - State 2 difference time courses against 0 were utilised to compare occurrence probabilities of the two sensorimotor networks. Models utilised for the replication analysis are depicted in Figure A2.9 .

## Data availability

The conditions of our ethics approval do not permit public archiving of the data supporting the sustained-gripping task experiment. Sharing data requires a formal data-sharing agreement in accordance with ethics procedures governing the re-use of sensitive data. Readers seeking access to the data should contact me.

Data from “The Swedish National Facility for Parkinson’s Disease Dataset” is openly available (Vinding, Eriksson, et al., 2024) and can be accessed via the EBRAINS Human Data Gateway (https://doi.org/10.25493/NMD2-2FW).

# Results

## Decreased beta power in the MRD period following grip-release in individuals with PD.

To investigate changes in movement-related beta-power modulations in PD relative to HCs, I compared trial-averaged TFRs between the two groups. Prior to this, I assessed beta-power group differences in the time window used for baseline correction (Figure 2.3B) and observed significantly decreased beta power for PD volunteers ($t(22) = 3.33$, $p = .003$). Given the short resting periods between grips, it is likely that PMBR-related beta-power changes occurred in this window and contributed to the observed group differences. Significant associations between baseline window beta power and participants' resting-state beta power ($r = .88$, $p < .001$; Figure 2.3C), obtained earlier during the MEG-scanning session, suggest that interindividual beta-power differences were comparable between the baseline window and the resting-state scan. Despite this, potential differences in absolute beta power due to the presence of PMBR cannot be ruled out.

The group comparison of trial-averaged TFRs of motor cortical activity revealed a 13 to 35-Hz cluster with significantly decreased beta power in the MRD period after grip release in HCs ($p = .04$) (Figure 2.3A; Figure A2.2). This suggests that the MRD is attenuated in individuals with PD.

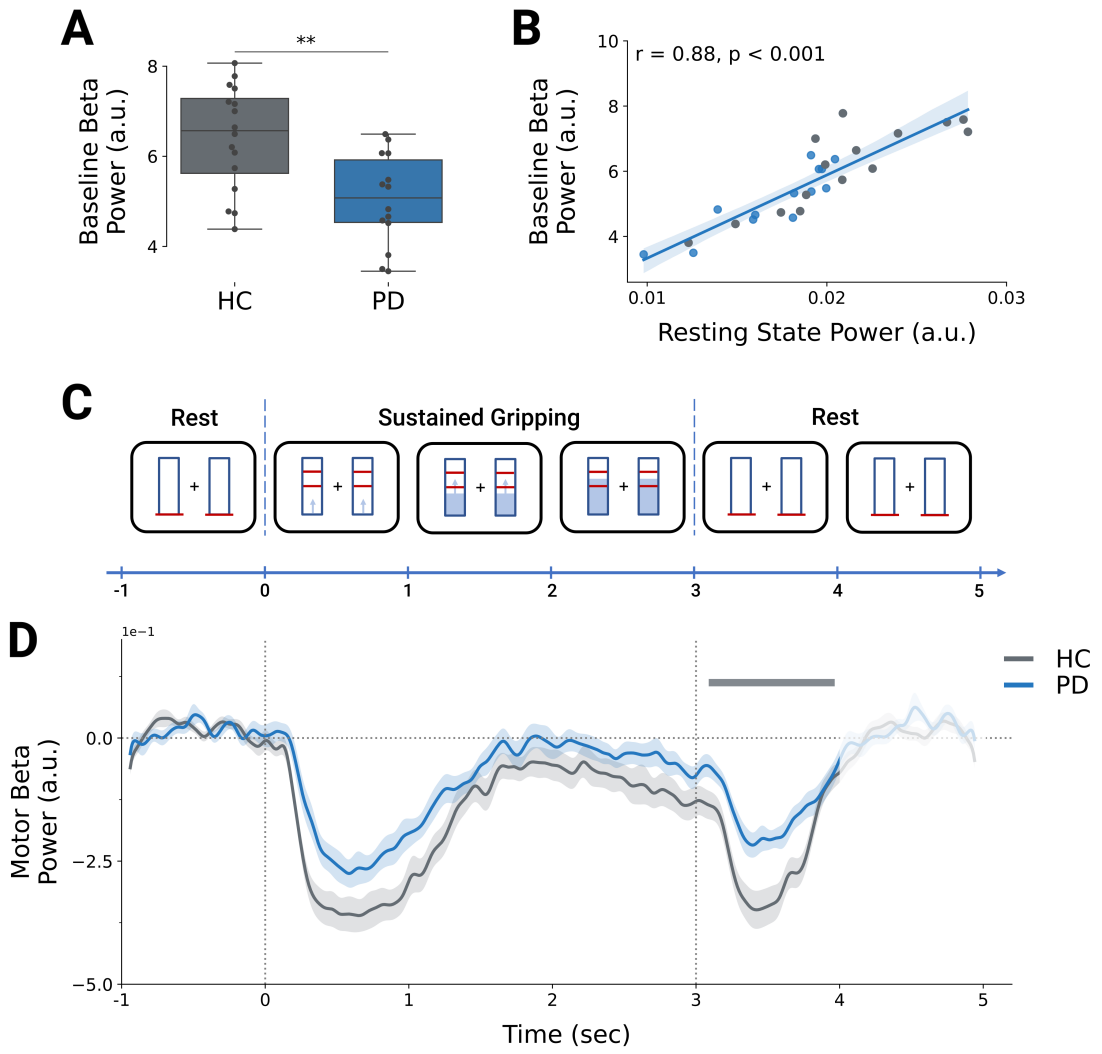


**Figure 2.3. Trial-averaged motor cortical beta power during the MRD period is significantly decreased in individuals with PD. (A)** Beta power in the trial-averaged -1 to 0-second baseline window is significantly smaller in PD. Each participant's average beta power is represented by a dot. **(B)** Baseline window beta power is significantly associated with individuals' resting-state beta power. Each dot represents the values of one participant, and the shaded line depicts the 95%-confidence interval of the estimate. **(C)** Schematic of a trial of the sustained-gripping task. Red lines in bars indicate the bimanual gripping strength to be exerted, while the blue shading within bars represents online feedback about the exerted gripping strength. The participants' task was to match the height of the blue shading to the red lines. Red lines indicate grips for a period of

3 seconds followed by a resting period of 2 seconds. **(D)** Results of the TFR cluster-based permutation test are visualised by showing trial-average motor cortical power time courses averaged across the 13 to 35-Hz range as defined by the significant time-frequency cluster. Prior to averaging across the 13 to 35Hz range, TFRs were baseline corrected for each frequency bin separately by expressing them as the percentage of the respective frequency bin's mean power in the -1 to 0-second baseline window. Trial-averaged time courses of HC (grey) and PD (blue) groups are depicted. Clusters with significant power differences are marked with a grey line on top of the beta time courses. The shaded areas around the two lines depict the group's standard error for each time point. The 4 to 5-second interval is shaded white since, due to the epoching, the data in this interval overlaps with the data in the -1 to 0-second period. ** indicate $p < .01$ and * $p < .05$.

## Fast, transient network dynamics described by TDE-HMM.

Spectral descriptions of the spatiotemporal large-scale networks extracted with the TDE-HMM are presented in Figure 2.4. Power covariance and phase connectivity patterns of the states are consistent with previous studies that have used a TDE-HMM to extract large-scale networks from MEG task data (Quinn et al., 2018).

Based on the spectral descriptions, I identified three large-scale networks with clearly increased oscillatory wideband power in motor parcels: State 1 occurrences were characterised by an increase in wideband power and coherence in motor cortical areas, while activity in other areas was decreased. State 2 activations were linked to increased wideband power and coherence in motor cortical, superior temporal, parietal, and occipital areas. State 3 visits were associated with a strong increase in

wideband power throughout the whole cortex and increased wideband coherence in frontal and central areas of the brain. Interestingly, states similar to State 1 and 3 were observed in the resting-state analyses in Chapter 1, and States similar to State 2 have been observed in other papers analysing task data (Higgins et al., 2021; Quinn et al., 2018).

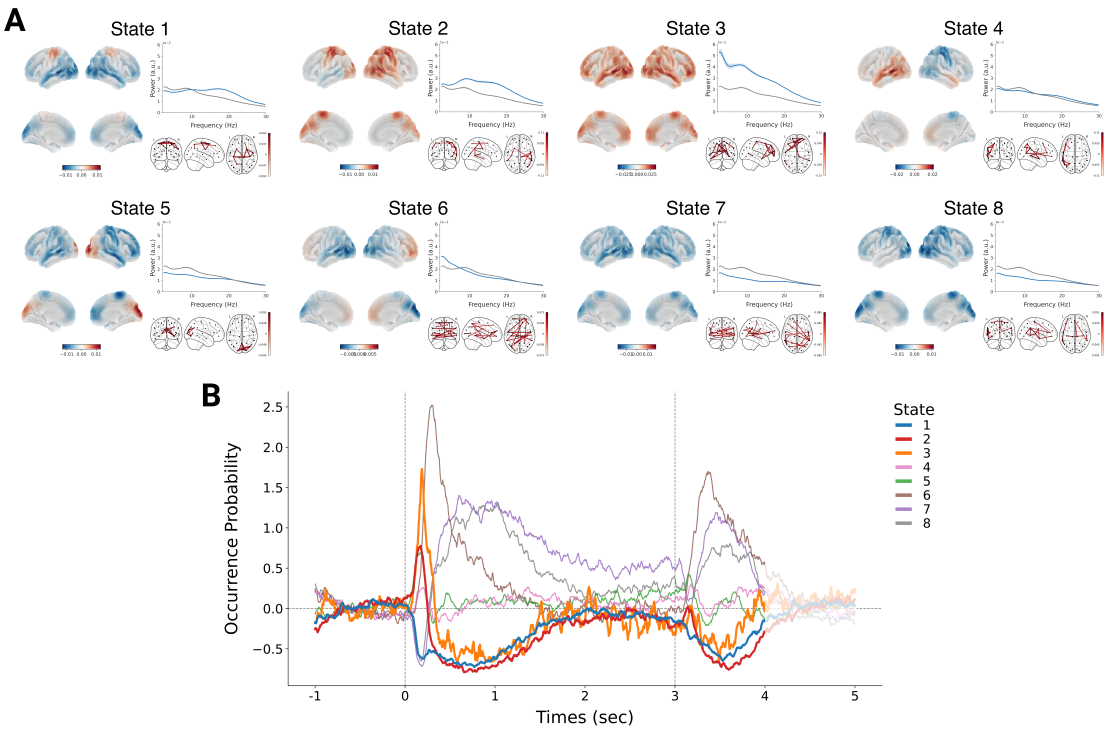


**Figure 2.4. Description of the dynamically switching large-scale networks inferred with TDE-HMM. (A)** Each network state's spectral properties are described in 3 ways: 1) Wideband power of each parcel (relative to the average power across all states) projected onto a cortical surface. 2) Superior motor cortical state power spectra (blue line) shown alongside superior motor cortical state power spectra averaged across all states (grey line). 3) State-specific wideband coherence networks (relative to the mean coherence across all states) projected onto a volumetric brain. States are sorted in descending order according to their association between the respective state's trial-averaged

occurrence probability time course and trial-averaged task-related beta-power modulations. **(B)** Trial-averaged state occurrence probabilities time-locked to gripping-stimulus onset, depicted as percentage of their occurrence probability during the baseline window. Occurrence probabilities of states with increased oscillatory wideband power in superior motor cortical parcels are shown in vivid colours. Trial-averaged state occurrence probabilities without baseline correction applied are presented in Figure A2.4).

The TDE-HMM state metrics provide a summary of the temporal dynamics of the large-scale networks captured by the TDE-HMM. State and participant-specific fractional occupancy values were smaller than 42% and larger than 1% (Figure A2.3), indicating that the brain networks mix well within participants, i.e., all networks were visited for each participant. Subject-averaged fractional occupancies ranged from 11% to 16%, lifetimes from 51 to 88 ms, and interval times from 361 to 559 ms for all States, except for State 3. Subject averaged fractional occupancies of State 3 were 3% and intervals times were 2.8 seconds, indicating that this state was less likely to occur than the other states. Importantly, state metrics falling within similar ranges, including one state with lower fractional occupancies and longer interval times, have been reported in previous TDE-HMM analyses of task data (Quinn et al., 2018).

## Sensorimotor networks show distinct spectral patterns

Interestingly, both State 1 and State 2 exhibited a distinct peak in the beta band. Specifically, State 2 seemed to peak at a lower beta frequency compared to State 1 (Figure 2.5A). State 2-specific spectra also reveal a prominent alpha peak, and the overall peak frequency was significantly lower than in State 1 ($t(26) = 5.16$; $p < .001$ )

(Figure 2.5B). These observations highlight that occurrences of different large-scale networks can lead to distinct spectral profiles in activity measured in the same parcels.

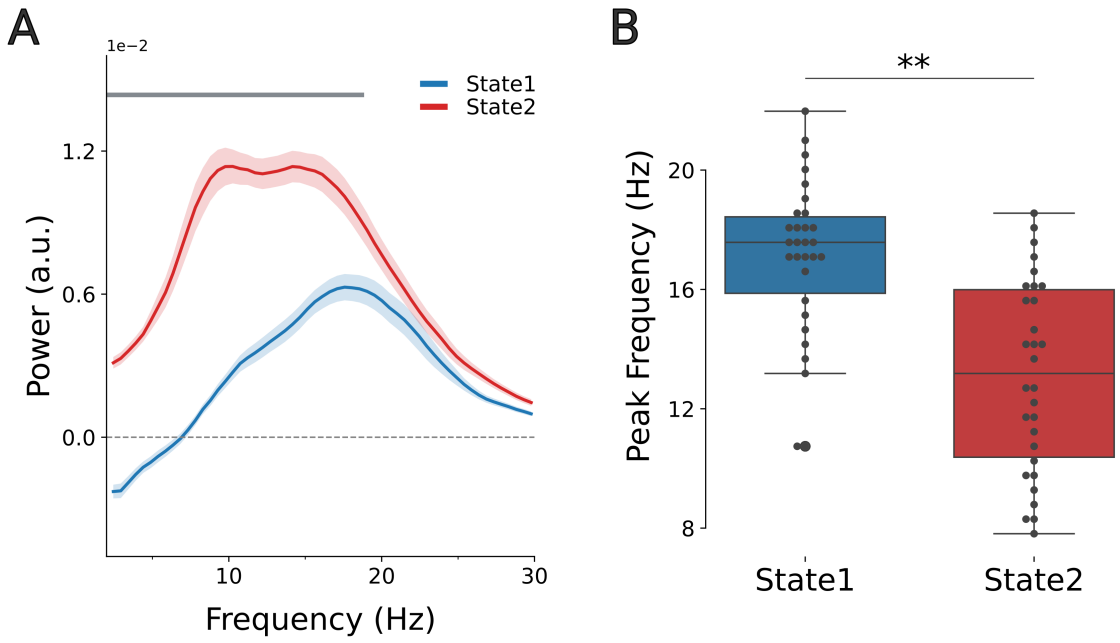


**Figure 2.5. Comparison of motor cortical state-specific spectra of sensorimotor (State 1) and posterior sensorimotor network (State 2) extracted from the sustained-gripping task data. (A)** State-specific power spectral change during occurrences of the sensorimotor and posterior sensorimotor network are depicted next to each other. State-specific power spectral change is calculated by subtracting the power spectrum averaged across all states from the state-specific power spectrum. Values of 0 indicated no change from the (static) average power spectrum (dashed line). Positive values indicate increases and negative values indicate decreases from the average power spectrum. Shaded areas around the lines represent the standard error for each frequency bin. The grey line on top of the spectra marks frequency bins that show significantly lower power in State 1 compared to State 2. **(B)** Peak frequencies of state-specific spectra of the sensorimotor network are significantly higher than peak frequencies of the posterior sensorimotor network. Each dot represents a

participant's peak frequency of the respective network-specific spectrum. ** indicate $p < .01$ and * $p < .05$

## Dynamics of sensorimotor networks are modulated by movements and gripping force.

Next, I assessed whether the dynamics of large-scale networks were modulated by the sustained-gripping task. Investigation of the trial-averaged state-probability time courses suggested that state occurrence probabilities varied systematically across trials in response to the task demands (Figure 2.4B; Figure 2.6). States 2, 3 and 6 exhibited prominent peaks in occurrence probability approximately 144 to 280 ms after the onset of the visual stimulus, likely reflecting the evoked responses to the stimulus (Figure A2.5). State 1 and 2 probability time courses showed pronounced decreases in occurrence probabilities during actual movement execution, such as gripping and releasing, while demonstrating increasing activations during periods associated with the PMBR and tonic muscle contraction. Notably, these modulations in state-occurrence probabilities closely mirrored the task-related changes observed in beta power during the same periods in the TFR analysis (Figure 2.3). Correlations between trial-averaged state-probability time courses and trial-averaged 13 to 35-Hz beta-power time courses, concatenated across participants, revealed strong positive correlations, suggesting that State 1 and State 2 underpin movement-related modulations of beta power (Figure 2.6A). Correlations between State 3 occurrence probabilities and movement-related beta-power modulations were weak, suggesting

that State 3 dynamics are unlikely to underpin movement-related beta-power modulations.

To ascertain that State 1 and 2 occurrence probabilities were not only modulated by movements but also scaled with movement intensity, I compared 13 to 35-Hz power and state occurrence probabilities between trials with low and high gripping strength (Figure 2.6B). I found significantly greater decreases in normalized 13 to 35-Hz power as well as normalised State 1 and State 2 occurrence probabilities during periods of sustained gripping (all *p*s < .05) in trials with higher gripping force exertion. In contrast, differences between the two grip-force conditions were less pronounced for State 3 probabilities, with only two short significant clusters observed at the end of the sustained-gripping period.

Based on these findings, combined with spatial activation patterns of the states, from here on I will refer to State 1 as the sensorimotor network and to State 2 as the posterior sensorimotor network.

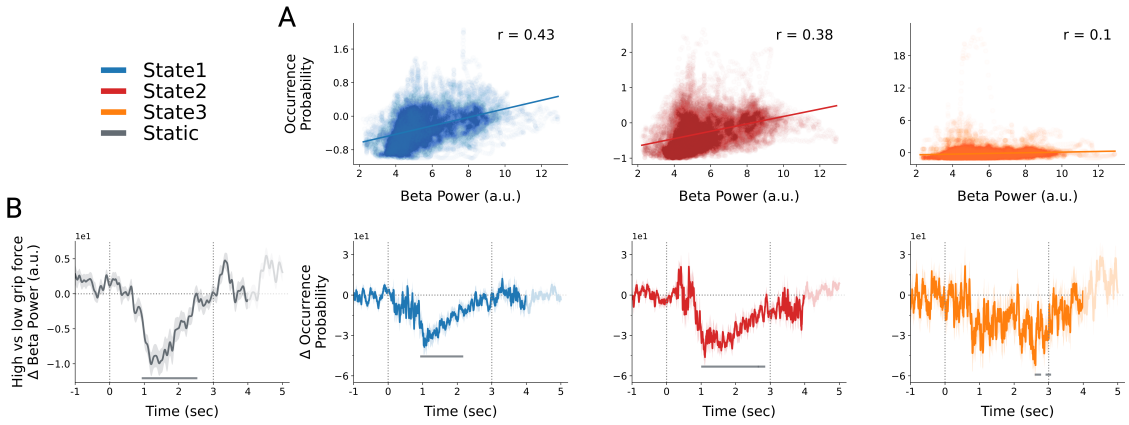

**Figure 2.6. Dynamics of sensorimotor networks are modulated by movements and gripping force. (A)** Trial-average occurrence probabilities of sensorimotor (State 1, blue) and posterior sensorimotor (State 2, red) networks are strongly associated with trial-averaged motor cortical beta-power time courses, whereas State 3 (orange) occurrence probabilities are not. Each dot represents beta-power and state-occurrence probability at a given sample of the participants' trial-averaged beta-power and state-probability time courses. Averaged beta-power and state-probability time courses are calculated as percentage of their average in the -1 to 0-second baseline window. **(B)** The normalised difference of superior motor cortical beta power (grey) and state occurrence probabilities (State1: blue, State 2: red, State 3: orange) between trials with high or low gripping force exertion. Negative values indicate lower beta-power or occurrence probabilities in the high grip force condition. Clusters with significant power or state occurrence probability differences are marked with a grey line at the bottom of the time course. The shaded areas around the lines depict the standard error across all participants for each time point.

## No significant differences in network dynamics between HCs and PD volunteers

After demonstrating that the dynamic large-scale networks extracted by the TDE-HMM describe task dynamics from a network perspective, I proceeded to investigate whether dynamic features of these networks differed between HCs and PD volunteers. Comparisons of metrics summarising the dynamics of large-scale networks across the entire scan did not reveal significant group differences. Fractional Occupancies (all $p > .75$), lifetimes (all $p > .67$), and interval times (all $p > .2$) of all states were not significantly altered in PD. Cluster-based permutation tests comparing task-evoked

network occurrence probability time courses, which provide a temporal description of state dynamics throughout a trial, also did not yield any clusters with significantly altered occurrence probabilities (Figure 2.7A; Figure A2.6).

## State-specific motor beta power is decreased in posterior sensorimotor network

I next assessed whether motor cortical beta power specific to large-scale networks differed between the HC and PD groups. Group comparisons of network-specific beta power revealed no significant changes in beta power in the sensorimotor network ($t(22)=1.929$, $p = .26$). However, the PD group showed a significant decrease in beta power in the posterior sensorimotor network ($t(22)=3.383$, $p = .004$)(Fig 2.7B,C) and significant increase in beta power in State 6 ($t(22)=-3.02$, $p = .032$). Group comparisons of state-specific beta power for all other states did not reveal any significant differences (all $p > .06$) (Figure A2.7). In all these analyses, I applied correction for multiple comparisons across states using maximum T-statistic permutation tests. Repeating this analysis for the 89 remaining HMMs extracting 8, 10, or 12 States demonstrated that the observed group differences in the posterior sensorimotor network and state 6 were robust across different HMM inferences and number of states (Figure A2.7 ).

Furthermore, peak frequencies of state-specific spectra for both the sensorimotor ($t(22)=2.99$; $p = .014$) and posterior sensorimotor ($t(22)=2.47$; $p = .046$) networks were significantly reduced in the PD group (Figure A2.8).

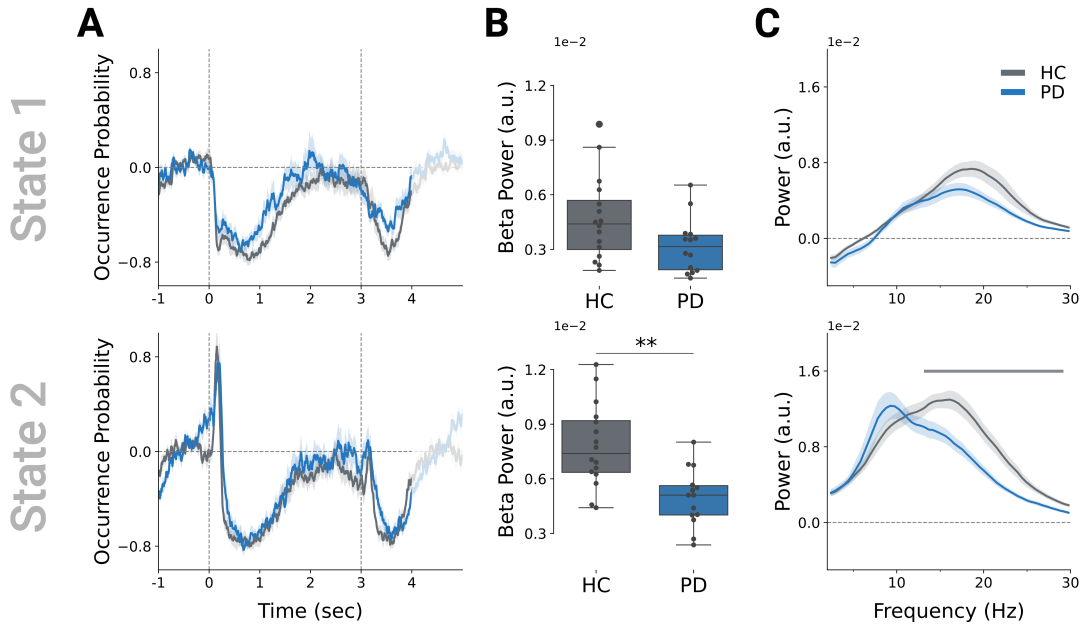


**Figure 2.7. Occurrence probabilities of sensorimotor networks are not changed in PD, but the state-specific beta power of the posterior sensorimotor network is significantly decreased in PD. (A)** Baseline-corrected trial-averaged occurrence probabilities of sensorimotor network (State 1) and posterior sensorimotor network (State 2) do not differ between HCs (grey) and PD (blue). **(B)** 13 to 30-Hz average of state-specific power is significantly decreased in PD in posterior sensorimotor network. **(C)** State-specific spectrum of posterior sensorimotor network is significantly decreased in beta range in PD. Clusters with significant power group differences are marked with a grey line at the top of the power spectrum. The shaded areas around the lines in (A) and (C) depict the standard error across the groups' participants for each time point or frequency bin. ** indicate $p < .01$ and * $p < .05$.

## Replication of beta-power changes in sensorimotor networks, while probability time courses do not differ

I repeated key analyses from the sustained-gripping task using open-access MEG recordings from HCs and PD volunteers performing a passive-movement task. This replication aimed to assess the generalisability of our key findings across different datasets and other types of movements.

### Time-Frequency Representation (TFR) Analysis

Group comparisons of motor cortical oscillatory power during the passive-movement task found a 20 to 31.5-Hz cluster with significantly decreased beta power in the PMBR period in the HC compared to the PD group ($p$ = .03) (Figure 2.8B; Figure A2.10 ). This finding replicates earlier observations of attenuated PMBR in a distinct PD cohort performing the same task (Vinding et al., 2019).

### Large-scale network description

Spectral descriptions of the large-scale networks inferred using a TDE-HMM revealed two distinct sensorimotor states with similar spatial distributions of wideband power (Figure 2.8A). Comparable to the sensorimotor network observed in the sustained-gripping task, State 1 exhibited activations in superior motor cortical areas, while activity in posterior regions of the brain was decreased. Conversely, during State 2 visits, stronger and broader activations of the motor cortex were observed, aligning with observations of the posterior sensorimotor network in the sustained-gripping task. Notably, parietal activations were less prominent and occipital activations were not present during State 2 visits in the passive-movement task. State-specific motor

cortical power spectra of State 1 and State 2 resembled the state-specific spectra of the sensorimotor and posterior sensorimotor states of the sustained-gripping task, respectively (Figure A2.11). Additionally, State 2 state-specific spectra exhibited a significantly lower peak frequency compared to State 1 state-specific spectra ($t(250) = 8.73$, $p < .001$) (Figure A2.11). Given these similarities, from now on I refer to State 1 as the sensorimotor network, and State 2 as the posterior sensorimotor network.

## Sensorimotor network occurrences are modulated by passive movements

Relative to the baseline period, state occurrence probability time courses of both sensorimotor networks decreased shortly after the onset of the 300ms-long passive movement, followed by an increase after the end of the passive movement, as expected for sensorimotor networks (Figure 2.8B). Importantly, this pattern closely mirrored task-related modulations of beta power, suggesting that sensorimotor network occurrence probabilities underpin task-related beta-power modulations (Figure 2.8C). Despite this resemblance, the network-occurrence probability time courses also showed differences between the two networks: The posterior sensorimotor network was less likely to occur during the MRD period (cluster $p = .002$) and took longer to reach its strongest deactivation ($t(250) = -5.55$, $p < .001$). In the PMBR period, the posterior sensorimotor network was more likely to be present than the sensorimotor network (all cluster $p$s <= .005) (Figure A2.12).

## Network-specific beta power, but not network occurrences were altered in PD

Next, I assessed whether the pattern of significantly decreased beta power in the posterior sensorimotor network, without notable differences in network probability time courses, could also be observed in the passive-movement task.

Cluster-based permutation tests conducted on state occurrence probability time courses of both sensorimotor networks revealed no significant differences between HCs and PD volunteers (Figure 2.8D). However, state-specific beta power of the posterior sensorimotor network was significantly decreased in individuals with PD ($t(119) = 3.57$; $p = .003$), mirroring observations from the sustained-gripping task (Figure 2.8E,F). Interestingly, state-specific beta power during sensorimotor state visits was also significantly decreased in PD patients ($t(119) = 3.0$; $p = .0175$) (Figure 2.8E,F), in contrast to the results from the sustained-gripping task analysis. Peak frequencies of state-specific spectra of the sensorimotor network ($t(119) = 1.88$; $p = .11$) did not exhibit significant differences between the two groups, whereas State 2 peak frequencies were significantly reduced in PD volunteers ($t(119)=1.88$; $p < .001$) (Figure A2.13).

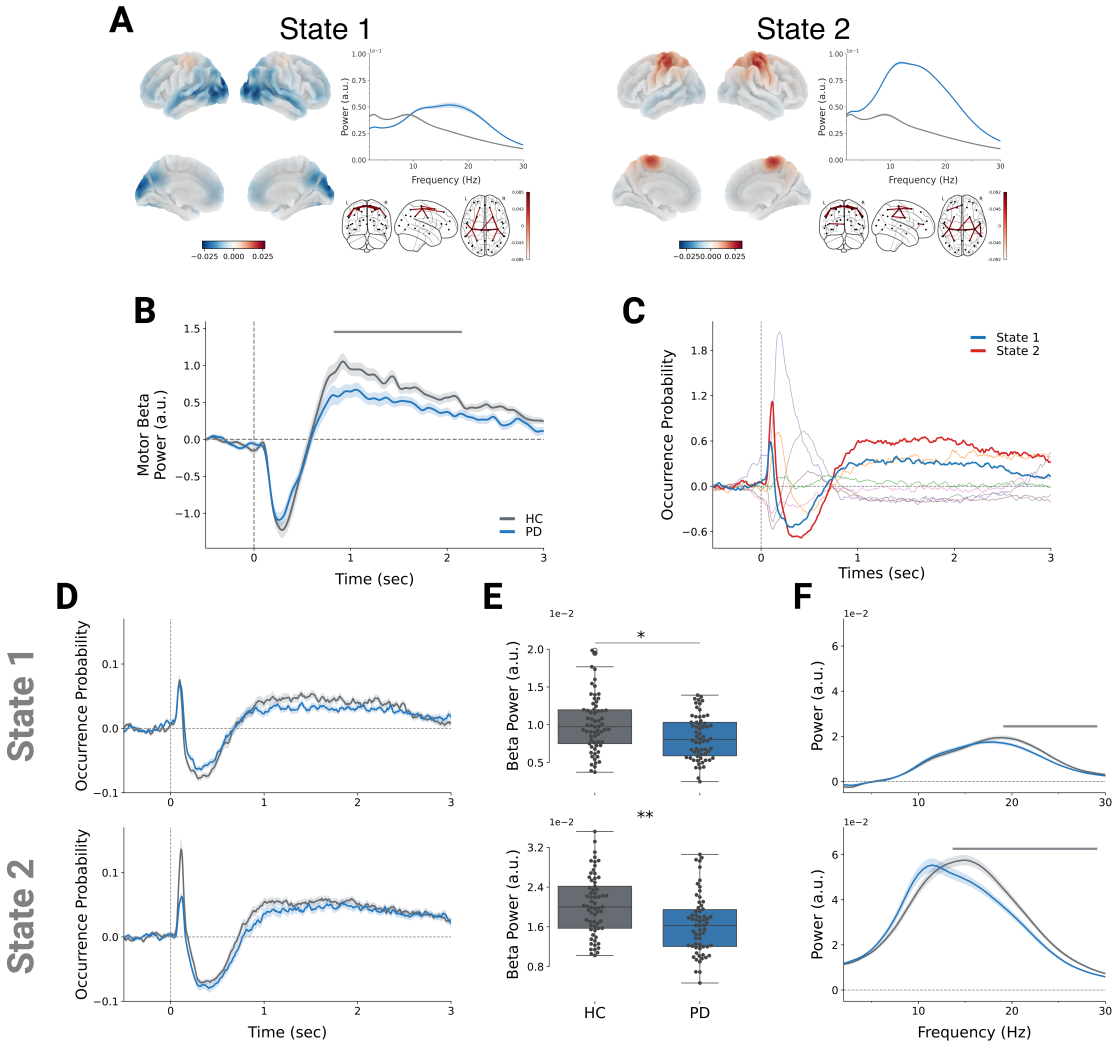


**Figure 2.8. Findings of generalisanility analysis. (A)** Spectral description of networks. Wideband power maps, state-specific coherence networks, and state power spectra of the superior, lateral motor cortex (blue) are presented. (See Fig. 2.4 for a more detailed description). **(B)** Results of the TFR cluster-based permutation test are displayed, showing trial-average motor cortical power time-courses averaged across the 20 to 31.5-Hz range, as defined by the significant cluster. Trial-averaged time courses of HC (grey) and PD group (blue) are depicted. Clusters with significant power differences are marked with a grey line on top of the beta time courses. **(C)** Trial-averaged state occurrence probabilities time-locked to passive-movement onset are shown as percentage of their occurrence probabilities during the baseline window. Occurrence probabilities of sensorimotor networks are shown in vivid colours. **(D)** Trial-averaged occurrence

probabilities of sensorimotor network (State 1) and posterior sensorimotor network (State 2) for HCs (grey) and PD volunteers (blue). **(E)** State-specific beta power in superior, lateral motor cortex for HC (grey) and PD (blue) groups for sensorimotor networks. **(F)** State-specific power spectrum of sensorimotor networks for HC (grey) and PD (blue) groups. Clusters with significant power group differences are marked by grey lines at the top of the power spectrum. The shaded areas around the lines in (A), (B), (D), and (F) depict the group's standard error for each time point or frequency bin.

# Discussion

## Summary

In this present Chapter, I aimed to enhance our understanding of the pathophysiological changes underlying PD by investigating movement-related beta-power modulations through dynamic, large-scale network analyses. The findings revealed significant attenuation of beta-power modulations during MRD periods in a gripping task and PMBR periods following passive movements. I propose that these beta-power modulations are influenced by various large-scale networks, in particular by two distinct networks exhibiting increased activations in motor areas. One network primarily activates superior motor areas (sensorimotor network), while the other shows more widespread activation across motor cortical, superior temporal, parietal, and occipital regions. Although the network occurrence dynamics of these networks did not differ between HCs and PD volunteers, state-specific spectra of both networks indicated decreases in beta power and peak frequencies in PD. The results emphasize the importance of considering the large-scale network context when analysing motor cortical activations, providing insights into the complex changes in movement-related oscillatory activity in PD.

## Task-related oscillatory beta-power modulations are attenuated in PD

Time-resolved motor cortical beta power was significantly modulated by movements during both tasks, with attenuated modulations observed in PD volunteers. During the sustained-gripping task, individuals with PD demonstrated significantly higher beta

power during the MRD period, consistent with prior reports (Heinrichs-Graham, Wilson, et al., 2014). Elevated motor beta power during movement execution has been linked to difficulties in planning and initiating new motor plans, potentially hindering the modification of the motor system's 'status quo' (Engel & Fries, 2010). Thus, higher beta power during the MRD period in individuals with PD may contribute to problems in initiating movements in PD (Heinrichs-Graham, Wilson, et al., 2014).

However, it is crucial to note that the time window utilized for baseline correction likely contained beta activity related to PMBR, showing significantly higher beta power in HCs compared to PD volunteers. This has two consequences: Firstly, conclusions regarding beta-power changes during PMBR periods cannot be drawn. Secondly, differences in MRD changes might be exaggerated due to subtracting significantly higher baseline values for HCs compared to PD volunteers. Nonetheless, given the high correlation between beta power in the baseline window and participants' resting-state beta power, and the documented PD-related decreases in MRD in previous studies (Heinrichs-Graham, Wilson, et al., 2014), I speculate that the changes observed in the sustained-gripping task are influenced by, but not solely attributable to, the baseline correction.

In the passive-movement task, I observed lower levels of beta power during the PMBR period in PD volunteers, replicating previous findings of attenuated PMBR in a nearly identical passive-movement task (Vinding et al., 2019). The authors suggested that attenuated PMBR may indicate PD-related impairments in processing and integrating proprioceptive feedback, as demonstrated in various behavioural studies (Abbruzzese & Berardelli, 2003; Adamovich et al., 2001; Bronstein et al., 1990; Demirci et al., 1997;

Jacobs & Horak, 2006; Nowak & Hermsdörfer, 2006; Rabin et al., 2010; Rickards, 1997). Erroneous models regarding one's body or limb position, resulting from such impairments, could contribute to motor symptoms in PD.

Since movements were not actively initiated, brain processes related to movement planning, initiation, or execution were unlikely to occur during the MRD period. Consequently, it is likely that the observed MRD primarily reflects the brain's immediate response to afferent signals resulting from the passive movement. The lack of significant group differences in beta power during the MRD period suggests that the sensorimotor system's initial response to afferent signals remains intact in PD. However, later processes involving the integration of proprioceptive feedback to update models of the participant's body position, occurring during the PMBR, are likely impaired.

In summary, these findings replicate previous research indicating that motor cortical beta power is modulated by movements and that these modulations are attenuated in PD, likely contributing to motor impairments in the disease.

## Two distinct spatiotemporal networks underpin movement-related beta-power modulations

Describing the data of both datasets in terms of dynamic, large-scale networks revealed two sensorimotor networks with distinct spatiotemporal patterns. Network probabilities of both sensorimotor networks were modulated by movements and scaled with gripping strength; mirroring observed beta-power modulations. Based on this, paired with the observation of increased motor cortical beta power during the

occurrences of these two states, I hypothesise that both networks may underpin movement-related beta-power modulations.

## Spatiotemporal patterns of sensorimotor and posterior sensorimotor networks hint at different functionalities

Based on the topography of the oscillatory wideband activations, network-specific power spectra, and network-occurrence probabilities of the sensorimotor and posterior sensorimotor network, I hypothesise that they may serve functionally distinct processes.

### Sensorimotor network reflects initial sensorimotor activity related to hand movements

The sensorimotor network exhibited its strongest activations in superior, lateral motor parcels, which correspond to areas implicated in the motor functioning of the hand and fingers (Gordon et al., 2023; Penfield & Boldrey, 1937). Moreover, the peak frequencies of state-specific spectra of the sensorimotor network were around 17.1 Hz (SD = 2.6) for the sustained-gripping task and around 17.8 Hz (SD = ±3.0) for the passive-movement task, aligning with previous reports of ~17-Hz beta frequencies during hand movements (Neuper & Pfurtscheller, 2001; Pfurtscheller et al., 2000). Notably, the state's spatial activation pattern did not vary a lot between the sustained-gripping and passive-movement task, suggesting similar activation patterns during both active and passive movements. Given this similarity in activation patterns confined to sensorimotor areas, I hypothesise that this network is unlikely to drive higher-order cognitive processes related to movements, such as integration of task-

related visual and proprioceptive feedback, but instead is more closely associated with the immediate processing of movements. Future research assessing sensorimotor network activity during carefully designed experimental tasks that allow for the dissociation of movement-related processes within the same participants may provide means to test this hypothesis.

## Posterior sensorimotor network reflects motor planning and goal-directed integration of bottom-up visual and proprioceptive information

In contrast to the sensorimotor network, the posterior sensorimotor network exhibited variations in the extent of the spatial activation between the sustained-gripping and passive-movement task. In the sustained-gripping task, strong activations occurred throughout the entire motor cortex, parietal cortex, and occipital cortex. In contrast, in the passive-movement task activations were predominantly observed in superior and medial motor areas, as well as superior parietal regions. This variation suggests that the posterior sensorimotor network displays broader activations in parietal and occipital areas during tasks that require online integration of visual and proprioceptive feedback, as well as movement planning to adjust gripping strength according to the integrated feedback.

Strikingly, in both tasks, superior parietal areas showed increased activation during occurrences of the posterior sensorimotor network. Superior parietal regions have been implicated in receiving proprioceptive feedback (Chilvers et al., 2021; Delhaye et al., 2018; Kalaska, 1996; McGuire & Sabes, 2011), highlighting that the posterior sensorimotor network is likely involved in the processing of proprioceptive feedback. This interpretation is further supported by the observation that the posterior

sensorimotor network is more strongly modulated by passive movements than the sensorimotor network, suggesting that proprioceptive feedback from passive finger movements more strongly influences the occurrences of the posterior sensorimotor network.

Posterior parietal regions, which were exclusively active during posterior sensorimotor occurrences in the sustained-gripping task, have been linked to the integration of motor plans and visual information (Chung et al., 2017; Clower et al., 1996; Desmurget et al., 1999; Hanakawa et al., 2008; Heinrichs-Graham & Wilson, 2015; Mountcastle et al., 1975; Wiesman et al., 2020), as well as continuous estimation of limb kinematics during online correction of movements (Archambault et al., 2015; Battaglia-Mayer et al., 2014; Gaveau et al., 2014). Considering that the sustained-gripping task requires the continuous integration of visual and proprioceptive feedback, along with the updating of movement plans to adjust the exerted grip force, it is expected that activity in these parietal areas plays a prominent role in this task. Given that these areas were only activated during posterior sensorimotor network occurrences in the sustained-gripping task, may suggest that the posterior sensorimotor network is involved in the integration of visual and proprioceptive feedback, as well as updating of movement plans.

Taken together, these findings suggest that both sensorimotor networks are likely involved in separate sensorimotor functions: The posterior sensorimotor network may contribute to motor planning and goal-directed integration of bottom-up visual and proprioceptive information, whereas the sensorimotor network is more likely involved in the immediate processing of sensorimotor information related to limb movements.

## Sensorimotor networks may underpin beta oscillations with varying peak frequencies

Previous studies investigating motor cortical beta oscillations in non-human primates during various task periods suggested the presence of different beta oscillations with distinct frequencies in motor cortical areas, which change with behavioural context or movement direction (Chandrasekaran et al., 2019; Kilavik et al., 2012; Szurhaj et al., 2003). It was hypothesised that different network activations underpin the variations in motor cortical beta frequencies (Chandrasekaran et al., 2019; Kilavik et al., 2012). Importantly, our analysis revealed that state-specific motor cortical spectra and peak frequencies of both sensorimotor networks were significantly different in both datasets, suggesting that varying network activations might indeed underpin task-related variations in beta frequencies. Although the beta frequencies reported by these studies are higher than the observed network peak frequencies in our data, it is tempting to speculate that different motor cortical beta frequencies reflect activations of different large-scale sensorimotor networks.

## Spectral properties of networks are significantly changed in PD whereas occurrence dynamics are maintained

In both the sustained-gripping and passive-movement task, I did not observe significant changes in the sensorimotor networks' occurrence probabilities in PD. However, the posterior sensorimotor network exhibited decreased beta power and peak frequencies in both tasks, which might contribute to attenuations of task-related beta-power modulations in PD. Given that the occurrence probabilities of the posterior

sensorimotor network are significantly associated with task-related beta-power modulations, the decrease in state-specific beta power likely results in lower fluctuations in beta power throughout the task. The decrease of beta power during passive movements has been discussed to reflect impairments in the proprioceptive processing of PD volunteers (Vinding et al., 2019), which aligns with reports of impaired high-level proprioceptive integration (Nowak & Hermsdörfer, 2006; Rabin et al., 2010; Rickards, 1997) and increased reliance on visual feedback compared to proprioceptive feedback in PD (Abbruzzese & Berardelli, 2003; Adamovich et al., 2001; Bronstein et al., 1990; Demirci et al., 1997; Jacobs & Horak, 2006). This, combined with the observation that the posterior sensorimotor network was more strongly modulated by the passive-movement task than the sensorimotor network, poses the hypothesis that changes in state-specific beta power of the posterior sensorimotor network relate to impairments in proprioceptive processing in PD.

The sensorimotor network exhibited significantly decreased beta power in PD volunteers during the passive-movement task, with a non-significant trend towards decreased beta power in the sustained-gripping task. The lack of significance might be due to the small sample size of this comparison. These state-specific decreases in beta power likely contribute to task-related beta-power modulations in a manner similar to the posterior sensorimotor network. As discussed above, the sensorimotor network is likely involved in initial sensorimotor processes related to hand movements. Therefore, significantly decreased state-specific beta-power changes might be closely linked to motor impairments in PD.

Crucially, both HC and PD groups were able to perform the sustained-gripping task without prominent differences in task performance (Zokaei et al., 2021). Thus, conclusions about impaired functioning in PD volunteers based solely on significant changes in network properties should be treated with caution.

## Potential underpinnings of alterations in state-specific spectra of sensorimotor networks

An explanation for the observed changes, considering that both networks were modulated by PD in a very similar manner, could be that state-specific beta-power changes reflect a shared underlying PD-related pathology impacting motor cortex functioning across both networks in a similar way. In other words, persistent pathological changes in a specific region may influence various large-scale networks that rely on this region for their operations.

A common mechanism underpinning the decreases in state-specific beta power could be a slowing of the oscillatory beta frequencies in motor cortex, linked to altered dopaminergic functioning (Iskhakova et al., 2021). I observed a significant slowing of peak frequencies accompanied by a qualitatively observed slowing of beta oscillations in motor cortical regions during occurrences of the posterior sensorimotor network (and during occurrences of the sensorimotor network during the sustained-gripping task). It has been demonstrated that the frequency of beta oscillations in non-human primates and PD volunteers reflects the brain's dopaminergic tone (Iskhakova et al., 2021). Therefore, peak frequency decreases in both states might reflect alterations in dopaminergic functioning in PD volunteers.

Alternatively, this pattern of slowing might be part of a broader, more static slowing of cortical oscillatory power (Boon et al., 2023; Krösche et al., 2023; Stoffers et al., 2007; Wiesman et al., 2023) that has been discussed to result from neurotransmitter system dysfunction (Bosboom et al., 2009; Rea et al., 2021; Wiesman et al., 2023), local cortical atrophy (Krösche et al., 2023), or protein pathology (Wiesman et al., 2022).

In both cases, changes in the motor cortical state-specific spectra would reflect impaired motor cortical functioning in PD, which becomes particularly prevalent during motor cortical recruitment and affects both sensorimotor networks and their functioning. Interestingly, I observed these changes in both tasks, despite participants in the passive-movement task being on dopaminergic medication. This suggests that motor cortical oscillatory beta power of both sensorimotor networks is altered regardless of medication status or active vs. passive movements. In the context of previous work reporting that oscillatory slowing in MEG recordings is not substantially affected by dopaminergic medication (Stoffers et al., 2007), it seems likely that the observed beta-power changes are more likely a result of widespread oscillatory slowing rather than altered dopaminergic functioning. Future studies systematically investigating how oscillatory slowing affects motor cortical beta-power changes in PD, and how dopaminergic medication influences this, may help to explain which mechanisms are driving the observed oscillatory changes in motor cortex. Moreover, studies further investigating whether oscillatory slowing varies across dynamic large-scale networks might provide further insights into the dynamics of this phenomenon.

## Limitations

Differing spatial patterns of state-specific wideband activation of the posterior sensorimotor network in the two tasks were attributed to the distinct task requirements of sustained-gripping and passive-movement tasks. However, it is important to note that the datasets were collected from different cohorts. Crucially, PD volunteers in the sustained-gripping task were off medication, while those in the passive-movement task were on medication. This suggests that observed differences between the tasks could potentially be influenced by interindividual variations among participants or differences in medication status. Due to studies reporting attenuated movement-related beta-power modulations in PD volunteers on medication (Pfurtscheller et al., 1998; Vinding et al., 2019) compared to healthy controls, it is unlikely that observed differences between the two tasks are solely due to medication status. Future studies comparing large-scale networks during active and passive movements in the same PD volunteers, both on and off medication, could help clarify whether observed differences stem from interindividual differences among participants, varying medication states, or task requirements.

Additionally, it is worth noting that TDE-HMMs, which were used to extract dynamic large-scale networks, assume that brain network states are mutually exclusive. While the mutual exclusivity of states was somewhat softened post-hoc by averaging state occurrences over trials, this approach is not optimised to precisely describe coactivation patterns of dynamic large-scale networks. However, methods such as DyNeMo (Gohil et al., 2022) model brain activity in terms of continuous brain modes without relying on the assumption of mutual exclusivity. This approach likely offers a

more precise description of simultaneously activated large-scale networks during task performance (Gohil, Kohl, et al., 2024). By capturing the dynamic interplay between different brain states in a more nuanced manner, DyNeMo has the potential to enhance our understanding of the large-scale network underpinnings of movement-related brain activity.

## Conclusion

This chapter reveals that motor cortical beta power is changed during movement performance in PD volunteers. Through investigation of dynamic large-scale networks, I identified alterations in network-specific beta power within two distinct sensorimotor networks that likely underpin PD-related changes in movement-related beta-power modulations. These findings emphasize the importance of considering the large-scale network context when analysing motor cortical activations because it provides insights into the underpinnings of altered movement-related oscillatory activity in PD.

Building upon the findings of Chapters 1 and 2, which highlighted changes in both time-averaged oscillatory power and dynamic large-scale network properties in PD volunteers, my next objective is to assess whether such alterations are detectable in individuals with a high risk of progressing to PD. If this is the case, the identified signatures hold promise as markers for early stages of PD.

# Chapter 3 – Cortical electrophysiological markers of REM-Sleep Behaviour Disorder

## Introduction

REM-Sleep Behaviour Disorder (RBD) is a sleep disorder characterised by decreased inherent muscle atonia that occurs during REM sleep resulting in enactment of dreams (Hu, 2020; Postuma, Gagnon, et al., 2015; Roguski et al., 2020). Imbalances between excitation and inhibition in brainstem areas, such as the pontine sub coeruleus nucleus and ventral medulla, are suggested to dysregulate muscle tone during REM sleep (Peever et al., 2014; Weber et al., 2015). Furthermore, alterations in various neurotransmitter systems including serotonergic, cholinergic, noradrenergic, and dopaminergic pathways (Barber et al., 2018; Knudsen et al., 2018), as well as changes in the pyramidal motor tract (Roguski et al., 2020) and the amygdala (Hu, 2020) have been implicated in the pathology of RBD.

### RBD as a prodromal stage of alpha-synucleinopathies

Importantly, growing evidence highlights RBD as a promising marker for prodromal stages of alpha-synucleinopathies. Studies found that 90% of individuals with RBD eventually develop alpha-synucleinopathies, with 44% eventually progressing to Parkinson's Disease (PD) and 25% to dementia with Lewy Bodies (DLB) (Galbiati et al., 2019; Iranzo et al., 2014). Notably, RBD onset typically precedes the PD diagnosis by 12 to 14 years (Postuma et al., 2012). Furthermore, RBD has been reported to manifest 8 years prior to the onset of cognitive or motor symptoms, ultimately leading to a clinical

diagnosis of either PD or DLB (Postuma et al., 2019). Given these high conversion rates and the early onset, RBD is a remarkably specific marker for alpha-synucleinopathies (Postuma et al., 2012). The study of this disorder provides a unique window into prodromal neurodegenerative processes of alpha-synucleinopathies including PD (Hu, 2020).

## Non-invasive electrophysiological studies on RBD

Various electroencephalogram (EEG) studies have consistently reported a marked slowing of cortical oscillatory activity in individuals with RBD. Typically, this oscillatory slowing is quantified through increases in delta and theta frequency band power, slow-to-fast frequency power ratio ((delta + theta)/(alpha + beta)), or a decrease of the occipital peak frequency.

Studies assessing oscillatory slowing in terms of theta power or slow-to-fast frequency ratio, reported widespread patterns of increased slowing (Livia Fantini et al., 2003; Massicotte-Marquez et al., 2008) that were particularly pronounced in RBD volunteers with mild cognitive impairment (Iranzo et al., 2010; Rodrigues Brazète et al., 2013) or in RBD volunteers that progressed to PD, DLB, or multiple system atrophy (MSA) over a period of 3.5 years (Rodrigues Brazète et al., 2016). Moreover, Montreal Cognitive Assessment (MOCA) scores showed an inverse relationship with delta, theta, and beta power in occipital areas or delta power in central regions (Sasai et al., 2013). Strikingly, RBD volunteers progressing to DLB exhibit even more pronounced increases in the slow-to-high frequency ratio compared to those progressing to PD or MSA (Rodrigues Brazète et al., 2016).

Similarly, a reduction of the occipital peak frequency was observed in individuals with RBD (Bang et al., 2017; Livia Fantini et al., 2003), particularly those with mild cognitive impairment (MCI) (Rodrigues Brazète et al., 2013), or those progressing to PD, MSA, or DLB (Rodrigues Brazète et al., 2016). Conversely, RBD volunteers without MCI or progression to these disorders did not differ significantly from healthy controls (HC) (Rodrigues Brazète et al., 2013, 2016). Taken together, these studies suggest a significant slowing of cortical oscillatory activity in RBD, particularly pronounced in individuals progressing to alpha-synucleinopathies.

## Slowing in PD

Magnetoencephalogram (MEG) and EEG studies investigating cortical oscillatory dynamics across the entire brain in PD consistently reported widespread patterns of oscillatory slowing, particularly prominent in posterior brain regions (Boon et al., 2023; Bosboom et al., 2006; Krösche et al., 2023; Neufeld et al., 1988; Olde Dubbelink, Stoffers, Deijen, Twisk, Stam, & Berendse, 2013; Soikkeli et al., 1991; Stanzione et al., 1996; Stoffers et al., 2007; Wiesman et al., 2023). Cross-sectional comparisons reveal that untreated, early-stage PD patients (~0.9 years post-diagnosis) already exhibit widespread increases in theta and alpha power alongside decreased beta power across most brain regions, excluding frontal areas (Stoffers et al., 2007). In more progressed stages of PD (~8 to 10 years post-diagnosis), studies also reported increased theta power in non-frontal regions and decreased beta power, particularly in parietal and occipital regions (Bosboom et al., 2006). PD volunteers with dementia (~11.23 years post-diagnosis) showed even more pronounced alterations, including widespread increases in delta power, centrally heightened theta power, widespread decreases in

alpha power, and diminished beta power in frontal, central, and parietal areas compared to non-demented PD volunteers (Bosboom et al., 2006).

Longitudinal studies provided further evidence for this continuous pattern of slowing, demonstrating widespread increases in theta power and decreases in alpha power (Boon et al., 2023; Olde Dubbelink, Stoffers, Deijen, Twisk, Stam, & Berendse, 2013), as well as changes in the high-to-low frequency power ratio (Morita et al., 2009), as the disease progresses. Strikingly, this pattern of slowing correlates with cognitive decline (Boon et al., 2023; Bosboom et al., 2006; Geraedts et al., 2018; Morita et al., 2011; Olde Dubbelink, Stoffers, Deijen, Twisk, Stam, & Berendse, 2013; Wiesman et al., 2023) and progression to PD with dementia (Olde Dubbelink et al., 2014). The association between oscillatory slowing and motor symptom severity is less clear, with some studies observing significant associations (Boon et al., 2023; Olde Dubbelink, Stoffers, Deijen, Twisk, Stam, & Berendse, 2013), while others do not (Bosboom et al., 2006; Geraedts et al., 2018; Stoffers et al., 2007).

Taken together, these findings suggest a progressive increase in low-frequency power and decrease in high-frequency power throughout PD progression that is associated with worsening cognitive performance. Oscillatory slowing has been discussed to reflect various pathological mechanisms: impairments in various neurotransmitter systems, e.g., dopaminergic-, noradrenergic-, serotonergic systems (Bosboom et al., 2006; Stoffers et al., 2007); thalamocortical circuits (Boon et al., 2019; Steriade et al., 1990); neurodegeneration of the cholinergic nucleus of Meynert (Bosboom et al., 2009); or local pathology (Ranasinghe et al., 2020; Wiesman et al., 2022). Overall, this suggests that observed patterns of change are not merely a consequence of

dysregulation in the basal ganglia-thalamocortical loop, but likely also reflect other pathological changes in PD.

## Parametrisation of neural power spectra

Recent research has emphasised the importance of dividing power spectra into periodic and aperiodic components, based on the idea that they correspond to contributions from neuronal oscillatory and arrhythmic activity respectively (Donoghue et al., 2020; He, 2014; Wen & Liu, 2016). The power spectrum of the arrhythmic component typically follows a 1/f-like shape, commonly referred to as the "1/f-Slope". While the oscillatory components of the signal are thought to reflect oscillatory activity in neuronal populations (Buzsáki & Draguhn, 2004; Engel et al., 2001), the exact underpinning of the aperiodic component remains an open question. One possibility is that the aperiodic component comprises diverse oscillatory activities, characterised by various oscillations occurring at varying frequencies, each exhibiting transient behaviours. Alternatively, it has been proposed that the 1/f-Slope is sensitive to the balance between excitatory (glutamate) and inhibitory (GABA) synaptic inputs, known as E/I balance (Gao et al., 2017). Computational modelling (Gao et al., 2017), electrophysiological STN recordings of dopamine-depleted rats (Wiest et al., 2023), and electrophysiological studies of drug-induced changes in E/I balance in humans and non-human primates (Colombo et al., 2019; Gao et al., 2017; Muthukumaraswamy & Liley, 2018; Waschke et al., 2021) have provided supporting evidence for this hypothesis. However, it should be stressed that variations in 1/f-Slopes in neural power spectra can also be influenced by a variety of factors beyond sophisticated

biological mechanisms. For instance, variations in noise within a nonlinear dynamical system, such as the brain, can also contribute to changes in 1/f-Slope (Kramer & Chu, 2023).

Most of the literature on power spectral changes in RBD or PD volunteers predates these discussions and therefore, did not examine alterations in power spectral 1/f-Slopes. This is crucial because 1/f-Slopes have been reported to be steeper in PD volunteers (Helson et al., 2023; Wang et al., 2022; Wiesman et al., 2022, 2024), likely influencing estimations of narrowband power (Donoghue et al., 2020).

In the present chapter, I will investigate alterations in 1/f-Slopes associated with PD and RBD, alongside comparisons of conventional frequency range power, and dynamic large-scale network features. This will enable me to investigate PD- and RBD-related changes in cortical oscillatory power, 1/f-Slopes, and properties of dynamic large-scale networks. Moreover, I hope to establish associations between static oscillatory power and 1/f-Slope alterations with specific dynamic large-scale networks, enhancing our understanding of disease-related changes and how they are underpinned by dynamic large-scale networks.

## Chapter Overview

In this chapter, I aim to investigate static oscillatory power, 1/f-Slopes, and dynamic large-scale networks in resting-state recordings of RBD volunteers and HCs, which I collected as part of my PhD. All analyses will be performed alongside the PD dataset analysed in Chapter 1, to compare patterns of change between the PD and RBD group. Given the high conversion rate from RBD to PD, markers that exhibit changes in both

groups hold promise as potential candidates for prodromal stages of alpha-synucleinopathies, particularly PD.

First, I aim to replicate the previously described patterns of power spectral alterations in the RBD and PD datasets. Subsequently, I will explore associations between frequency band power and cognitive performance quantified with Addenbrooke's cognitive examination (ACE). Following this, I will compare 1/f-Slopes between the groups and investigate their relationship with cognitive performance scores. I will then extract state metrics and state-specific spectra of dynamic large-scale networks with a time-delay embedded Hidden Markov Model (TDE-HMM) and contrast them between the groups. This enables us to evaluate whether RBD volunteers show similar patterns of change in sensorimotor network dynamics as observed in the PD group in Chapter 1 and to explore how power spectral changes across the entire brain are underpinned by dynamic large-scale networks. Finally, I will demonstrate that key findings for the RBD group, obtained using the TDE-HMM analysis, can be also observed when fitting the TDE-HMM solely to the RBD dataset; potentially providing a more precise description of RBD-related alterations in large-scale network dynamics.

# Materials and Methods

## Sample

The study received ethical approval from the Medical Sciences Interdivisional Research Ethics Committee of the University of Oxford (Ethics Approval Reference: R81839/RE001) and NHS Oxford C Research Ethics Committee (REC reference: 18/SC/0560) and followed the principles of the Declaration of Helsinki. All participants gave written and informed consent before participating.

All RBD volunteers were recruited from the Oxford Discovery Cohort (Hu, 2017) and were diagnosed based on polysomnography. HCs were recruited from the Joint Dementia Research UK database, with inclusion criteria covering fluency in English, normal or corrected-to-normal vision and hearing, no history of neurological or neuropsychiatric disorder, no psychoactive medication use, and the ability to undergo an MRI scan.

Resting-State MEG recordings of 20 HCs and 20 RBD volunteers were recorded. Prior to the MEG scans, the cognitive performance of all participants was assessed with Addenbrooke's Cognitive Examination (ACE) (Mathuranath et al., 2000). Demographic information and ACE scores are presented in Table 3.1.

During the MEG recordings, participants were instructed to maintain loose visual fixation on the centre of the screen for 8 minutes while not thinking about anything in particular. The scanning procedure was matched to that of the PD dataset analysed in Chapter 1. Data were acquired at a sampling rate of 1000 Hz using an Elekta Neo

Scanner, together with electrocardiogram (ECG) and electrooculogram (EOG) recordings.

Following the MEG scan, each HC underwent an MRI scan to obtain a structural T1 scan. T1 scans of RBD volunteers were retrieved from the Oxford Discovery Cohort (Hu, 2017) and obtained on average 7.6 (SD = ±3.4) months prior to the MEG scan.

The RBD dataset was analysed alongside the PD dataset described in Chapter 1.

Table 3.1 Descriptive statistics of included participants for both datasets.

| Demographics | RBD Data Set | | PD Data Set | |
|---|---|---|---|---|
| | Healthy Controls | REM Sleep Behaviour Disorder | Healthy Controls | Parkinson's Disease |
| N | 20 | 20 | 36 | 34 |
| Sex (female/male) | 1/19 | 0/20 | 15/21 | 18/16 |
| Handedness (right/left) | 18/2 | 19/1 | 34/2 | 31/3 |
| Age (years) (mean, range) | 67.45 (45-78) | 66.8 (51-80) | 68.36 (60-80) | 67.53 (54-79) |
| Education (years) (mean, range) | 15.52 (10-19) | 14.6 (10-23) | 15.36 (10-21) | 15.21 (10-24) |
| Years since Diagnosis (years) (mean, range) | N/A | 5.95 (1-16) | N/A | 2.85 (1-7) |
| ACE Total score (mean, range) | 95.4 (89-99) | 92 (80-98) | 97 (86-100) | 96.5 (90-100) |
| UPDRS III motor score (mean, range) | N/A | N/A | N/A | 30.41 (11-50) |

N = number of participants; ACE = Addenbrooke's Cognitive Examination; UPDRS = Unified Parkinson Disease Rating Scale;
In the PD dataset, ACE values were only available for 13 HCs and 17 PD volunteers.
Provided values were calculated across all available values in cases where values were not available for all participants.

## Software

All analyses were performed in Python 3.10. Pre-processing was conducted with the Python implementation of the Oxford Centre for Human Brain Activity Software Library (OSL) (https://github.com/OHBA-analysis/osl/) and MNE (https://mne.tools/stable/index.html) (Gramfort, 2013). Hidden Markov Model Analyses were run with OSL-Dynamics (https://github.com/OHBA-analysis/osl-dynamics) and statistical analyses of group contrasts and associations were performed with GLMOOLs (https://pypi.org/project/glmtools/).

## Pre-processing

The PD and RBD datasets underwent similar pre-processing procedures, as described in Chapter 2. Raw data were first maxfiltered using Maxfilter 2.2 with the temporal extension (-tsss) option to attenuate signals originating from sources outside the head. Further, the -headpos and -movecomp options were applied to compensate for movement-related changes in the signal. Next, the maxfiltered data underwent broadband filtering between 0.5 and 125 Hz, with notch filters applied at 17, 50 and 100 Hz to remove line noise and a 17-Hz fan artefact specific to the RBD dataset. To maintain consistency, the 17-Hz notch filter was applied to both the PD and RBD datasets. Subsequently, bad segments in the data were identified by dividing

magnetometer and gradiometer data into 2-second windows and calculating the standard deviation of each window. Outlier windows were identified using Generalised Extreme Studentized Deviate outlier detection (Rosner, 1983) and marked as bad. This process was repeated for the differential of the magnetometer and gradiometer time courses. Bad channels were detected based on the standard deviation of the magnetometer and gradiometer time courses, and the signal at bad sensor locations was interpolated using the spherical spline method (Perrin et al., 1989) implemented in MNE. In the RBD dataset, no bad channels were identified, and on average 6.9% (SD = ±4.7) of the magnetometer time courses and 3.8% (SD = ±1.9) of the gradiometer time courses were marked as bad segments. In the PD dataset, no bad channels were identified, and on average 3.5% (SD =± 3.3) of the magnetometer time courses and 1% (SD = ±1.1) of the gradiometer time courses were identified as bad segments.

Next, signal-space projection (SSP) (Uusitalo & Ilmoniemi, 1997) was applied to repair ECG and EOG artefacts in the data. One EOG projection was removed for each participant in both datasets. In the RBD dataset, an average of 1.5 (SD = 0.9) ECG projections were removed, while in the PD dataset, an average of 1.4 (SD = 0.7) ECG projections were removed. For two participants in the PD dataset, ECG and EOG were not recorded, hampering SSP, because of what manual independent component analysis (ICA) artefact rejection was performed. Four and six components containing ECG and EOG artefacts were manually identified and rejected. Prior to and after SSP or manual ICA, power spectra of all channels were carefully inspected to ensure adequate artefact removal.

The cleaned data were then registered to participants' structural MRI scans using RHINO (Registration of Headshapes Including Nose) without using the nose because it was not fully captured in all MRI scans of the RBD group. For four PD volunteers and two RBD volunteers without available structural MRI scans, co-registration was performed using an 8-mm MNI152 standard brain template. The alignment between MEG data and MRI scans was manually verified for all participants.

Sensor normalisation was applied to ensure equal contribution from magnetometer and gradiometer channels to the source localisation (Woolrich et al., 2011). After broadband filtering the MEG data from 1 to 45 Hz, the filtered data were projected onto an 8-mm MNI152 standard brain template using a linearly constraint Minimum Variance (LCMV) vector beamformer (Van Veen & Buckley, 1988; Woolrich et al., 2011) with a principal component analysis (PCA) regularisation rank of 60. Voxel time courses were parcellated into 52 parcels using a parcellation (Kohl et al., 2023) derived from the Glasser Parcellation (Glasser et al., 2016) as described by Tait et al. (2021). For each parcel, a time course was calculated as the first principal component across all voxel time courses allocated to this parcel. To reduce direct and inherited spatial leakage and "ghost interactions"(Palva et al., 2018), symmetric multivariate leakage reduction was performed on the data (Colclough et al., 2015). Finally, sign-flipping was applied to reduce 180-degree ambiguity in the dipole direction by aligning the signs of the parcel time courses across participants.

## Static Power Spectral Analysis

A relative power spectrum was computed for each parcel's time course signal for all participants to compare oscillatory power differences across the entire brain between the groups. Parcel-wise power spectra were derived from z-standardised time courses with Welch's method, using 2-second time windows with a 50% overlap. The resulting relative power spectra exhibited a dip between 16 and 18 Hz due to the 17-Hz notch filter applied during the pre-processing. To address this, values in this interval were interpolated with the interpolate_spectrum function provided in the "fooof" package (Donoghue et al., 2020). Interpolated spectra were then compared between the groups either frequency-bin-wise or by averaging across theta (5 to 8 Hz), alpha (8 to 12 Hz), and beta (13 to 30 Hz) frequency ranges. The fooof function was applied to the 2 to 40-Hz range of power spectra of all participants and parcels to extract 1/f-Slopes. The quality of fooof fits for all parcels was qualitatively checked for 28 (15 HC1, 3 PD, 8 HC2, 2 RBD) individuals whose across-parcels average r-squared value was below 0.975. Most of these participants showed acceptable fits, albeit slightly worse, for parcels in the inferior dorsolateral prefrontal cortex and inferior frontal gyrus. Only one participant of the PD group demonstrated poor fits throughout the entire brain and was excluded from all analyses including 1/f-Slopes. An overview of r-squared values, errors, aperiodic component offsets, and aperiodic exponents can be found in Figure A3.1.

## Time-Delay Embedded Hidden Markov Model (TDE-HMM)

A time-delay embedded Hidden Markov Model (TDE-HMM) was employed to the standardised parcel time courses to compare dynamic large-scale network features between the groups. TDE-HMMs identify dynamic brain states characterised by distinct patterns of multi-region oscillatory activity, i.e., distinct power covariations and phase synchrony patterns (Vidaurre, Hunt, et al., 2018). For a more detailed description of the TDE-HMM and the calculation of state power, state-specific power and coherence, as well as state metrics, please refer to Chapters 1 and 2.

Importantly, the TDE-HMM was run on the combined PD and RBD datasets. The larger sample size of the PD dataset compared to the RBD dataset has the consequence that inferred HMM-states are more strongly influenced by oscillatory activity in the PD dataset. Consequently, specific details of large-scale networks in RBD volunteers may not be fully captured if these networks exhibit different patterns of change between RBD and PD. This discrepancy could potentially lead to reduced sensitivity in detecting changes between RBD volunteers and HCs. To account for the risk of obtaining null findings solely due to imprecise descriptions of large-scale networks, I conducted an additional TDE-HMM analysis solely on the RBD sample. This additional analysis allowed us to confirm that observed null findings were not solely due to training the TDE-HMM on both datasets.

## Statistical Analysis

Group contrasts for static power spectral variables, ACE values, state metrics, and various variables extracted from state spectra were assessed using Generalised Linear

Models (GLMs). These models included group constants along with age, sex, and education as covariates to control for potential confounding factors (Figure 3.1A). The significance of all GLMs was determined using maximum t-statistic permutation tests. Specifically, group labels were shuffled 1000 times before computing the above-described contrasts to generate null distributions. Maximum t-statistic pooling was applied to control for multiple comparisons across parcels, frequency bands, frequency bands and parcels, or brain states by constructing a single null distribution based on the largest t-statistic across all comparisons per permutation. Observed t-statistics were considered significant if they exceeded the threshold of $p < .05$ obtained from the null distribution.

Furthermore, a PCA was conducted on the cognitive domain scores obtained with the ACE for all participants to extract a single summary value representing the cognitive performance of each participant. Associations between ACE scores and frequency band power, calculated from either static or state-specific power spectra, or 1/f-Slopes were assessed using GLMs. These GLMs included group constants, age, sex, education, and ACE scores as regressors, with ACE scores z-scored across all participants before being separated into different ACE group regressors (Figure 3.1B). Similar to group contrast GLMs, significance was assessed using maximum t-statistic permutation tests with 1000 permutations. For each of the neuronal markers, I accounted for multiple comparisons by pooling maximum t-statistics across either parcels or frequency bands and parcels when constructing null distributions for the significance assessment.

Additionally, relationships between state fractional occupancies and power within frequency bands and bins or 1/f-Slopes were calculated using separate GLMs for each

of the 8 states. These GLMs contained an intercept and the respective state's fractional occupancy values as regressors. Significance was assessed with maximum t-statistic permutation tests pooling across parcels or frequency bins.

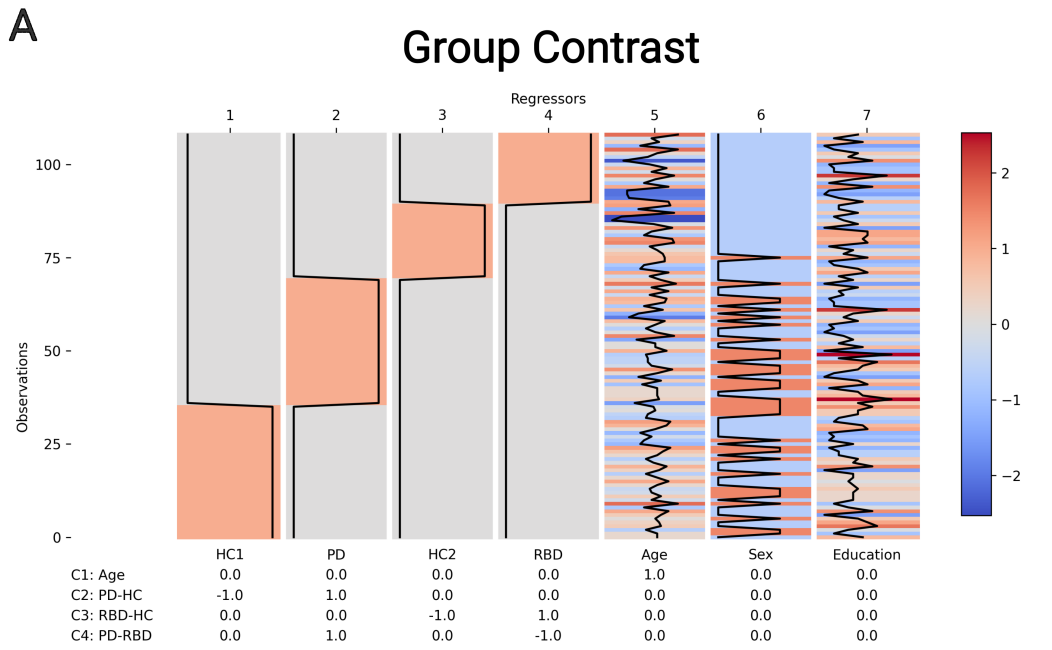


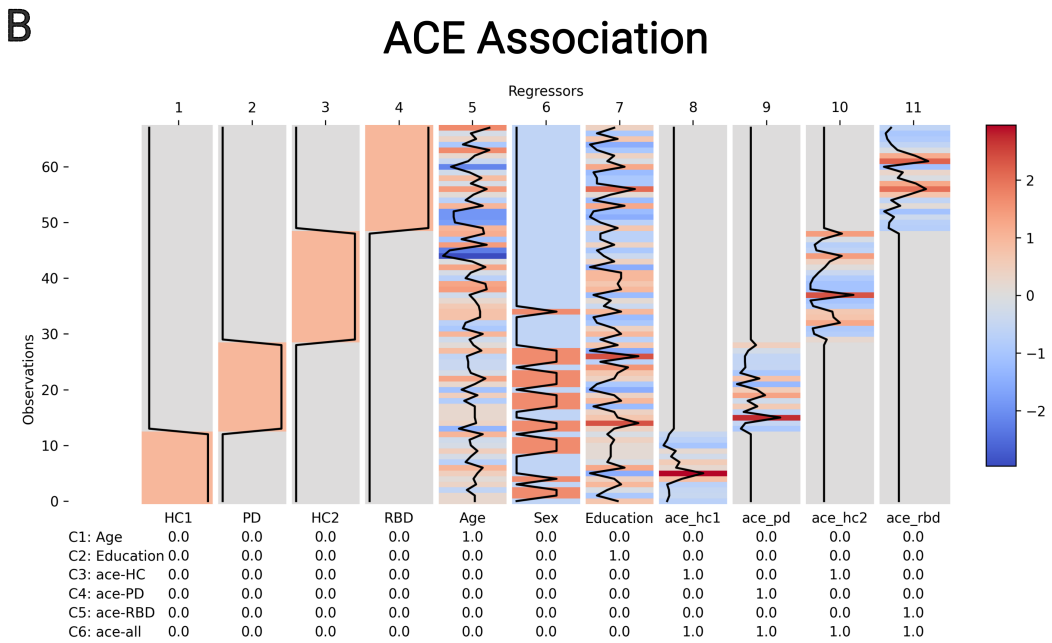

**Figure 3.1. Overview of the GLMs used to calculate group contrasts and associations between spectral power and ACE scores. (A)** Summary of the GLM used to investigate group differences in the data. Regressors are represented as bars with each entry representing the regressor value of a single participant. **(B)** Summary of the GLM used to assess associations between spectral variables and ACE scores. Regressors are represented as bars with each entry representing the regressor value of a single participant. ACE scores were z-scored across all participants before they were separated into distinct ACE group regressors.

# Results

## Static oscillatory power is changed in PD and RBD volunteers

First, I investigated whether PD and RBD volunteers exhibited alterations in static cortical oscillatory power.

Comparing PD volunteers with HCs (Figure 3.2A) revealed widespread increases in theta power across the entire brain, alongside elevated alpha power predominantly in frontal, central, and parietal regions, likely driven by alterations in low alpha frequencies. Conversely, beta power was significantly decreased across most brain regions, except for a few frontal areas.

RBD volunteers showed significantly increased theta power in occipital, inferior temporal, and inferior frontal areas, alongside reduced beta power in occipital regions compared to their HC group (Figure 3.2B). Interestingly, frequency-bin-wise group comparisons suggest that beta-power decreases were likely driven by reductions in high-beta frequencies.

Comparing PD and RBD volunteers revealed distinct patterns: PD volunteers exhibited larger theta power in central areas, increased alpha power in parietal areas, and decreased beta power in superior parietal, central and frontal areas.

Qualitative observations of frequency-bin-resolved group comparisons indicate that static oscillatory power alterations in PD and RBD did not simply affect the same areas or frequencies to varying degrees (Figure 3.2C). RBD volunteers showed the strongest increases in theta power around 6 to 7 Hz, whereas PD volunteers exhibited more

prominent alterations in high-theta to low-alpha frequencies. Similarly, PD volunteers demonstrated decreased power across the entire beta range, whereas RBD volunteers showed more pronounced decreases in high-beta frequencies. These findings suggest that cortical oscillatory alterations in PD and RBD were characterized by distinct regional and frequency-specific patterns.

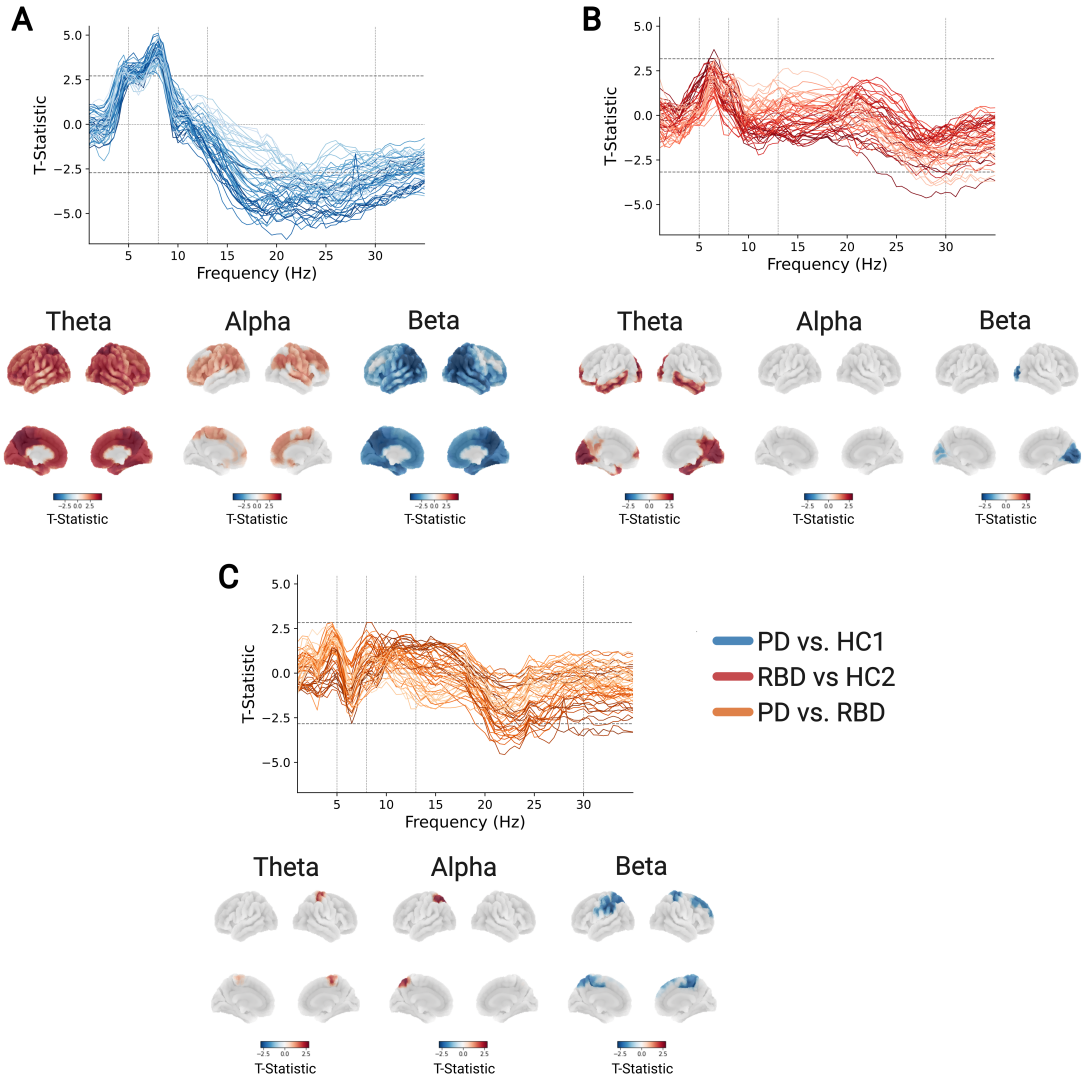


**Figure 3.2. Cortical oscillatory power is changed in PD and RBD volunteers in resting-state MEG.** Each panel presents results of group-level GLMs assessing **(A)**

HC vs PD (blue), **(B)** HC vs RBD (red), and **(C)** PD vs RBD (orange) group contrasts. In the top section, each line represents t-statistics of group contrasts for all frequency bins for a single parcel. Parcels located at frontal positions are depicted in brighter colours, with colour darkness gradually increasing for parcels located further posteriorly. Horizontal dashed lines indicated significance thresholds obtained from maximum t-statistic permutation tests, pooling across frequency bins and parcels. Below, t-statistics of group contrasts of theta-, alpha-, and beta-power averages are presented. T-statistics of parcels that yield significant group differences are projected onto brain surfaces after controlling for multiple comparisons with maximum t-statistic permutation testing pooling across parcels and frequency bands.

## Beta Oscillatory power in RBD is associated with cognitive performance

Next, I investigated the relationship between static oscillatory power and cognitive performance across the different groups. To do so, I conducted a PCA on the standardised cognitive domain scores from the ACE across all participants.

The first principal component (PC1), which explained 39% of the variance, loaded negatively on scores of all cognitive domains. Among the cognitive domains, memory loaded strongest on the first principal component (Figure 3.3A). Group contrasts of the PC1's values did not yield significant differences between the HCs and PD volunteers ($t(37) = -0.28$, $p = .79$). However, RBD volunteers exhibited significantly higher PC1 values compared to their respective HCs ($t(37) = -2.57$, $p = .014$), indicating poorer cognitive performance in RBD volunteers (Figure 3.3B). Importantly, among RBD volunteers, only four had ACE sum scores below 88 and two had scores below 82,

which have been discussed as thresholds for cognitive impairments (Hsieh et al., 2013; Mathuranath et al., 2000).

GLMs assessing associations between frequency-band power and PC1 values did not yield any significant associations for HCs (all $p > .89$) and PD volunteers (all $p > .87$). However, RBD volunteers exhibited a negative association in the left occipital cortex, suggesting that decreased beta power in this region correlates with worse cognitive performance ($t(46) = -3.7$, $p = .046$) (Figure 3.3C,D). I corrected for multiple comparisons by assessing the significance of associations between frequency-band power and PC1 values with maximum t-statistic permutation tests, pooling across frequency bins and parcels.

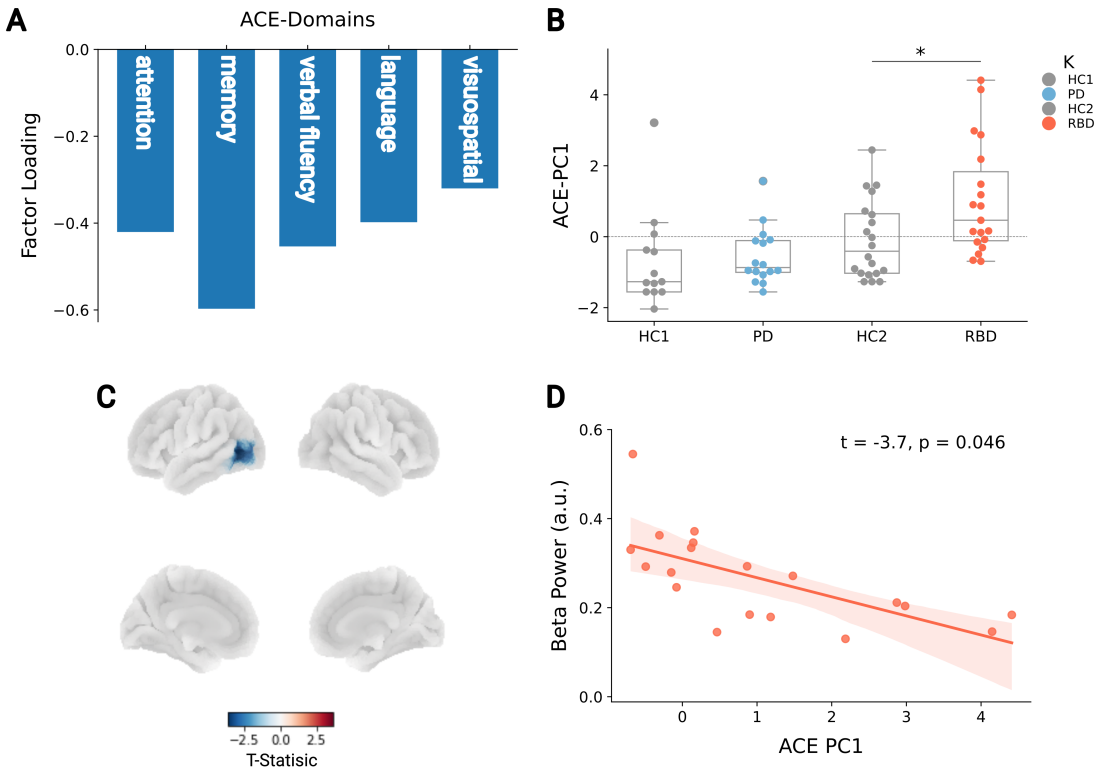

**Figure 3.3. RBD volunteers show significantly worse cognitive performance, which is negatively associated with occipital beta power. (A)** Factor Loadings of ACE's cognitive domains on the first principal component (PC1) of the PCA applied to standardised ACE's cognitive domain scores. **(B)** Participants' values of PC1 are depicted for each group, respectively. **(C)** Significant associations between beta power and PC1 values of the RBD group are presented by projecting t-statistics of parcels that yield significant associations onto brain surfaces. Multiple comparison correction for comparisons across parcels and frequency bands was performed with maximum t-statistic permutation testing. **(D)** Scatter plot illustrating negative association at parcels with the strongest association between PC1 and beta power in (C).
** indicates $p < .01$ and * $p < .05$.

## Aperiodic Exponent significantly changed in PD and RBD

Previous research reported increases in 1/f-Slopes among PD volunteers (Helson et al., 2023; Wang et al., 2022; Wiesman et al., 2024, 2024), which likely contribute to narrow band power group differences reported above.

Thus, I next investigated whether the 1/f-Slopes, estimated with the fooof package (Donoghue et al., 2020), are significantly altered in both RBD and PD volunteers (Figure 3.4A). PD volunteers exhibited significantly steeper 1/f-Slopes across the entire brain compared to their HCs, whereas RBD volunteers demonstrated steeper 1/f-Slopes in occipital and frontal regions. When directly comparing the two groups, PD volunteers exhibited steeper slopes in superior parietal, central, and frontal areas, whereas RBD volunteers demonstrated steeper slopes in a left inferior occipital parcel. Notably, the spatial patterns of 1/f-Slope change in the PD and RBD groups largely mirrored the

spatial patterns of theta and beta-power alterations identified in the power spectral analysis.

Similar to findings regarding beta power, occipital 1/f-Slopes among RBD volunteers – though not among PD volunteers or HCs – showed a negative relationship with PC1 values obtained from the PCA-analysis of the ACE domains ($t(46) = 3.64$, $p = .024$) (Figure 3.4B). The fact that both 1/f-Slope and beta-power associations reached significance at the same occipital parcel further suggests that 1/f-Slope changes likely contribute to observed power spectral group differences.

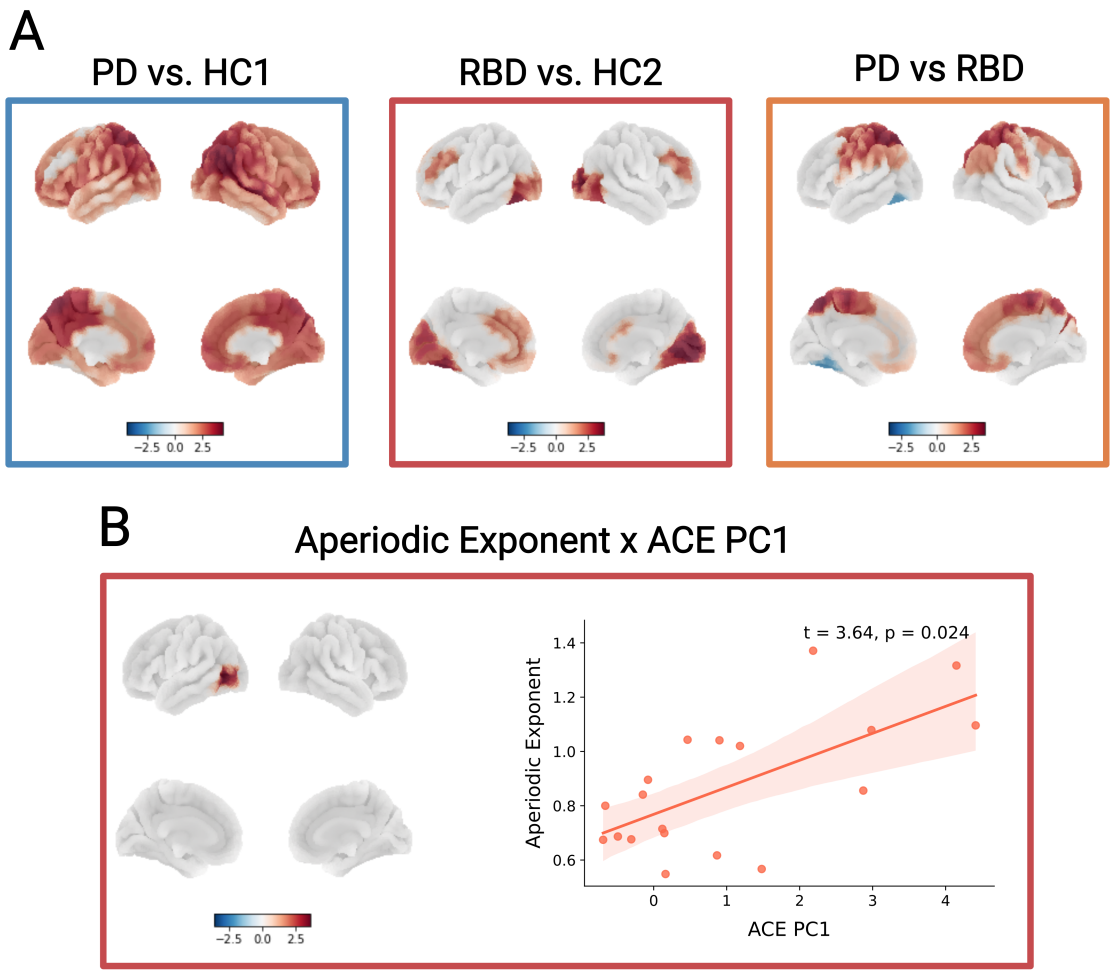

**Figure 3.4. 1/f-Slopes are significantly changed in RBD and PD volunteers and are associated with cognitive performance in the RBD group. (A)** Spatial distribution of significant 1/f-Slope group differences. T-statistics of GLMs comparing the groups at each parcel, reaching significance, are projected onto brain surfaces. Significance was assessed with maximum t-statistic permutation tests pooled across parcels to account for multiple comparisons. **(B)** Spatial distribution of significant associations between 1/f-Slopes and first principal component scores (PC1) obtained from the PCA analysis of ACE's cognitive domain scores. T-statistics of GLMs assessing the association between aperiodic components and PC1 values, reaching significance, are projected onto brain surfaces. Significance was assessed by maximum t-statistic permutation tests pooled across parcels. A scatter plot illustrating the association between 1/f-Slopes and PC1 scores at the only significant parcel is displayed next to the surface plots.

## Removing the aperiodic component diminishes beta-power group differences

Considering the spatial overlap observed between significant theta and beta-power alterations, and 1/f-Slope changes within the PD and RBD groups, I aimed to assess the impact of removing the aperiodic component from all power spectra before calculating power spectral group differences. Although the estimation of the aperiodic component by fooof may not be perfect, this analysis enables to better understand the contribution of 1/f-Slope group differences in conventional power spectral group comparisons.

Strikingly, beta-power group differences were largely diminished after aperiodic component subtraction, whereas theta-power group differences seemed less affected (Figure 3.5A,B). Differences between the PD and RBD groups failed to reach significance across all frequency bands after subtracting the aperiodic component (Figure 3.5C). Associations between ACE scores and occipital beta power also failed to reach significance, whereas theta power in left inferior temporal parcels showed significant associations with ACE PC1 scores ($t(46) = 4.01$, $p = .02$) (Figure 3.5D). Overall, these findings suggest that significant group differences in 1/f-Slope likely contribute to widespread decreases in beta power in PD, as well as occipital beta-power decreases in RBD, while theta-power alterations in both groups are less affected by such differences.

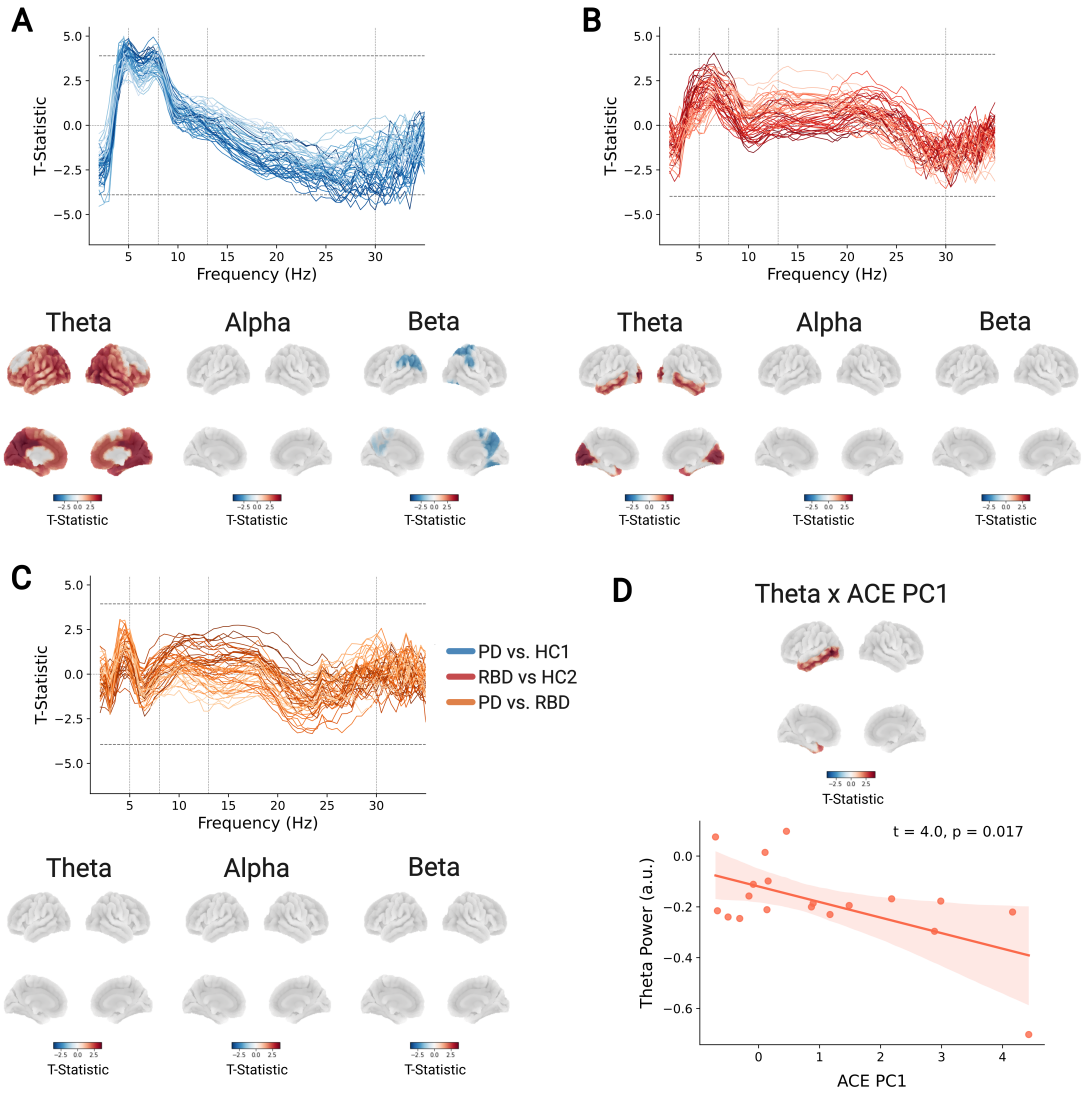


**Figure 3.5. Cortical oscillatory power alterations in PD and RBD volunteers are attenuated when the aperiodic component is removed prior to group comparisons.** The first three panels visualise results of GLMs calculating **(A)** HC vs PD (blue), **(B)** HC vs RBD (red), and **(C)** PD vs RBD (orange) group contrasts. In the top section, each line represents t-statistics of group contrasts for all frequency bins for a single parcel. Parcels located at frontal positions are depicted in brighter colours, with colour darkness gradually increasing for parcels located further posteriorly. Horizontal dashed lines indicated significance thresholds obtained from maximum t-statistic permutation tests pooled across frequency bins and parcels to control for multiple comparisons. Below, t-statistics of group contrasts of theta, alpha, and beta-power averages are

presented. T-statistics of parcels that yield significant group differences are projected onto brain surfaces. Maximum t-statistic permutation testing pooled across frequency bins and parcels was applied to control for multiple comparisons. **(D)** Relationship between theta power and first principal component scores (PC1) obtained from a PCA analysis on ACE's cognitive domains scores. In the top panel, t-statistics of parcels with significant associations between theta power and ACE PC1 scores are projected onto brain surfaces. Significance was assessed using maximum t-statistic permutation tests pooled across parcels and frequency bands. Bottom panel, illustration of the relationship between theta power and PC1 ACE scores at parcel with the highest t-statistic.

## HMM Description

Having demonstrated in Chapter 1 that time-averaged power spectral group differences between HCs and PD volunteers are likely underpinned by dynamic large-scale networks, I next investigated whether dynamic large-scale networks also provide a more fine-grained description of the observed alterations in spectral power and 1/f-Slopes in the RBD and PD group. To achieve this, I applied a TDE-HMM to extract dynamic large-scale networks from the sign-flipped parcel time courses, containing both oscillatory and aperiodic components of the signal. Consequently, both oscillatory and aperiodic components of the signal are represented in the dynamic large-scale network description provided by the TDE-HMM.

The inferred large-scale networks (Figure 3.6) resemble those extracted from the PD dataset in Chapter 1. State 2 occurrences were associated with increased wideband power and coherence in sensorimotor areas. Given this activation pattern and the high

similarity of the motor cortical power spectrum of State 2 to the sensorimotor network identified in Chapter 1, I concluded that State 2 corresponds to the sensorimotor network. Interestingly, within the combined RBD and PD data set, a brain state characterised by widespread increases in wideband power, predominantly in parietal regions, resulted in even stronger motor cortical beta-power increases. Thus, the ordering of the states is different to Chapter 1. State 4 was the only state that demonstrated marked increases in low-frequency power throughout the whole brain, following a 1/f pattern.

Metrics characterising the dynamics of the obtained large-scale networks were in similar ranges as those inferred in Chapter 1. An overview of mean fractional occupancies, lifetimes, and interval times is presented in Figure A3.2. Mean fractional occupancies of all states ranged between 4% and 17%. Fractional occupancy values across all participants and states were larger than 1% and smaller than 50% indicating a good mixing of states, i.e., each network was visited by each participant. The mean lifetimes of the networks varied between 53 to 104 ms, while mean interval times varied between 346 and 1781 ms.

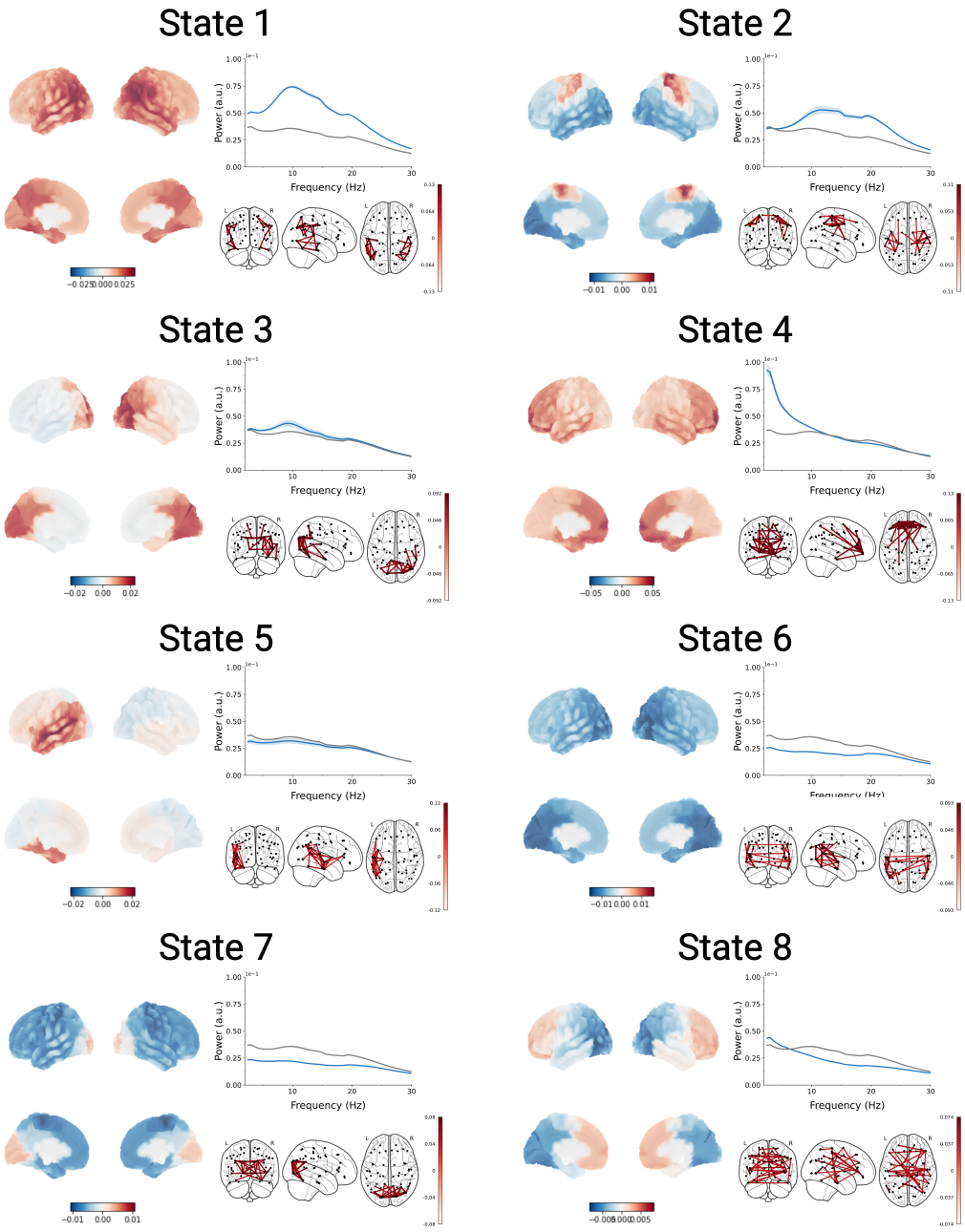


**Figure 3.6. Description of the dynamic large-scale networks inferred with TDE-HMM.** Spectral properties of each state are described in 3 ways: 1) Wideband power of each parcel (relative to the average power across all states) is projected onto a cortical surface. 2) State-averaged power spectrum (grey) is displayed alongside absolute state power spectra (blue) in the superior motor cortex. Importantly, in these spectra, the aperiodic component was not removed. 3) State-specific coherence networks averaged across frequency bins, as specified

by a low-frequency spectral factor obtained from the NNMF (relative to the mean coherence across all states), are shown below the motor power spectra. States are sorted according to their state-specific beta power in the superior motor parcel.

## Large-scale network occurrence probabilities are associated with static oscillatory power

I calculated correlations between brain state fractional occupancies and static frequency band power values to elucidate the relationship between brain state occurrences and static oscillatory power. For each State, a GLM was applied to predict frequency band power based on an intercept and the respective state's fractional occupancies.

Increased occurrence probability of the sensorimotor network was significantly associated with an increase in beta power in the sensorimotor cortex but also adjacent frontal and parietal areas (Figure 3.7A,C). This suggests that sensorimotor network occurrences coincide with static power increases in the sensorimotor cortex and neighbouring regions. Interestingly, both State 1 and State 7 demonstrate positive associations with beta power in frontal areas and parts of the sensorimotor cortex (Figure A3.3), indicating that several states contribute to sensorimotor cortical beta power.

Widespread theta-power increases were only significantly associated with State 4 occurrence probabilities (Figure 3.7B,D), implying that an increase in the occurrence of

this state is linked to heightened theta power. Furthermore, this state was associated with decreased alpha power in inferior temporal, parietal, and occipital areas, and widespread decreases in beta power.

Given that this pattern of change could result from an increase in 1/f-Slope and the 1/f-like shape of the State 4-specific spectrum, I next calculated GLMs to assess the relationship between State 4 fractional occupancy and 1/f-Slopes across the entire brain. This analysis revealed a significant positive association between State 4 occurrence probability and 1/f-Slopes across all brain regions except a few frontal and occipital regions (Figure 3.7D).

Based on these association patterns, I hypothesised that if theta power and 1/f-differences, observed in the static power analysis, vary over time, the large-scale network metrics of State 4 should capture these theta-power alterations.

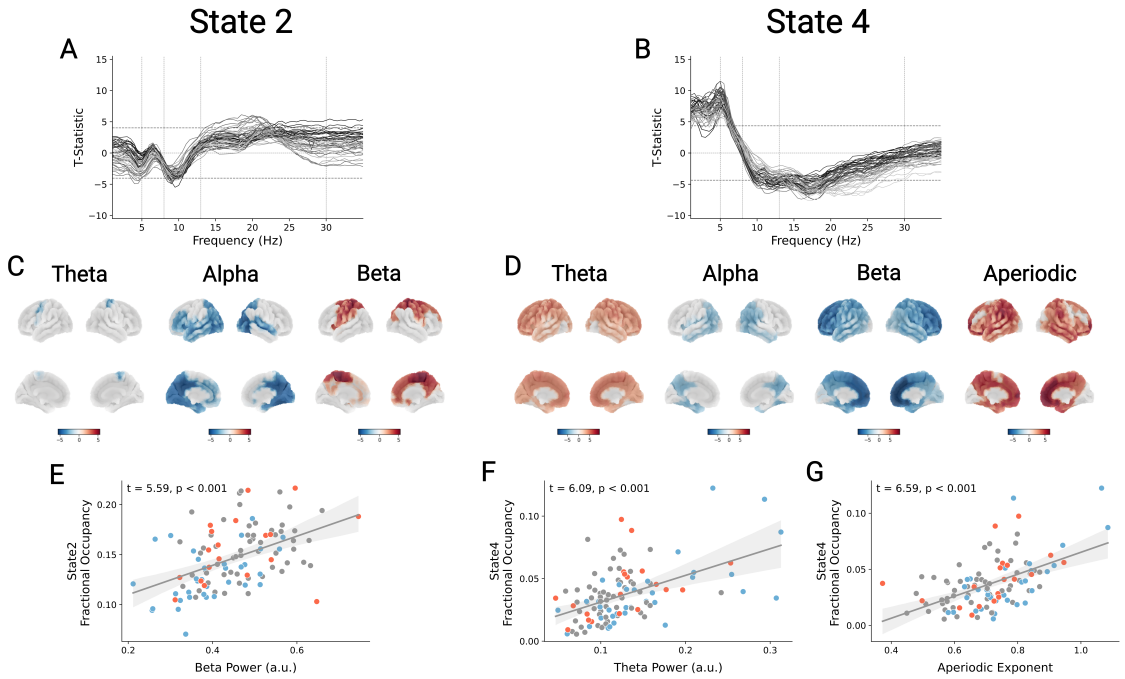


**Figure 3.7. Occurrence probabilities of dynamic large-scale networks are associated with static oscillatory power. (A)** T-statistics of association between sensorimotor network fractional occupancy and frequency bin power across participants. Each line represents t-statistics for a single parcel. Parcels with centre coordinates located in frontal brain regions are depicted in lighter greys, with lines darkening as parcel centres move posteriorly. Horizontal dashed lines indicate significance thresholds obtained from maximum t-statistic permutation tests pooled across frequency bins and parcels. **(B)** T-statistics of associations between State 4 fractional occupancy and frequency bin power across participants. **(C)** T-statistics of GLMs assessing the association between fractional occupancy of sensorimotor network and theta, alpha, and beta power across all participants. T-statistics for all parcels exhibiting significant associations after correcting for multiple comparisons with maximum t-statistic permutation tests pooled across parcels and frequency bands, are plotted onto the brain surfaces. **(D)** T-statistics of GLMs assessing the association between fractional occupancy of State 4 and theta, alpha, and beta power or 1/f-Slopes across all participants. **(E)** Correlation between sensorimotor network fractional occupancies and beta power across all participants at the parcel with the strongest association in GLMs

presented in (C). **(F)** Correlation between State 4 fractional occupancies and beta power across all participants at the parcel with the strongest association in GLMs presented in (D). **(G)** Correlation between State 4 fractional occupancies and 1/f-Slopes across all participants at the parcel with the strongest association in GLMs presented in (D).

## Large-scale network dynamics are not altered in RBD volunteers

After demonstrating how the extracted large-scale networks relate to static spectral power, I next assessed whether dynamic features of these large-scale networks were significantly changed in the PD and RBD groups.

Consistent with observations reported in Chapter 1, the sensorimotor network exhibited significant alterations in PD volunteers compared to HCs. Specifically, it was significantly less likely to be present ($t(95) = -3.9$, $p < .001$ ), and intervals between its occurrences were significantly longer ($t(95) = 2.26$, $p = .031$) (Figure 3.8A). Surprisingly, in this analysis sensorimotor network lifetimes were also significantly decreased in PD ($t(95) = -2.17$, $p = .036$), while occurrence rates did not differ between the two groups ($t(95) = -2.02$; $p = .056$), contrary to the findings in Chapter 1.

In contrast, dynamic features of the sensorimotor network did not differ between RBD volunteers and HCs, suggesting that sensorimotor network dynamics were not significantly different between the two groups (all $p > .158$) (Figure 3.8A). Similar to HCs, the sensorimotor network was significantly more likely to be present in RBD volunteers than in PD volunteers ($t(95) = -2.96$, $p = .002$). These results, combined with the strong association observed between the sensorimotor network and static cortical

beta power, suggest that differences in the fractional occupancy of the sensorimotor network likely underpin beta-power decreases in the sensorimotor cortex and neighbouring areas observed in PD but not in RBD volunteers.

Dynamic features of State 4 did not show any significant alterations in PD and RBD volunteers relative to their respective control groups (all $p > .159$) (Figure 3.8B). Consequently, it is unlikely that the dynamics of State 4 fully explain static theta power changes in the RBD or PD group.

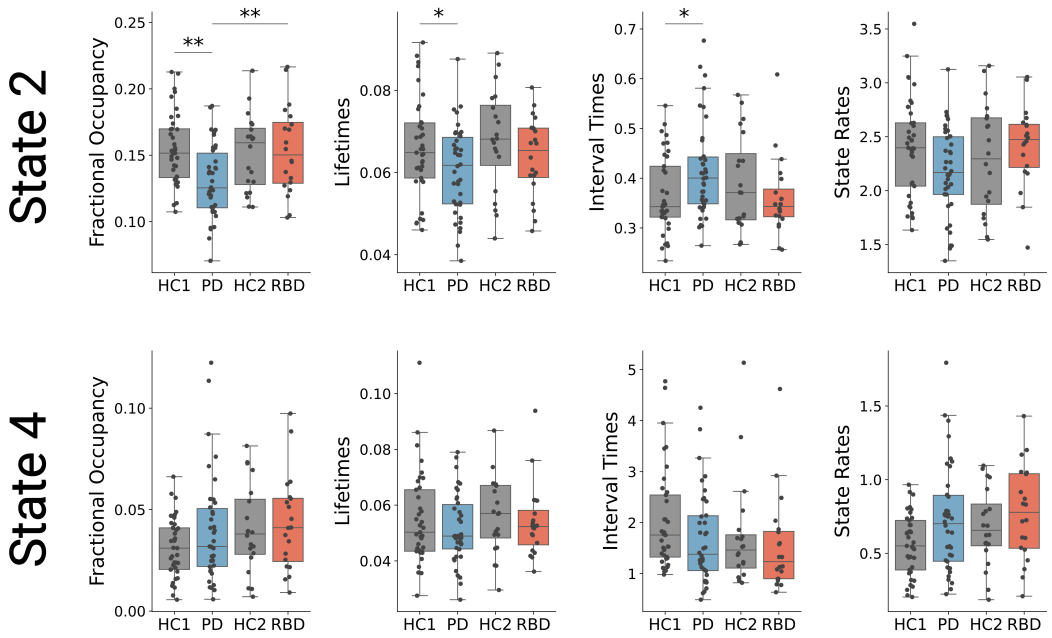


**Figure 3.8. Sensorimotor network is less likely to be present in PD, whereas RBD volunteers show no change in large-scale network dynamics.** State metric values of all participants for the sensorimotor network (State 1) and State 4 are presented for each group, respectively.
** indicates $p < .01$ and * $p < .05$.

## State 4-specific spectra do not underpin significant changes in static oscillatory power

Following the observation that the large-scale network dynamics of State 4 were not altered in PD or RBD, I next investigated whether State 4-specific spectra differed between the groups. State-specific spectra of State 4 were calculated by subtracting the mean across all state spectra from State 4 power spectra. Such group differences could potentially underpin the alterations in static theta power observed in PD and RBD within the static power spectral analysis.

Interestingly, State 4-specific spectra group comparisons did not reveal widespread increases in theta power or decreases in beta power. Instead, they showed significant increases solely in right medial parietal beta power in PD (Figure 3.9A) and left lateral frontal alpha power in RBD (Figure 3.9B). None of the frequency band power group contrasts between PD and RBD volunteers reached significance (Figure 3.9C). Crucially, also none of the other states exhibited widespread decreases in theta or increases in beta power. Only States 3 and 5 showed decreased theta power in a few parcels (Figure A3.4), which are unlikely to underpin widespread theta and beta-power alterations in the static power spectrum analysis.

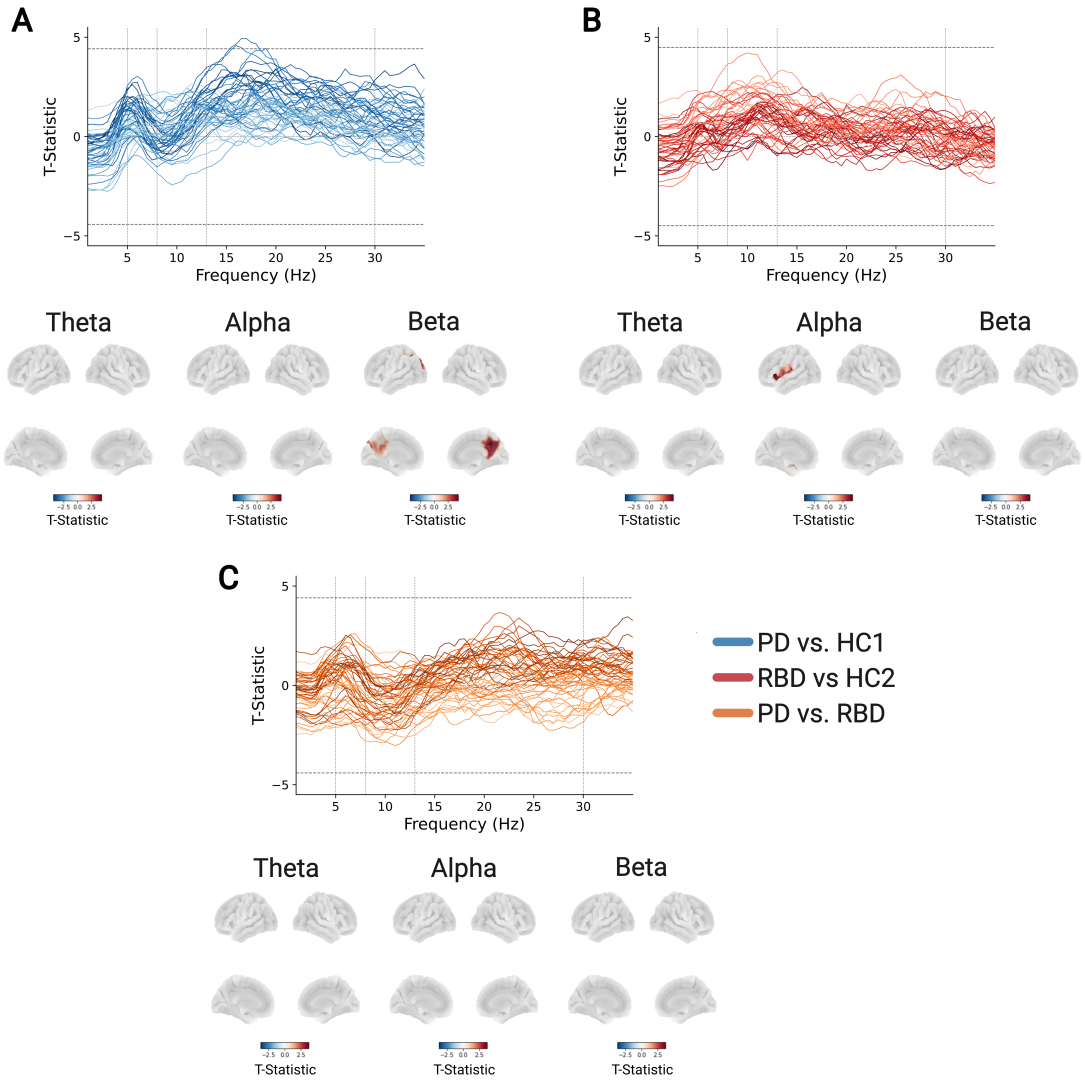


**Figure 3.9. State-specific spectra of State 4 are unlikely to underpin static theta-power differences between the patient groups and their respective control groups.** State 4-specific spectra were calculated by subtracting the mean across all state spectra from State 4 power spectra. Each panel presents results of GLMs assessing **(A)** HC vs PD (blue), **(B)** HC vs RBD (red), and **(C)** PD vs RBD (orange) group contrasts. In the top section, each line represents t-statistics of group contrasts for State 4-specific frequency bin power for a single parcel. Parcels located at frontal positions are depicted in brighter colours, with colour darkening for parcels located further posteriorly. Horizontal dashed lines indicated significance thresholds obtained from maximum t-statistic permutation tests pooled across frequency bins and parcels. Below, t-statistics of group

contrasts of state-specific theta, alpha, and beta power are presented. T-statistics of parcels that yield significant group differences are projected onto brain surfaces. Multiple comparison correction for comparisons across parcels and frequency bands was performed with maximum t-statistic permutation testing.

## Mean across state spectra shows significant differences observed in static power spectral analysis

Given that state-specific spectra and state metrics did not capture static theta and beta-power, as well as 1/f-Slope alterations in the RBD and PD group, I next checked whether these changes were present in the average across all state spectra (= state-averaged spectra). This would suggest that these alterations are present in several state spectra, and thus, are more persistent than the dynamics captured in the HMM description.

Group-level GLMs comparing frequency band power and 1/f-Slopes between PD and RBD volunteers and their respective control groups yielded patterns of change that closely resembled the alterations observed in the static power spectrum analysis. PD volunteers exhibited widespread increases in theta and alpha power, whereas beta power was significantly decreased across the entire brain (Figure 3.10A). Similarly, RBD volunteers exhibited increased theta power in occipital, inferior temporal, and inferior frontal areas, along with decreased beta power in occipital regions (Figure 3.10B). Comparisons between PD and RBD volunteers revealed increased theta and alpha

power in parietal and sensorimotor areas, while beta power was decreased in parietal, sensorimotor and frontal areas in PD volunteers (Figure 3.10C).

Furthermore, group differences of 1/f-Slopes also mirrored 1/f-Slope alterations observed in the static 1/f-Slope analysis (Figure 3.10D). PD volunteers demonstrated widespread 1/f-Slope increases, while RBD volunteers showed increased 1/f-Slopes in occipital, inferior temporal, and medial frontal regions. Comparisons of 1/f-Slopes between PD and RBD volunteers found significantly steeper 1/f-Slopes in parietal, sensorimotor, and frontal areas of PD volunteers, whereas RBD volunteers exhibited steeper 1/f-Slopes in left inferior temporal parcels.

Moreover, the majority of the state spectra, when the mean across states was not subtracted, demonstrated the changes described above (Figure A3.5), highlighting that observed alterations were present in the majority of states. Overall, these alteration patterns largely overlap with the results of the static power spectrum comparison. This suggests that these effects are more persistent than the dynamics captured by the TDE-HMM analysis, i.e., the theta and beta power changes in the RBD sample manifest at time scales slower than those captured by the TDE-HMM analysis.

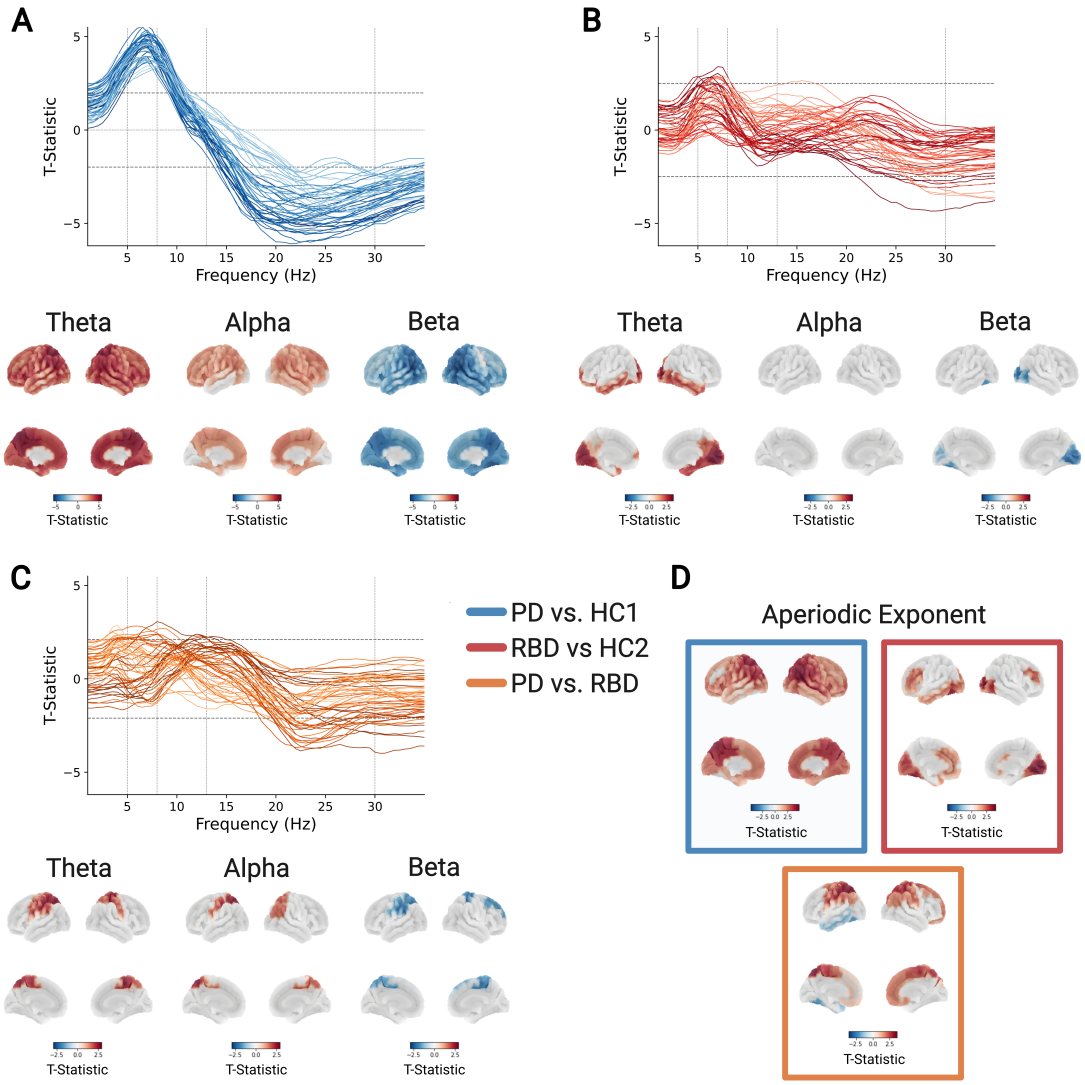


**Figure 3.10. Mean across all state spectra demonstrates significant group differences in cortical power, similar to findings of static power spectrum analysis.** Panel (A), (B), and (C) depict results of GLMs calculating **(A)** HC vs PD (blue), **(B)** HC vs RBD (red), and **(C)** PD vs RBD (orange) group contrasts. In the top figure, t-statistics of group contrasts comparing frequency bin power at each parcel are depicted. Each line represents t-statistics of group contrasts for all frequency bins for a single parcel. Parcels positioned frontally are coloured in brighter shades, gradually darkening as parcel centres move posteriorly. Horizontal dashed lines indicate significance thresholds obtained from maximum t-statistic permutation tests, pooling across frequency bins and parcels. Below, t-statistics of group contrasts of theta, alpha, and beta power are presented. T-

statistics of parcels whose group contrasts yielded significance after controlling for multiple comparisons with maximum t-statistic permutation testing, pooling across parcels and frequency bands, are projected onto brain surfaces. (D) Results of GLMs comparing 1/f-Slopes between the groups. T-statistics of parcels whose group contrasts yielded significance after controlling for multiple comparisons with maximum t-statistic permutation testing, pooling across parcels, are projected onto brain surfaces.

## Occipital theta power and 1/f Slopes, extracted from the mean across state spectra, are significantly associated with cognitive performance

Having established that static theta and beta-power alterations are represented in the mean across state spectra, I next investigated whether frequency range power and 1/f-Slopes, calculated from the mean across state spectra, were also associated with cognitive performance.

In contrast to the static power spectrum analysis, I did not observe any significant associations between beta power and ACE PC1 scores ($p < .1$). However, I observed a significant positive association between theta power and ACE PC1 scores ($t(46) = 3.52$; $p = .04$) at the same occipital parcel that exhibited significant associations between static beta power and ACE PC1 scores (Figure 3.11A). This suggests that higher theta power is associated with poorer cognitive performance.

Identical to the static 1/f-Slope analysis, steeper 1/f-Slopes at exactly the same parcel were linked to worse cognitive performance in the RBD group ($t(46) = 4.1$; $p = .005$)

(Figure 3.11B). Associations between 1/f-Slopes ($p < 0.31$), theta ($p < .96$), alpha ($p < .91$), and beta power ($p < .96$) for all other groups did not reach significance.

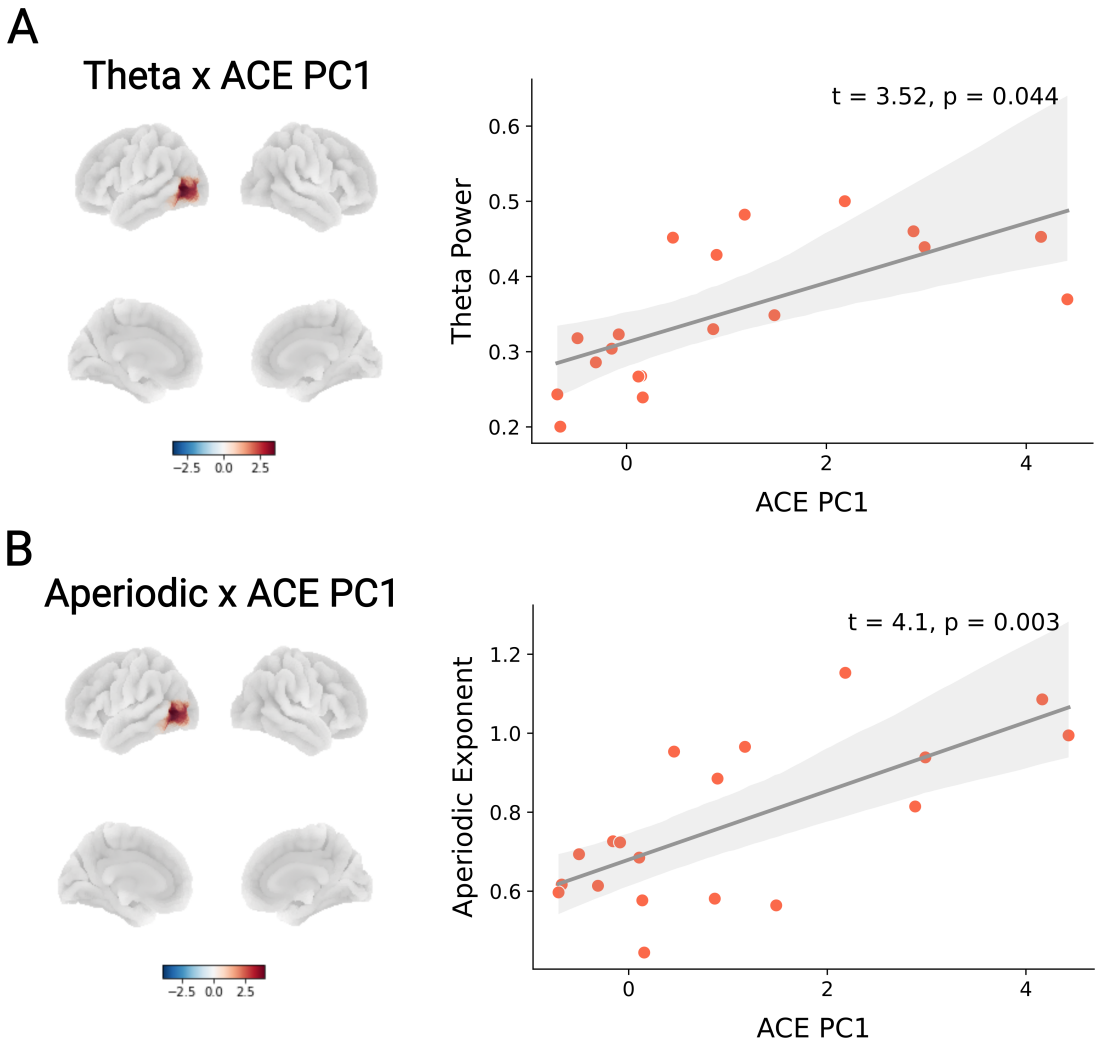


**Figure 3.11. Occipital theta power and 1/f-Slopes of the average across state spectra exhibit significant associations with ACE scores. (A)** Relationships between theta power, extracted from the average across state spectra, and first principal component values obtained from the PCA analysis (PC1) on ACE's cognitive domains. In the left panel, t-statistics of parcels with significant associations between theta power and ACE PC1 scores are projected onto brain surfaces. Positive t-statistics indicate positive associations between theta power

and ACE scores. Significance was assessed using maximum t-statistic permutation tests, pooling across parcels and frequency bands. In the right panel, the relationship between theta power and ACE PC1 scores at the parcel with the highest t-statistic is visualised. **(B)** Similarly, relationships between ACE PC1 scores and 1/f-Slopes, extracted from the average across state spectra, are presented.

## Repeating the analyses on solely the RBD dataset yields similar findings.

The preceding analyses suggest that differences in theta and beta power observed in the static power spectrum analysis are not captured by metrics focusing on dynamic features of individual large-scale networks. Instead, these differences manifest in the mean across state spectra, indicating that they occur at slower timescales. To ensure that this observation for the RBD sample is not merely a result of training the TDE-HMM on the combined RBD and PD dataset, potentially leading to a suboptimal network description for the RBD sample, I replicated all analyses using an HMM fitted solely on the RBD dataset.

The networks extracted with the TDE-HMM on the RBD dataset closely resembled those derived from the combined PD and RBD dataset (Figure A3.6). It identified a sensorimotor network and State 5 mirroring characteristics of State 4 extracted with the TDE-HMM on the combined dataset (Figure 3.12A). State metrics of State 5 ($p <$ .99) (Figure 3.12B) and all other large-scale networks did not differ between RBD volunteers and HCs ($p <$ .84). RBD vs. HC group contrasts did not yield significant

differences in theta or beta power in any of the state-specific spectra ($p < .25$) (Figure 3.12C).

The mean across state spectra pointed towards increased theta power in the RBD group, although the theta frequency band power contrasts did not yield significant group differences ($t(31) = 3.42$; $p = .29$) (Figure 3.12D). The lack of significance might be attributed to reduced power in the GLMs due to including only the 40 participants of the RBD dataset.

Similar to the findings from the combined analysis of the PD and RBD dataset, the group contrast of 1/f-Slopes calculated from the mean spectrum across states revealed significantly increased 1/f-Slopes in occipital areas in the RBD sample (Figure 3.12E). Overall, these findings suggest that theta and beta-power changes in the RBD sample manifest at time scales slower than those captured by the TDE-HMM analysis.

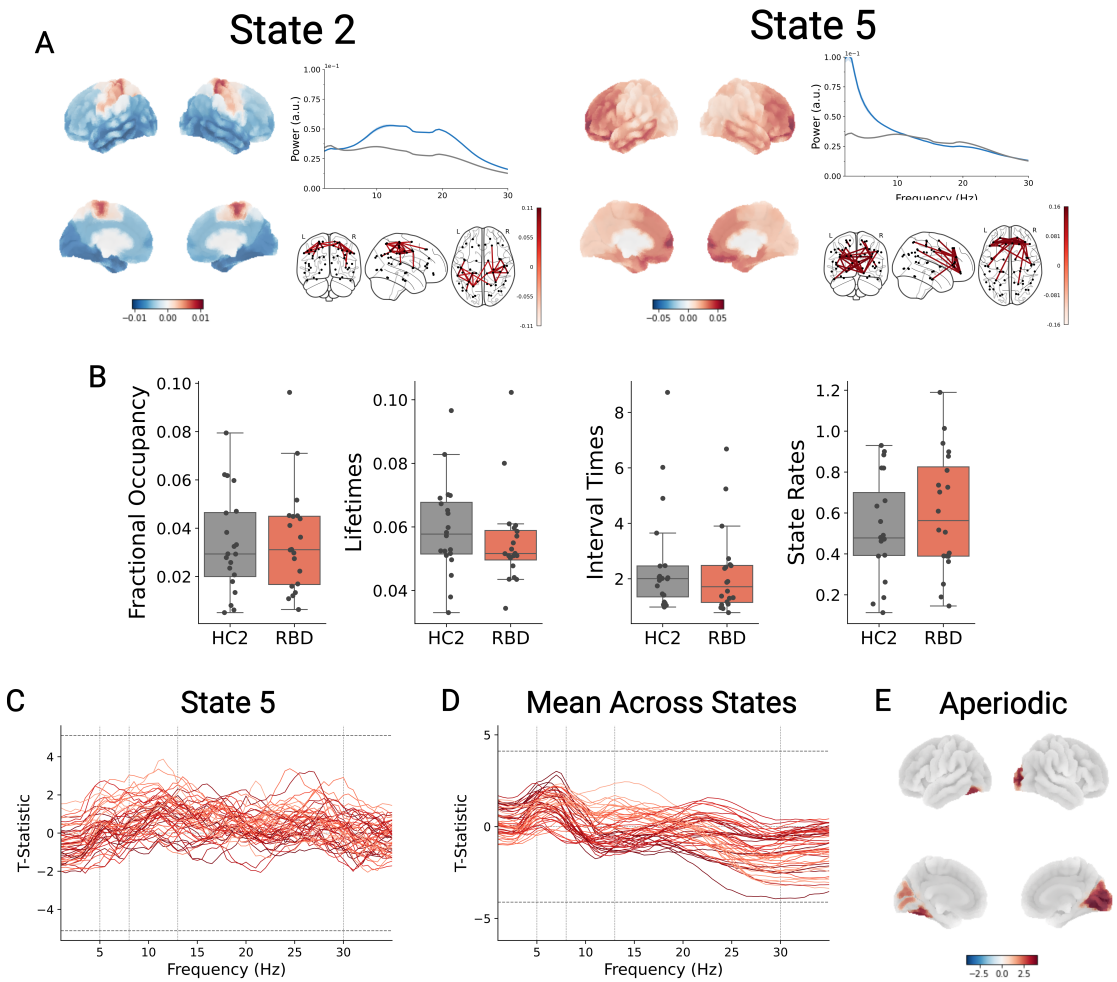


**Figure 3.12. TDE-HMM analysis on RBD dataset confirms that RBD-related power spectral alterations are not underpinned by changes in a single large-scale network but rather by more static alterations spanning across various states. (A)** Spectral state description of sensorimotor network and network with widespread low-frequency power increases (State 5), extracted by fitting the TDE-HMM to the RBD dataset. (Refer to Fig 3.6 for a detailed explanation of the state description). **(B)** Group comparisons of State 5 state metrics do not yield significant alterations between HCs (grey) and the RBD group (red). **(C)** Frequency bin-wise group contrasts of state-specific power spectral changes do not yield significant group differences. Parcels at frontal positions are depicted in brighter colours, becoming progressively darker towards more posterior parcels. Horizontal dashed lines denote significance thresholds obtained from maximum t-statistic permutation tests, pooling across frequency bins, parcels, and

networks. **(D)** Frequency bin-wise group contrasts of the average across state spectra reveal clearer patterns of change in t-statistics but do not reach significance. Parcels at frontal positions are depicted in brighter colours, becoming progressively darker towards more posterior parcels. Horizontal dashed lines denote significance thresholds obtained from maximum t-statistic permutation tests, pooling across frequency bins and parcels. **(E)** 1/f-Slopes calculated from the average across state spectra are significantly steeper at occipital parcels in RBD. T-statistics of parcels exhibiting significant group differences are projected onto brain surfaces. Higher values indicate steeper 1/f-Slopes in the RBD group.

# Discussion

## Summary

In the present chapter, I aimed to investigate static aperiodic and oscillatory power as well as dynamic large-scale networks in PD and RBD volunteers to identify candidates for prodromal markers of PD. RBD volunteers demonstrated focal increases of theta power in occipital, inferior temporal, and inferior frontal areas and beta-power decreases in occipital areas, whereas PD volunteers exhibited widespread increases in theta power and decreases in beta power. Similarly, 1/f-Slopes were steeper throughout the whole brain in PD volunteers, whereas RBD volunteers showed marked decreases in occipital and frontal areas. Both steeper 1/f-Slopes and smaller beta power in occipital areas of RBD volunteers were associated with worse cognitive performance. Control analyses suggested that 1/f-Slope group differences likely contribute to beta-power findings whereas theta-power findings were less affected. Examining only static power spectra does not allow for distinguishing whether the observed changes are underpinned by alterations in specific dynamic brain networks or by persistent changes over time. To investigate these possibilities, I applied a TDE-HMM to investigate how observed aperiodic and oscillatory power alterations are represented in a dynamical large-scale network description. Neither metrics of network dynamics nor network-specific spectral changes demonstrated alteration patterns explaining static theta and beta-power alterations in PD and RBD. Consequently, I investigated whether such power spectral group differences were captured by the majority of states and therefore, can be observed in the average

across state spectra. Indeed, group comparisons between the average across state spectra yielded theta and beta power as well as 1/f-Slope changes similar to alterations observed in the static power spectrum analysis. This finding suggests that observed power spectral alterations in PD and RBD reflect a more persistent change that is not specifically tied to particular dynamic networks. In conclusion, RBD volunteers demonstrated static oscillatory and aperiodic activity alterations in inferior regions of the brain also affected in PD volunteers, which can be considered as promising candidates for prodromal markers of PD and alpha-synucleinopathies.

## Cortical oscillatory and aperiodic activity is altered in RBD

This project is one of the first projects analysing electrophysiological activity recorded with MEG from RBD volunteers. Similar to previous EEG studies (Bang et al., 2017; Iranzo et al., 2010; Livia Fantini et al., 2003; Massicotte-Marquez et al., 2008; Rodrigues Brazète et al., 2013, 2016), RBD volunteers showed significant alterations in cortical oscillatory activity that suggest an increase in low-frequency power and a decrease in high-frequency power, also referred to as oscillatory slowing. More specifically, I observed increased theta power in occipital, inferior temporal, and inferior frontal areas and decreased beta power in occipital areas. In contrast to this, previous EEG studies that usually assessed the brain in terms of 10 coarse regions (frontal, central, temporal, parietal, and occipital) reported increases in theta power and slow-to-fast frequency power ratio throughout the entire brain (Iranzo et al., 2010; Livia Fantini et al., 2003; Rodrigues Brazète et al., 2013, 2016). This difference may be due to the more rigorous multiple comparison correction that I applied in our

analysis to correct for multiple comparisons across 52 parcels and 3 frequency bands which makes it less sensitive to smaller differences.

Strikingly, 1/f-Slopes were significantly increased in RBD volunteers and the spatial pattern of change overlapped considerably with the spatial distribution of theta and beta-power changes. Given that steeper 1/f-Slopes result in higher power in low frequencies and reduced power in higher frequencies, it seems likely that 1/f-alterations contribute to observed changes in oscillatory power. In line with this, I observed that beta-power alterations in the RBD group failed to reach significance after removing the aperiodic part of each participant's power spectrum, whereas theta-power differences remained significant. This suggests that 1/f-alterations in RBD likely contribute to previously observed patterns of power spectral change, in particular, in beta power.

Power spectral alterations in RBD have been proposed to reflect dysfunction of the cholinergic neurotransmitter system (Sasai et al., 2013). Cholinergic dysfunction in RBD has been observed in various PET studies (Bedard et al., 2019; Stær et al., 2020; Stokholm et al., 2020) and was linked to worse cognitive performance (Stokholm et al., 2020). Notably, PD patients with RBD show stronger cholinergic denervation (Kotagal et al., 2012) and increased theta power in frontal, temporal, parietal, and occipital areas (Gagnon et al., 2004) than PD patients without RBD. This further supports the notion that cholinergic dysfunction in RBD might affect cortical oscillatory power. Crucially, theta and beta power, especially in occipital and inferior temporal areas of PD volunteers were observed to be the best electrophysiological predictors for the progression to PD with dementia after a period of 7 years (Olde Dubbelink et al.,

2014). The fact that these areas largely overlap with the theta and beta-power alterations observed in this chapter combined with studies that discussed RBD as an indicator of a cholinergic (Pasquini et al., 2021) or body-first PD subtypes (Borghammer, 2021) linked to cognitive impairments, make it tempting to speculate that the spectral changes observed in this study are early markers for such a PD-subtype with more severe cognitive impairments (Borghammer, 2021; Pasquini et al., 2021). This notion is further supported by observed associations between spectral changes in beta and theta power and cognitive performance.

In addition to cholinergic neurotransmitter system alterations, several other factors could contribute to observed spectral changes:

- Alterations of 1/f-Slopes.

  I observed that 1/f-Slopes in occipital and frontal areas were significantly increased, likely underpinning occipital beta-power differences. 1/f-Slopes have been previously demonstrated to be modulated by drugs affecting the E/I-balance of synaptic inputs (Colombo et al., 2019; Gao et al., 2017; Muthukumaraswamy & Liley, 2018; Waschke et al., 2021) because of what it may be hypothesized that observed alterations in the RBD group demonstrate changes in the occipital and frontal E/I-balance. This interpretation should be treated carefully, because even though 1/f-Slopes are sensitive to E/I balance variations, they still may also reflect variations in other biologically meaningful mechanisms (Kramer & Chu, 2023).

- Local Accumulation of alpha-synuclein pathology:

  Power spectral changes especially observed in inferomedial temporal and

frontal areas could be hypothesized to reflect the accumulation of proteinopathy, given that anteromedial portions of the temporal lobe were observed to be the first cortical areas that express Lewy Bodies (Braak et al., 2003). However, it should be noted that in Braak Stage 4, in which cortical Lewy Body accumulations were first reported, clinical signs of PD are assumed to be strong enough to diagnose PD. Thus, it may be that power spectral alterations in our sample predate periods in which Lewy Bodies accumulate in anteromedial portions of the temporal lobe. With new cerebrospinal fluid- (Poggiolini et al., 2022) and blood-based (Yan et al., 2023) markers of alpha-synuclein on the horizon the relationship between alpha-synuclein and observed power spectral alterations may be tested in the near future.

- Noradrenergic neurotransmitter system dysfunction:

  Increasing loss of brain noradrenaline has been linked to cognitive decline in PD (Aarsland et al., 2021). PD volunteers with RBD and cognitive decline demonstrated decreased noradrenaline transporter availability measured with PET that was associated with stronger oscillatory slowing in EEG recordings (increased theta power and decreased alpha power and peak frequency) (Sommerauer et al., 2018).

  Given that MRI signals sensitive to neuromelanin concentration in the locus coeruleus, a key region of the noradrenergic system, have been observed to be reduced in RBD volunteers (Ehrminger et al., 2016), it may be that alterations in the noradrenergic system contribute to observed oscillatory changes in the RBD group. However, since reduced neuromelanin-sensitive MRI of the locus coeruleus has been shown to be associated with higher alpha power in mostly

frontal and central regions of PD volunteers (Wiesman et al., 2024), it seems unlikely that observed theta and beta-power changes in occipital, inferior temporal or inferior frontal areas can be explained by noradrenergic alterations in RBD volunteers.

In sum, findings in the RBD dataset demonstrate focal aperiodic and oscillatory changes in occipital, inferior temporal, and inferior frontal areas of the brain which may be linked to various pathological processes. Future research, attempting to disentangle contributions of the discussed mechanisms may help to further pinpoint pathological processes that underpin observed power spectral changes and enrich our understanding of cortical dysfunction in RBD.

## Widespread alterations in cortical oscillatory activity in PD

Similar to RBD volunteers, individuals with PD also showed altered aperiodic activity and cortical oscillatory power, particularly in theta and beta frequency ranges. In contrast to the RBD group, theta power was increased throughout the entire brain and beta power was decreased in all but a few frontal parcels replicating previous work on de-novo and more progressed PD volunteers (Boon et al., 2023; Bosboom et al., 2006; Morita et al., 2009; Stanzione et al., 1996; Stoffers et al., 2007). In contrast to previous studies (Boon et al., 2023; Bosboom et al., 2006; Geraedts et al., 2018; Morita et al., 2011; Olde Dubbelink, Stoffers, Deijen, Twisk, Stam, & Berendse, 2013; Wiesman et al., 2023), I did not observe significant associations between theta, alpha, or beta power and cognitive performance in PD volunteers. This may be due to the small variability of ACE scores in the PD sample.

Similar to the RBD literature, oscillatory slowing in PD has been discussed to reflect various underpinning processes: Various neurotransmitter systems, including dopaminergic, serotonergic, GABAergic, and noradrenergic systems, have been linked to oscillatory slowing (Wiesman et al., 2023). Cholinesterase inhibitors were observed to increase alpha and beta power while decreasing frontocentral and parietooccipital delta power in PD patients with dementia, suggesting involvement of the cholinergic system, which has been discussed to be an important factor for cognitive impairments and dementia in PD (Bosboom et al., 2009). DBS of the STN was suggested to reverse cortical oscillatory slowing by increasing high alpha and beta power throughout the entire brain while decreasing delta, theta, and low alpha power in scattered brain regions, likely reflecting a contribution of thalamocortical circuits or 1/f-Slope alterations (Boon et al., 2019). Lastly, various spectral markers, discussed to indicate oscillatory slowing, have been linked to cerebrospinal fluid (CSF) and positron emission tomography (PET) markers of neuropathology in mild cognitive impairment and Alzheimer's Disease (Coomans et al., 2021; Maestú et al., 2021; Nakamura et al., 2018; Ranasinghe et al., 2020, 2021; Smailovic et al., 2018; Stomrud et al., 2010; Wiesman et al., 2022). As co-localisation between spatially resolved spectral and such neuropathological CSF- and PET-markers has been reported (Ranasinghe et al., 2020; Wiesman et al., 2022), accumulation of local pathology may be another factor implicated in oscillatory slowing. In summary, patterns observed in the present chapter likely reflect alterations in various underpinning pathological processes.

## RBD and PD group show similar but not identical patterns of change

Direct comparisons of oscillatory and aperiodic variables between PD and RBD volunteers revealed that individuals with PD had significantly higher theta power in superior sensorimotor areas, higher alpha power in superior parietal areas, and lower beta power in superior parietal, sensorimotor, and frontal areas. Similar to power spectral comparisons between disease groups and their respective HC groups, significant 1/f-Slope alterations spatially overlapped with oscillatory group differences. I observed steeper 1/f-Slopes in superior parietal, sensorimotor, and frontal areas in PD and significantly steeper 1/f-Slopes in an inferior temporal parcel in the RBD group. Crucially, subtracting 1/f-Slopes prior to calculating oscillatory power group contrasts attenuated group differences so that none of them reached significance. This suggests that steeper 1/f-Slopes strongly contribute to observed group differences between individuals with PD and RBD. Future studies carefully assessing pathological mechanisms modulating 1/f-Slopes in especially superior parietal, sensorimotor, and frontal areas may provide insights about pathological processes differentiating individuals in potentially prodromal stages of PD from PD.

Remarkably, alterations of oscillatory and aperiodic variables in the PD group spread throughout the entire brain whereas they were spatially limited to inferior regions in the RBD group. This suggests that spectral changes in the PD and RBD group do not reflect different degrees of pathology in overlapping areas but that functional alterations in PD are more distributed. This observation is not surprising given that PD is a progressive neurodegenerative disorder with increasing distribution of pathology (Braak et al., 2003). Thus, PD volunteers likely exhibit stronger and more widespread

neurodegeneration, probably affecting various of the above-mentioned processes that all contribute to power spectral alterations. In contrast, prodromal stages of alpha-synucleinopathies that may be present in RBD (Hu, 2020), likely include lower and more focal neurodegeneration. Pathology is probably more localised to brain stem areas and without extensive spread into cortical regions (Borghammer, 2021), which could result in sparser effects of neurodegenerative processes on cortical oscillatory power. Consequently, cortical oscillatory alterations in PD may initially emerge in areas identified in the RBD dataset and gradually spread throughout the entire brain as the disease progresses. Longitudinal studies will be important to identify patterns of systematic progression associated with conversion of RBD to PD.

## Alterations of oscillatory activity occur at different timescales

Theta and beta power as well as 1/f-alterations in both PD and RBD were prevalent during visits to multiple states and could not be explained by metrics of individual states. This suggests that the observed spectral changes likely reflect more general consequences of underlying pathological processes that are not differentially modulated by varying large-scale network occurrences over time. This implies that the pathological processes underpinning the observed spectral changes do not affect the functioning of single networks but rather the functioning of certain brain areas consistently over time.

Unsurprisingly, the large-scale network description provided by the TDE-HMM replicated findings of reduced occurrence probability of the sensorimotor network in PD, presented in Chapter 1, which shows that meaningful dynamic variations are

captured by the fitted TDE-HMM. This demonstrates that PD yields various kinds of cortical oscillatory change that manifest at different timescales. The state-specific reduced sensorimotor network occurrences in PD are embedded witing more consistent and widespread patterns of theta-power increase, beta-power decrease, and steepening of 1/f-Slopes. Similarly, I observed State 4 occurrences to be significantly associated with 1/f-Slopes, while the alterations in 1/f-Slopes related to PD and RBD were not reflected in the State 4 power spectra. Conversely, the group differences in 1/f-Slopes were captured by all states except State 4. This suggests that 1/f-Slopes may have a more dynamic time-varying component (Wilson et al., 2022) as well as a more static component. My findings suggest that the latter contribute more to the 1/f-Slope alterations in RBD and PD. These findings regarding oscillatory power and 1/f-Slopes demonstrate that time-varying and static measures likely pinpoint processes manifesting at different timescales, providing complementary information. This complementary information may yield a better understanding of dysfunctional processes and pathology in PD and other disorders.

## Limitations

Even though scanning protocols for both datasets were matched, the explanatory power of the PD vs. RBD group contrast is limited because both data sets were recorded with different scanners in different time periods. Thus, it cannot be ruled out that observed group differences reflect differences between scanners or scanner environments. Importantly, control groups of the two datasets were collected with the same scanner and period as the respective disorder group because of what HCs vs disorder group comparisons are not affected by this limitation.

I assumed that power spectral alterations prevalent in both the PD and the RBD dataset are promising candidates for prodromal stages of PD. This assumption is likely not true for PD in general but rather for specific subtypes of PD associated with RBD, autonomic dysfunction, cognitive impairments, faster progression, and larger degrees of neurodegeneration upon PD diagnosis (Borghammer, 2021; Fereshtehnejad et al., 2015; Pasquini et al., 2021). Additionally, individuals with RBD do not only progress to PD but also Multiple System Atrophy and Dementia with Lewy Bodies. Given that I observed worse cognitive performance in RBD volunteers compared to their HC group and that worse cognitive performance best predicts progression to dementia as the primary disease manifestation (Postuma et al., 2019), I cannot rule out that observed spectral alterations in the RBD group are driven by participants eventually progressing to alpha-synucleinopathies associated with impaired cognition and dementia. Follow-up assessments providing information about the phenoconversion of the included volunteers will help to clarify whether certain types of phenoconverters drove the observed spectral alterations.

Power spectra were derived from z-scored time course signals, potentially introducing associations between peak frequency power and beta/gamma power, as well as mixing alterations in theta power and 1/f-Slopes with those in beta power in PD and RBD (see Figure A4.1 to Figure A4.5). Notably, both RBD and PD volunteers exhibited alterations in theta power, which spatially overlapped with changes in beta power and 1/f-Slopes. Consequently, it may be that differences observed in beta power simply reflect alterations in peak frequency power and 1/f-Slopes that were inadvertently incorporated through z-scoring parcel time courses. See “Effects of normalising power

spectra on beta power" section in the discussion of this thesis and Figure A4.1 to Figure A4.5 for a more detailed discussion.

## Conclusion

In summary, the present chapter demonstrated that oscillatory and aperiodic power spectral markers in primarily inferior regions of the brain are altered in RBD. These alterations constitute promising markers for prodromal stages of PD or alpha-synucleinopathies due to the high conversion rates from RBD to alpha-synucleinopathies. This notion was further supported by observing that PD volunteers show change in the same power spectral markers with overlapping but more diffuse spatial distribution. Extracting a rich large-scale network description of the data by fitting a TDE-HMM to it, I noticed that observed power spectral changes reflect a static phenomenon. This suggests that pathophysiological alterations of cortical oscillatory and aperiodic activity are stable and not specific to single large-scale networks. The pathophysiology underpinning these changes remains an open question given the multitude of processes that have been observed to modulate observed patterns of power spectral alterations.

# Discussion

The overarching goal of my doctoral thesis was to identify oscillatory brain activity signatures associated with PD within non-invasive electrophysiological recordings, which may hold promise as markers for early stages of Parkinson's disease (PD). To achieve this, I investigated cortical oscillatory and network activity, comparing Healthy Controls (HCs) with individuals diagnosed with PD across both resting and task-related states. Through these analyses, I identified alterations in brain activity linked to PD. Furthermore, I extended my investigation to include individuals with REM-Sleep Behaviour Disorder (RBD), a population at high risk of developing PD. I explored whether the identified markers of PD-related brain activity were already detectable in resting-state brain activity recordings of individuals with RBD. This exploration enabled the identification of cortical oscillatory signatures for detecting prodromal stages of PD. In the concluding chapter of my thesis, I will summarise and discuss the empirical findings of my research. Initially, I will focus on electrophysiological markers observed to be altered in PD. Subsequently, I will shift the focus to markers that exhibited changes in individuals with RBD and PD, thus presenting potential candidates for prodromal PD markers. Finally, I will outline the implications of these findings for future research, emphasizing steps that can be taken to further solidify the role of non-invasive electrophysiological measures as markers for PD.

# Electrophysiological Signatures of Parkinson's Disease

## Static and dynamic alterations of cortical oscillatory power in PD

In each of the chapters in the thesis, I investigated oscillatory signatures of PD using electrophysiological recordings obtained with Magnetoencephalography (MEG). In Chapter 1, I observed significantly decreased beta power within sensorimotor areas, which was accompanied by widespread decreases in beta power across the entire brain, as demonstrated in Chapter 3. In Chapter 1, I further demonstrated that decreases in the occurrence probability of the sensorimotor network likely contribute to the decrease in sensorimotor beta power. In contrast, the more widespread beta-power decreases may reflect more consistent, static changes, which affect various large-scale networks. More specifically, they were neither associated with large-scale network dynamics nor state-specific spectral changes of certain states. These observations suggest that pathological changes in PD affect cortical oscillatory activity in various ways and across different time scales.

This is not surprising given the multitude of pathophysiological changes that have been reported for PD (Kalia & Lang, 2015; Kouli et al., 2018). In addition to the loss of dopaminergic neurons in the substantia nigra pars compacta – the pathological hallmark of PD – neurodegeneration impacts various cortical (Braak et al., 2003; Laansma et al., 2021) and subcortical regions as well as neurotransmitter systems (Dickson, 2012; Kalia & Lang, 2015). Although a few multimodal studies have attempted to relate markers of subcortical structural integrity (Wiesman et al., 2024), cortical structural integrity (Vinding, Waldthaler, et al., 2024), subthalamic nucleus

(STN) activity (Tinkhauser et al., 2018), or neurotransmitter systems (Bosboom et al., 2009; Wiesman et al., 2023) to cortical oscillatory activity, it remains an open question how pathological processes underpin observed cortical oscillatory alterations in PD.

Given that dynamics of transient beta events in the STN have been identified as the primary electrophysiological hallmark of PD (Lofredi et al., 2023; Tinkhauser, Pogosyan, Little, et al., 2017; Tinkhauser, Pogosyan, Tan, et al., 2017), it is tempting to speculate that PD-related alterations in the dynamics of the sensorimotor network relate to these changes in basal ganglia-thalamocortical loop functioning. Invasive studies observed significant overlaps between burst occurrences in STN and motor cortex (Tinkhauser et al., 2018) and reported beta synchronisation between supplementary motor cortex (SMA) and STN (Litvak et al., 2011; Oswal et al., 2016, 2021). In line with this, markers describing dynamics of sensorimotor beta oscillations have distinguished between HCs and PD volunteers (Pauls et al., 2022; Vinding et al., 2020; Vinding, Waldthaler, et al., 2024), although observed patterns of change were inconsistent across studies. Notably, only one of these studies showed burst-dynamic alterations in line with what has been reported in STN recordings (Pauls et al., 2022). As outlined in Chapter 1, these inconsistencies may be resolved by considering the large-scale network context of sensorimotor beta activations, potentially enabling researchers to focus on beta activations related to PD. However, various other factors, i.e., varying disease progression, symptomatology, motor states in the scanner, assessment of intervention effects vs. HC vs. PD group contrasts, or differences in the scale of measurements, likely contribute to these inconsistencies.

In contrast, widespread changes in static beta oscillations, which are not captured by network dynamics, may stem from other pathological processes, including neurotransmitter system dysfunction, local neurodegeneration and protein pathology, or compensatory mechanisms. In line with this, drug-induced modulations of the cholinergic system were linked to beta-power changes across the entire brain (Bosboom et al., 2009). However, various other pathological alterations likely contribute to power spectral changes in PD (Boon et al., 2020; Vinding, Waldthaler, et al., 2024; Wiesman et al., 2023, 2024). Potential contributing factors are presented in the discussion of Chapter 3 in more detail.

Even though it remains an open question to what degree certain PD-related pathophysiological processes affect cortical oscillatory changes, this thesis provides evidence that adopting both static and dynamic perspectives on PD-related cortical oscillatory alterations pinpoints complementary patterns of change. These patterns of change are likely associated with different pathophysiological processes. Thus, it will be crucial to carefully disentangle contributions of pathophysiological processes to cortical oscillatory alterations in PD to establish a precise understanding of what alterations in these signatures reflect.

## Sensorimotor network as a marker for PD during rest and task performance

In Chapters 1 and 2, I observed significant changes in sensorimotor network features in PD during both resting and task conditions. During resting-state scans, these alterations were associated with decreases in time-averaged motor cortical beta power, while during task performance, they were suggested to underpin decreases in

movement-related beta-power modulations. Interestingly, in resting-state recordings the occurrence probability of the sensorimotor network was changed, whereas state-specific beta power during sensorimotor network occurrences was altered during task performance. These findings are somewhat paradoxical, suggesting that PD volunteers demonstrate alterations in different sensorimotor network features in resting-state and task conditions. A possible, albeit speculative, explanation for this discrepancy may be that the observed alterations in dynamic and spectral features are driven by distinct processes.

It may be that alterations in sensorimotor-network dynamics are more noticeable in resting-state conditions because no external constraints are present, dictating the occurrence of specific brain states at certain time points. In such an unrestricted state, alterations in intrinsic dynamics of the pathologically impaired sensorimotor network may become more apparent. Conversely, during task performance, the brain may be forced into an action-oriented state to accomplish a predetermined goal, which is identical for all participants. Since achieving the goal strongly influences network dynamics, alterations in intrinsic network dynamics may be less evident. Considering that PD volunteers did not show prominently impaired performance in the sustained-gripping task (Zokaei et al., 2021), one could hypothesise that similar task performance renders network dynamics more alike.

The observation that the sensorimotor networks demonstrated decreased beta power in PD volunteers during movement performance but not during rest, could reflect more persistent alterations closely related to motor cortical functioning. As both the sensorimotor network and the posterior sensorimotor network showed decreases in

motor cortical beta power and peak frequencies in Chapter 2, I discussed that these changes may reflect more static impairments of motor cortical functioning that become particularly prominent during periods of motor cortical activation. Crucially, in Chapter 1, there was a non-significant trend towards decreased sensorimotor network-specific beta power in PD volunteers (majority of t values in robustness test > 2; Figure 1.7D). It may be that such functional alterations within the sensorimotor network become more pronounced when it engages in the processing of actual movements. Alternatively, it may be that increased occurrences of the sensorimotor network during task performance (mean fractional occupancy: rest = 12%; sustained-gripping task = 15%), combined with longer durations of the sustained-gripping task scans (scan duration per participant: rest = ~8min; sustained-gripping task = ~ 12min), enhance the signal-to-noise ratio when estimating sensorimotor network-specific power spectra. Consequently, PD-related motor cortical alterations could become apparent in the sustained-gripping task due to the increased signal-to-noise ratio.

Overall, the findings from Chapters 1 and 2 suggest that the sensorimotor network is significantly altered during rest and task performance in PD, although with variations in the specific features that are affected under these conditions. It remains an open question whether alterations in sensorimotor network dynamics and sensorimotor network-specific motor cortical beta power stem from similar or distinct pathological mechanisms. Future research should aim to dissect how pathological mechanisms contribute to observed changes by comparing effects of dopaminergic medication on vs. off conditions (Heinrichs-Graham, Kurz, et al., 2014) or markers of more static changes (Vinding, Waldthaler, et al., 2024; Wiesman et al., 2024) on sensorimotor

network features. Furthermore, future studies could explore whether PD-related alterations become more pronounced during sensorimotor network activations by assessing whether sensorimotor network-specific motor cortical alterations in beta power become more pronounced during tasks requiring strong motor cortical recruitment compared to tasks requiring little motor cortical recruitment. Similarly, within scans, one could investigate whether motor cortical alterations in PD volunteers are more pronounced during motor cortical activations, defined as burst or sensorimotor-network occurrences.

## Electrophysiological markers of prodromal stages of Parkinson's Disease

In the empirical work of this thesis, I observed alterations in both time-average cortical oscillatory and aperiodic activity, as well as changes in large-scale network dynamics in PD volunteers. Could these observed patterns of change serve as markers for prodromal stages of PD? To address this question, I collected and analysed resting-state recordings from HCs and RBD volunteers, a population at high risk of developing PD.

Dynamic sensorimotor network features differentiated between PD volunteers and HCs during rest and task performance and provided a fine-grain description of movement-related brain activity modulations. Despite this, sensorimotor network features were not significantly altered in individuals with RBD. This is somewhat surprising, given previous reports of decreased basal ganglia functional connectivity in

RBD, which suggests that basal ganglia functional connectivity may already be altered in RBD (Rolinski et al., 2016). However, the authors observed decreased functional connectivity only between basal ganglia and frontal cortical areas, hinting that sensorimotor areas might not be affected by subcortical changes in this prodromal stage. Another explanation could be that only 34% of RBD volunteers show subtle motor impairments (Postuma et al., 2019), making it unlikely that the sample of 20 RBD volunteers, investigated in Chapter 3, included a sufficiently large number of RBD volunteers with motor impairments.

In contrast to this, I observed marked changes in static cortical oscillatory and aperiodic activity in both PD and RBD volunteers. RBD volunteers demonstrated significantly increased theta power in occipital, inferior temporal, and inferior frontal areas, whereas occipital beta power was decreased. These changes were partially associated with worse cognitive performance and largely overlapped with regions where theta- and beta-power changes have been identified as strong predictors for the progression from PD without dementia to PD with dementia (Olde Dubbelink et al., 2014). These observations make it tempting to hypothesise that these alterations are markers for prodromal stages of a specific PD subtype associated with cognitive impairments and progression to dementia (Borghammer, 2021; Pasquini et al., 2021). Considering that cholinergic dysfunction has been implicated in PD with dementia (Aarsland et al., 2021; Pasquini et al., 2021; Shimada et al., 2009) and has also been observed in RBD (Bedard et al., 2019; Stær et al., 2020; Stokholm et al., 2020) and PD volunteers with RBD (Kotagal et al., 2012), it seems possible that cholinergic dysfunction underpins observed power spectral changes. This hypothesis could be

tested by extracting the grey matter volume of the participants' nucleus basalis of Meynert, a key node in the cholinergic network (Mesulam & Geula, 1988), from their structural MRI scans and correlating it with spectral power.

However, it is important to note that not all individuals with RBD progress to PD, and that indeed, cognitive impairments in RBD are a strong predictor for the conversion to alpha-synucleinopathies with dementia as primary manifestation of the disease (Postuma et al., 2019). Thus, the observed alterations might serve as markers for prodromal stages of alpha-synucleinopathies with dementia as their primary disease manifestation rather than PD in general. Following up on the phenoconversion and subsequent disease progression of the included RBD volunteers would help to clarify this further.

Nevertheless, decreases in theta power in occipital, inferior temporal, and inferior frontal regions, as well as reductions in occipital beta power, are very promising candidates for prodromal markers of alpha-synucleinopathies, including PD.

## Implications for future research

Finally, I would like to discuss a few implications for future research based on the research during my doctoral training. Firstly, I will examine various factors that potentially contribute to the inconsistencies observed in electrophysiological research on PD. Following this, I will explore potential improvements or alternative analyses for quantifying electrophysiological alterations in PD, aiming to better capture PD-related power spectral changes. Finally, I will highlight two particularly promising avenues for

future research that could further solidify the potential of MEG-derived electrophysiological markers for PD.

## Inconsistency in non-invasive electrophysiological research on PD

To provide meaningful markers for PD, MEG research must address the inconsistencies within non-invasive studies but also between non-invasive and invasive studies. Studies investigating oscillatory power changes throughout the entire brain consistently report increases in low-frequency power and decreases in high-frequency power (Boon et al., 2019). However, studies investigating sensorimotor beta power or dynamics yield inconsistent findings (Boon et al., 2019; Underwood & Parr-Brownlie, 2021). Furthermore, these findings are often difficult to reconcile with well-established findings from invasive recordings of the STN or motor cortex. Resolving these inconsistencies is crucial to obtain a clear understanding of how PD affects cortical oscillatory activity and to bridge the gap between non-invasive and invasive electrophysiological research on PD.

Reconciling these inconsistent findings will be very challenging because the variability across studies likely arises from a multitude of disorder-related and disorder-unrelated factors. Identifying these factors, understanding their effects, and implementing measures to mitigate their impact are essential steps to realise the full potential of non-invasive electrophysiological measurements in PD research. In the following, I want to discuss a few of these factors and outline avenues for future research.

## Effects of normalising power spectra on beta power

In the MEG literature, there are variations in whether and how power spectra are normalised. Such normalisations are usually performed by either standardising time courses prior to power spectrum calculation (Chapters 1 to 3) or expressing frequency bin power relative to the overall spectral power (Boon et al., 2023; Stoffers et al., 2007; Wiesman et al., 2023). This normalisation step is usually undertaken to account for variations in the overall power of recorded signals due to differing distances between the signal sources and the sensors (Gross et al., 2013). However, it is worth noting that approaches used to standardise power spectra introduce associations between beta-power values and the peak frequency power (Figure D.1; Figure A4.1 to Figure A4.5).

Considering the well-established finding that theta to low-alpha power is significantly increased throughout the entire brain in PD compared to HCs (Boon et al., 2019, 2023; Bosboom et al., 2006; Soikkeli et al., 1991; Stoffers et al., 2007), standardising power spectra likely results in a mixing of these alterations in peak power and alterations in beta power (Figure D.1). Consequently, this raises the question of whether widespread decreases in beta power, as observed in Chapter 3 and other studies, truly reflect genuine changes in beta power or simply stem from significant group differences in peak power. In line with this, EEG studies on RBD (Rodrigues Brazète et al., 2016) and non-demented PD volunteers (Soikkeli et al., 1991) observed significant increases in absolute and standardised theta power, whereas only standardised, but not absolute, beta power was significantly decreased.

Given the prominent role of beta oscillations and oscillatory slowing in PD, it is crucial to carefully explore the impact of standardising power spectra on beta power, and to establish gold standards for conducting frequency-band power comparisons. Excitingly, new technologies such as optically pumped magnetometers that can be attached to flexible caps or helmets will enable to reduce the variability in the distance between participants' heads and sensors.

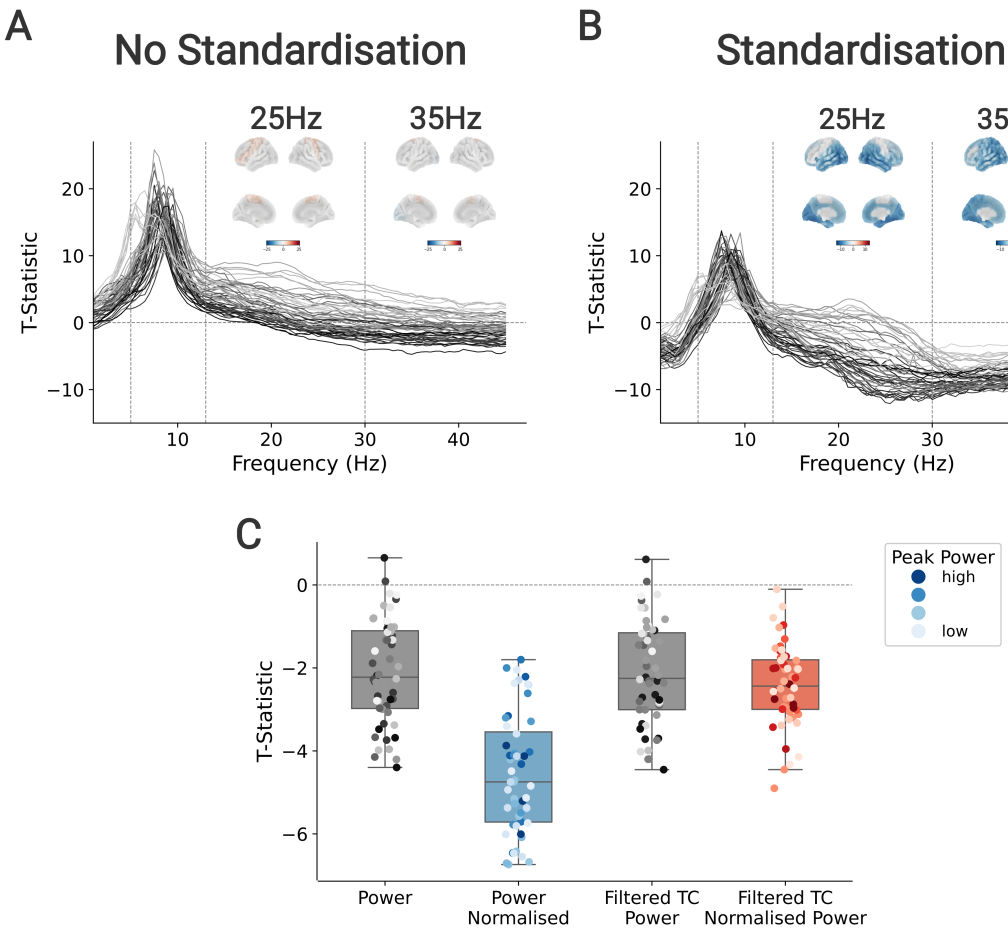


**Figure D.1. Standardising time courses prior to power spectra calculation introduces correlations between unstandardised peak power and beta power, likely mixing peak power and beta-power group differences in comparisons of z-standardised power spectra.** All figures are calculated on the pre-processed

data presented in Chapter 3. **(A)** GLMs assessing frequency bin-wise associations between peak power and frequency-bin power in unstandardised power spectra. Each line represents t-statistics for a single parcel. Parcels with low peak frequency power are depicted in brighter colours, with shades gradually darkening as parcel peak power increases. Surface plots depict t-statistics of parcels that yield significant associations after correcting for multiple comparisons with FDR correction across parcels and frequency bins. **(B)** Similarly, GLMs assessing frequency bin-wise associations between peak power in unstandardised power spectra and frequency-bin power in power spectra calculated from z-standardised time courses. Crucially, beta power calculated from standardised time courses exhibits strong negative associations with unstandardised peak power (B) whereas beta power from unstandardised time courses does not (A). The colours of the lines indicate that negative associations are stronger in parcels with high unstandardised peak power. **(C)** HC vs. PD beta-power group contrasts were calculated for power spectra of unstandardised (grey) and standardised (blue) time courses. Additionally, beta power was calculated from 13 to 30-Hz filtered time courses (grey) and 13 to 30-Hz filtered and z-scored time courses (red) and contrasted between the two groups. Each dot represents the t-statistic at a single parcel. Crucially, calculating beta power from standardised power spectra results in larger group differences between the two groups, which are likely driven by alterations in peak power and beta power. For more detailed analyses see Figure A4.1 to Figure A4.5.

## Understanding how variations in PD volunteers affect MEG measurements

Another factor contributing to inconsistent findings in the non-invasive M/EEG literature lies in the heterogeneity of the PD cohorts. Variations in disease progression, PD subtypes, medication status, and motor state in the scanner can introduce

variability in the measures of interest. In the following, I consider three of these factors and propose potential avenues to address them in future research.

### *Medication status and resting tremor*

Among these factors, only the influence of medication status, particularly levodopa intake, has been investigated. Studies suggest that levodopa intake increases motor cortical beta power (Cao et al., 2020; Heinrichs-Graham, Kurz, et al., 2014; Melgari, 2014; Salenius et al., 2002) thereby normalising beta-power decreases relative to HCs (Heinrichs-Graham, Kurz, et al., 2014). To validate whether decreased beta power during the off-medication condition truly reflects the brain's response to the drug, it may be important to assess the volunteers' discomfort and motor state while they are in the scanner.

In particular, resting tremors occurring during the off-medication condition are a potential confound, as concurrent tremors have been observed to decrease motor cortical beta power (Hirschmann et al., 2013; Qasim et al., 2016). PD volunteers in the analysed PD dataset were included based on low UPDRS-tremor scores to reduce the risk of tremors during the scans. Additionally, electromyogram (EMG) signals were qualitatively assessed to ensure that strong tremor activity was absent during scans. Future studies simultaneously recording EMG and MEG (similar to our approach) should qualitatively inspect EMG signals for signs of tremor. Alternatively, extracting quantitative markers of tremor activity could be beneficial as confound regressors to control for the influence of resting tremors on motor cortical beta-power decreases in off-medication conditions.

*Disease Progression, dopaminergic system pathology, and DBS-surgery*

Other variables such as disease progression or levodopa equivalent dosage (LED) scores are rarely considered, despite their potential contribution to inconsistencies between non-invasive MEG studies (Boon et al., 2019) or between MEG studies and invasive Electrocorticography (EcOG) or Deep Brain Stimulation (DBS) studies.

DBS surgery typically becomes an option for the treatment of PD symptoms when PD patients develop dyskinesia or experience the 'wearing off' of initially effective dopaminergic medication over the course of the disease, resulting in motor symptoms impacting their quality of life (Armstrong & Okun, 2020; Bloem et al., 2021). As a result, PD patients undergoing DBS surgery are typically at more advanced disease stages, when medication alone no longer provides sufficient symptom control.

This has two important implications for comparisons between invasive DBS or ECoG studies and non-invasive M/EEG studies on PD:

- **PD samples in invasive studies may be more homogenous due to qualification criteria for DBS surgery.**
- **PD volunteers included in invasive studies are likely in more advanced disease stages and receive higher medication dosages.** Figure D.2 (see also Table A1 & Figure A1.1), depicting years since diagnosis, UPDRS scores on- and off-medication, and LED scores of all studies referenced in the introduction of Chapter 1, provides evidence for this notion. Crucially, invasive studies investigated more progressed PD volunteers (>8 years disease duration),

whereas the majority of non-invasive studies focused on early-stage PD volunteers (<5 years disease duration).

Interestingly, 'wearing off' effects of dopaminergic medication have been discussed to reflect pathophysiological changes in the striatal dopaminergic system, i.e. loss of the long-time responses to dopaminergic drugs, a reduction in pre- and post-synaptic storage capacity for extra dopamine, or strong fluctuations in striatal dopamine levels due to levodopa intake (Chou et al., 2018). Thus, it seems likely that PD patients included in invasive studies exhibit more severe pathology in the striatal dopaminergic system, which likely contributes to inconsistencies between invasive and non-invasive studies. Additionally, variability in non-invasive studies may be introduced by the inclusion of PD volunteers with varying disease progressions that likely exhibit varying degrees of pathophysiological changes in the striatal dopaminergic system.

The fact that early-stage PD patients do not undergo DBS surgery highlights an important potential of non-invasive electrophysiological recordings: the ability to assess cortical oscillatory power throughout the entire course of the disease, from earliest to most advanced stages, and in volunteers that do not require or are ineligible for surgery. Surprisingly, oscillatory power of PD volunteers at progressed disease stages (>5 years) is rarely studied with M/EEG, despite its feasibility. Cross-sectional assessments of PD volunteers at various disease stages or longitudinal studies with frequent follow-up measurements could shed light on how widespread theta power and motor cortical beta power are affected across different disease stages.

Furthermore, studies testing progressed PD volunteers who have not undergone DBS surgery may help clarify whether the observed increase in motor cortical beta power in patients with DBS surgery (Crowell et al., 2012; O'Keeffe et al., 2020; Pauls et al., 2022) generalises to volunteers who have not had the surgery, or group comparisons of noninvasively recorded power between PD volunteers and HCs. Interestingly, the only two studies that compared non-invasive recordings of PD volunteers prior to DBS surgery (> 9.9 years disease duration) with HCs did not report significant changes in beta power in central brain regions (Cao et al., 2015, 2017). In contrast to this, the only study comparing motor cortical beta bursts obtained from non-invasive recordings between HCs and PD volunteers who underwent DBS surgery observed increased burst amplitudes and lifetimes in PD (Pauls et al., 2022), suggesting elevated levels of motor cortical beta power. This discrepancy may imply that there are systematic differences in motor cortical beta power between progressed PD volunteers who underwent DBS surgery and those who did not. However, it is important to note that the studies on PD volunteers prior to DBS surgery had a coarse spatial resolution (frontal, central, temporal, and occipital areas) (Cao et al., 2015, 2017), making it difficult to draw clear conclusions about motor cortical beta power. Future studies investigating alterations in motor cortical beta power in progressed PD volunteers should aim to clarify whether changes in non-invasively recorded motor cortical beta power are consistent in both progressed PD volunteers with and without DBS surgery.

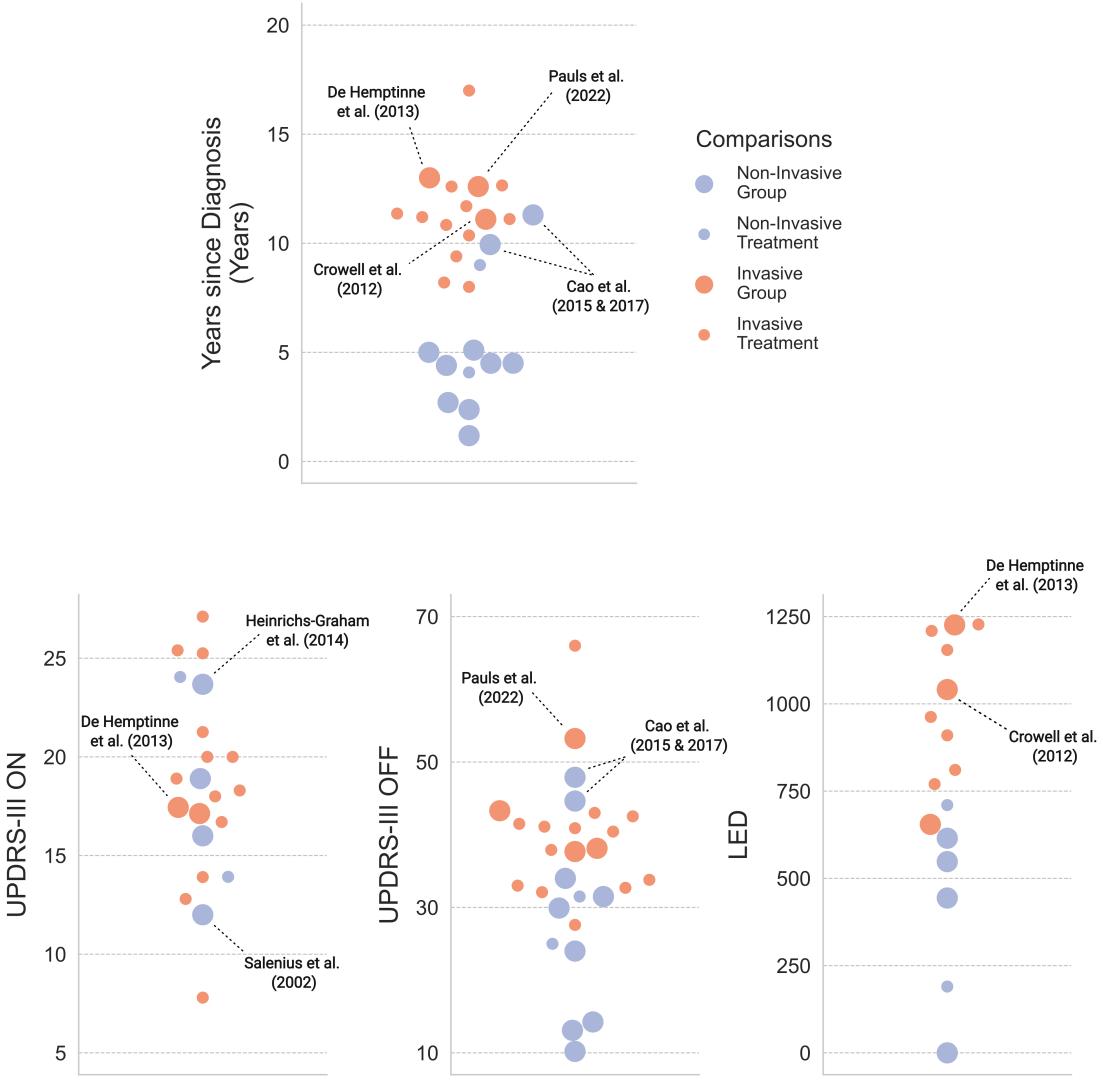


**Figure D.2. Overview of clinical variables across all studies on beta oscillations in the basal ganglia-thalamocortical loop and motor cortex referenced in the introduction of Chapter 1.** Years since diagnosis, UPDRS-III scores on- and off-medication, and levodopa equivalent dose (LED) scores were extracted from all papers. Each paper that provided average values or a table with values for the respective metric was included in these figures. Dot colours indicate whether included participants underwent an invasive DBS or EcOG surgery (purple) or not (red). Large dots represent studies that conducted group contrasts between HCs and PD volunteers, while smaller dost indicate studies in which the effect of either dopaminergic medication or DBS was investigated. For a detailed

description of the creation and discussion of the figure see Table A1 and Figure A1.1.

### *Sample sizes and replication in openly available data sets*

Another factor likely contributing to the variability of findings across various studies are the often very small sample sizes (including Chapter 2) due to complex recruitment procedures for patients and high scanning costs. Crucially, in recent years openly available datasets of MEG recordings of large PD and HC samples during rest and task performance have been published (Niso et al., 2016; Vinding, Eriksson, et al., 2024). Even though variations of above-discussed factors between samples and the openly available datasets should be considered, these datasets pose a great opportunity to replicate study findings in independent, large datasets. Such replications will hopefully help to clarify inconsistencies in the literature.

## Precise descriptions of PD-related electrophysiological alterations

Large parts of the present thesis, as well as the electrophysiological literature on PD, focus on altered frequency band power as a signature for PD. However, other markers such as peak frequencies (Iskhakova et al., 2021), functional connectivity (Olde Dubbelink, Stoffers, Deijen, Twisk, Stam, Hillebrand, et al., 2013; Yassine et al., 2022), signal complexity (Averna et al., 2023), and dynamics of bursts (Pauls et al., 2022; Vinding et al., 2020), or large-scale networks (Chapters 1 and 2) have also been discussed. It may be that inconsistencies in the literature on motor cortical electrophysiological alterations result from the fact that oscillatory power variations

do not provide an optimal operationalisation of PD-related changes. In the following, paragraphs I will highlight four aspects that may enable to capture PD-related alterations more precisely.

## Peak frequency as a marker for dopaminergic functioning in PD?

In Chapter 2, I observed significant alterations in peak frequencies within sensorimotor networks across two distinct datasets. Crucially, variations in the peak frequency of beta oscillations have been discussed as potential markers of dopaminergic tone in both non-human primates and PD volunteers, whereas power or phase-amplitude coupling were not systematically associated with dopaminergic tone (Iskhakova et al., 2021). Consequently, peak frequencies of motor cortical beta oscillations may be a more precise marker of dopaminergic functioning in PD and should be systematically explored in future research.

## Supplementary Motor Area (SMA) as window to pathological cortico-basal ganglia hyperconnectivity?

Another important aspect that needs to be considered when investigating cortical oscillatory signatures related to basal ganglia-thalamocortical loop functioning in PD, is the spatial resolution with which sensorimotor areas are investigated. Hypersynchronisation between the STN and supplementary motor areas (SMA) via the hyperdirect pathway has been implicated to play an important role in PD pathology (Oswal et al., 2021). Consequently, it may be crucial to specifically target sensorimotor areas such as the SMA or mesial motor cortex to focus on regions implicated in PD-related subcortical-cortical pathological changes. M/EEG analyses using parcellations with sufficient granularity to target these regions, e.g., with a finer-grained description

of sensorimotor regions (Kohl et al., 2023), will be important to focus on cortical regions involved in subcortical-cortical hyperconnectivity. Alternatively, defining a specific cortical region of interest from simultaneous STN-MEG recordings that demonstrates hypersynchronisation with STN might provide an effective window to subcortical electrophysiological hallmarks of PD.

Similarly, identifying and isolating dynamic cortical networks that reflect the cortical counterpart of exaggerated synchronisation between STN and mesial motor cortex or SMA (Litvak et al., 2011, 2021; Oswal et al., 2016, 2021), might provide temporal windows in which effects of PD-related subcortical-cortical hyperactivity can be measured in the cortex.

### Capturing PD-related changes of alpha/theta oscillations

Qualitative comparisons of group power spectra between HCs and individuals with PD indicate an increase in power of the dominant alpha peak, while its peak frequency appears to slow down from alpha to low alpha or theta frequencies in individuals with PD (e.g., Figure 1.4). However, PD-related changes in oscillatory activity are usually operationalised in terms of power in generic frequency bands (Bosboom et al., 2006; Hall et al., 2014; Heinrichs-Graham, Kurz, et al., 2014; Olde Dubbelink, Stoffers, Deijen, Twisk, Stam, & Berendse, 2013; Pollok et al., 2012; Stoffers et al., 2007; Vinding, Waldthaler, et al., 2024; Wiesman et al., 2023). Thus, this pattern of alpha oscillatory change is indirectly measured by observing theta power increases in PD that actually reflect a slowing of alpha oscillations into the theta range. Crucially, this indirect description cannot distinguish between slowing of the peak frequency and increasing of peak frequency power which can be both observed in PD. A more precise

description of this pattern will better capture PD-related changes in cortical oscillatory activity, and thereby provide improved means to describe pathological changes in PD.

Interestingly, qualitative observations of power spectra presented in longitudinal studies of PD volunteers (Boon et al., 2023; Olde Dubbelink, Stoffers, Deijen, Twisk, Stam, & Berendse, 2013) suggest that disease progression results in increasing slowing of peak frequency, while peak power is not changed or even decreased. One caution, however, is that peak power was not quantified in these two studies, thus restricting interpretability. Future research should assess whether alterations in peak frequency slowing and peak frequency power covary and thus, likely reflect the same underpinning pathological processes. In general, efforts aimed at capturing this pattern of change more precisely will provide better makers of cortical oscillatory activity that reflect PD pathology, particularly associated with impaired cognition (Boon et al., 2019; Caviness et al., 2007; Geraedts et al., 2018; Olde Dubbelink et al., 2014).

### Continuous Rather Than Bursting Large-Scale Network Perspective

Finally, careful consideration of brain processes captured in large-scale network descriptions may be crucial for improving our mechanistic understanding of brain activity changes in PD. Theories on communication between brain areas propose that network formation is realised through phase-locking periodic fluctuations in neuronal excitability across different regions (Fries, 2005). Phase-locked excitability rhythms between brain areas result in common periods of increased excitability, facilitating communication while preventing interaction with other areas whose excitation phases do not align. Findings from Chapters 1 and 2 suggest that describing brain activity in

terms of transient and mutually exclusive large-scale networks is useful for distinguishing HCs from PD volunteers. Lifetimes of these large-scale networks identified with the TDE-HMM typically range between 50 and 100 ms, capturing only single cycles of alpha and beta oscillations or parts of cycles of theta and delta oscillations. Consequently, 50 to 100 ms occurrences of networks with low frequency (>10 Hz) oscillatory activity and coherence are challenging to explain within the context of theories on communication within the brain.

This contradiction can be reconciled by assuming that large-scale networks are continuously active with varying degrees of activation strength, rather than activating only for short periods (Deco & Corbetta, 2011; Deco & Jirsa, 2012). The HMM's description of continuous data in terms of mutually exclusive states cannot accurately capture these simultaneous activity patterns. In this scenario, short TDE-HMM network visits would reflect moments of strongest network activations, i.e., when a particular network is more strongly activated than all other identified networks. Therefore, the 50 to 100ms lifetimes of large-scale networks would not imply that the networks activate only for these brief periods. Instead, they indicate how long a certain network remains more strongly activated than other simultaneously active networks.

Careful interpretation of large-scale networks inferred with TDE-HMMs and brain processes that they may capture might lead to a more precise perspective on large-scale network alterations in PD. Additionally, this could motivate the use of methods such as DyNeMo (Gohil et al., 2022), which describe brain activity in terms of continuously and simultaneously active networks, potentially capturing brain processes more accurately.

## Disentangling simultaneously occurring pathological changes

In Chapter 3, I observed changes in time-averaged cortical oscillatory and aperiodic activity in both PD and RBD volunteers. RBD volunteers demonstrated significantly increased theta power in occipital, inferior temporal, and inferior frontal areas, whereas occipital beta power was increased. In contrast, PD volunteers demonstrated widespread increases in theta power and decreases in beta power. Various factors, including changes in neurotransmitter systems (Bosboom et al., 2009; Wiesman et al., 2023, 2024), thalamocortical interactions and 1/f-Slopes (Boon et al., 2020), and the accumulation of local protein pathology (Ranasinghe et al., 2020; Wiesman et al., 2022) or neurodegeneration (Van Schependom et al., 2021), have been discussed to influence cortical oscillatory activity. Since PD-pathology likely affects various of these processes, it will be crucial to improve our understanding of how their alterations impact cortical oscillatory activity. Pharmaco-MEG or multimodal studies capable of mimicking or quantifying these pathological processes (Bosboom et al., 2009; Wiesman et al., 2024) and linking them to cortical spatiotemporal oscillatory patterns will be crucial for this endeavour. Delineating distinct cortical oscillatory patterns associated with specific pathological processes may help guide interpretation of findings across studies and disorders, and potentially define sensitive and disorder-specific markers.

## Embedding subcortical literature into cortical network context

Another crucial endeavour will be to link well-established findings in invasive STN recordings to non-invasive recordings of cortical oscillatory activity. Research on electrophysiological STN activity identified low-beta hypersychronisation, underpinned

by prolonged low-beta bursts, as an electrophysiological hallmark of PD (Brown et al., 2001; Eusebio et al., 2011; Hammond et al., 2007; Lofredi et al., 2023; Oswal et al., 2016; Tinkhauser, Pogosyan, Little, et al., 2017; Tinkhauser, Pogosyan, Tan, et al., 2017). Despite demonstrating temporal overlaps between beta bursts in STN and motor cortex (Tinkhauser et al., 2018), it remains an open question how subcortical pathological hallmarks affect widespread patterns of cortical oscillatory activation.

Excitingly, various studies demonstrated significant high-beta coherence between STN and mesial motor regions and the SMA (Litvak et al., 2011, 2021; Oswal et al., 2016, 2021), which potentially contributes to low-beta hypersynchronisation in the STN (Oswal et al., 2021). Considering this link between cortical activity and subcortical oscillatory signatures of PD, future research should attempt to identify cortical activation patterns associated with synchronisation between STN and cortex (Litvak et al., 2021).

In Chapter 1, I demonstrated that the large-scale network context of motor cortical activations may be crucial to dissect motor cortical activations related to PD. Similarly, identifying large-scale networks linked to STN beta bursts may help to dissect motor cortical activations related to STN activity from unrelated activations. Furthermore, I observed significant relationships between motor symptom severity scores and beta bursts co-occurring with a brain state associated with increased synchronisation between motor cortex and all other regions. Given that motor cortical high beta coherence during occurrences of this state was increased in the PD group, I hypothesised that hypersychonisation between STN and sensorimotor areas may be embedded in a cortical state with low oscillatory power but widespread

hypersynchronisation. Future studies analysing simultaneous STN-MEG recordings could test this hypothesis by time-locking large-scale network occurrences to STN beta burst occurrences or investigating temporal overlaps between STN beta bursts and large-scale network occurrences.

Establishing cortical patterns associated with STN-cortex hypersynchronisation may provide non-invasive markers for subcortical dysfunction that could be measured from the earliest stages of PD. Such markers would enable to track the progression of basal-ganglia dysfunction across the disease duration. Additionally, large-scale networks associated with STN-cortex connectivity may offer promising spatiotemporal windows for non-invasive stimulation targeting STN activity via the hyperdirect pathway.

## Conclusion

The present thesis demonstrates significant alterations in cortical oscillatory activity measured non-invasively with MEG in Parkinson's Disease. These alterations manifest as persistent changes in 1/f-Slopes, theta, or beta power and dynamic or spectral features of sensorimotor networks, likely reflecting distinct pathological changes in PD. Excitingly, patterns of altered theta and beta power, along with 1/f-Slopes, were observed in both PD and RBD volunteers, particularly in occipital, inferior frontal, and inferior temporal regions. These cortical oscillatory signatures hold promise as markers for prodromal stages of alpha-synucleinopathies, including PD, that may facilitate the development of drugs and enable earlier treatment for PD patients. Further research, including replication of these findings and clarification of inconsistencies in non-

invasive research on PD, is necessary to solidify the potential of these signatures as non-invasive electrophysiological markers of PD.

# References

Aarsland, D., Batzu, L., Halliday, G. M., Geurtsen, G. J., Ballard, C., Ray Chaudhuri, K., & Weintraub, D. (2021). Parkinson disease-associated cognitive impairment. *Nature Reviews Disease Primers*, *7*(1), 47. https://doi.org/10.1038/s41572-021-00280-3

Abbasi, O., Hirschmann, J., Storzer, L., Özkurt, T. E., Elben, S., Vesper, J., Wojtecki, L., Schmitz, G., Schnitzler, A., & Butz, M. (2018). Unilateral deep brain stimulation suppresses alpha and beta oscillations in sensorimotor cortices. *NeuroImage*, *174*, 201–207. https://doi.org/10.1016/j.neuroimage.2018.03.026

Abbruzzese, G., & Berardelli, A. (2003). Sensorimotor integration in movement disorders. *Movement Disorders*, *18*(3), 231–240. https://doi.org/10.1002/mds.10327

Adamovich, S. V., Berkinblit, M. B., Hening, W., Sage, J., & Poizner, H. (2001). The interaction of visual and proprioceptive inputs in pointing to actual and remembered targets in Parkinson's disease. *Neuroscience*, *104*(4), 1027–1041. https://doi.org/10.1016/S0306-4522(01)00099-9

Adams-Carr, K. L., Bestwick, J. P., Shribman, S., Lees, A., Schrag, A., & Noyce, A. J. (2016). Constipation preceding Parkinson's disease: A systematic review and meta-analysis. *Journal of Neurology, Neurosurgery & Psychiatry*, *87*(7), 710–716. https://doi.org/10.1136/jnnp-2015-311680

Alegre, M., Labarga, A., Gurtubay, I. G., Iriarte, J., Malanda, A., & Artieda, J. (2002). Beta electroencephalograph changes during passive movements: Sensory afferences contribute to beta event-related desynchronization in humans. *Neuroscience Letters*, *331*(1), 29–32. https://doi.org/10.1016/S0304-3940(02)00825-X

Androulidakis, A. G., Doyle, L. M. F., Gilbertson, T. P., & Brown, P. (2006). Corrective movements in response to displacements in visual feedback are more effective during periods of 13-35 Hz oscillatory synchrony in the human corticospinal system. *European Journal of Neuroscience*, *24*(11), 3299–3304. https://doi.org/10.1111/j.1460-9568.2006.05201.x

Androulidakis, A. G., Doyle, L. M. F., Yarrow, K., Litvak, V., Gilbertson, T. P., & Brown, P. (2007). Anticipatory changes in beta synchrony in the human corticospinal system and associated improvements in task performance. *European Journal of Neuroscience*, *25*(12), 3758–3765. https://doi.org/10.1111/j.1460-9568.2007.05620.x

Archambault, P. S., Ferrari-Toniolo, S., Caminiti, R., & Battaglia-Mayer, A. (2015). Visually-guided correction of hand reaching movements: The neurophysiological bases in the cerebral cortex. *Vision Research*, *110*, 244–256. https://doi.org/10.1016/j.visres.2014.09.009

Armstrong, M. J., & Okun, M. S. (2020). Diagnosis and Treatment of Parkinson Disease: A Review. *JAMA*, *323*(6), 548. https://doi.org/10.1001/jama.2019.22360

Averna, A., Coelli, S., Ferrara, R., Cerutti, S., Priori, A., & Bianchi, A. M. (2023). Entropy and fractal analysis of brain-related neurophysiological signals in Alzheimer's and Parkinson's disease. *Journal of Neural Engineering*, *20*(5), 051001. https://doi.org/10.1088/1741-2552/acf8fa

Baker, S. N. (2007). Oscillatory interactions between sensorimotor cortex and the periphery. *Current Opinion in Neurobiology*, *17*(6), 649–655. https://doi.org/10.1016/j.conb.2008.01.007

Bang, Y. R., Jeon, H. J., Youn, S., & Yoon, I.-Y. (2017). Alterations of awake EEG in idiopathic REM sleep behavior disorder without cognitive impairment. *Neuroscience Letters*, *637*, 64–69. https://doi.org/10.1016/j.neulet.2016.11.052

Barber, T. R., Griffanti, L., Muhammed, K., Drew, D. S., Bradley, K. M., McGowan, D. R., Crabbe, M., Lo, C., Mackay, C. E., Husain, M., Hu, M. T., & Klein, J. C. (2018). Apathy in rapid eye movement sleep behaviour disorder is associated with serotonin depletion in the dorsal raphe nucleus. *Brain*, *141*(10), 2848–2854. https://doi.org/10.1093/brain/awy240

Barber, T. R., Klein, J. C., Mackay, C. E., & Hu, M. T. M. (2017). Neuroimaging in pre-motor Parkinson's disease. *NeuroImage: Clinical*, *15*, 215–227. https://doi.org/10.1016/j.nicl.2017.04.011

Barnes, G. R., Hillebrand, A., Fawcett, I. P., & Singh, K. D. (2004). Realistic spatial sampling for MEG beamformer images. *Human Brain Mapping*, *23*(2), 120–127. https://doi.org/10.1002/hbm.20047

Barone, J., & Rossiter, H. E. (2021). Understanding the Role of Sensorimotor Beta Oscillations. *Frontiers in Systems Neuroscience*, *15*, 655886. https://doi.org/10.3389/fnsys.2021.655886

Battaglia-Mayer, A., Buiatti, T., Caminiti, R., Ferraina, S., Lacquaniti, F., & Shallice, T. (2014). Correction and suppression of reaching movements in the cerebral cortex: Physiological and neuropsychological aspects. *Neuroscience & Biobehavioral Reviews*, *42*, 232–251. https://doi.org/10.1016/j.neubiorev.2014.03.002

Bedard, M.-A., Aghourian, M., Legault-Denis, C., Postuma, R. B., Soucy, J.-P., Gagnon, J.-F., Pelletier, A., & Montplaisir, J. (2019). Brain cholinergic alterations in idiopathic REM sleep behaviour disorder: A PET imaging study with 18F-FEOBV. *Sleep Medicine*, *58*, 35–41. https://doi.org/10.1016/j.sleep.2018.12.020

Berg, D., Borghammer, P., Fereshtehnejad, S.-M., Heinzel, S., Horsager, J., Schaeffer, E., & Postuma, R. B. (2021). Prodromal Parkinson disease subtypes—Key to understanding heterogeneity. *Nature Reviews Neurology*, *17*(6), 349–361. https://doi.org/10.1038/s41582-021-00486-9

Berg, D., Postuma, R. B., Adler, C. H., Bloem, B. R., Chan, P., Dubois, B., Gasser, T., Goetz, C. G., Halliday, G., Joseph, L., Lang, A. E., Liepelt-Scarfone, I., Litvan, I., Marek, K., Obeso, J., Oertel, W., Olanow, C. W., Poewe, W., Stern, M., & Deuschl, G. (2015). MDS research criteria for prodromal Parkinson's disease: MDS Criteria for Prodromal PD. *Movement Disorders*, *30*(12), 1600–1611. https://doi.org/10.1002/mds.26431

Bloem, B. R., Okun, M. S., & Klein, C. (2021). Parkinson's disease. *The Lancet*, *397*(10291), 2284–2303. https://doi.org/10.1016/S0140-6736(21)00218-X

Boeve, B. F. (2010). REM sleep behavior disorder: Updated review of the core features, the REM sleep behavior disorder-neurodegenerative disease association, evolving concepts, controversies, and future directions. *Annals of the New York Academy of Sciences*, *1184*(1), 15–54. https://doi.org/10.1111/j.1749-6632.2009.05115.x

Boon, L. I., Geraedts, V. J., Hillebrand, A., Tannemaat, M. R., Contarino, M. F., Stam, C. J., & Berendse, H. W. (2019). A systematic review of MEG-based studies in Parkinson's disease: The motor system and beyond. *Human Brain Mapping*, *40*(9), 2827–2848. https://doi.org/10.1002/hbm.24562

Boon, L. I., Hillebrand, A., Potters, W. V., de Bie, R. M. A., Prent, N., Bot, M., Schuurman, P. R., Stam, C. J., van Rootselaar, A.-F., & Berendse, H. W. (2020). Motor effects of deep brain stimulation correlate with increased functional connectivity in Parkinson's disease: An MEG study. *NeuroImage: Clinical*, *26*, 102225. https://doi.org/10.1016/j.nicl.2020.102225

Boon, L. I., Hillebrand, A., Schoonheim, M. M., Twisk, J. W., Stam, C. J., & Berendse, H. W. (2023). Cortical and Subcortical Changes in MEG Activity Reflect Parkinson's Progression over a Period of 7 Years. *Brain Topography*, *36*(4), 566–580. https://doi.org/10.1007/s10548-023-00965-w

Borghammer, P. (2021). The α-Synuclein Origin and Connectome Model (SOC Model) of Parkinson's Disease: Explaining Motor Asymmetry, Non-Motor Phenotypes,

and Cognitive Decline. *Journal of Parkinson's Disease*, *11*(2), 455–474. https://doi.org/10.3233/JPD-202481

Bosboom, J. L. W., Stoffers, D., Stam, C. J., Berendse, H. W., & Wolters, E. Ch. (2009). Cholinergic modulation of MEG resting-state oscillatory activity in Parkinson's disease related dementia. *Clinical Neurophysiology*, *120*(5), 910–915. https://doi.org/10.1016/j.clinph.2009.03.004

Bosboom, J. L. W., Stoffers, D., Stam, C. J., van Dijk, B. W., Verbunt, J., Berendse, H. W., & Wolters, E. Ch. (2006). Resting state oscillatory brain dynamics in Parkinson's disease: An MEG study. *Clinical Neurophysiology*, *117*(11), 2521–2531. https://doi.org/10.1016/j.clinph.2006.06.720

Braak, H., Tredici, K. D., Rüb, U., de Vos, R. A. I., Jansen Steur, E. N. H., & Braak, E. (2003). Staging of brain pathology related to sporadic Parkinson's disease. *Neurobiology of Aging*, *24*(2), 197–211. https://doi.org/10.1016/S0197-4580(02)00065-9

Brittain, J., Sharott, A., & Brown, P. (2014). The highs and lows of beta activity in cortico-basal ganglia loops. *European Journal of Neuroscience*, *39*(11), 1951–1959. https://doi.org/10.1111/ejn.12574

Bronstein, A. M., Hood, J. D., Gresty, M. A., & Panagi, C. (1990). VISUAL CONTROL OF BALANCE IN CEREBELLAR AND PARKINSONIAN SYNDROMES. *Brain*, *113*(3), 767–779. https://doi.org/10.1093/brain/113.3.767

Brooks, D. J., & Pavese, N. (2011). Imaging biomarkers in Parkinson's disease. *Progress in Neurobiology*, *95*(4), 614–628. https://doi.org/10.1016/j.pneurobio.2011.08.009

Brown, P., Oliviero, A., Mazzone, P., Insola, A., Tonali, P., & Di Lazzaro, V. (2001). Dopamine Dependency of Oscillations between Subthalamic Nucleus and Pallidum in Parkinson's Disease. *The Journal of Neuroscience*, *21*(3), 1033–1038. https://doi.org/10.1523/JNEUROSCI.21-03-01033.2001

Buzsáki, G., & Draguhn, A. (2004). Neuronal Oscillations in Cortical Networks. *Science*, *304*(5679), 1926–1929. https://doi.org/10.1126/science.1099745

Campbell, M. C., Koller, J. M., Snyder, A. Z., Buddhala, C., Kotzbauer, P. T., & Perlmutter, J. S. (2015). CSF proteins and resting-state functional connectivity in Parkinson disease. *Neurology*, *84*(24), 2413–2421. https://doi.org/10.1212/WNL.0000000000001681

Cao, C., Li, D., Jiang, T., Ince, N. F., Zhan, S., Zhang, J., Sha, Z., & Sun, B. (2015). Resting State Cortical Oscillations of Patients With Parkinson Disease and With and Without Subthalamic Deep Brain Stimulation: A Magnetoencephalography Study. *Journal of Clinical Neurophysiology*, *32*(2), 109–118. https://doi.org/10.1097/WNP.0000000000000137

Cao, C., Li, D., Zhan, S., Zhang, C., Sun, B., & Litvak, V. (2020). L-dopa treatment increases oscillatory power in the motor cortex of Parkinson's disease patients. *NeuroImage: Clinical*, *26*, 102255. https://doi.org/10.1016/j.nicl.2020.102255

Cao, C., Zeng, K., Li, D.-Y., Zhan, S.-K., Li, X.-L., & Sun, B.-M. (2017). Modulations on cortical oscillations by subthalamic deep brain stimulation in patients with Parkinson disease: A MEG study. *Neuroscience Letters*, *636*, 95–100. https://doi.org/10.1016/j.neulet.2016.11.009

Cassim, F., Monaca, C., Szurhaj, W., Bourriez, J.-L., Defebvre, L., Derambure, P., & Guieu, J.-D. (2001). Does post-movement beta synchronization reflect an idling motor cortex?: *Neuroreport*, *12*(17), 3859–3863. https://doi.org/10.1097/00001756-200112040-00051

Castellanos, G., Fernández-Seara, M. A., Lorenzo-Betancor, O., Ortega-Cubero, S., Puigvert, M., Uranga, J., Vidorreta, M., Irigoyen, J., Lorenzo, E., Muñoz-Barrutia, A., Ortiz-de-Solorzano, C., Pastor, P., & Pastor, M. A. (2015). Automated Neuromelanin Imaging as a Diagnostic Biomarker for Parkinson's Disease. *Movement Disorders*, *30*(7), 945–952. https://doi.org/10.1002/mds.26201

Caviness, J. N., Hentz, J. G., Evidente, V. G., Driver-Dunckley, E., Samanta, J., Mahant, P., Connor, D. J., Sabbagh, M. N., Shill, H. A., & Adler, C. H. (2007). Both early and late cognitive dysfunction affects the electroencephalogram in Parkinson's disease. *Parkinsonism & Related Disorders*, *13*(6), 348–354. https://doi.org/10.1016/j.parkreldis.2007.01.003

Caviness, J. N., Lue, L.-F., Hentz, J. G., Schmitz, C. T., Adler, C. H., Shill, H. A., Sabbagh, M. N., Beach, T. G., & Walker, D. G. (2016). Cortical phosphorylated α-Synuclein levels correlate with brain wave spectra in Parkinson's disease: Biochemical

Correlates of Brain Waves. *Movement Disorders*, *31*(7), 1012–1019. https://doi.org/10.1002/mds.26621

Chandrasekaran, C., Bray, I. E., & Shenoy, K. V. (2019). Frequency Shifts and Depth Dependence of Premotor Beta Band Activity during Perceptual Decision-Making. *The Journal of Neuroscience*, *39*(8), 1420–1435. https://doi.org/10.1523/JNEUROSCI.1066-18.2018

Chaudhuri, K. R., Healy, D. G., & Schapira, A. H. (2006). Non-motor symptoms of Parkinson's disease: Diagnosis and management. *The Lancet Neurology*, *5*(3), 235–245. https://doi.org/10.1016/S1474-4422(06)70373-8

Checkoway, H., Lundin, J. I., & Kelada, S. N. (2011). Neurodegenerative diseases. In *Application of Biomarkers to Disease* (1–5, pp. 407–420).

Cheng, H.-C., Ulane, C. M., & Burke, R. E. (2010). Clinical progression in Parkinson disease and the neurobiology of axons. *Annals of Neurology*, *67*(6), 715–725. https://doi.org/10.1002/ana.21995

Chilvers, M. J., Hawe, R. L., Scott, S. H., & Dukelow, S. P. (2021). Investigating the neuroanatomy underlying proprioception using a stroke model. *Journal of the Neurological Sciences*, *430*, 120029. https://doi.org/10.1016/j.jns.2021.120029

Chou, K. L., Stacy, M., Simuni, T., Miyasaki, J., Oertel, W. H., Sethi, K., Fernandez, H. H., & Stocchi, F. (2018). The spectrum of "off" in Parkinson's disease: What have we learned over 40 years? *Parkinsonism & Related Disorders*, *51*, 9–16. https://doi.org/10.1016/j.parkreldis.2018.02.001

Chung, J. W., Ofori, E., Misra, G., Hess, C. W., & Vaillancourt, D. E. (2017). Beta-band activity and connectivity in sensorimotor and parietal cortex are important for accurate motor performance. *NeuroImage*, *144*, 164–173. https://doi.org/10.1016/j.neuroimage.2016.10.008

Clower, D. M., Hoffman, J. M., Votaw, J. R., Faber, T. L., Woods, R. P., & Alexander, G. E. (1996). Role of posterior parietal cortex in the recalibration of visually guided reaching. *Nature*, *383*(6601), 618–621. https://doi.org/10.1038/383618a0

Cochrane, C. J., & Ebmeier, K. P. (2013). Diffusion tensor imaging in parkinsonian syndromes: A systematic review and meta-analysis. *Neurology*, *80*(9), 857–864. https://doi.org/10.1212/WNL.0b013e318284070c

Cohen, M. X. (2014). *Analyzing Neural Time Series Data: Theory and Practice*. The MIT Press. https://doi.org/10.7551/mitpress/9609.001.0001

Colclough, G. L., Brookes, M. J., Smith, S. M., & Woolrich, M. W. (2015). A symmetric multivariate leakage correction for MEG connectomes. *NeuroImage*, *117*, 439–448. https://doi.org/10.1016/j.neuroimage.2015.03.071

Cole, S., Donoghue, T., Gao, R., & Voytek, B. (2019). NeuroDSP: A package for neural digital signal processing. *Journal of Open Source Software*, *4*(36), 1272. https://doi.org/10.21105/joss.01272

Colombo, M. A., Napolitani, M., Boly, M., Gosseries, O., Casarotto, S., Rosanova, M., Brichant, J.-F., Boveroux, P., Rex, S., Laureys, S., Massimini, M., Chieregato, A., & Sarasso, S. (2019). The spectral exponent of the resting EEG indexes the

presence of consciousness during unresponsiveness induced by propofol, xenon, and ketamine. *NeuroImage*, *189*, 631–644. https://doi.org/10.1016/j.neuroimage.2019.01.024

Connolly, B. S., & Lang, A. E. (2014). Pharmacological Treatment of Parkinson Disease: A Review. *JAMA*, *311*(16), 1670. https://doi.org/10.1001/jama.2014.3654

Coomans, E. M., Schoonhoven, D. N., Tuncel, H., Verfaillie, S. C. J., Wolters, E. E., Boellaard, R., Ossenkoppele, R., Den Braber, A., Scheper, W., Schober, P., Sweeney, S. P., Ryan, J. M., Schuit, R. C., Windhorst, A. D., Barkhof, F., Scheltens, P., Golla, S. S. V., Hillebrand, A., Gouw, A. A., & Van Berckel, B. N. M. (2021). In vivo tau pathology is associated with synaptic loss and altered synaptic function. *Alzheimer's Research & Therapy*, *13*(1), 35. https://doi.org/10.1186/s13195-021-00772-0

Crowell, A. L., Ryapolova-Webb, E. S., Ostrem, J. L., Galifianakis, N. B., Shimamoto, S., Lim, D. A., & Starr, P. A. (2012). Oscillations in sensorimotor cortex in movement disorders: An electrocorticography study. *Brain*, *135*(2), 615–630. https://doi.org/10.1093/brain/awr332

Dammers, J., Schiek, M., Boers, F., Silex, C., Zvyagintsev, M., Pietrzyk, U., & Mathiak, K. (2008). Integration of Amplitude and Phase Statistics for Complete Artifact Removal in Independent Components of Neuromagnetic Recordings. *IEEE Transactions on Biomedical Engineering*, *55*(10), 2353–2362. https://doi.org/10.1109/TBME.2008.926677

Dauer, W., & Przedborski, S. (2003). Parkinson's Disease. *Neuron*, *39*(6), 889–909. https://doi.org/10.1016/S0896-6273(03)00568-3

De Hemptinne, C., Ryapolova-Webb, E. S., Air, E. L., Garcia, P. A., Miller, K. J., Ojemann, J. G., Ostrem, J. L., Galifianakis, N. B., & Starr, P. A. (2013). Exaggerated phase–amplitude coupling in the primary motor cortex in Parkinson disease. *Proceedings of the National Academy of Sciences*, *110*(12), 4780–4785. https://doi.org/10.1073/pnas.1214546110

Deco, G., & Corbetta, M. (2011). The Dynamical Balance of the Brain at Rest. *The Neuroscientist*, *17*(1), 107–123. https://doi.org/10.1177/1073858409354384

Deco, G., & Jirsa, V. K. (2012). Ongoing Cortical Activity at Rest: Criticality, Multistability, and Ghost Attractors. *The Journal of Neuroscience*, *32*(10), 3366–3375. https://doi.org/10.1523/JNEUROSCI.2523-11.2012

Del Tredici, K., & Braak, H. (2012). Lewy pathology and neurodegeneration in premotor Parkinson's disease. *Movement Disorders*, *27*(5), 597–607. https://doi.org/10.1002/mds.24921

Delhaye, B. P., Long, K. H., & Bensmaia, S. J. (2018). Neural Basis of Touch and Proprioception in Primate Cortex. In Y. S. Prakash (Ed.), *Comprehensive Physiology* (1st ed., pp. 1575–1602). Wiley. https://doi.org/10.1002/cphy.c170033

DeMaagd, G., & Philip, A. (2015). Parkinson's Disease and Its Management: Part 1: Disease Entity, Risk Factors, Pathophysiology, Clinical Presentation, and

Diagnosis. *P & T: A Peer-Reviewed Journal for Formulary Management*, *40*(8), 504–532.

Demirci, M., Grill, S., McShane, L., & Hallett, M. (1997). A mismatch between kinesthetic and visual perception in Parkinson's disease. *Annals of Neurology*, *41*(6), 781–788. https://doi.org/10.1002/ana.410410614

Deng, H., Wang, P., & Jankovic, J. (2018). The genetics of Parkinson disease. *Ageing Research Reviews*, *42*, 72–85. https://doi.org/10.1016/j.arr.2017.12.007

Desmurget, M., Epstein, C. M., Turner, R. S., Prablanc, C., Alexander, G. E., & Grafton, S. T. (1999). Role of the posterior parietal cortex in updating reaching movements to a visual target. *Nature Neuroscience*, *2*(6), 563–567. https://doi.org/10.1038/9219

Deuschl, G., Schüpbach, M., Knudsen, K., Pinsker, M. O., Cornu, P., Rau, J., Agid, Y., & Schade-Brittinger, C. (2013). Stimulation of the subthalamic nucleus at an earlier disease stage of Parkinson's disease: Concept and standards of the EARLYSTIM-study. *Parkinsonism & Related Disorders*, *19*(1), 56–61. https://doi.org/10.1016/j.parkreldis.2012.07.004

Devos, D., Labyt, E., Cassim, F., Bourriez, J. L., Reyns, N., Touzet, G., Blond, S., Guieu, J. D., Derambure, P., Destee, A., & Defebvre, L. (2003). Subthalamic stimulation influences postmovement cortical somatosensory processing in Parkinson's disease. *European Journal of Neuroscience*, *18*(7), 1884–1888. https://doi.org/10.1046/j.1460-9568.2003.02925.x

Dib, M. (2005). Issues for Clinical Drug Development in Neurodegenerative Diseases: *Drugs*, *65*(17), 2463–2479. https://doi.org/10.2165/00003495-200565170-00004

Dickson, D. W. (2012). Parkinson's Disease and Parkinsonism: Neuropathology. *Cold Spring Harbor Perspectives in Medicine*, *2*(8), a009258–a009258. https://doi.org/10.1101/cshperspect.a009258

Donoghue, T., Haller, M., Peterson, E. J., Varma, P., Sebastian, P., Gao, R., Noto, T., Lara, A. H., Wallis, J. D., Knight, R. T., Shestyuk, A., & Voytek, B. (2020). Parameterizing neural power spectra into periodic and aperiodic components. *Nature Neuroscience*, *23*(12), 1655–1665. https://doi.org/10.1038/s41593-020-00744-x

Dorsey, E. R., Elbaz, A., Nichols, E., Abbasi, N., Abd-Allah, F., Abdelalim, A., Adsuar, J. C., Ansha, M. G., Brayne, C., Choi, J.-Y. J., Collado-Mateo, D., Dahodwala, N., Do, H. P., Edessa, D., Endres, M., Fereshtehnejad, S.-M., Foreman, K. J., Gankpe, F. G., Gupta, R., … Murray, C. J. L. (2018). Global, regional, and national burden of Parkinson's disease, 1990–2016: A systematic analysis for the Global Burden of Disease Study 2016. *The Lancet Neurology*, *17*(11), 939–953. https://doi.org/10.1016/S1474-4422(18)30295-3

Dorsey, E. R., Sherer, T., Okun, M. S., & Bloem, B. R. (2018). The Emerging Evidence of the Parkinson Pandemic. *Journal of Parkinson's Disease*, *8*(s1), S3–S8. https://doi.org/10.3233/JPD-181474

Dugger, B. N., & Dickson, D. W. (2017). Pathology of Neurodegenerative Diseases. *Cold Spring Harbor Perspectives in Biology*, *9*(7), a028035. https://doi.org/10.1101/cshperspect.a028035

Ehrminger, M., Latimier, A., Pyatigorskaya, N., Garcia-Lorenzo, D., Leu-Semenescu, S., Vidailhet, M., Lehericy, S., & Arnulf, I. (2016). The coeruleus/subcoeruleus complex in idiopathic rapid eye movement sleep behaviour disorder. *Brain*, *139*(4), 1180–1188. https://doi.org/10.1093/brain/aww006

Engel, A. K., & Fries, P. (2010). Beta-band oscillations—Signalling the status quo? *Current Opinion in Neurobiology*, *20*(2), 156–165. https://doi.org/10.1016/j.conb.2010.02.015

Engel, A. K., Fries, P., & Singer, W. (2001). Dynamic predictions: Oscillations and synchrony in top–down processing. *Nature Reviews Neuroscience*, *2*(10), 704–716. https://doi.org/10.1038/35094565

Eusebio, A., Thevathasan, W., Doyle Gaynor, L., Pogosyan, A., Bye, E., Foltynie, T., Zrinzo, L., Ashkan, K., Aziz, T., & Brown, P. (2011). Deep brain stimulation can suppress pathological synchronisation in parkinsonian patients. *Journal of Neurology, Neurosurgery & Psychiatry*, *82*(5), 569–573. https://doi.org/10.1136/jnnp.2010.217489

Fahn, S. (1987). Unified Parkinson's disease rating scale. *Recent Developments in Parkinson's Disease*, 153–163.

Feigin, V. L., Abajobir, A. A., Abate, K. H., Abd-Allah, F., Abdulle, A. M., Abera, S. F., Abyu, G. Y., Ahmed, M. B., Aichour, A. N., Aichour, I., Aichour, M. T. E., Akinyemi, R. O., Alabed, S., Al-Raddadi, R., Alvis-Guzman, N., Amare, A. T., Ansari, H., Anwari, P., Ärnlöv, J., … Vos, T. (2017). Global, regional, and national burden of neurological disorders during 1990–2015: A systematic analysis for the Global Burden of Disease Study 2015. *The Lancet Neurology*, *16*(11), 877–897. https://doi.org/10.1016/S1474-4422(17)30299-5

Feingold, J., Gibson, D. J., DePasquale, B., & Graybiel, A. M. (2015). Bursts of beta oscillation differentiate postperformance activity in the striatum and motor cortex of monkeys performing movement tasks. *Proceedings of the National Academy of Sciences*, *112*(44), 13687–13692. https://doi.org/10.1073/pnas.1517629112

Fereshtehnejad, S.-M., Romenets, S. R., Anang, J. B. M., Latreille, V., Gagnon, J.-F., & Postuma, R. B. (2015). New Clinical Subtypes of Parkinson Disease and Their Longitudinal Progression: A Prospective Cohort Comparison With Other Phenotypes. *JAMA Neurology*, *72*(8), 863. https://doi.org/10.1001/jamaneurol.2015.0703

Fereshtehnejad, S.-M., Yao, C., Pelletier, A., Montplaisir, J. Y., Gagnon, J.-F., & Postuma, R. B. (2019). Evolution of prodromal Parkinson's disease and dementia with Lewy bodies: A prospective study. *Brain*, *142*(7), 2051–2067. https://doi.org/10.1093/brain/awz111

Fox, S. H., Katzenschlager, R., Lim, S., Barton, B., De Bie, R. M. A., Seppi, K., Coelho, M., Sampaio, C., & on behalf of the Movement Disorder Society Evidence-Based Medicine Committee. (2018). International Parkinson and movement disorder society evidence-based medicine review: Update on treatments for the motor symptoms of Parkinson's disease. *Movement Disorders*, *33*(8), 1248–1266. https://doi.org/10.1002/mds.27372

Frauscher, B., Ehrmann, L., & Högl, B. (2013). Defining muscle activities for assessment of rapid eye movement sleep behavior disorder: From a qualitative to a quantitative diagnostic level. *Sleep Medicine*, *14*(8), 729–733. https://doi.org/10.1016/j.sleep.2012.09.028

Fries, P. (2005). A mechanism for cognitive dynamics: Neuronal communication through neuronal coherence. *Trends in Cognitive Sciences*, *9*(10), 474–480. https://doi.org/10.1016/j.tics.2005.08.011

Friston, K. J., Ashburner, J., Kiebel, S., Nichols, T., & Penny, W. (Eds.). (2007). *Statistical parametric mapping: The analysis of funtional brain images* (1st ed). Elsevier/Academic Press.

Gagnon, J.-F., Fantini, M. L., Bedard, M.-A., Petit, D., Carrier, J., Rompre, S., Decary, A., Panisset, M., & Montplaisir, J. (2004). Association between waking EEG slowing and REM sleep behavior disorder in PD without dementia. *Neurology*, *62*(3), 401–406. https://doi.org/10.1212/01.WNL.0000106460.34682.E9

Galbiati, A., Verga, L., Giora, E., Zucconi, M., & Ferini-Strambi, L. (2019). The risk of neurodegeneration in REM sleep behavior disorder: A systematic review and

meta-analysis of longitudinal studies. *Sleep Medicine Reviews*, *43*, 37–46. https://doi.org/10.1016/j.smrv.2018.09.008

Gao, R., Peterson, E. J., & Voytek, B. (2017). Inferring synaptic excitation/inhibition balance from field potentials. *NeuroImage*, *158*, 70–78. https://doi.org/10.1016/j.neuroimage.2017.06.078

Gaveau, V., Pisella, L., Priot, A.-E., Fukui, T., Rossetti, Y., Pélisson, D., & Prablanc, C. (2014). Automatic online control of motor adjustments in reaching and grasping. *Neuropsychologia*, *55*, 25–40. https://doi.org/10.1016/j.neuropsychologia.2013.12.005

Geraedts, V. J., Boon, L. I., Marinus, J., Gouw, A. A., van Hilten, J. J., Stam, C. J., Tannemaat, M. R., & Contarino, M. F. (2018). Clinical correlates of quantitative EEG in Parkinson disease: A systematic review. *Neurology*, *91*(19), 871–883. https://doi.org/10.1212/WNL.0000000000006473

Giguère, N., Burke Nanni, S., & Trudeau, L.-E. (2018). On Cell Loss and Selective Vulnerability of Neuronal Populations in Parkinson's Disease. *Frontiers in Neurology*, *9*, 455. https://doi.org/10.3389/fneur.2018.00455

Gilbertson, T., Lalo, E., Doyle, L., Di Lazzaro, V., Cioni, B., & Brown, P. (2005). Existing Motor State Is Favored at the Expense of New Movement during 13-35 Hz Oscillatory Synchrony in the Human Corticospinal System. *The Journal of Neuroscience*, *25*(34), 7771–7779. https://doi.org/10.1523/JNEUROSCI.1762-05.2005

Glasser, M. F., Coalson, T. S., Robinson, E. C., Hacker, C. D., Harwell, J., Yacoub, E., Ugurbil, K., Andersson, J., Beckmann, C. F., Jenkinson, M., Smith, S. M., & Van Essen, D. C. (2016). A multi-modal parcellation of human cerebral cortex. *Nature*, *536*(7615), 171–178. https://doi.org/10.1038/nature18933

Goetz, C. G., Tilley, B. C., Shaftman, S. R., Stebbins, G. T., Fahn, S., Martinez-Martin, P., Poewe, W., Sampaio, C., Stern, M. B., Dodel, R., Dubois, B., Holloway, R., Jankovic, J., Kulisevsky, J., Lang, A. E., Lees, A., Leurgans, S., LeWitt, P. A., Nyenhuis, D., … LaPelle, N. (2008). Movement Disorder Society-sponsored revision of the Unified Parkinson's Disease Rating Scale (MDS-UPDRS): Scale presentation and clinimetric testing results: MDS-UPDRS: Clinimetric Assessment. *Movement Disorders*, *23*(15), 2129–2170. https://doi.org/10.1002/mds.22340

Gohil, C., Huang, R., Roberts, E., Van Es, M. W., Quinn, A. J., Vidaurre, D., & Woolrich, M. W. (2024). Osl-dynamics, a toolbox for modeling fast dynamic brain activity. *eLife*, *12*, RP91949. https://doi.org/10.7554/eLife.91949.3

Gohil, C., Kohl, O., Huang, R., Van Es, M. W. J., Parker Jones, O., Hunt, L. T., Quinn, A. J., & Woolrich, M. W. (2024). *Dynamic Network Analysis of Electrophysiological Task Data* [Preprint]. Neuroscience. https://doi.org/10.1101/2024.01.12.567026

Gohil, C., Roberts, E., Timms, R., Skates, A., Higgins, C., Quinn, A., Pervaiz, U., van Amersfoort, J., Notin, P., Gal, Y., Adaszewski, S., & Woolrich, M. (2022).

Mixtures of large-scale dynamic functional brain network modes. *NeuroImage*, 119595. https://doi.org/10.1016/j.neuroimage.2022.119595

Gordon, E. M., Chauvin, R. J., Van, A. N., Rajesh, A., Nielsen, A., Newbold, D. J., Lynch, C. J., Seider, N. A., Krimmel, S. R., Scheidter, K. M., Monk, J., Miller, R. L., Metoki, A., Montez, D. F., Zheng, A., Elbau, I., Madison, T., Nishino, T., Myers, M. J., … Dosenbach, N. U. F. (2023). A somato-cognitive action network alternates with effector regions in motor cortex. *Nature*, *617*(7960), 351–359. https://doi.org/10.1038/s41586-023-05964-2

Gramfort, A. (2013). MEG and EEG data analysis with MNE-Python. *Frontiers in Neuroscience*, *7*. https://doi.org/10.3389/fnins.2013.00267

Gross, J. (2019). Magnetoencephalography in Cognitive Neuroscience: A Primer. *Neuron*, *104*(2), 189–204. https://doi.org/10.1016/j.neuron.2019.07.001

Gross, J., Baillet, S., Barnes, G. R., Henson, R. N., Hillebrand, A., Jensen, O., Jerbi, K., Litvak, V., Maess, B., Oostenveld, R., Parkkonen, L., Taylor, J. R., van Wassenhove, V., Wibral, M., & Schoffelen, J.-M. (2013). Good practice for conducting and reporting MEG research. *NeuroImage*, *65*, 349–363. https://doi.org/10.1016/j.neuroimage.2012.10.001

Hall, S. D., Prokic, E. J., McAllister, C. J., Ronnqvist, K. C., Williams, A. C., Yamawaki, N., Witton, C., Woodhall, G. L., & Stanford, I. M. (2014). GABA-mediated changes in inter-hemispheric beta frequency activity in early-stage Parkinson's disease. *Neuroscience*, *281*, 68–76. https://doi.org/10.1016/j.neuroscience.2014.09.037

Hämäläinen, M., Hari, R., Ilmoniemi, R. J., Knuutila, J., & Lounasmaa, O. V. (1993). Magnetoencephalography—Theory, instrumentation, and applications to noninvasive studies of the working human brain. *Reviews of Modern Physics*, *65*(2), 413–497. https://doi.org/10.1103/RevModPhys.65.413

Hammond, C., Bergman, H., & Brown, P. (2007). Pathological synchronization in Parkinson's disease: Networks, models and treatments. *Trends in Neurosciences*, *30*(7), 357–364. https://doi.org/10.1016/j.tins.2007.05.004

Han, C.-X., Wang, J., Yi, G.-S., & Che, Y.-Q. (2013). Investigation of EEG abnormalities in the early stage of Parkinson's disease. *Cognitive Neurodynamics*, *7*(4), 351–359. https://doi.org/10.1007/s11571-013-9247-z

Hanakawa, T., Dimyan, M. A., & Hallett, M. (2008). Motor Planning, Imagery, and Execution in the Distributed Motor Network: A Time-Course Study with Functional MRI. *Cerebral Cortex*, *18*(12), 2775–2788. https://doi.org/10.1093/cercor/bhn036

Hari, R. (2017). *Magnetoencephalography* (D. L. Schomer & F. H. Lopes Da Silva, Eds.; Vol. 1). Oxford University Press. https://doi.org/10.1093/med/9780190228484.003.0035

He, B. J. (2014). Scale-free brain activity: Past, present, and future. *Trends in Cognitive Sciences*, *18*(9), 480–487. https://doi.org/10.1016/j.tics.2014.04.003

Heideman, S. G., Quinn, A. J., Woolrich, M. W., van Ede, F., & Nobre, A. C. (2020). Dissecting beta-state changes during timed movement preparation in

Parkinson's disease. *Progress in Neurobiology*, *184*, 101731. https://doi.org/10.1016/j.pneurobio.2019.101731

Heinrichs-Graham, E., Kurz, M. J., Becker, K. M., Santamaria, P. M., Gendelman, H. E., & Wilson, T. W. (2014). Hypersynchrony despite pathologically reduced beta oscillations in patients with Parkinson's disease: A pharmaco-magnetoencephalography study. *Journal of Neurophysiology*, *112*(7), 1739–1747. https://doi.org/10.1152/jn.00383.2014

Heinrichs-Graham, E., & Wilson, T. W. (2015). Coding complexity in the human motor circuit. *Human Brain Mapping*, *36*(12), 5155–5167. https://doi.org/10.1002/hbm.23000

Heinrichs-Graham, E., Wilson, T. W., Santamaria, P. M., Heithoff, S. K., Torres-Russotto, D., Hutter-Saunders, J. A. L., Estes, K. A., Meza, J. L., Mosley, R. L., & Gendelman, H. E. (2014). Neuromagnetic Evidence of Abnormal Movement-Related Beta Desynchronization in Parkinson's Disease. *Cerebral Cortex*, *24*(10), 2669–2678. https://doi.org/10.1093/cercor/bht121

Heinzel, S., Berg, D., Gasser, T., Chen, H., Yao, C., Postuma, R. B., & the MDS Task Force on the Definition of Parkinson's Disease. (2019). Update of the MDS research criteria for prodromal Parkinson's disease. *Movement Disorders*, *34*(10), 1464–1470. https://doi.org/10.1002/mds.27802

Helson, P., Lundqvist, D., Svenningsson, P., Vinding, M. C., & Kumar, A. (2023). Cortex-wide topography of 1/f-exponent in Parkinson's disease. *Npj Parkinson's Disease*, *9*(1), 109. https://doi.org/10.1038/s41531-023-00553-6

Higgins, C., Liu, Y., Vidaurre, D., Kurth-Nelson, Z., Dolan, R., Behrens, T., & Woolrich, M. (2021). Replay bursts in humans coincide with activation of the default mode and parietal alpha networks. *Neuron*, *109*(5), 882-893.e7. https://doi.org/10.1016/j.neuron.2020.12.007

Hirschmann, J., Hartmann, C. J., Butz, M., Hoogenboom, N., Özkurt, T. E., Elben, S., Vesper, J., Wojtecki, L., & Schnitzler, A. (2013). A direct relationship between oscillatory subthalamic nucleus–cortex coupling and rest tremor in Parkinson's disease. *Brain*, *136*(12), 3659–3670. https://doi.org/10.1093/brain/awt271

Hornykiewicz, O., & Kish, S. J. (1987). Biochemical pathophysiology of Parkinson's disease. *Advances in Neurology*, *45*, 19–34.

Horsager, J., Andersen, K. B., Knudsen, K., Skjærbæk, C., Fedorova, T. D., Okkels, N., Schaeffer, E., Bonkat, S. K., Geday, J., Otto, M., Sommerauer, M., Danielsen, E. H., Bech, E., Kraft, J., Munk, O. L., Hansen, S. D., Pavese, N., Göder, R., Brooks, D. J., … Borghammer, P. (2020). Brain-first versus body-first Parkinson's disease: A multimodal imaging case-control study. *Brain*, *143*(10), 3077–3088. https://doi.org/10.1093/brain/awaa238

Hsieh, S., Schubert, S., Hoon, C., Mioshi, E., & Hodges, J. R. (2013). Validation of the Addenbrooke's Cognitive Examination III in Frontotemporal Dementia and Alzheimer's Disease. *Dementia and Geriatric Cognitive Disorders*, *36*(3–4), 242–250. https://doi.org/10.1159/000351671

Hu, M. (2017). *Oxford Parkinson's Disease Centre Discovery CohortOPDC Discovery* [dataset]. [object Object]. https://doi.org/10.48532/036000

Hu, M. T. (2020). REM sleep behavior disorder (RBD). *Neurobiology of Disease*, *143*, 104996. https://doi.org/10.1016/j.nbd.2020.104996

Iranzo, A., Fernández-Arcos, A., Tolosa, E., Serradell, M., Molinuevo, J. L., Valldeoriola, F., Gelpi, E., Vilaseca, I., Sánchez-Valle, R., Lladó, A., Gaig, C., & Santamaría, J. (2014). Neurodegenerative Disorder Risk in Idiopathic REM Sleep Behavior Disorder: Study in 174 Patients. *PLoS ONE*, *9*(2), e89741. https://doi.org/10.1371/journal.pone.0089741

Iranzo, A., Isetta, V., Molinuevo, J. L., Serradell, M., Navajas, D., Farre, R., & Santamaria, J. (2010). Electroencephalographic slowing heralds mild cognitive impairment in idiopathic REM sleep behavior disorder. *Sleep Medicine*, *11*(6), 534–539. https://doi.org/10.1016/j.sleep.2010.03.006

Iskhakova, L., Rappel, P., Deffains, M., Fonar, G., Marmor, O., Paz, R., Israel, Z., Eitan, R., & Bergman, H. (2021). Modulation of dopamine tone induces frequency shifts in cortico-basal ganglia beta oscillations. *Nature Communications*, *12*(1), 7026. https://doi.org/10.1038/s41467-021-27375-5

Jacobs, J. V., & Horak, F. B. (2006). Abnormal proprioceptive-motor integration contributes to hypometric postural responses of subjects with parkinson's disease. *Neuroscience*, *141*(2), 999–1009. https://doi.org/10.1016/j.neuroscience.2006.04.014

Jones, S. R. (2016). When brain rhythms aren't 'rhythmic': Implication for their mechanisms and meaning. *Current Opinion in Neurobiology*, *40*, 72–80. https://doi.org/10.1016/j.conb.2016.06.010

Kalaska, J. F. (1996). Parietal cortex area 5 and visuomotor behavior. *Canadian Journal of Physiology and Pharmacology*, *74*(4), 483–498. https://doi.org/10.1139/y96-040

Kalia, L. V., Brotchie, J. M., & Fox, S. H. (2013). Novel nondopaminergic targets for motor features of Parkinson's disease: Review of recent trials. *Movement Disorders*, *28*(2), 131–144. https://doi.org/10.1002/mds.25273

Kalia, L. V., & Lang, A. E. (2015). Parkinson's disease. *The Lancet*, *386*(9996), 896–912. https://doi.org/10.1016/S0140-6736(14)61393-3

Kalinderi, K., Bostantjopoulou, S., & Fidani, L. (2016). The genetic background of Parkinson's disease: Current progress and future prospects. *Acta Neurologica Scandinavica*, *134*(5), 314–326. https://doi.org/10.1111/ane.12563

Khawaldeh, S., Tinkhauser, G., Torrecillos, F., He, S., Foltynie, T., Limousin, P., Zrinzo, L., Oswal, A., Quinn, A. J., Vidaurre, D., Tan, H., Litvak, V., Kühn, A., Woolrich, M., & Brown, P. (2022). Balance between competing spectral states in subthalamic nucleus is linked to motor impairment in Parkinson's disease. *Brain: A Journal of Neurology*, *145*(1), 237–250. https://doi.org/10.1093/brain/awab264

Kilavik, B. E., Ponce-Alvarez, A., Trachel, R., Confais, J., Takerkart, S., & Riehle, A. (2012). Context-Related Frequency Modulations of Macaque Motor Cortical LFP Beta Oscillations. *Cerebral Cortex*, *22*(9), 2148–2159. https://doi.org/10.1093/cercor/bhr299

Kilavik, B. E., Zaepffel, M., Brovelli, A., MacKay, W. A., & Riehle, A. (2013). The ups and downs of beta oscillations in sensorimotor cortex. *Experimental Neurology*, *245*, 15–26. https://doi.org/10.1016/j.expneurol.2012.09.014

Knudsen, K., Fedorova, T. D., Hansen, A. K., Sommerauer, M., Otto, M., Svendsen, K. B., Nahimi, A., Stokholm, M. G., Pavese, N., Beier, C. P., Brooks, D. J., & Borghammer, P. (2018). In-vivo staging of pathology in REM sleep behaviour disorder: A multimodality imaging case-control study. *The Lancet Neurology*, *17*(7), 618–628. https://doi.org/10.1016/S1474-4422(18)30162-5

Kohl, O., Woolrich, M., Nobre, A. C., & Quinn, A. (2023). *Glasser52: A parcellation for MEG-Analysis* [dataset]. Zenodo. https://doi.org/10.5281/ZENODO.10401793

Kotagal, V., Albin, R. L., Müller, M. L. T. M., Koeppe, R. A., Chervin, R. D., Frey, K. A., & Bohnen, N. I. (2012). Symptoms of rapid eye movement sleep behavior disorder are associated with cholinergic denervation in Parkinson disease. *Annals of Neurology*, *71*(4), 560–568. https://doi.org/10.1002/ana.22691

Kouli, A., Torsney, K. M., & Kuan, W.-L. (2018). Parkinson's Disease: Etiology, Neuropathology, and Pathogenesis. In T. B. Stoker & J. C. Greenland (Eds.), *Parkinson's Disease: Pathogenesis and Clinical Aspects* (pp. 3–26). Codon Publications. https://doi.org/10.15586/codonpublications.parkinsonsdisease.2018.ch1

Kramer, M. A., & Chu, C. J. (2023). *The 1/f-like behavior of neural field spectra are a natural consequence of noise driven brain dynamics* [Preprint]. Neuroscience. https://doi.org/10.1101/2023.03.10.532077

Krösche, M., Kannenberg, S., Butz, M., Hartmann, C. J., Florin, E., Schnitzler, A., & Hirschmann, J. (2023). Slowing of Frontal β Oscillations in Atypical Parkinsonism. *Movement Disorders*, *38*(5), 806–817. https://doi.org/10.1002/mds.29378

Kühn, A. A., Kempf, F., Brucke, C., Gaynor Doyle, L., Martinez-Torres, I., Pogosyan, A., Trottenberg, T., Kupsch, A., Schneider, G.-H., Hariz, M. I., Vandenberghe, W., Nuttin, B., & Brown, P. (2008). High-Frequency Stimulation of the Subthalamic Nucleus Suppresses Oscillatory Activity in Patients with Parkinson's Disease in Parallel with Improvement in Motor Performance. *Journal of Neuroscience*, *28*(24), 6165–6173. https://doi.org/10.1523/JNEUROSCI.0282-08.2008

Kühn, A. A., Kupsch, A., Schneider, G.-H., & Brown, P. (2006). Reduction in subthalamic 8-35 Hz oscillatory activity correlates with clinical improvement in Parkinson's disease: STN activity and motor improvement. *European Journal of Neuroscience*, *23*(7), 1956–1960. https://doi.org/10.1111/j.1460-9568.2006.04717.x

Kühn, A. A., Tsui, A., Aziz, T., Ray, N., Brücke, C., Kupsch, A., Schneider, G.-H., & Brown, P. (2009). Pathological synchronisation in the subthalamic nucleus of patients with Parkinson's disease relates to both bradykinesia and rigidity. *Experimental Neurology*, *215*(2), 380–387. https://doi.org/10.1016/j.expneurol.2008.11.008

Laansma, M. A., Bright, J. K., Al-Bachari, S., Anderson, T. J., Ard, T., Assogna, F., Baquero, K. A., Berendse, H. W., Blair, J., Cendes, F., Dalrymple-Alford, J. C., Bie, R. M. A., Debove, I., Dirkx, M. F., Druzgal, J., Emsley, H. C. A., Garraux, G.,

Guimarães, R. P., Gutman, B. A., … The ENIGMA-Parkinson's Study. (2021). International Multicenter Analysis of Brain Structure Across Clinical Stages of Parkinson's Disease. *Movement Disorders*, mds.28706. https://doi.org/10.1002/mds.28706

Lang, A. E., & Lozano, A. M. (1998). Parkinson's Disease. *New England Journal of Medicine*, *339*(15), 1044–1053. https://doi.org/10.1056/NEJM199810083391506

Lanskey, J. H., Kocagoncu, E., Quinn, A. J., Cheng, Y.-J., Karadag, M., Pitt, J., Lowe, S., Perkinton, M., Raymont, V., Singh, K. D., Woolrich, M., Nobre, A. C., Henson, R. N., & Rowe, J. B. (2022). New Therapeutics in Alzheimer's Disease Longitudinal Cohort study (NTAD): Study protocol. *BMJ Open*, *12*(12), e055135. https://doi.org/10.1136/bmjopen-2021-055135

Levy, R., Ashby, P., Hutchison, W. D., Lang, A. E., Lozano, A. M., & Dostrovsky, J. O. (2002). Dependence of subthalamic nucleus oscillations on movement and dopamine in Parkinson's disease. *Brain*, *125*(6), 1196–1209. https://doi.org/10.1093/brain/awf128

Little, S., Pogosyan, A., Kuhn, A. A., & Brown, P. (2012). Beta band stability over time correlates with Parkinsonian rigidity and bradykinesia. *Experimental Neurology*, *236*(2), 383–388. https://doi.org/10.1016/j.expneurol.2012.04.024

Litvak, V., Florin, E., Tamás, G., Groppa, S., & Muthuraman, M. (2021). EEG and MEG primers for tracking DBS network effects. *NeuroImage*, *224*, 117447. https://doi.org/10.1016/j.neuroimage.2020.117447

Litvak, V., Jha, A., Eusebio, A., Oostenveld, R., Foltynie, T., Limousin, P., Zrinzo, L., Hariz, M. I., Friston, K., & Brown, P. (2011). Resting oscillatory cortico-subthalamic connectivity in patients with Parkinson's disease. *Brain*, *134*(2), 359–374. https://doi.org/10.1093/brain/awq332

Livia Fantini, M., Gagnon, J.-F., Petit, D., Rompré, S., Décary, A., Carrier, J., & Montplaisir, J. (2003). Slowing of electroencephalogram in rapid eye movement sleep behavior disorder: Electroencephalogram in RBD. *Annals of Neurology*, *53*(6), 774–780. https://doi.org/10.1002/ana.10547

Lofredi, R., Okudzhava, L., Irmen, F., Brücke, C., Huebl, J., Krauss, J. K., Schneider, G.-H., Faust, K., Neumann, W.-J., & Kühn, A. A. (2023). Subthalamic beta bursts correlate with dopamine-dependent motor symptoms in 106 Parkinson's patients. *Npj Parkinson's Disease*, *9*(1), 2. https://doi.org/10.1038/s41531-022-00443-3

Lofredi, R., Tan, H., Neumann, W.-J., Yeh, C.-H., Schneider, G.-H., Kühn, A. A., & Brown, P. (2019). Beta bursts during continuous movements accompany the velocity decrement in Parkinson's disease patients. *Neurobiology of Disease*, *127*, 462–471. https://doi.org/10.1016/j.nbd.2019.03.013

Lopes da Silva, F. (2013). EEG and MEG: Relevance to Neuroscience. *Neuron*, *80*(5), 1112–1128. https://doi.org/10.1016/j.neuron.2013.10.017

Lozano, A. M., Lipsman, N., Bergman, H., Brown, P., Chabardes, S., Chang, J. W., Matthews, K., McIntyre, C. C., Schlaepfer, T. E., Schulder, M., Temel, Y., Volkmann, J., & Krauss, J. K. (2019). Deep brain stimulation: Current challenges

and future directions. *Nature Reviews Neurology*, *15*(3), 148–160. https://doi.org/10.1038/s41582-018-0128-2

Luoma, J., Pekkonen, E., Airaksinen, K., Helle, L., Nurminen, J., Taulu, S., & Mäkelä, J. P. (2018). Spontaneous sensorimotor cortical activity is suppressed by deep brain stimulation in patients with advanced Parkinson's disease. *Neuroscience Letters*, *683*, 48–53. https://doi.org/10.1016/j.neulet.2018.06.041

Maestú, F., De Haan, W., Busche, M. A., & DeFelipe, J. (2021). Neuronal excitation/inhibition imbalance: Core element of a translational perspective on Alzheimer pathophysiology. *Ageing Research Reviews*, *69*, 101372. https://doi.org/10.1016/j.arr.2021.101372

Mahlknecht, P., Marini, K., Werkmann, M., Poewe, W., & Seppi, K. (2022). Prodromal Parkinson's disease: Hype or hope for disease-modification trials? *Translational Neurodegeneration*, *11*(1), 11. https://doi.org/10.1186/s40035-022-00286-1

Massicotte-Marquez, J., Decary, A., Gagnon, J.-F., Vendette, M., Mathieu, A., Postuma, R. B., Carrier, J., & Montplaisir, J. (2008). Executive dysfunction and memory impairment in idiopathic REM sleep behavior disorder. *Neurology*, *70*(15), 1250–1257. https://doi.org/10.1212/01.wnl.0000286943.79593.a6

Mathuranath, P. S., Nestor, P. J., Berrios, G. E., Rakowicz, W., & Hodges, J. R. (2000). A brief cognitive test battery to differentiate Alzheimer's disease and frontotemporal dementia. *Neurology*, *55*(11), 1613–1620. https://doi.org/10.1212/01.wnl.0000434309.85312.19

McGuire, L. M. M., & Sabes, P. N. (2011). Heterogeneous Representations in the Superior Parietal Lobule Are Common across Reaches to Visual and Proprioceptive Targets. *The Journal of Neuroscience*, *31*(18), 6661–6673. https://doi.org/10.1523/JNEUROSCI.2921-10.2011

Melgari, J.-M. (2014). Alpha and beta EEG power reflects L-dopa acute administration in parkinsonian patients. *Frontiers in Aging Neuroscience*, *6*. https://doi.org/10.3389/fnagi.2014.00302

Mesulam, M., & Geula, C. (1988). Nucleus basalis (Ch4) and cortical cholinergic innervation in the human brain: Observations based on the distribution of acetylcholinesterase and choline acetyltransferase. *Journal of Comparative Neurology*, *275*(2), 216–240. https://doi.org/10.1002/cne.902750205

Morita, A., Kamei, S., & Mizutani, T. (2011). Relationship Between Slowing of the EEG and Cognitive Impairment in Parkinson Disease: *Journal of Clinical Neurophysiology*, 1. https://doi.org/10.1097/WNP.0b013e3182273211

Morita, A., Kamei, S., Serizawa, K., & Mizutani, T. (2009). The Relationship Between Slowing EEGs and the Progression of Parkinson's Disease. *Journal of Clinical Neurophysiology*, *26*(6), 426–429. https://doi.org/10.1097/WNP.0b013e3181c2bce6

Mountcastle, V. B., Lynch, J. C., Georgopoulos, A., Sakata, H., & Acuna, C. (1975). Posterior parietal association cortex of the monkey: Command functions for operations within extrapersonal space. *Journal of Neurophysiology*, *38*(4), 871–908. https://doi.org/10.1152/jn.1975.38.4.871

Munkres, J. (1957). Algorithms for the Assignment and Transportation Problems. *Journal of the Society for Industrial and Applied Mathematics*, *5*(1), 32–38. https://doi.org/10.1137/0105003

Murakami, S., & Okada, Y. (2006). Contributions of principal neocortical neurons to magnetoencephalography and electroencephalography signals. *The Journal of Physiology*, *575*(3), 925–936. https://doi.org/10.1113/jphysiol.2006.105379

Muthukumaraswamy, S. D., & Liley, D. Tj. (2018). 1/f electrophysiological spectra in resting and drug-induced states can be explained by the dynamics of multiple oscillatory relaxation processes. *NeuroImage*, *179*, 582–595. https://doi.org/10.1016/j.neuroimage.2018.06.068

Nakamura, A., Cuesta, P., Fernández, A., Arahata, Y., Iwata, K., Kuratsubo, I., Bundo, M., Hattori, H., Sakurai, T., Fukuda, K., Washimi, Y., Endo, H., Takeda, A., Diers, K., Bajo, R., Maestú, F., Ito, K., & Kato, T. (2018). Electromagnetic signatures of the preclinical and prodromal stages of Alzheimer's disease. *Brain*, *141*(5), 1470–1485. https://doi.org/10.1093/brain/awy044

Neufeld, M. Y., Inzelberg, R., & Korczyn, A. D. (1988). EEG in demented and non-demented parkinsonian patients. *Acta Neurologica Scandinavica*, *78*(1), 1–5. https://doi.org/10.1111/j.1600-0404.1988.tb03609.x

Neumann, W.-J., Steiner, L. A., & Milosevic, L. (2023). Neurophysiological mechanisms of deep brain stimulation across spatiotemporal resolutions. *Brain*, awad239. https://doi.org/10.1093/brain/awad239

Neuper, C., & Pfurtscheller, G. (2001). Evidence for distinct beta resonance frequencies in human EEG related to specific sensorimotor cortical areas. *Clinical Neurophysiology*, *112*(11), 2084–2097. https://doi.org/10.1016/S1388-2457(01)00661-7

Nichols, T. E., & Holmes, A. P. (2002). Nonparametric permutation tests for functional neuroimaging: A primer with examples. *Human Brain Mapping*, *15*(1), 1–25. https://doi.org/10.1002/hbm.1058

Niso, G., Rogers, C., Moreau, J. T., Chen, L.-Y., Madjar, C., Das, S., Bock, E., Tadel, F., Evans, A. C., Jolicoeur, P., & Baillet, S. (2016). OMEGA: The Open MEG Archive. *NeuroImage*, *124*, 1182–1187. https://doi.org/10.1016/j.neuroimage.2015.04.028

Nowak, D. A., & Hermsdörfer, J. (2006). Predictive and reactive control of grasping forces: On the role of the basal ganglia and sensory feedback. *Experimental Brain Research*, *173*(4), 650–660. https://doi.org/10.1007/s00221-006-0409-7

O'Keeffe, A. B., Malekmohammadi, M., Sparks, H., & Pouratian, N. (2020). Synchrony Drives Motor Cortex Beta Bursting, Waveform Dynamics, and Phase-Amplitude Coupling in Parkinson's Disease. *The Journal of Neuroscience*, *40*(30), 5833–5846. https://doi.org/10.1523/JNEUROSCI.1996-19.2020

Olde Dubbelink, K. T. E., Hillebrand, A., Twisk, J. W. R., Deijen, J. B., Stoffers, D., Schmand, B. A., Stam, C. J., & Berendse, H. W. (2014). Predicting dementia in Parkinson disease by combining neurophysiologic and cognitive markers. *Neurology*, *82*(3), 263–270. https://doi.org/10.1212/WNL.0000000000000034

Olde Dubbelink, K. T. E., Stoffers, D., Deijen, J. B., Twisk, J. W. R., Stam, C. J., & Berendse, H. W. (2013). Cognitive decline in Parkinson's disease is associated with slowing of resting-state brain activity: A longitudinal study. *Neurobiology of Aging*, *34*(2), 408–418. https://doi.org/10.1016/j.neurobiolaging.2012.02.029

Olde Dubbelink, K. T. E., Stoffers, D., Deijen, J. B., Twisk, J. W. R., Stam, C. J., Hillebrand, A., & Berendse, H. W. (2013). Resting-state functional connectivity as a marker of disease progression in Parkinson's disease: A longitudinal MEG study. *NeuroImage: Clinical*, *2*, 612–619. https://doi.org/10.1016/j.nicl.2013.04.003

Oswal, A., Beudel, M., Zrinzo, L., Limousin, P., Hariz, M., Foltynie, T., Litvak, V., & Brown, P. (2016). Deep brain stimulation modulates synchrony within spatially and spectrally distinct resting state networks in Parkinson's disease. *Brain*, *139*(5), 1482–1496. https://doi.org/10.1093/brain/aww048

Oswal, A., Cao, C., Yeh, C.-H., Neumann, W.-J., Gratwicke, J., Akram, H., Horn, A., Li, D., Zhan, S., Zhang, C., Wang, Q., Zrinzo, L., Foltynie, T., Limousin, P., Bogacz, R., Sun, B., Husain, M., Brown, P., & Litvak, V. (2021). Neural signatures of hyperdirect pathway activity in Parkinson's disease. *Nature Communications*, *12*(1), 5185. https://doi.org/10.1038/s41467-021-25366-0

Palva, J. M., Wang, S. H., Palva, S., Zhigalov, A., Monto, S., Brookes, M. J., Schoffelen, J.-M., & Jerbi, K. (2018). Ghost interactions in MEG/EEG source space: A note of caution on inter-areal coupling measures. *NeuroImage*, *173*, 632–643. https://doi.org/10.1016/j.neuroimage.2018.02.032

Pan, P., Zhang, Y., Liu, Y., Zhang, H., Guan, D., & Xu, Y. (2017). Abnormalities of regional brain function in Parkinson's disease: A meta-analysis of resting state functional magnetic resonance imaging studies. *Scientific Reports*, *7*(1), 40469. https://doi.org/10.1038/srep40469

Parkinson, J. (2002). An Essay on the Shaking Palsy. *The Journal of Neuropsychiatry and Clinical Neurosciences*, *14*(2), 223–236. https://doi.org/10.1176/jnp.14.2.223

Pasquini, J., Brooks, D. J., & Pavese, N. (2021). The Cholinergic Brain in Parkinson's Disease. *Movement Disorders Clinical Practice*, *8*(7), 1012–1026. https://doi.org/10.1002/mdc3.13319

Pauls, K. A. M., Korsun, O., Nenonen, J., Nurminen, J., Liljeström, M., Kujala, J., Pekkonen, E., & Renvall, H. (2022). Cortical beta burst dynamics are altered in Parkinson's disease but normalized by deep brain stimulation. *NeuroImage*, *257*, 119308. https://doi.org/10.1016/j.neuroimage.2022.119308

Peever, J., Luppi, P.-H., & Montplaisir, J. (2014). Breakdown in REM sleep circuitry underlies REM sleep behavior disorder. *Trends in Neurosciences*, *37*(5), 279–288. https://doi.org/10.1016/j.tins.2014.02.009

Penfield, W., & Boldrey, E. (1937). SOMATIC MOTOR AND SENSORY REPRESENTATION IN THE CEREBRAL CORTEX OF MAN AS STUDIED BY ELECTRICAL STIMULATION. *Brain*, *60*(4), 389–443. https://doi.org/10.1093/brain/60.4.389

Perrin, F., Pernier, J., Bertrand, O., & Echallier, J. F. (1989). Spherical splines for scalp potential and current density mapping. *Electroencephalography and Clinical*

*Neurophysiology*, *72*(2), 184–187. https://doi.org/10.1016/0013-4694(89)90180-6

Petersson, P., Kühn, A. A., Neumann, W.-J., & Fuentes, R. (2020). Basal ganglia oscillations as biomarkers for targeting circuit dysfunction in Parkinson's disease. In *Progress in Brain Research* (Vol. 252, pp. 525–557). Elsevier. https://doi.org/10.1016/bs.pbr.2020.02.002

Pfurtscheller, G., Neuper, C., Pichler-Zalaudek, K., Edlinger, G., & Lopes Da Silva, F. H. (2000). Do brain oscillations of different frequencies indicate interaction between cortical areas in humans? *Neuroscience Letters*, *286*(1), 66–68. https://doi.org/10.1016/S0304-3940(00)01055-7

Pfurtscheller, G., Pichler-Zalaudek, K., Ortmayr, B., Diez, J., & Reisecker, &Na; (1998). Postmovement Beta Synchronization in Patients With Parkinson's Disease: *Journal of Clinical Neurophysiology*, *15*(3), 243–250. https://doi.org/10.1097/00004691-199805000-00008

Pfurtscheller, G., Stancák, A., & Neuper, C. (1996). Post-movement beta synchronization. A correlate of an idling motor area? *Electroencephalography and Clinical Neurophysiology*, *98*(4), 281–293. https://doi.org/10.1016/0013-4694(95)00258-8

Pizzo, F., Roehri, N., Medina Villalon, S., Trébuchon, A., Chen, S., Lagarde, S., Carron, R., Gavaret, M., Giusiano, B., McGonigal, A., Bartolomei, F., Badier, J. M., & Bénar, C. G. (2019). Deep brain activities can be detected with

magnetoencephalography. *Nature Communications*, *10*(1), 971. https://doi.org/10.1038/s41467-019-08665-5

Poewe, W., Seppi, K., Marini, K., & Mahlknecht, P. (2020). New hopes for disease modification in Parkinson's Disease. *Neuropharmacology*, *171*, 108085. https://doi.org/10.1016/j.neuropharm.2020.108085

Poggiolini, I., Gupta, V., Lawton, M., Lee, S., El-Turabi, A., Querejeta-Coma, A., Trenkwalder, C., Sixel-Döring, F., Foubert-Samier, A., Pavy-Le Traon, A., Plazzi, G., Biscarini, F., Montplaisir, J., Gagnon, J.-F., Postuma, R. B., Antelmi, E., Meissner, W. G., Mollenhauer, B., Ben-Shlomo, Y., … Parkkinen, L. (2022). Diagnostic value of cerebrospinal fluid alpha-synuclein seed quantification in synucleinopathies. *Brain*, *145*(2), 584–595. https://doi.org/10.1093/brain/awab431

Pollok, B., Krause, V., Martsch, W., Wach, C., Schnitzler, A., & Südmeyer, M. (2012). Motor-cortical oscillations in early stages of Parkinson's disease: Suppression of motor cortical beta oscillations is altered in early PD. *The Journal of Physiology*, *590*(13), 3203–3212. https://doi.org/10.1113/jphysiol.2012.231316

Postuma, R. B., Aarsland, D., Barone, P., Burn, D. J., Hawkes, C. H., Oertel, W., & Ziemssen, T. (2012). Identifying prodromal Parkinson's disease: Pre-Motor disorders in Parkinson's disease. *Movement Disorders*, *27*(5), 617–626. https://doi.org/10.1002/mds.24996

Postuma, R. B., & Berg, D. (2019). Prodromal Parkinson's Disease: The Decade Past, the Decade to Come. *Movement Disorders*, *34*(5), 665–675. https://doi.org/10.1002/mds.27670

Postuma, R. B., Berg, D., Stern, M., Poewe, W., Olanow, C. W., Oertel, W., Obeso, J., Marek, K., Litvan, I., Lang, A. E., Halliday, G., Goetz, C. G., Gasser, T., Dubois, B., Chan, P., Bloem, B. R., Adler, C. H., & Deuschl, G. (2015). MDS clinical diagnostic criteria for Parkinson's disease: MDS-PD Clinical Diagnostic Criteria. *Movement Disorders*, *30*(12), 1591–1601. https://doi.org/10.1002/mds.26424

Postuma, R. B., Gagnon, J. F., Rompré, S., & Montplaisir, J. Y. (2010). Severity of REM atonia loss in idiopathic REM sleep behavior disorder predicts Parkinson disease. *Neurology*, *74*(3), 239–244. https://doi.org/10.1212/WNL.0b013e3181ca0166

Postuma, R. B., Gagnon, J.-F., Bertrand, J.-A., Génier Marchand, D., & Montplaisir, J. Y. (2015). Parkinson risk in idiopathic REM sleep behavior disorder: Preparing for neuroprotective trials. *Neurology*, *84*(11), 1104–1113. https://doi.org/10.1212/WNL.0000000000001364

Postuma, R. B., Iranzo, A., Hu, M., Högl, B., Boeve, B. F., Manni, R., Oertel, W. H., Arnulf, I., Ferini-Strambi, L., Puligheddu, M., Antelmi, E., Cochen De Cock, V., Arnaldi, D., Mollenhauer, B., Videnovic, A., Sonka, K., Jung, K.-Y., Kunz, D., Dauvilliers, Y., … Pelletier, A. (2019). Risk and predictors of dementia and parkinsonism in idiopathic REM sleep behaviour disorder: A multicentre study. *Brain*, *142*(3), 744–759. https://doi.org/10.1093/brain/awz030

Priori, A., Foffani, G., Pesenti, A., Tamma, F., Bianchi, A., Pellegrini, M., Locatelli, M., Moxon, K., & Villani, R. (2004). Rhythm-specific pharmacological modulation of subthalamic activity in Parkinson's disease. *Experimental Neurology*, *189*(2), 369–379. https://doi.org/10.1016/j.expneurol.2004.06.001

Proudfoot, M., Woolrich, M. W., Nobre, A. C., & Turner, M. R. (2014). Magnetoencephalography. *Practical Neurology*, *14*(5), 336–343. https://doi.org/10.1136/practneurol-2013-000768

Qasim, S. E., De Hemptinne, C., Swann, N. C., Miocinovic, S., Ostrem, J. L., & Starr, P. A. (2016). Electrocorticography reveals beta desynchronization in the basal ganglia-cortical loop during rest tremor in Parkinson's disease. *Neurobiology of Disease*, *86*, 177–186. https://doi.org/10.1016/j.nbd.2015.11.023

Quinn, A. J., van Ede, F., Brookes, M. J., Heideman, S. G., Nowak, M., Seedat, Z. A., Vidaurre, D., Zich, C., Nobre, A. C., & Woolrich, M. W. (2019). Unpacking Transient Event Dynamics in Electrophysiological Power Spectra. *Brain Topography*, *32*(6), 1020–1034. https://doi.org/10.1007/s10548-019-00745-5

Quinn, A. J., Vidaurre, D., Abeysuriya, R., Becker, R., Nobre, A. C., & Woolrich, M. W. (2018). Task-Evoked Dynamic Network Analysis Through Hidden Markov Modeling. *Frontiers in Neuroscience*, *12*, 603. https://doi.org/10.3389/fnins.2018.00603

Rabin, E., Muratori, L., Svokos, K., & Gordon, A. (2010). Tactile/proprioceptive integration during arm localization is intact in individuals with Parkinson's

disease. *Neuroscience Letters*, *470*(1), 38–42. https://doi.org/10.1016/j.neulet.2009.12.051

Ramaker, C., Marinus, J., Stiggelbout, A. M., & Van Hilten, B. J. (2002). Systematic evaluation of rating scales for impairment and disability in Parkinson's disease. *Movement Disorders*, *17*(5), 867–876. https://doi.org/10.1002/mds.10248

Ranasinghe, K. G., Cha, J., Iaccarino, L., Hinkley, L. B., Beagle, A. J., Pham, J., Jagust, W. J., Miller, B. L., Rankin, K. P., Rabinovici, G. D., Vossel, K. A., & Nagarajan, S. S. (2020). Neurophysiological signatures in Alzheimer's disease are distinctly associated with TAU, amyloid-β accumulation, and cognitive decline. *Science Translational Medicine*, *12*(534), eaaz4069. https://doi.org/10.1126/scitranslmed.aaz4069

Ranasinghe, K. G., Petersen, C., Kudo, K., Mizuiri, D., Rankin, K. P., Rabinovici, G. D., Gorno-Tempini, M. L., Seeley, W. W., Spina, S., Miller, B. L., Vossel, K., Grinberg, L. T., & Nagarajan, S. S. (2021). Reduced synchrony in alpha oscillations during life predicts *post mortem* neurofibrillary tangle density in early-onset and atypical Alzheimer's disease. *Alzheimer's & Dementia*, *17*(12), 2009–2019. https://doi.org/10.1002/alz.12349

Rea, R. C., Berlot, R., Martin, S. L., Craig, C. E., Holmes, P. S., Wright, D. J., Bon, J., Pirtošek, Z., & Ray, N. J. (2021). Quantitative EEG and cholinergic basal forebrain atrophy in Parkinson's disease and mild cognitive impairment. *Neurobiology of Aging*, *106*, 37–44. https://doi.org/10.1016/j.neurobiolaging.2021.05.023

Rickards, C. (1997). Proprioceptive control of wrist movements in Parkinson's disease. Reduced muscle vibration-induced errors. *Brain*, *120*(6), 977–990. https://doi.org/10.1093/brain/120.6.977

Rodrigues Brazète, J., Gagnon, J.-F., Postuma, R. B., Bertrand, J.-A., Petit, D., & Montplaisir, J. (2016). Electroencephalogram slowing predicts neurodegeneration in rapid eye movement sleep behavior disorder. *Neurobiology of Aging*, *37*, 74–81. https://doi.org/10.1016/j.neurobiolaging.2015.10.007

Rodrigues Brazète, J., Montplaisir, J., Petit, D., Postuma, R. B., Bertrand, J.-A., Génier Marchand, D., & Gagnon, J.-F. (2013). Electroencephalogram slowing in rapid eye movement sleep behavior disorder is associated with mild cognitive impairment. *Sleep Medicine*, *14*(11), 1059–1063. https://doi.org/10.1016/j.sleep.2013.06.013

Roguski, A., Rayment, D., Whone, A. L., Jones, M. W., & Rolinski, M. (2020). A Neurologist's Guide to REM Sleep Behavior Disorder. *Frontiers in Neurology*, *11*, 610. https://doi.org/10.3389/fneur.2020.00610

Rolinski, M., Griffanti, L., Piccini, P., Roussakis, A. A., Szewczyk-Krolikowski, K., Menke, R. A., Quinnell, T., Zaiwalla, Z., Klein, J. C., Mackay, C. E., & Hu, M. T. M. (2016). Basal ganglia dysfunction in idiopathic REM sleep behaviour disorder parallels that in early Parkinson's disease. *Brain*, *139*(8), 2224–2234. https://doi.org/10.1093/brain/aww124

Rosner, B. (1983). Percentage Points for a Generalized ESD Many-Outlier Procedure. *Technometrics*, *25*(2), 165–172. https://doi.org/10.1080/00401706.1983.10487848

Ross, G. W., Petrovitch, H., Abbott, R. D., Nelson, J., Markesbery, W., Davis, D., Hardman, J., Launer, L., Masaki, K., Tanner, C. M., & White, L. R. (2004). Parkinsonian signs and substantia nigra neuron density in decendents elders without PD. *Annals of Neurology*, *56*(4), 532–539. https://doi.org/10.1002/ana.20226

Rossi, A., Berger, K., Chen, H., Leslie, D., Mailman, R. B., & Huang, X. (2018). Projection of the prevalence of Parkinson's disease in the coming decades: Revisited. *Movement Disorders*, *33*(1), 156–159. https://doi.org/10.1002/mds.27063

Salenius, S., Avikainen, S., Kaakkola, S., Hari, R., & Brown, P. (2002). Defective cortical drive to muscle in Parkinson's disease and its improvement with levodopa. *Brain*, *125*(3), 491–500. https://doi.org/10.1093/brain/awf042

Sasai, T., Matsuura, M., & Inoue, Y. (2013). Electroencephalographic Findings Related With Mild Cognitive Impairment in Idiopathic Rapid Eye Movement Sleep Behavior Disorder. *Sleep*, *36*(12), 1893–1899. https://doi.org/10.5665/sleep.3224

Schapira, A. H. V., Chaudhuri, K. R., & Jenner, P. (2017). Non-motor features of Parkinson disease. *Nature Reviews Neuroscience*, *18*(7), 435–450. https://doi.org/10.1038/nrn.2017.62

Schmidt, R., Herrojo Ruiz, M., Kilavik, B. E., Lundqvist, M., Starr, P. A., & Aron, A. R. (2019). Beta Oscillations in Working Memory, Executive Control of Movement and Thought, and Sensorimotor Function. *The Journal of Neuroscience*, *39*(42), 8231–8238. https://doi.org/10.1523/JNEUROSCI.1163-19.2019

Schneider, L., Seeger, V., Timmermann, L., & Florin, E. (2020). Electrophysiological resting state networks of predominantly akinetic-rigid Parkinson patients: Effects of dopamine therapy. *NeuroImage: Clinical*, *25*, 102147. https://doi.org/10.1016/j.nicl.2019.102147

Schuepbach, W. M. M., Rau, J., Knudsen, K., Volkmann, J., Krack, P., Timmermann, L., Hälbig, T. D., Hesekamp, H., Navarro, S. M., Meier, N., Falk, D., Mehdorn, M., Paschen, S., Maarouf, M., Barbe, M. T., Fink, G. R., Kupsch, A., Gruber, D., Schneider, G.-H., … Deuschl, G. (2013). Neurostimulation for Parkinson's Disease with Early Motor Complications. *New England Journal of Medicine*, *368*(7), 610–622. https://doi.org/10.1056/NEJMoa1205158

Segal, A., Parkes, L., Aquino, K., Kia, S. M., Wolfers, T., Franke, B., Hoogman, M., Beckmann, C. F., Westlye, L. T., Andreassen, O. A., Zalesky, A., Harrison, B. J., Davey, C. G., Soriano-Mas, C., Cardoner, N., Tiego, J., Yücel, M., Braganza, L., Suo, C., … Fornito, A. (2023). Regional, circuit and network heterogeneity of brain abnormalities in psychiatric disorders. *Nature Neuroscience*, *26*(9), 1613–1629. https://doi.org/10.1038/s41593-023-01404-6

Sharott, A., Magill, P. J., Harnack, D., Kupsch, A., Meissner, W., & Brown, P. (2005). Dopamine depletion increases the power and coherence of β-oscillations in the

cerebral cortex and subthalamic nucleus of the awake rat. *European Journal of Neuroscience*, *21*(5), 1413–1422. https://doi.org/10.1111/j.1460-9568.2005.03973.x

Shimada, H., Hirano, S., Shinotoh, H., Aotsuka, A., Sato, K., Tanaka, N., Ota, T., Asahina, M., Fukushi, K., Kuwabara, S., Hattori, T., Suhara, T., & Irie, T. (2009). Mapping of brain acetylcholinesterase alterations in Lewy body disease by PET. *Neurology*, *73*(4), 273–278. https://doi.org/10.1212/WNL.0b013e3181ab2b58

Shirahige, L., Berenguer-Rocha, M., Mendonça, S., Rocha, S., Rodrigues, M. C., & Monte-Silva, K. (2020). Quantitative Electroencephalography Characteristics for Parkinson's Disease: A Systematic Review. *Journal of Parkinson's Disease*, *10*(2), 455–470. https://doi.org/10.3233/JPD-191840

Singh, A. (2018). Oscillatory activity in the cortico-basal ganglia-thalamic neural circuits in Parkinson's disease. *European Journal of Neuroscience*, *48*(8), 2869–2878. https://doi.org/10.1111/ejn.13853

Smailovic, U., Koenig, T., Kåreholt, I., Andersson, T., Kramberger, M. G., Winblad, B., & Jelic, V. (2018). Quantitative EEG power and synchronization correlate with Alzheimer's disease CSF biomarkers. *Neurobiology of Aging*, *63*, 88–95. https://doi.org/10.1016/j.neurobiolaging.2017.11.005

Soikkeli, R., Partanen, J., Soininen, H., Pääkkönen, A., & Riekkinen, P. (1991). Slowing of EEG in Parkinson's disease. *Electroencephalography and Clinical Neurophysiology*, *79*(3), 159–165. https://doi.org/10.1016/0013-4694(91)90134-P

Sommerauer, M., Fedorova, T. D., Hansen, A. K., Knudsen, K., Otto, M., Jeppesen, J., Frederiksen, Y., Blicher, J. U., Geday, J., Nahimi, A., Damholdt, M. F., Brooks, D. J., & Borghammer, P. (2018). Evaluation of the noradrenergic system in Parkinson's disease: An 11C-MeNER PET and neuromelanin MRI study. *Brain*, *141*(2), 496–504. https://doi.org/10.1093/brain/awx348

Spillantini, M. G., Schmidt, M. L., Lee, V. M.-Y., Trojanowski, J. Q., Jakes, R., & Goedert, M. (1997). α-Synuclein in Lewy bodies. *Nature*, *388*(6645), 839–840. https://doi.org/10.1038/42166

Stær, K., Iranzo, A., Stokholm, M. G., Østergaard, K., Serradell, M., Otto, M., Svendsen, K. B., Garrido, A., Vilas, D., Santamaria, J., Møller, A., Gaig, C., Brooks, D. J., Borghammer, P., Tolosa, E., & Pavese, N. (2020). Cortical cholinergic dysfunction correlates with microglial activation in the substantia innominata in REM sleep behavior disorder. *Parkinsonism & Related Disorders*, *81*, 89–93. https://doi.org/10.1016/j.parkreldis.2020.10.014

Stanzione, P., Marciani, M. G., Maschio, M., Bassetti, M. A., Spanedda, F., Pierantozzi, M., Semprini, R., & Bernardi, G. (1996). Quantitative EEG changes in non-demented Parkinson's disease patients before and during L-dopa therapy. *European Journal of Neurology*, *3*(4), 354–362. https://doi.org/10.1111/j.1468-1331.1996.tb00229.x

Steriade, M., Gloor, P., Llinás, R. R., Lopes Da Silva, F. H., & Mesulam, M.-M. (1990). Basic mechanisms of cerebral rhythmic activities. *Electroencephalography and*

*Clinical Neurophysiology*, *76*(6), 481–508. https://doi.org/10.1016/0013-4694(90)90001-Z

Stoffers, D., Bosboom, J. L. W., Deijen, J. B., Wolters, E. C., Berendse, H. W., & Stam, C. J. (2007). Slowing of oscillatory brain activity is a stable characteristic of Parkinson's disease without dementia. *Brain*, *130*(7), 1847–1860. https://doi.org/10.1093/brain/awm034

Stokholm, M. G., Iranzo, A., Østergaard, K., Serradell, M., Otto, M., Bacher Svendsen, K., Garrido, A., Vilas, D., Fedorova, T. D., Santamaria, J., Møller, A., Gaig, C., Hiraoka, K., Brooks, D. J., Okamura, N., Borghammer, P., Tolosa, E., & Pavese, N. (2020). Cholinergic denervation in patients with idiopathic rapid eye movement sleep behaviour disorder. *European Journal of Neurology*, *27*(4), 644–652. https://doi.org/10.1111/ene.14127

Stomrud, E., Hansson, O., Minthon, L., Blennow, K., Rosén, I., & Londos, E. (2010). Slowing of EEG correlates with CSF biomarkers and reduced cognitive speed in elderly with normal cognition over 4 years. *Neurobiology of Aging*, *31*(2), 215–223. https://doi.org/10.1016/j.neurobiolaging.2008.03.025

Swann, N. C., De Hemptinne, C., Aron, A. R., Ostrem, J. L., Knight, R. T., & Starr, P. A. (2015). Elevated synchrony in Parkinson disease detected with electroencephalography. *Annals of Neurology*, *78*(5), 742–750. https://doi.org/10.1002/ana.24507

Szewczyk-Krolikowski, K., Menke, R. A. L., Rolinski, M., Duff, E., Salimi-Khorshidi, G., Filippini, N., Zamboni, G., Hu, M. T. M., & Mackay, C. E. (2014). Functional

connectivity in the basal ganglia network differentiates PD patients from controls. *Neurology*, *83*(3), 208–214. https://doi.org/10.1212/WNL.0000000000000592

Szurhaj, W., Derambure, P., Labyt, E., Cassim, F., Bourriez, J.-L., Isnard, J., Guieu, J.-D., & Mauguière, F. (2003). Basic mechanisms of central rhythms reactivity to preparation and execution of a voluntary movement: A stereoelectroencephalographic study. *Clinical Neurophysiology*, *114*(1), 107–119. https://doi.org/10.1016/S1388-2457(02)00333-4

Tahmasian, M., Eickhoff, S. B., Giehl, K., Schwartz, F., Herz, D. M., Drzezga, A., van Eimeren, T., Laird, A. R., Fox, P. T., Khazaie, H., Zarei, M., Eggers, C., & Eickhoff, C. R. (2017). Resting-state functional reorganization in Parkinson's disease: An activation likelihood estimation meta-analysis. *Cortex*, *92*, 119–138. https://doi.org/10.1016/j.cortex.2017.03.016

Tait, L., Özkan, A., Szul, M. J., & Zhang, J. (2021). A systematic evaluation of source reconstruction of resting MEG of the human brain with a new high-resolution atlas: Performance, precision, and parcellation. *Human Brain Mapping*, *42*(14), 4685–4707. https://doi.org/10.1002/hbm.25578

Tambasco, N., Nigro, P., Romoli, M., Prontera, P., Simoni, S., & Calabresi, P. (2016). A53T in a parkinsonian family: A clinical update of the SNCA phenotypes. *Journal of Neural Transmission*, *123*(11), 1301–1307. https://doi.org/10.1007/s00702-016-1578-6

Tan, H., Jenkinson, N., & Brown, P. (2014). Dynamic Neural Correlates of Motor Error Monitoring and Adaptation during Trial-to-Trial Learning. *The Journal of Neuroscience*, *34*(16), 5678–5688. https://doi.org/10.1523/JNEUROSCI.4739-13.2014

Tan, H., Wade, C., & Brown, P. (2016). Post-Movement Beta Activity in Sensorimotor Cortex Indexes Confidence in the Estimations from Internal Models. *The Journal of Neuroscience*, *36*(5), 1516–1528. https://doi.org/10.1523/JNEUROSCI.3204-15.2016

Tinkhauser, G., Pogosyan, A., Little, S., Beudel, M., Herz, D. M., Tan, H., & Brown, P. (2017). The modulatory effect of adaptive deep brain stimulation on beta bursts in Parkinson's disease. *Brain*, *140*(4), 1053–1067. https://doi.org/10.1093/brain/awx010

Tinkhauser, G., Pogosyan, A., Tan, H., Herz, D. M., Kühn, A. A., & Brown, P. (2017). Beta burst dynamics in Parkinson's disease OFF and ON dopaminergic medication. *Brain*, *140*(11), 2968–2981. https://doi.org/10.1093/brain/awx252

Tinkhauser, G., Torrecillos, F., Duclos, Y., Tan, H., Pogosyan, A., Fischer, P., Carron, R., Welter, M.-L., Karachi, C., Vandenberghe, W., Nuttin, B., Witjas, T., Régis, J., Azulay, J.-P., Eusebio, A., & Brown, P. (2018). Beta burst coupling across the motor circuit in Parkinson's disease. *Neurobiology of Disease*, *117*, 217–225. https://doi.org/10.1016/j.nbd.2018.06.007

Torrecillos, F., Tinkhauser, G., Fischer, P., Green, A. L., Aziz, T. Z., Foltynie, T., Limousin, P., Zrinzo, L., Ashkan, K., Brown, P., & Tan, H. (2018). Modulation of Beta Bursts

in the Subthalamic Nucleus Predicts Motor Performance. *The Journal of Neuroscience*, *38*(41), 8905–8917. https://doi.org/10.1523/JNEUROSCI.1314-18.2018

Underwood, C. F., & Parr-Brownlie, L. C. (2021). Primary motor cortex in Parkinson's disease: Functional changes and opportunities for neurostimulation. *Neurobiology of Disease*, *147*, 105159. https://doi.org/10.1016/j.nbd.2020.105159

Uusitalo, M. A., & Ilmoniemi, R. J. (1997). Signal-space projection method for separating MEG or EEG into components. *Medical & Biological Engineering & Computing*, *35*(2), 135–140. https://doi.org/10.1007/BF02534144

van Ede, F., Quinn, A. J., Woolrich, M. W., & Nobre, A. C. (2018). Neural Oscillations: Sustained Rhythms or Transient Burst-Events? *Trends in Neurosciences*, *41*(7), 415–417. https://doi.org/10.1016/j.tins.2018.04.004

Van Schependom, J., Vidaurre, D., Costers, L., Sjøgård, M., Sima, D. M., Smeets, D., D'hooghe, M. B., D'haeseleer, M., Deco, G., Wens, V., De Tiège, X., Goldman, S., Woolrich, M., & Nagels, G. (2021). Increased brain atrophy and lesion load is associated with stronger lower alpha MEG power in multiple sclerosis patients. *NeuroImage: Clinical*, *30*, 102632. https://doi.org/10.1016/j.nicl.2021.102632

Van Veen, B. D., & Buckley, K. M. (1988). Beamforming: A versatile approach to spatial filtering. *IEEE ASSP Magazine*, *5*(2), 4–24. https://doi.org/10.1109/53.665

Vardy, A. N., van Wegen, E. E. H., Kwakkel, G., Berendse, H. W., Beek, P. J., & Daffertshofer, A. (2011). Slowing of M1 activity in Parkinson's disease during rest and movement – An MEG study. *Clinical Neurophysiology*, *122*(4), 789–795. https://doi.org/10.1016/j.clinph.2010.10.034

Vidaurre, D., Abeysuriya, R., Becker, R., Quinn, A. J., Alfaro-Almagro, F., Smith, S. M., & Woolrich, M. W. (2018). Discovering dynamic brain networks from big data in rest and task. *NeuroImage*, *180*, 646–656. https://doi.org/10.1016/j.neuroimage.2017.06.077

Vidaurre, D., Hunt, L. T., Quinn, A. J., Hunt, B. A. E., Brookes, M. J., Nobre, A. C., & Woolrich, M. W. (2018). Spontaneous cortical activity transiently organises into frequency specific phase-coupling networks. *Nature Communications*, *9*(1), 2987. https://doi.org/10.1038/s41467-018-05316-z

Vidaurre, D., Quinn, A. J., Baker, A. P., Dupret, D., Tejero-Cantero, A., & Woolrich, M. W. (2016). Spectrally resolved fast transient brain states in electrophysiological data. *NeuroImage*, *126*, 81–95. https://doi.org/10.1016/j.neuroimage.2015.11.047

Vidaurre, D., Smith, S. M., & Woolrich, M. W. (2017). Brain network dynamics are hierarchically organized in time. *Proceedings of the National Academy of Sciences*, *114*(48), 12827–12832. https://doi.org/10.1073/pnas.1705120114

Vijiaratnam, N., Simuni, T., Bandmann, O., Morris, H. R., & Foltynie, T. (2021). Progress towards therapies for disease modification in Parkinson's disease. *The Lancet Neurology*, *20*(7), 559–572. https://doi.org/10.1016/S1474-4422(21)00061-2

Vinding, M. C., Eriksson, A., Comarovschii, I., Waldthaler, J., Manting, C. L., Oostenveld, R., Ingvar, M., Svenningsson, P., & Lundqvist, D. (2023). *The Swedish National Facility for Magnetoencephalography Parkinson's Disease Dataset (v1.1)* [dataset]. EBRAINS. https://doi.org/10.25493/DSY2-W2P

Vinding, M. C., Eriksson, A., Comarovschii, I., Waldthaler, J., Manting, C. L., Oostenveld, R., Ingvar, M., Svenningsson, P., & Lundqvist, D. (2024). The Swedish National Facility for Magnetoencephalography Parkinson's disease dataset. *Scientific Data*, *11*(1), 150. https://doi.org/10.1038/s41597-024-02987-w

Vinding, M. C., Eriksson, A., Ting Low, C. M., Waldthaler, J., Ferreira, D., Ingvar, M., Svenningsson, P., & Lundqvist, D. (2021). *Changes in non-oscillatory features of the cortical sensorimotor rhythm in Parkinson's disease across age* [Preprint]. Neurology. https://doi.org/10.1101/2021.06.27.21259592

Vinding, M. C., & Oostenveld, R. (2022). Sharing individualised template MRI data for MEG source reconstruction: A solution for open data while keeping subject confidentiality. *NeuroImage*, *254*, 119165. https://doi.org/10.1016/j.neuroimage.2022.119165

Vinding, M. C., Tsitsi, P., Piitulainen, H., Waldthaler, J., Jousmäki, V., Ingvar, M., Svenningsson, P., & Lundqvist, D. (2019). Attenuated beta rebound to proprioceptive afferent feedback in Parkinson's disease. *Scientific Reports*, *9*(1), 2604. https://doi.org/10.1038/s41598-019-39204-3

Vinding, M. C., Tsitsi, P., Waldthaler, J., Oostenveld, R., Ingvar, M., Svenningsson, P., & Lundqvist, D. (2020). Reduction of spontaneous cortical beta bursts in

Parkinson's disease is linked to symptom severity. *Brain Communications*, *2*(1), fcaa052. https://doi.org/10.1093/braincomms/fcaa052

Vinding, M. C., Waldthaler, J., Eriksson, A., Manting, C. L., Ferreira, D., Ingvar, M., Svenningsson, P., & Lundqvist, D. (2024). Oscillatory and non-oscillatory features of the magnetoencephalic sensorimotor rhythm in Parkinson's disease. *Npj Parkinson's Disease*, *10*(1), 51. https://doi.org/10.1038/s41531-024-00669-3

Wang, Z., Mo, Y., Sun, Y., Hu, K., Peng, C., Zhang, S., & Xue, S. (2022). Separating the aperiodic and periodic components of neural activity in Parkinson's disease. *European Journal of Neuroscience*, *56*(6), 4889–4900. https://doi.org/10.1111/ejn.15774

Waschke, L., Donoghue, T., Fiedler, L., Smith, S., Garrett, D. D., Voytek, B., & Obleser, J. (2021). Modality-specific tracking of attention and sensory statistics in the human electrophysiological spectral exponent. *eLife*, *10*, e70068. https://doi.org/10.7554/eLife.70068

Weber, F., Chung, S., Beier, K. T., Xu, M., Luo, L., & Dan, Y. (2015). Control of REM sleep by ventral medulla GABAergic neurons. *Nature*, *526*(7573), 435–438. https://doi.org/10.1038/nature14979

Wen, H., & Liu, Z. (2016). Separating Fractal and Oscillatory Components in the Power Spectrum of Neurophysiological Signal. *Brain Topography*, *29*(1), 13–26. https://doi.org/10.1007/s10548-015-0448-0

Wiesman, A. I., Da Silva Castanheira, J., Degroot, C., Fon, E. A., Baillet, S., & Network, Q. P. (2023). Adverse and compensatory neurophysiological slowing in Parkinson's disease. *Progress in Neurobiology*, *231*, 102538. https://doi.org/10.1016/j.pneurobio.2023.102538

Wiesman, A. I., Koshy, S. M., Heinrichs-Graham, E., & Wilson, T. W. (2020). Beta and gamma oscillations index cognitive interference effects across a distributed motor network. *NeuroImage*, *213*, 116747. https://doi.org/10.1016/j.neuroimage.2020.116747

Wiesman, A. I., Madge, V., Fon, E. A., Dagher, A., Collins, D. L., Baillet, S., PREVENT-AD Research Group, & Quebec Parkinson Network. (2024). *Associations between neuromelanin depletion and cortical rhythmic activity in Parkinson's disease* [Preprint]. Neurology. https://doi.org/10.1101/2024.02.16.24302958

Wiesman, A. I., Murman, D. L., Losh, R. A., Schantell, M., Christopher-Hayes, N. J., Johnson, H. J., Willett, M. P., Wolfson, S. L., Losh, K. L., Johnson, C. M., May, P. E., & Wilson, T. W. (2022). Spatially resolved neural slowing predicts impairment and amyloid burden in Alzheimer's disease. *Brain*, *145*(6), 2177–2189. https://doi.org/10.1093/brain/awab430

Wiest, C., Torrecillos, F., Pogosyan, A., Bange, M., Muthuraman, M., Groppa, S., Hulse, N., Hasegawa, H., Ashkan, K., Baig, F., Morgante, F., Pereira, E. A., Mallet, N., Magill, P. J., Brown, P., Sharott, A., & Tan, H. (2023). The aperiodic exponent of subthalamic field potentials reflects excitation/inhibition balance in Parkinsonism. *eLife*, *12*, e82467. https://doi.org/10.7554/eLife.82467

Willis, A. W. (2013). *Parkinson Disease in the Elderly Adult*. *110(5)*, 406–410.

Wilson, L. E., Da Silva Castanheira, J., & Baillet, S. (2022). Time-resolved parameterization of aperiodic and periodic brain activity. *eLife*, *11*, e77348. https://doi.org/10.7554/eLife.77348

Woolrich, M., Hunt, L., Groves, A., & Barnes, G. (2011). MEG beamforming using Bayesian PCA for adaptive data covariance matrix regularization. *NeuroImage*, *57*(4), 1466–1479. https://doi.org/10.1016/j.neuroimage.2011.04.041

Yan, S., Jiang, C., Janzen, A., Barber, T. R., Seger, A., Sommerauer, M., Davis, J. J., Marek, K., Hu, M. T., Oertel, W. H., & Tofaris, G. K. (2023). Neuronally Derived Extracellular Vesicle α-Synuclein as a Serum Biomarker for Individuals at Risk of Developing Parkinson Disease. *JAMA Neurology*. https://doi.org/10.1001/jamaneurol.2023.4398

Yang, W., Hamilton, J. L., Kopil, C., Beck, J. C., Tanner, C. M., Albin, R. L., Ray Dorsey, E., Dahodwala, N., Cintina, I., Hogan, P., & Thompson, T. (2020). Current and projected future economic burden of Parkinson's disease in the U.S. *Npj Parkinson's Disease*, *6*(1), 15. https://doi.org/10.1038/s41531-020-0117-1

Yassine, S., Gschwandtner, U., Auffret, M., Achard, S., Verin, M., Fuhr, P., & Hassan, M. (2022). Functional Brain Dysconnectivity in Parkinson's Disease: A 5-Year Longitudinal Study. *Movement Disorders*, *37*(7), 1444–1453. https://doi.org/10.1002/mds.29026

Zich, C., Quinn, A. J., Mardell, L. C., Ward, N. S., & Bestmann, S. (2020). Dissecting Transient Burst Events. *Trends in Cognitive Sciences*, *24*(10), 784–788. https://doi.org/10.1016/j.tics.2020.07.004

Zokaei, N., Quinn, A. J., Hu, M. T., Husain, M., van Ede, F., & Nobre, A. C. (2021). Reduced cortico-muscular beta coupling in Parkinson's disease predicts motor impairment. *Brain Communications*, *3*(3), fcab179. https://doi.org/10.1093/braincomms/fcab179

# Appendix

# A1

## Chapter 1

Literature referenced in introduction of Chapter 1 on beta oscillations in basal ganglia-thalamocortical loop

Table A1 Referenced literature on beta oscillations in basal ganglia-thalamocortical

| Author | Year | N | Comparisons | Age | Years Since Diagnosis | Medication Status | UPDRS-III | H&Y | LED | Findings |
|---|---|---|---|---|---|---|---|---|---|---|
| Non-invasive motor cortical beta power | | | | | | | | | | |
| Swann et al. | 2015 | 16 HC; 15 PD | HC vs PD; On vs Off-Medication | HC: 63.5 PD: 63.2 | 4.5 | On & Off | / | /; 2-3 | / | No significant group differences or dopaminergic medication effects for motor cortical (C3 and C4) beta power. |
| Heinrichs-Graham et al. | 2014 | 15 HC; 15 PD | HC vs PD; On vs Off-Medication | HC: 66.3 PD: 63.1 | 5 (only of in analysis included patients; n= 12) | On & Off | On: 23.69 Off: 29.92 | / | / | Decreased motor cortical beta power that normalises (increases) after dopaminergic drug intake. |
| Salenius et al. | 2002 | 8 HC; 18 PD | HC vs PD; On vs Off-Medication | HC: 48 PD: 49 | / | On & Off | On: 12 Off: 24 | /; 1-3 | / | Not significant trend towards decreased beta power in PD and normalisation upon |

| | | | | | | | | | | |
|---|---|---|---|---|---|---|---|---|---|---|
| | | | | | | | | | | dopaminergic medication intake. |
| Stanzione et al. | 1996 | 22 HC; 19 PD | HC vs PD | HC: 63 PD: 63.5 | 2.36 | Off | 5 Items from UPDRS-III (Fahn & Elton, 1987): 18:53 | 1.34; 1.5-3 | / | Whole-brain average demonstrates significantly decreased beta power in PD that is not modified by dopaminergic medication. |
| Vardy et al. | 2011 | 11 HC; 11 PD | PD vs HC | HC: / PD: 61 | 5.1 | On | Total UPDRS On: 22-71 | 2.58; 1.5-3 | 748[a] | Motor cortical beta power (average across all trials) decreased in PD. |
| Hall et al. | 2014 | 9 HC; 9 PD (drug-naive) | PD vs HC; PD vs PD zolpidem; PD zolopidem vs HC. | HC: 62.2 PD: 60.7 | / | On & Off zolopidem | Off: 14.25 | / | N/A | Increased beta power in hemisphere contralateral to symptom presentation in PD compared to controls. |
| Pollok et al. | 2012 | 20 PD (10 drug- | Drug-naïve PD vs. PD; | HC: 56.1 | De Novo: 1.18 | Off | PD-Off:13.1 | /; 1-2 | / | De novo (drug naïve) and early PD patients (Ldopa treated) both show |

| | | | | | | | | | | |
|---|---|---|---|---|---|---|---|---|---|---|
| | | naïve; 10 early but dopaminergic medication prescribed)<br><br>10 HC | Drug-naïve PD vs HC;<br><br>PD vs HC | De Novo: 58.7<br>PD: 54.6 | PD: 2.375 | | De Novo-Off: 10.2 | | | significantly increased motor cortical beta power. |
| Vinding et al. | 2020 | 19 HC; 19 PD | HC vs PD; On vs Off-Medication | HC: 69.3<br>PD: 67.3 | 4.5 | On & Off | Off: 34<br>On: 16 | /;<br>1-3 | 615 | Beta bursts decreased in PD; Bursts rates associated with Bradykinesia & postural/ kinetic tremor. Burst rates not modulated by dopaminergic medication. No significant differences in motor cortical beta power between HC and PD. |
| Vinding et al. | 2021 | 60 HC; 78 PD | HC vs. PD | HC: 63.93<br>PD: 65.6 | 4.4 | On | On: 18.9 | /;<br><br>1-3 | 548 | **Not peer reviewed.**<br>Beta Burst rate not significantly in PD compared to HC but associated with Bradykinesia scores. Burst rates decline faster with increasing age in PD. Significantly increased beta |

| | | | | | | | | | | |
|---|---|---|---|---|---|---|---|---|---|---|
| | | | | | | | | | | power. But in Chapter 3 we observe significantly decreased beta power. |
| Heidemann et al. | 2020 | 18 HC; 18 PD | HC vs. PD | HC: 67.3 PD: 68.5 | 2.7 | Off | Off: 31.5 | 1.75 | 443.75 | Beta burst interval times underpin decreased beta power during movement preparation in PD. |
| Dopaminergic Medication effect on motor cortical beta power | | | | | | | | | | |
| Cao et al. | 2020 | 21 PD | On vs Off-Medication | PD: 59.8 | 9 | On & Off | Off: 50.95 On: 24.05 | / | 710 | Dopaminergic medication increases motor cortical beta power. Increase in beat power scales with motor improvement. |
| Melgari et al. | 2014 | 24 PD (15 Naïve; 9 on dopamine replacement therapy) | On vs Off-Medication | PD: 72.63 | 4.08 | On & Off | Off: 25 On: 13.92 | 1.9; | 190 | |
| DBS effect on motor cortical beta power | | | | | | | | | | |

| | | | | | | | | | | |
|---|---|---|---|---|---|---|---|---|---|---|
| Cao et al. | 2015 | 11 HC; 16 PD (pre-operative); 16 PD (DBS) | HC vs PD (pre-surgery); On vs Off-DBS | HC: 56.6 PD (no-DBS): 55.8 PD (DBS): 55 | PD: 9.94 PD DBS: 8 | Off | PD (No-DBS): 44.63 PD (DBS): On-DBS: 12.8 Off-DBS: 33.8 | / | / | DBS increases beta power across the brain. |
| Cao et al. | 2017 | 13 HC; 14 PD (pre-operative); 13 PD (DBS) | HC vs PD (pre-surgery); On vs Off-DBS | HC: 56.6 PD (no-DBS): 58.1 PD (DBS): 55 | PD preoperative: 11.3 PD DBS: 9.4 | Off | PD (No-DBS): 47.9 PD (DBS): Off-DBS: 40.9 On-DBS: 20 | / | / | DBS increases beta power in temporal and occipital regions; but not in central (they call it parietal) regions |
| Abbasi et al. | 2018 | 9 PD | On vs Off-DBS | PD: 62.89 | 11.11 | Off | Off DBS: 41.11 On | / | 1154.44 | DBS decreases motor cortical beta power. |

| | | | | | | | | | | |
|---|---|---|---|---|---|---|---|---|---|---|
| | | | | | | | DBS: 27.11 | | | |
| Luoma et al. | 2018 | 16 PD | On vs Off-DBS | PD: 57.4 | 11.9 to surgery 0.75 since surgery<br><br>12.65 | On | Off DBS: 32.1 On DBS: 18 | / | 962.5 | DBS decreases motor cortical beta power. |
| Beta Oscillations in basal ganglia-thalamocortical loop | | | | | | | | | | |
| Tinkhauser, Pogosyan, Little, et al. | 2017 | 13 PD | On vs Off-DBS | PD: 56.8 | 8.2 | Off | Off: 41.5<br><br>ON: 16.7 | / | / | Adaptive DBS reducing the STN burst duration is more effective than normal DBS. DBS reduces long, high-amplitude bursts. |
| Tinkhauser, Pogosyan, Tan, et al. | 2017 | 8 PD | On vs Off-Medication | PD: 62.5 | 12.6 | Off | Off: 22<br><br>On: 18.9 | / | / | Dopaminergic Medication decreases STN burst duration. Drug-related decrease in duration is associated with motor improvement. Medication also reduces burst overlap between hemispheres. |
| Kuhn et al. | 2008 | 10 PD | DBS On | PD: 59.72 | 10.36 | Off | Off: 37.36[b] | / | 1227.64[a,b] | DBS reduces beta power in STN. Beta power reduction associated with better task performance (movement |

| | | | | | | | | | | |
|---|---|---|---|---|---|---|---|---|---|---|
| | | | | | | | On: 13.91[b] | | | amplitude in motor task improved). |
| Oswal et al. | 2016 | 15 PD | On vs Off-DBS | PD: 61 | 11.2 | Off | DBS-Off: 42.53 DBS-On: 25.4 | / | 1209.07 | DBS reduces high beta coupling between STN and mesial motor areas. Reduction in synchronisation does not scale with motor improvement. |
| Brown et al. | 2001 | 4 PD | On vs Off-Medication | PD: 59 | 17 | On but on reduced dosage (LED = 200mg) | Off: 66 On: 20 Unclear if preoperative. | / | 770 Unclear if preoperative. | Low frequency (<30 Hz) coupling between STN and GPi. Levodopa administration reduces low frequency coupling. New peak in coupling at 70 Hz. |
| Eusebio et al. | 2011 | 15 PD | PD during DBS stimulation. | Supplementary information not available | / | / | / | / | / | DBS supresses STN 11 to 30-Hz activity. Increasing stimulation yields stronger reduction. |

| | | | | | | | | | | |
|---|---|---|---|---|---|---|---|---|---|---|
| Lofredi et al. | 2023 | 106 PD | On vs Off-Medication | PD: 63.5 | 10.84 | ON & OFF | Off: 32.7<br><br>On: 18.3<br><br>27 preoperatively and 67 during recording session UPDRS | / | 810.64<br><br>Unclear; probably similar to UPDRS. | Motor impairment off medication associated with higher low-beta power and longer burst duration. Reduction of power and burst duration correlated with symptom alleviation due to dopaminergic medication. |
| Oswal, Cao, et al. | 2021 | 32 PD | Simultaneous STN-MEG recordings; On vs. Off-DBS | PD: 58.8 (average across all PD groups) | 11.36 | On | Off: 43<br>On: 25.25<br><br>Average across groups/ condition for which UPDRS scores were | / | 909.8 | Coherence between STN and supplementary motor area in high-beta (21 to 30 Hz) but not low-beta (13 to 21 Hz) range correlated with fibre density of hyperdirect pathway. Supplementary motor area is driving STN in high-beta frequencies, which in turn might result in low-beta hypersynchronisation in STN. |

| | | | | | | | | | | |
|---|---|---|---|---|---|---|---|---|---|---|
| | | | | | | | provided | | | |
| Tinkhauser et al. | 2018 | 9 PD (advance stage) | Simultaneous STN-EEG recordings | PD: 60.1 | 11.7 | Off | Off: 27.6<br>On: 7.8 | / | / | STN Burst significantly overlap with motor cortex bursts.<br>Coherence between STN and Motor Cortex larger during Bursts.<br>Overlap between Cortex and STN larger during long bursts. |
| Invasive recordings of motor cortical beta power | | | | | | | | | | |
| Crowell et al. | 2012 | 11 PD;<br>10 dystonia;<br>10 essential tremor<br><br>All PD scheduled for DBS implantation. | PD vs. dystonia vs. essential tremor | PD : 56.7<br>Dyst: 58.5<br>ET: 64 | PD: 11.1<br>Dys: 10.3<br>ET: 27.4 | Off | Off: 43.3 | / | PD: 1041 | PD patients have larger high-beta power than essential tremor or dystonia patients. |

| | | | | | | | | | | |
|---|---|---|---|---|---|---|---|---|---|---|
| O'Keeffe et al. | 2020 | 22 PD; 10 Essential Tremor | PD vs essential tremor | PD: 64.4 ET: 58.9 | / | Off | Off (probably): 35.23 | / | / | PD patients show significantly increased burst durations compared to essential tremor patients. Synchronisation between motor and premotor cortex precedes high-beta motor bursts and high-beta bursts are associated with changes in waveform shape and phase- amplitude coupling. |
| De Hemptinne et al. | 2013 | 16 PD; 9 Primary cranio-cervical dystonia; 9 epilepsy | PD vs. Epilepsy vs. cranio-cervical dystonia | PD: 64.6 Dyst: 56 Ep: 26.3 | PD: 13 Dyst: 8.7 | Off | Off: 37.69 On: 17.44 | / | 1226.19 | No significant differences between motor cortical beta power and other patient groups. |
| De Hemptinne et al. | 2015 | 23 PD | On vs Off-DBS | PD: 63.04 | / | Off | Off: 40.43 On: 21.26 | / | / | DBS stimulation does not change motor cortical beta power significantly. |

| | | | | | | | | | | |
|---|---|---|---|---|---|---|---|---|---|---|
| Pauls et al.[c] | 2022 | 16 HC;<br><br>21 PD | HC vs. PD;<br><br>On vs Off-DBS | HC: 60.6<br>PD: 59 | 12.6 | 13 On;<br>3 Off | On: 17.13<br>Off: 38.13 | / | 654.6 | Sensorimotor beta bursts show increased amplitudes and lifetimes compared to HCs. Both metrics are modulated by DBS. DBS-related reduction in burst amplitude associated with DBS-related reductions in motor impairment scores. No association for DBS-related changes of burst durations observed. |

Where no mean values were reported but values per participant were provided group means were calculated manually.

UPDRS and LED values in DBS studies were all acquired preoperatively. In cases where this is not the case, this is mentioned in the table.

[a]: LED calculated from SI table with: https://www.parkinsonsmeasurement.org/toolBox/levodopaEquivalentDose.htm

[b]: UPDRS and LED values prior to the surgery were noted because more comparable to other studies.

[c]: Pauls et al. 2022 investigate changes in motor cortical beta oscillations with MEG in PD patients who underwent DBS surgery. In contrast to other studies in this section, brain activity is recorded non-invasively. But since included participants all underwent DBS surgery this study is considered invasive.

# Systematic sample differences between invasive and non-invasive literature on beta oscillations in basal ganglia-thalamocortical loop

## Motivation

From the comprehensive overview presented in Table A1 , it is evident that the invasive literature consistently portrays exaggerated beta oscillations in the basal ganglia-thalamocortical loop and motor cortex. However, the non-invasive literature reveals inconsistent findings, often diverging from the expected outcomes based on invasive studies. This discrepancy may stem from various factors, including varying disease progressions, assessment of intervention effects or HC vs. PD group contrasts, or different spatial resolutions.

## Procedure

To get a better understanding of systematic differences between the invasive and non-invasive literature, I extracted and visualised PD sample properties such as years since diagnosis, UPDRS-III scores on- and off-medication, and levodopa equivalent dose (LED) scores from the studies listed in Table A1 . The following findings are by no means conclusive, as no systematic literature search was conducted. However, they may offer valuable insights into differences and similarities among samples included in both types of studies.

For qualitative comparisons, studies were categorized into invasive vs. non-invasive and group vs. treatment comparisons. Invasive studies included those involving PD volunteers who underwent ECoG or DBS surgery, encompassing M/EEG studies investigating PD volunteers who underwent DBS surgery (Cao et al., 2015, 2017; Pauls

et al., 2022). Group comparison studies compared PD volunteers with control groups, while treatment comparison studies examined the effects of dopaminergic medication or DBS within participants. For studies with different PD groups, such as De Novo vs. Normal PD volunteers (Pollok et al., 2012) or pre-DBS vs. post-DBS surgery PD volunteers (Cao et al., 2015, 2017), I treated each group as separate sample in the visualization.

## Findings & Discussion

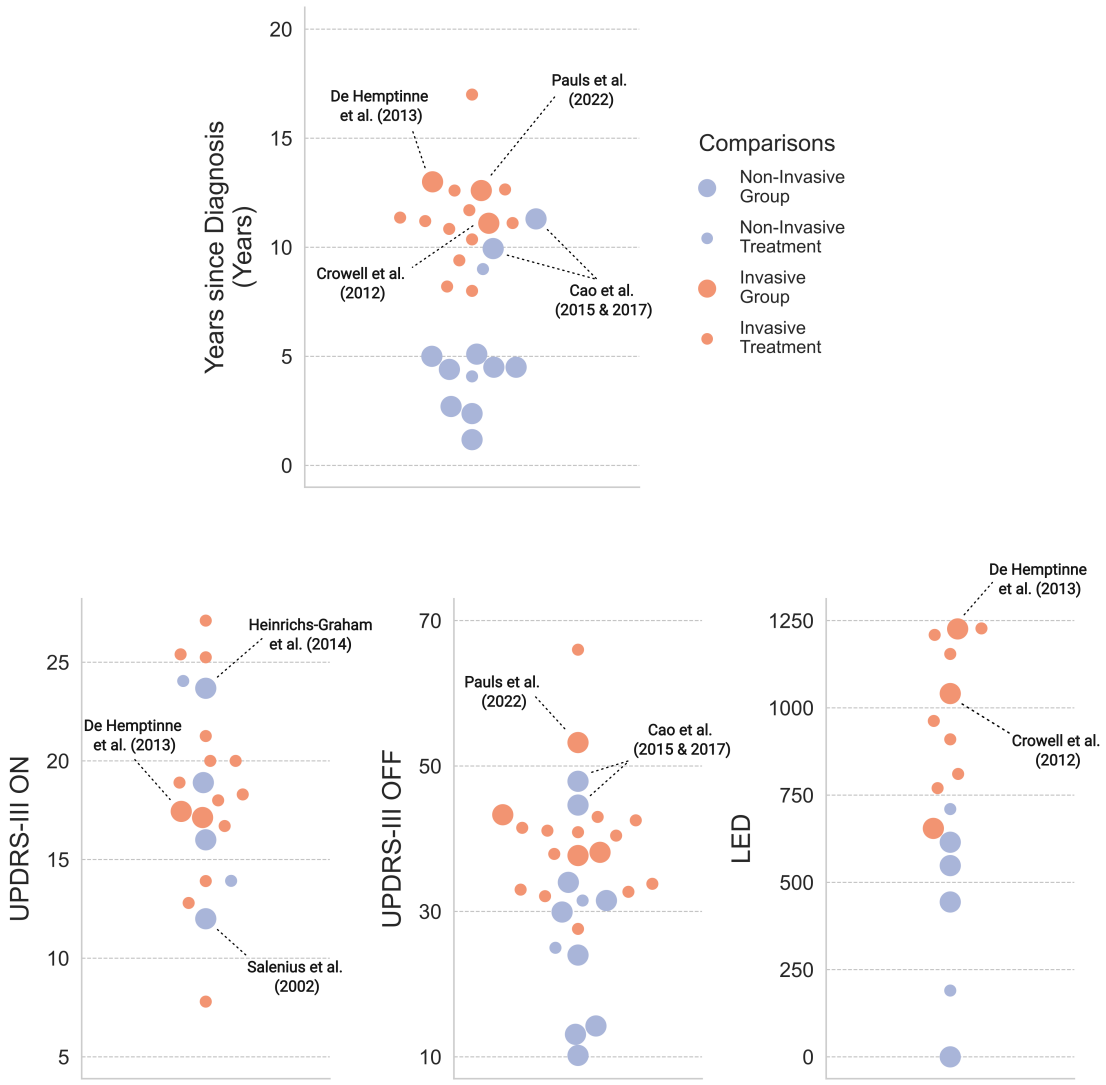

**Figure A1.1. Overview of clinical variables across all studies on beta oscillations in the basal ganglia-thalamocortical loop and motor cortex referenced in the introduction of Chapter 1.** Years since diagnosis, UPDRS-III scores on- and off-medication, and levodopa equivalent dose (LED) scores were extracted from all papers. Each paper that provided average values or a table with values for the respective metric was included in these figures. Dot colours indicate whether included participants underwent an invasive DBS or EcOG surgery (purple) or not (red). Large dots represent studies that conducted group contrasts between HCs and PD volunteers, while smaller dost indicate studies in which the effect of either dopaminergic medication or DBS was investigated.

Qualitative assessment of Table A1 . yields three main observations:

- Studies assessing non-invasive samples are more likely to compare PD volunteers with HCs, whereas invasive studies mostly investigate treatment effects.
- Participants included in non-invasive studies usually show shorter disease durations, lower UPDRS-Off scores, and lower LED scores. UPDRS-On scores do not seem to vary systematically between invasive and non-invasive samples.
- **Invasive and non-invasive studies systematically investigated PD volunteers with different disease progressions.** Invasive studies investigate more progressed PD volunteers (8 > years disease duration), whereas the majority of invasive studies focuses on early-stage PD volunteers (> 5 years disease duration).
-

Observation 1: Invasive studies primarily examine treatment effects due to the absence of control groups, as healthy individuals do not undergo surgery. The only exceptions are EcOG studies using recordings from patients with essential tremor or epilepsy as controls (Crowell et al., 2012; De Hemptinne et al., 2013; O'Keeffe et al., 2020), and non-invasive M/EEG recordings comparing PD volunteers who underwent DBS surgery with matched healthy controls (Pauls et al., 2022). These exceptions fairly consistently indicate increased motor cortical beta power (Crowell et al., 2012; O'Keeffe et al., 2020; Pauls et al., 2022).

Observation 2: Longer disease durations and higher LED scores in invasive samples are not surprising, given that PD patients undergoing DBS surgery typically have mean disease durations of approximately 10 to 13 years (Deuschl et al., 2013; Schuepbach et al., 2013). These observations may have important implications for reconciling non-invasive and invasive studies, as patients in more advanced stages often require higher levodopa dosages and exhibit motor symptom fluctuations assumed to reflect changes in the striatal dopaminergic system (Chou et al., 2018). Consequently, differences in disease stage and medication usage likely contribute to inconsistencies between invasive and non-invasive studies.

Observation 3: Studies focusing on early-stage PD patients are rare in invasive research due to the lack of necessity for DBS surgery, highlighting the importance of non-invasive M/EEG studies for examining cortical beta oscillatory power in early PD stages. However, non-invasive studies investigating progressed PD stages with or without DBS surgery remain scarce, despite feasibility. The only two studies that compared pre-DBS surgery PD volunteers (> 9.9 years disease duration) with healthy controls did not

report significant changes in beta power in central regions of the brain (Cao et al., 2015, 2017). Further research is needed to clarify whether the increased motor cortical beta power observed in DBS surgery patients extends to non-surgery patients at advanced disease stages.

## Detailed description of included PD samples

Table A1 1 Detailed descriptions of the two PD volunteer samples combined for this study.

| | Zokai et al. (2021) | Heideman et al. (2020) |
|---|---|---|
| N | 12 | 16 |
| Groups matched in | Age<br>Education | Age<br>Education |
| Inclusion Criteria | Currently not participation in ongoing drug trial<br>Not taking any of the following drugs:<br>Psychotropic hypertensive<br>Vasoactive medication<br>Long-acting dopamine agonists<br>No history of neurological or psychiatry disorders other than PD.<br>Tolerating coming off dopaminergic medication. | Being diagnosed with PD within the last 5 years.<br>Being able to understand written and spoken instructions in English.<br>Being older than 50 years.<br>Tolerating coming off dopaminergic medication. |
| Dopaminergic Medication | Off-Medication<br>Since 7 p.m. of previous day. | Off-Medication<br>Since 7pm of previous day. |
| UPDRS administration | By trained clinician. | By trained clinician. |
| Ethics-Reference | 12/SC/0650 | 12/SC/0650 |

| | | |
|---|---|---|
| Cohort | Participants were recruited from neurological clinics in Oxfordshire (UK). | Dementias and Neurodegeneration Speciality (https://dendron.org.uk) |
| Sex (female/male) | 8/4 | 7/9 |
| Handedness (right/left) | 11/1 | 14/2 |
| Age (years) (mean, range) | 68.5 (57-77) | 68.5 (54-79) |
| Education (years) (mean, range) | 16 (10-24) | 13.69 (10-23) |
| Years since Diagnosis (years) (mean, range) | 3 (1-7) | 2.75 (1-4) |
| UPDRS III motor score (mean, range) | 32.33 (20-55) | 28.86 (11-49) |
| Hoehn and Yahr scale (mean, range) | 1.75 (1-3) | 1.78 (1-3) |
| Levodopa-equivalent daily dose (mg/day) (mean, range) | 283.75 (150-540) | 488.39 (300-900)* |

N = number of participants; UPDRS = Unified Parkinson Disease Rating Scale

* Two volunteers with PD did not take Levodopa (or equivalent) medication.

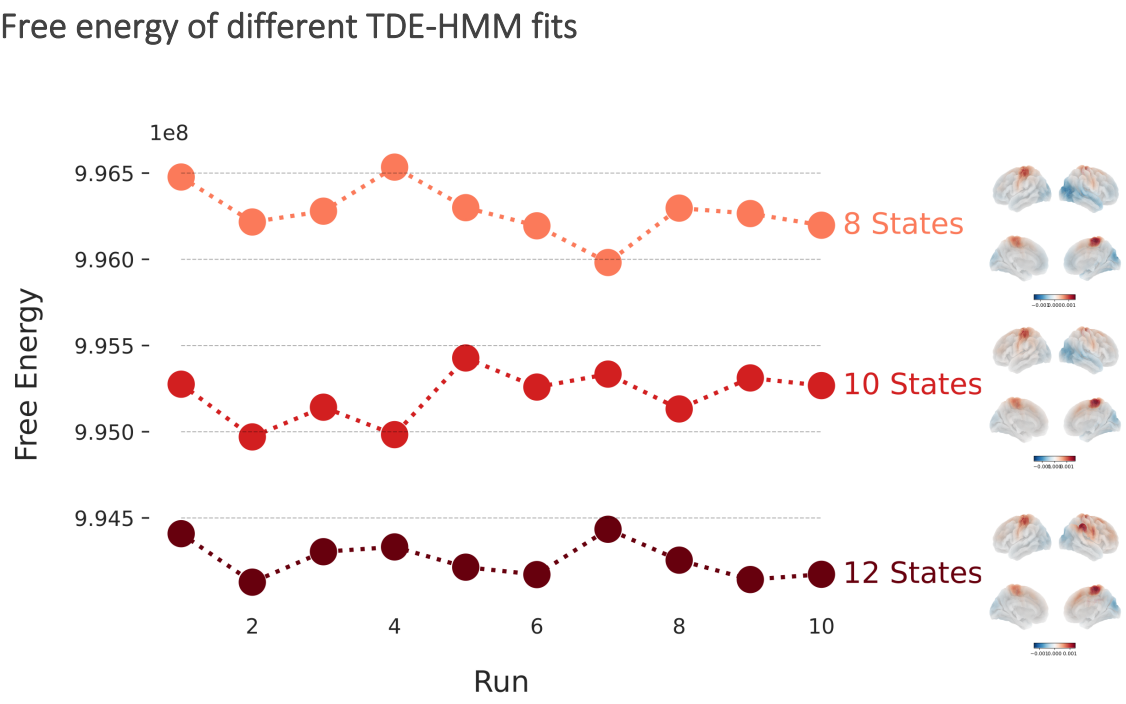


**Figure A1.2. Free Energy values of all HMM fits.** Free energy values for each of the 30 HMM fits are represented by a dot. Colours mark HMMs inferring different numbers of states. Wideband power maps of the sensorimotor network for the HMM fit with the lowest free energy of all HMMs extracting the same number of states are presented on the right.

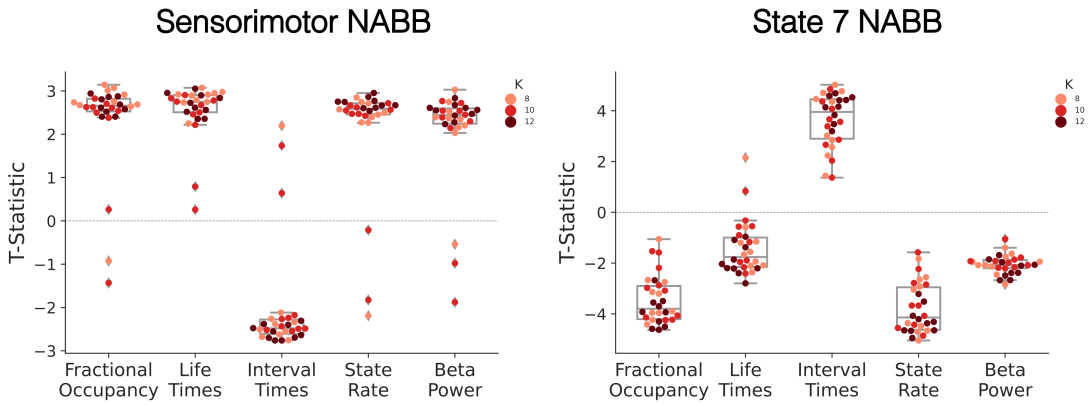


**Figure A1.3. Group differences of sensorimotor and State 7 NABB metrics are robust across all HMM inferences.** Each dot represents the t-statistic from the respective state metric's group contrast between HCs and PD patients for a different HMM inference. The colours of the dots indicate how many states were inferred for the depicted HMM inference.

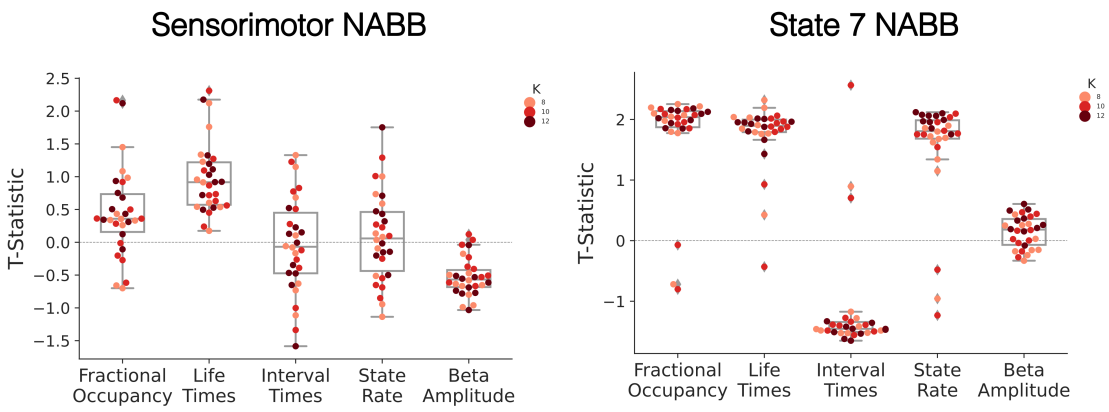


**Figure A1.4. Associations between State 7 NABB metrics and Bradykinesia/Rigidity scores are robust across all HMM inferences.** Each dot represents the t-statistic from the respective state metric's correlation with Bradykinesia/Rigidity score for a different HMM inference. The colours of the dots indicate how many states were inferred for the depicted HMM inference. Sensorimotor NABB metrics are not significantly associated with Bradykinesia/Rigidity scores.

# A2

## Chapter 2

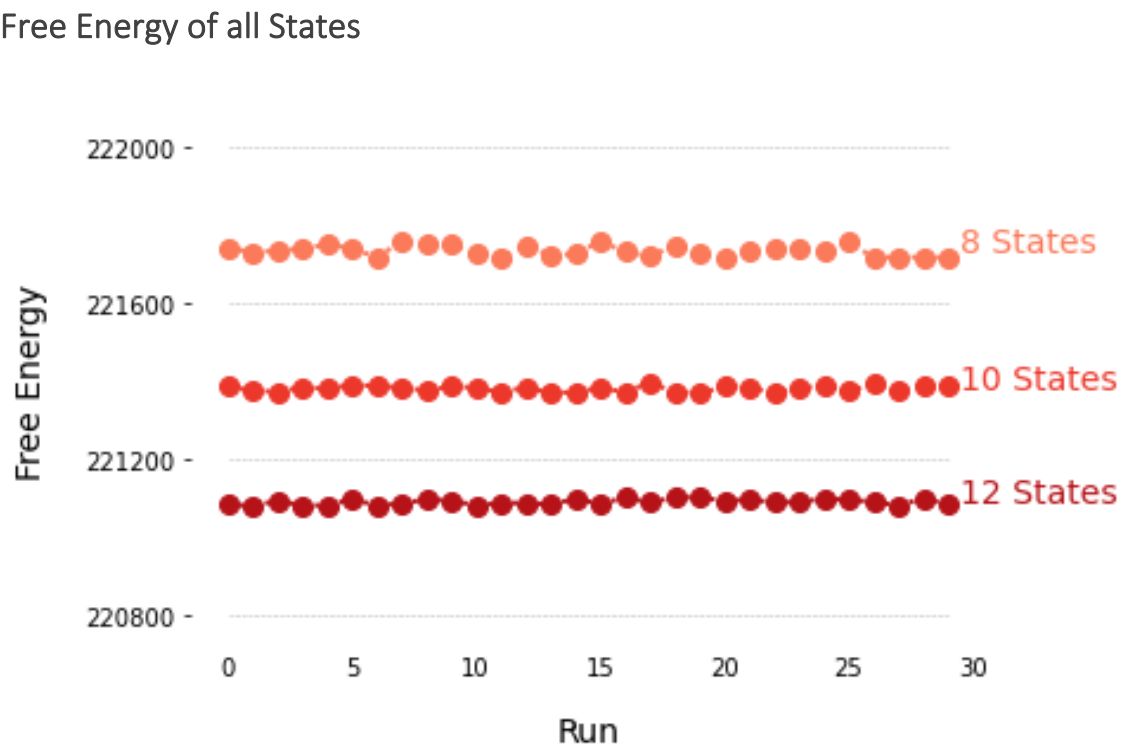


**Figure A2.1. Free Energy values of all HMM fits.** Free energy values for each of the 90 HMM fits are represented by a dot. Colours mark HMMs inferring different numbers of states.

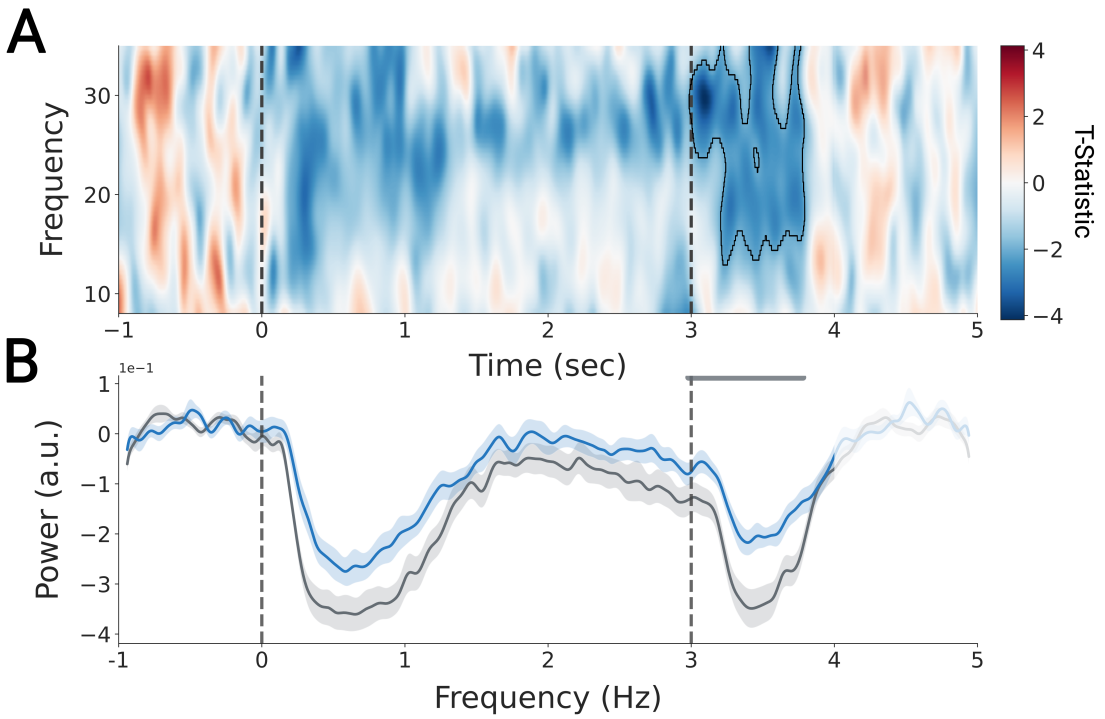


**Figure A2.2. Group contrast of motor cortical TFRs. (A)** T-statistic of baseline corrected TFR group contrast for each frequency bin and time point is depicted. Negative t-statistics indicate smaller values for PD patients. The black line outlines time-frequency cluster with significantly reduced beta power in PD volunteers that was identified with cluster-based permutation tests. **(B)** 13 to 35-Hz power time course of HCs (grey) and PD volunteers (blue) are shown to visualise the time course of beta power. The frequency range reflects the frequency range of the significant cluster obtained from cluster-based permutation tests on TFRs (A). Grey line on top of time courses marks time points in which significant cluster in TFR cluster-based permutation tests was identified.

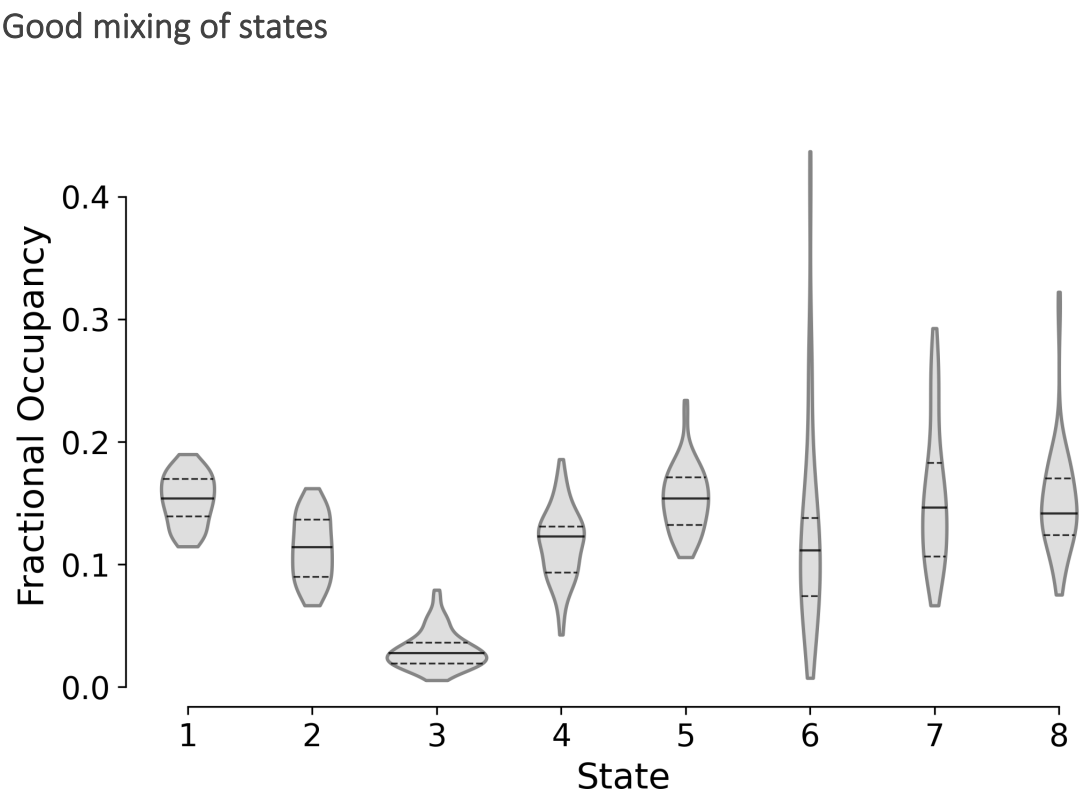


**Figure A2.3. Fractional Occupancies of all states indicate a good mixing of states.** Each violin represents the fractional occupancy values of all participants for the respective state. Crucially, the minimum fractional occupancy across all participants and states is larger than 0 and the maximum fractional occupancy across all participants and states is smaller than 1 demonstrating a good mixing of states. This reassures that the HMM-states do not represent interindividual differences between the participants but dynamic fluctuations with participants across the whole sample.

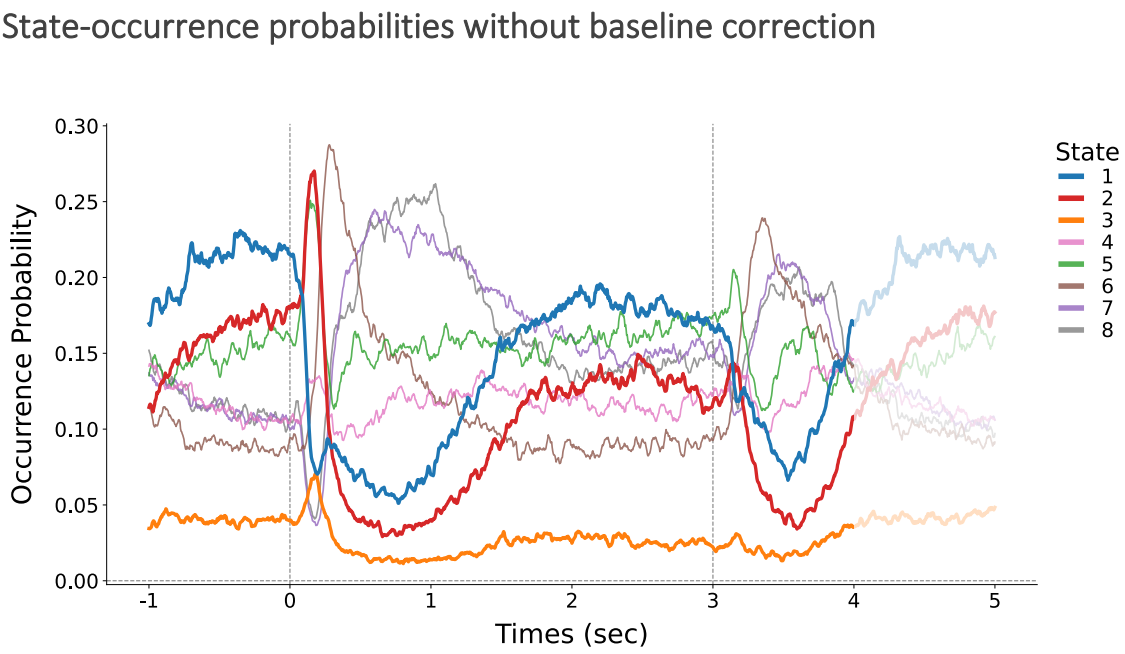


**Figure A2.4. Trial-averaged state occurrence probabilities without baseline correction time-locked to gripping-stimulus onset**. Each line reflects the average across participant of the percentage of all trials in which the respective state was present. Occurrence probabilities of states with increased oscillatory wideband power in superior motor cortical parcels are shown in vivid colours.

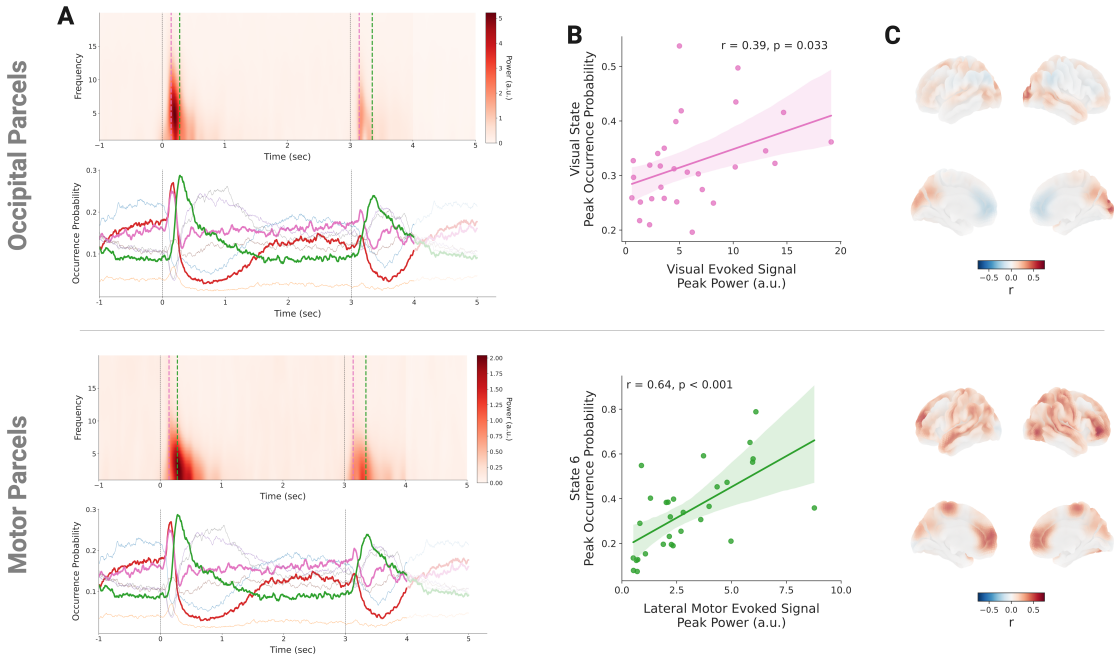


**Figure A2.5. Occurrence probability time courses of visual network and State 6 are linked to evoked responses. (A)** Peak state-occurrence probabilities of visual state and state 6 temporarily overlap with evoked responses in occipital and lateral motor parcels respectively. Time-frequency representations of all participants were calculated by averaging raw time courses of all trials, before a time-frequency analysis was calculated from each participant's trial-averaged parcel time course. TFRs were averaged across participants. Absolute occurrence probabilities are plotted under averaged TFRs to visualise temporal correspondence between state occurrence probabilities and evoked responses. Dashed lines indicate the time point with the maximum occurrence probability of the visual network (pink) and State 6 (green). Strikingly, the timing of maximal occurrence of visual networks overlaps with evoked response in occipital cortex, whereas maximal occurrence of State 6 overlaps with evoked response in motor parcels. **(B)** Peak occurrence probabilities of visual network and State 6 are significantly associated with peak power of evoked response in occipital and motor parcels. Peak power of evoked response was calculated as the average power across 1 to 5-Hz frequency bins. **(C)** Visual network peak occurrences

show the strongest association with the peak power of the evoked response in occipital parcels, whereas State 6 shows strong correlations with the peak power of the evoked response in frontal, motor, but also occipital regions of the brain. Correlation coefficients of visual network and State 6 peak occurrence probability with peak power of evoked response in each parcel are projected onto a brain surface.

## Group Contrasts of all network-probability time courses

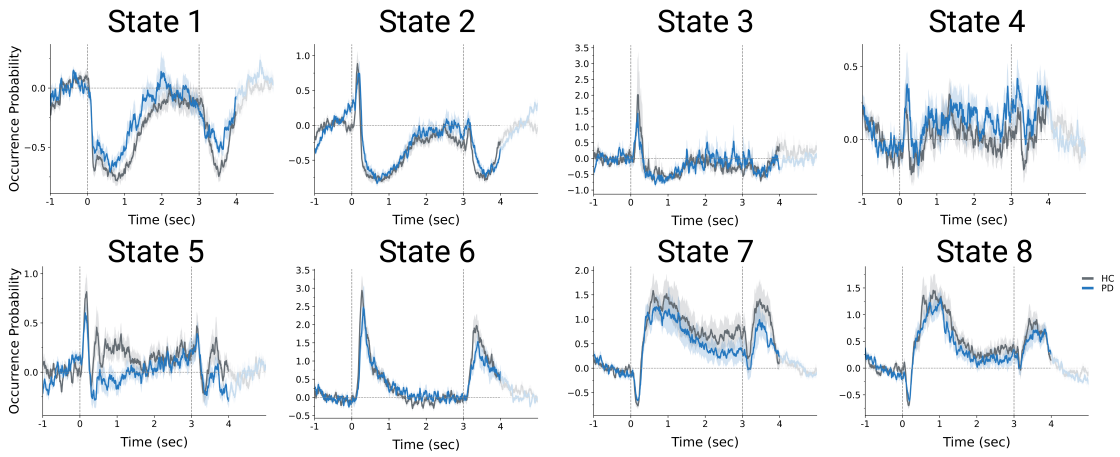


**Figure A2.6. Trial-averaged large-scale network occurrence probability group contrasts.** Trial average occurrence probabilities of each state are presented for HCs (grey) and PD volunteers (blue). The shaded areas around the two lines depict the group's standard error for each time point. Note, group contrasts calculated with cluster-based permutation tests did not yield significant group differences for any of the states.

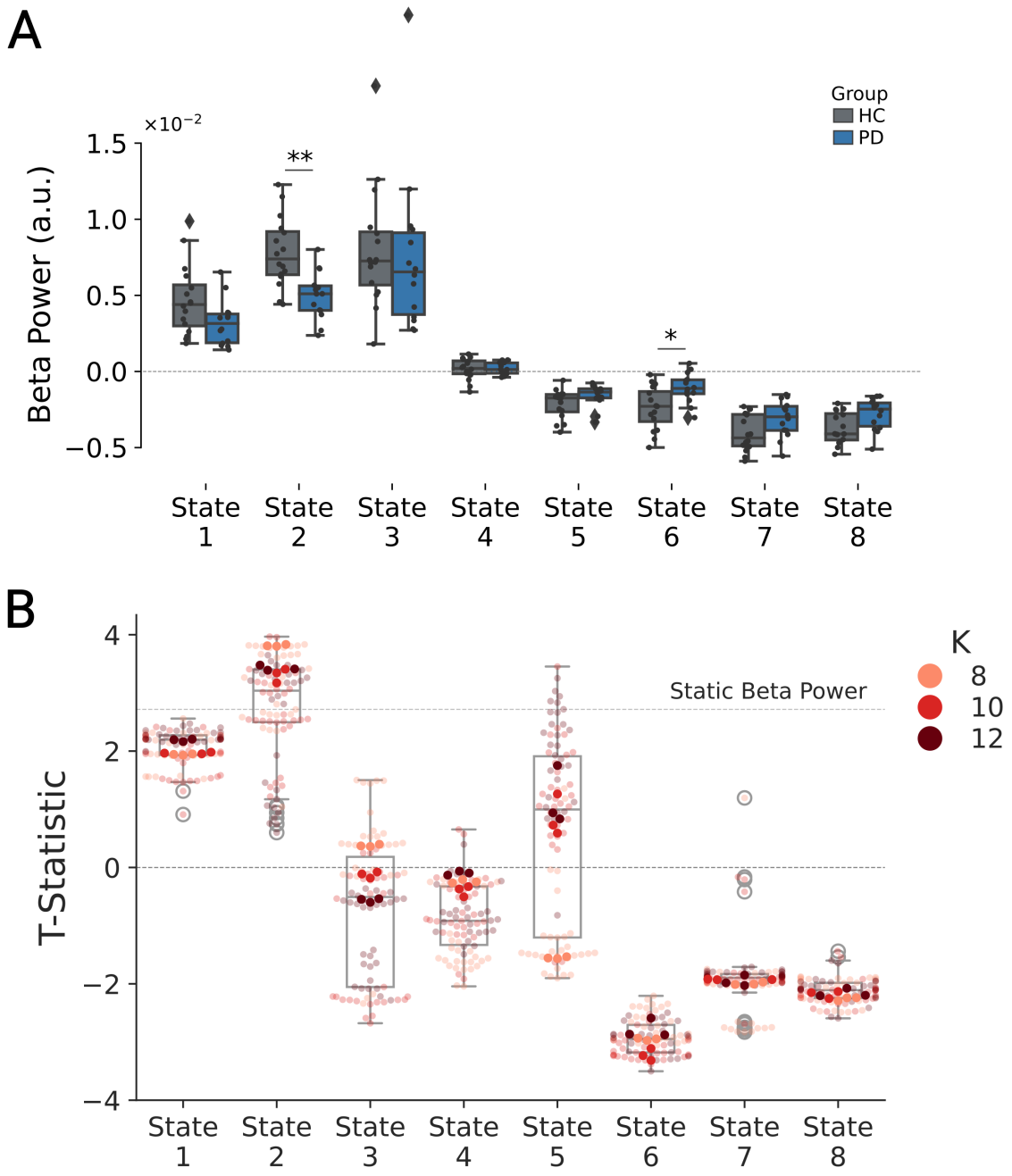


**Figure A2.7. State-specific beta-power group contrasts. (A)** State-specific beta power for each HMM state for HCs (grey) and PD volunteers (blue). Positive beta-power values indicate that respective state's beta power is larger than average beta power across states. Negative values indicate a decrease in beta power relative to the mean beta power across states. Asterisks indicate states in

which state-specific beta power is significantly different between the groups. Maximum t-statistic permutation tests pooled across states to correct for multiple comparisons across states. **(B)** Significant beta power group differences are not specific to selected HMM run. Each dot represents the t-statistic of the state-specific beta-power group contrasts for the respective state in one of the 90 HMMs. The colours of the dots indicate the number of states that the respective HMM-run was inferring. Positive t-values indicate larger state-specific beta power for HCs. The upper dotted line represents the t-statistic of the static beta-power group contrast (average across all states).
** indicate $p < .01$ and * $p < .05$

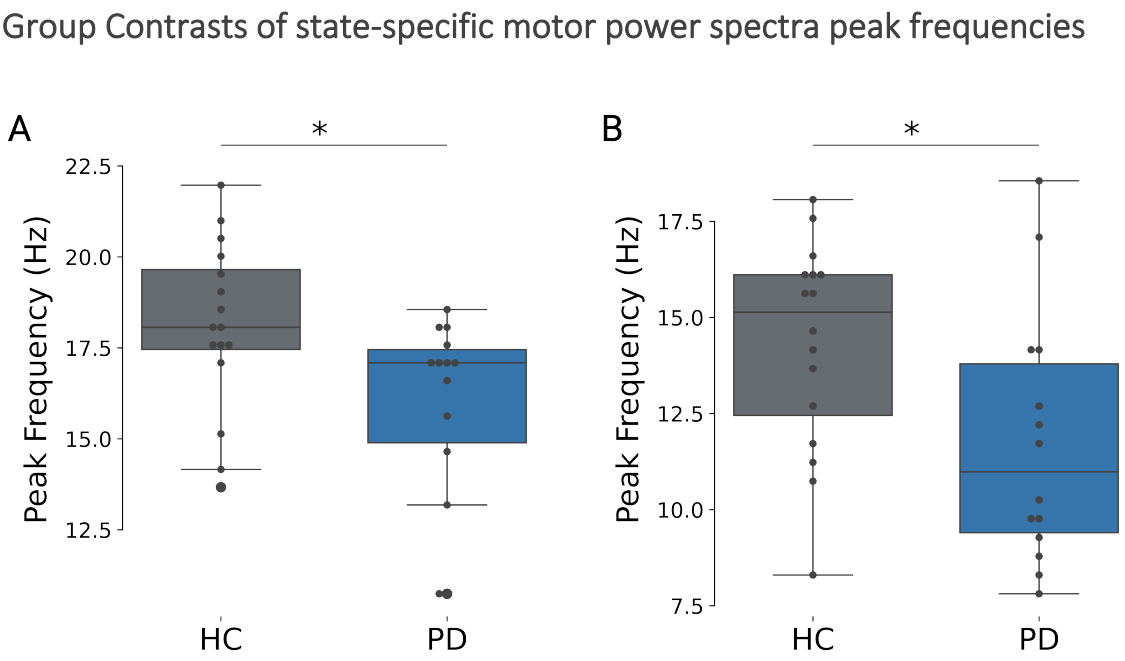


**Figure A2.8. Group comparisons of peak frequencies of motor cortical state-specific spectra of sensorimotor and posterior sensorimotor network extracted from the sustained-gripping task data between HCs (grey) and PD volunteers (blue). (A)** Peak frequencies of motor cortical state-specific spectra during sensorimotor network visits are significantly decreased in PD patients. Each dot represents peak frequency of a single participant. **(B)** Peak frequencies of motor cortical state-specific spectra during posterior sensorimotor network visits are significantly decreased in PD patients.

** indicate $p < .01$ and * $p < .05$

**A**

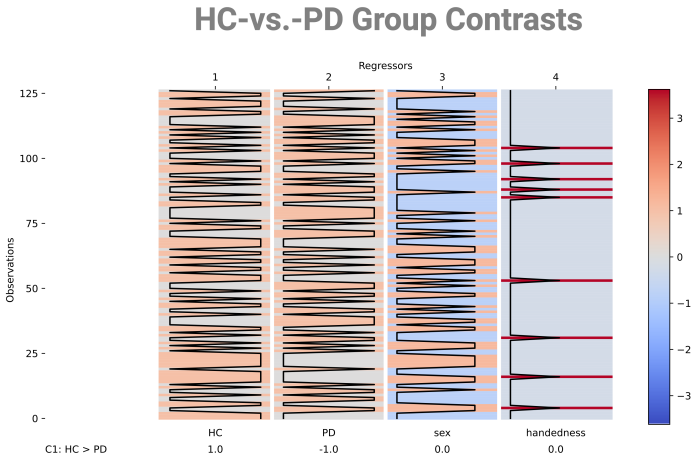
HC-vs.-PD Group Contrasts
Regressors
1
2
3
4
125
100
75
50
25
0
Observations
3
2
1
0
−1
−2
−3
HC
PD
sex
handedness
C1: HC > PD
1.0
-1.0
0.0
0.0

**B**

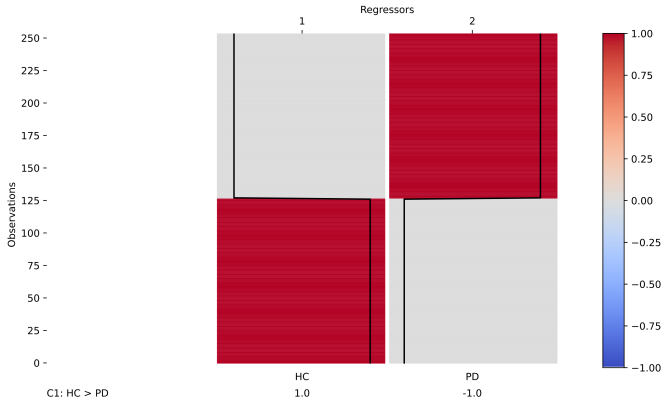
State1-vs.-State2 Contrasts
Regressors
1
2
250
225
200
175
150
125
100
75
50
25
0
Observations
1.00
0.75
0.50
0.25
0.00
−0.25
−0.50
−0.75
−1.00
HC
PD
C1: HC > PD
1.0
-1.0

**C**

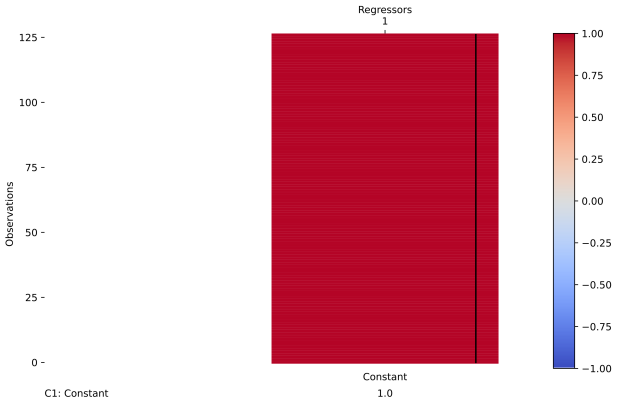
State Difference Contrasts
Regressors
1
125
100
75
50
25
0
Observations
1.00
0.75
0.50
0.25
0.00
−0.25
−0.50
−0.75
−1.00
Constant
C1: Constant
1.0

**Figure A2.9. Summary of GLMs used to compare variables between HCs and PD volunteers or States for the passive-movement task.** Regressors added to GLMs are represented as bars with each entry representing the z-scored regressor value of a single participant. Applied contrasts are depicted below the respective models. **(A)** Model for GLMs comparing metrics between HCs and PD volunteers. Note that the contrast is specified in such a manner that positive t-statistics indicate larger values for PD patients and negative t-statistics larger values for HCs. **(B)** GLM models for comparisons between State 1 and State 2 metrics. **(C)** Model for GLMs comparing State 1 - State 2 difference time courses against 0.

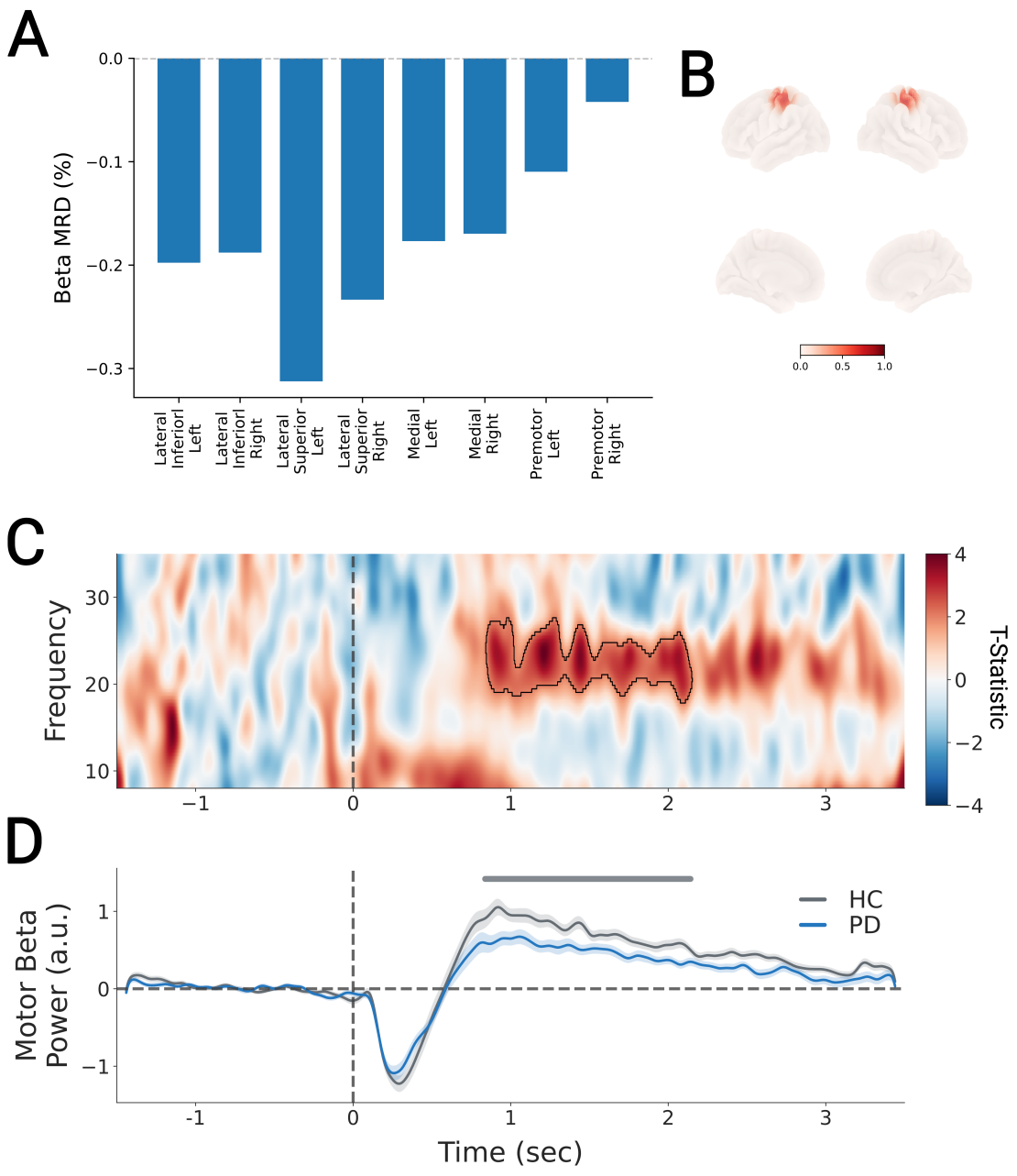


**Figure A2.10. Parcel selection and group contrasts of motor cortical TFRs. (A)** Average beta-power change in time window 50 to 110 ms after passive movement onset is plotted for each motor parcel. Region that showed strongest bilateral activation was selected as motor ROI for all following analyses of motor cortical power. **(B)** Visualisation of the location of the superior, lateral parcel that was selected based on findings in (A). **(C)** Group contrast of baseline corrected motor cortical TFRs. T-statistic of group contrast for each frequency bin and time

point is depicted. The significant cluster identified with cluster-based permutation tests is outlined with the black line. Maximum t-statistic permutation tests pooled across time points and frequency bins controlling for multiple comparisons. The dotted line at 0 seconds indicates the onset of the passive movement. **(D)** 20 to 31.5-Hz power time course of HCs (grey) and PD volunteers (blue) are shown to visualise beta-power time course of significant cluster. The frequency range reflects the frequency range of the significant cluster obtained from cluster-based permutation tests on TFR representations (C). Grey line on top of time courses marks time points in which significant cluster in TFR cluster-based permutation tests was identified.

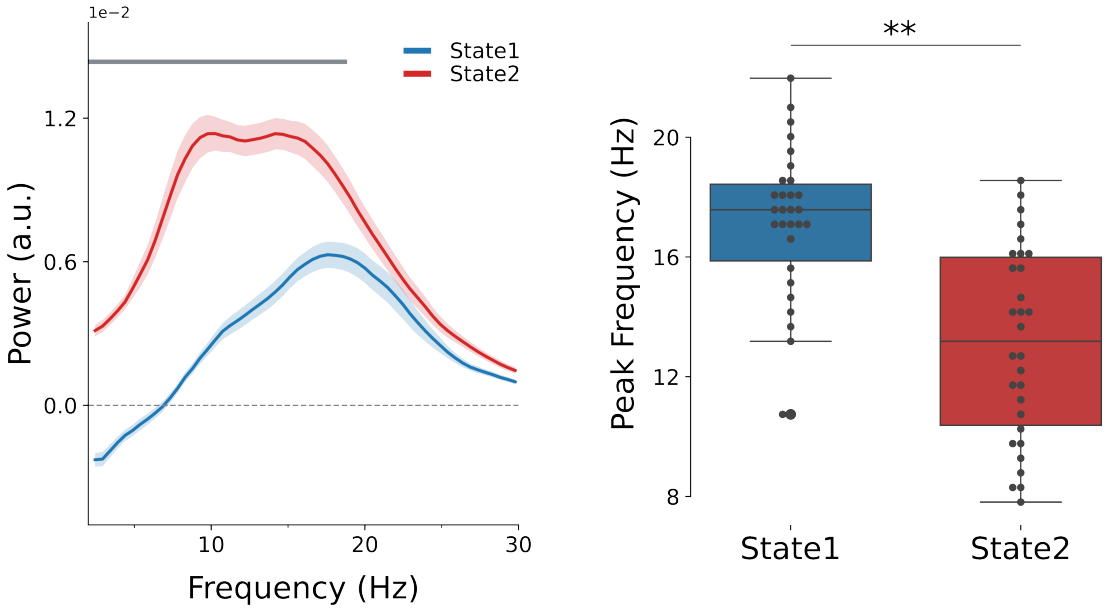


**Figure A2.11. Comparison of motor cortical state-specific spectra of sensorimotor and posterior sensorimotor network extracted from the passive movement task data. (A)** State-specific change during the sensorimotor (State 1) and posterior sensorimotor (State 2) network are depicted next to each other. State-specific beta-power change is calculated by subtracting the average power spectrum across all states from the state-specific power spectrum. Values of 0 indicated no change from the (static) average power spectrum (dashed line). Positive values indicate increases and negative values decreases from the average power spectrum. Shaded areas around the lines mark the 5 to 95% confidence interval. The grey line on top of the spectra marks frequency bins that show significantly lower power in State 1 compared to State 2 obtained from cluster-based permutation tests. **(B)** Peak frequency of state-specific spectra of the sensorimotor network are significantly higher than peak frequencies of the posterior sensorimotor network. Each dot represents a participant's peak frequency of the respective network-specific spectrum. ** indicate $p < .01$ and * $p < .05$

Comparison of dynamics of sensorimotor networks in passive movement-task

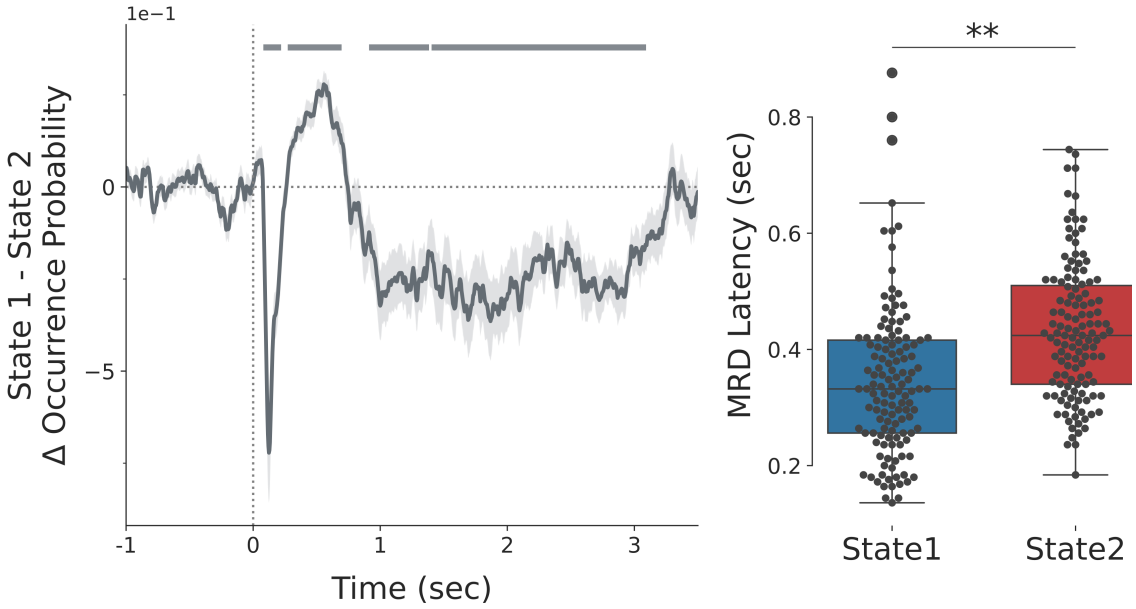


**Figure A2.12. Comparisons of dynamic metrics of sensorimotor and posterior sensorimotor networks. (A)** Difference between sensorimotor network and posterior sensorimotor network occurrences is significantly lower than zero during periods of evoked responses and post-movement beta rebounds, whereas it is significantly larger than zero during MRD period. Values lower than 0 indicate time points in which posterior network occurrence probabilities are larger than sensorimotor network occurrence probabilities and positive values mark time points in which sensorimotor network occurrence probabilities exceed occurrence probabilities of the posterior sensorimotor network. (B) The latency to the peak decrease of network occurrence probability in the MRD period is significantly longer for the posterior sensorimotor network.

** indicate $p < .01$ and * $p < .05$

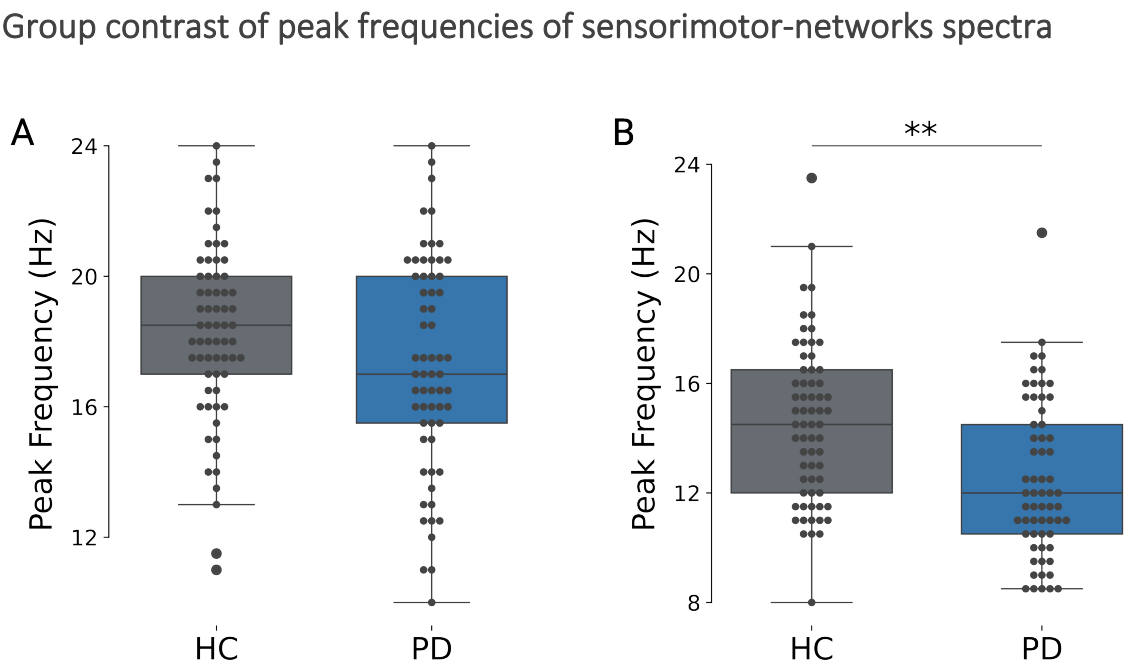


**Figure A2.13. Group comparisons of peak frequencies of motor cortical state-specific spectra of sensorimotor and posterior sensorimotor networks extracted from the sustained-gripping task data between HCs (grey) and PD volunteers (blue). (A)** Peak frequencies of motor cortical state-specific spectra during sensorimotor network visits are significantly decreased in PD patients. Each dot represents peak frequency of a single participant. **(B)** Peak frequencies of motor cortical state-specific spectra during posterior sensorimotor network visits are significantly decreased in PD patients.

** indicate $p < .01$ and * $p < .05$

# A3

## Chapter 3

Fooof fits across all participants and parcels

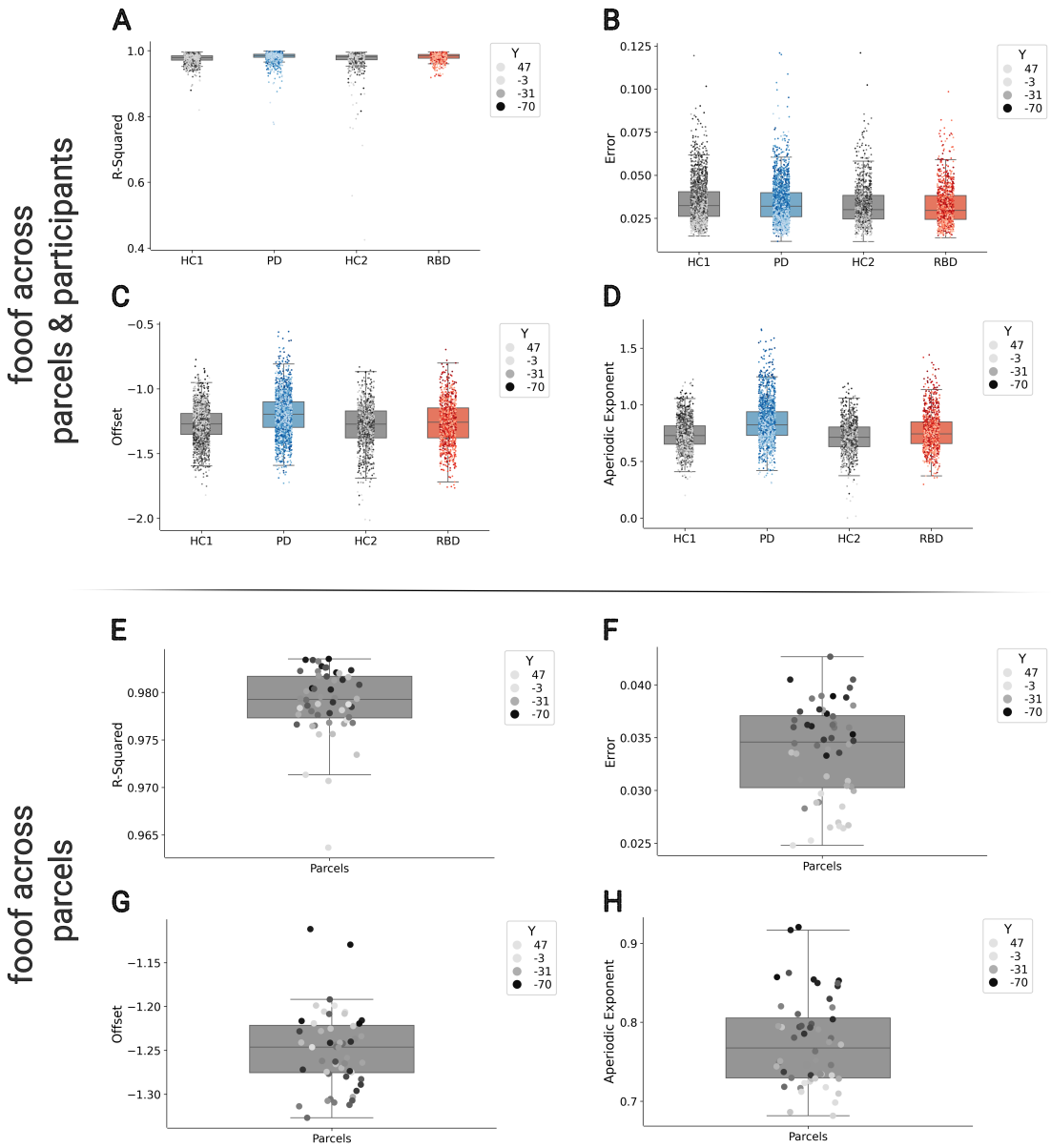


**Figure A3.1. Overview of fooof fits.** R-squared **(A)**, error **(B)**, aperiodic component offset **(C)**, and aperiodic exponent **(D)** values of fooof fits across all participants and parcels. Each dot represents the value extracted from a fooof fit to a power spectrum obtained from a single parcel of a single participant. Dots at frontal positions are depicted in brighter shades, becoming progressively darker towards more posterior parcels. R-squared **(E)**, error **(F)**, aperiodic component offset **(G)**, and aperiodic exponent **(H)** averaged across participants are depicted for each parcel. Dots at frontal positions are depicted in brighter shades,

becoming progressively darker towards more posterior parcels. Notably, R-squared values (A & E) in frontal parcels indicate qualitatively worse fits, and aperiodic exponents (D & H) follow well-established anterior-to-posterior gradients.

## Dynamic Metrics of large-scale networks

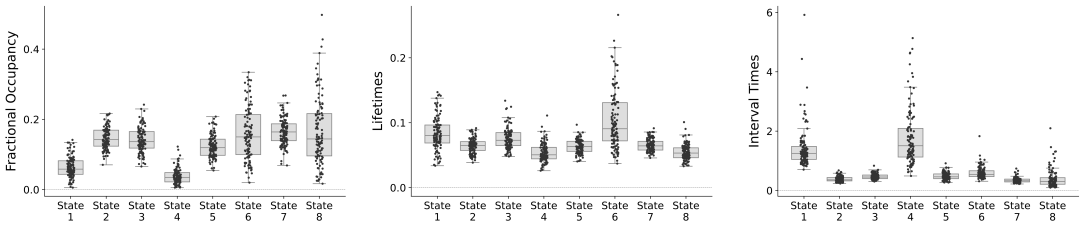


**Figure A3.2. Overview of metrics describing large-scale network metrics.** Fractional occupancies, lifetimes, and interval times of all participants are depicted for each state, respectively.

Large-scale network occurrences are associated with static oscillatory power

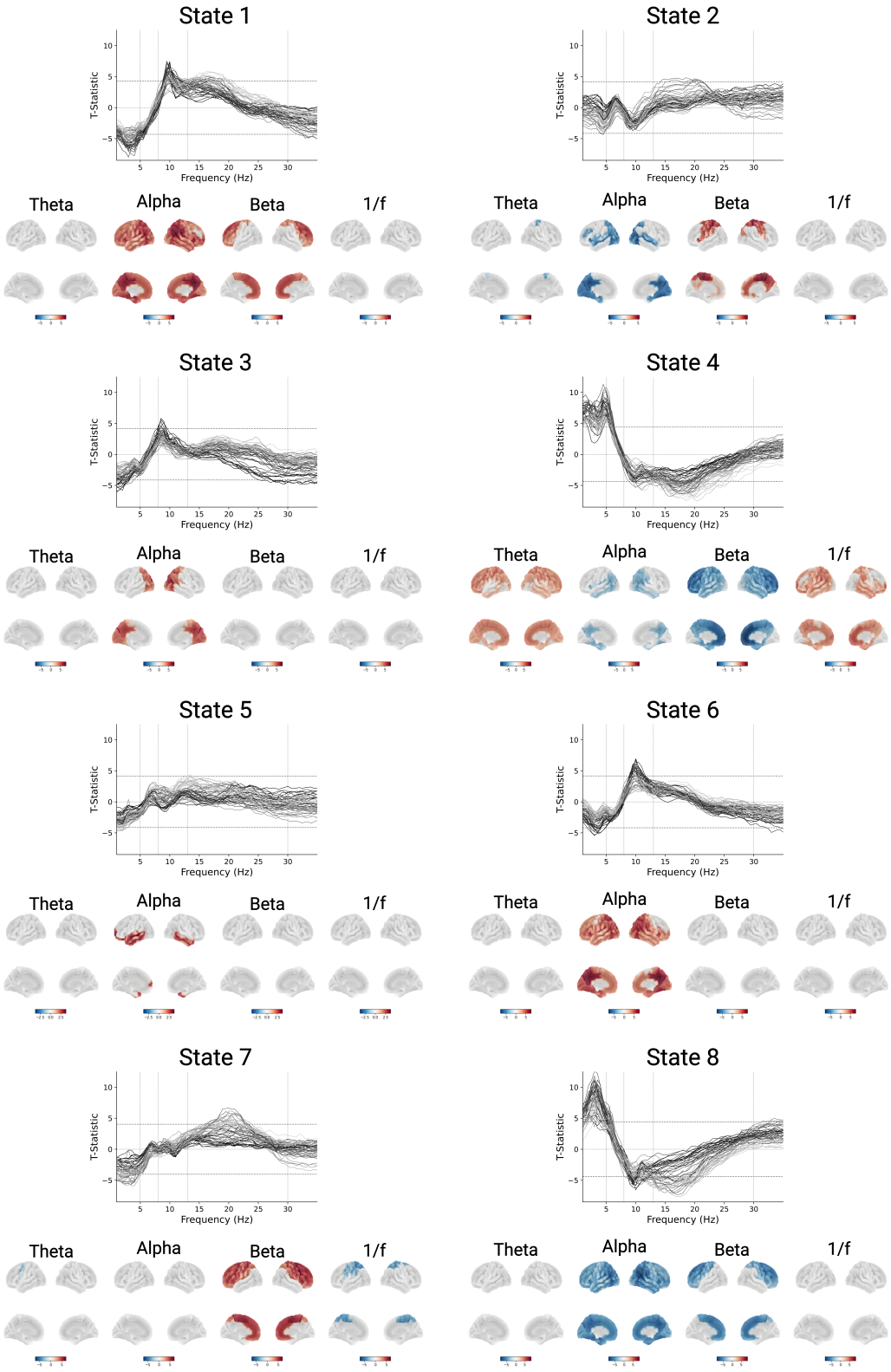

**Figure A3.3. Overview of associations between large-scale network fractional occupancies and static power spectral variables.** Each panel depicts associations for one of the large-scale networks extracted with the TDE-HMM. At the top of each panel, t-statistics of association between state's fractional occupancies and frequency bin power across participants are presented. Each line represents t-statistics for a single parcel. Parcels with centre coordinates located in frontal brain regions are depicted in brighter shades, with colour intensity gradually darkening as parcel centres move posteriorly. Horizontal dashed lines indicate significance thresholds obtained from maximum t-statistic permutation tests, pooling across frequency bins, parcels, and states. At the bottom of each panel, t-statistics of GLMs assessing the association between state's fractional occupancy and theta, alpha, and beta power, as well as 1/f-Slopes across all participants, are depicted. T-statistic of parcels exhibiting significant associations after correcting for multiple comparisons with maximum t-statistic permutation tests, pooling across parcels and frequency bands are plotted onto the brain surfaces.

Power spectral alterations are not represented in state-specific power changes

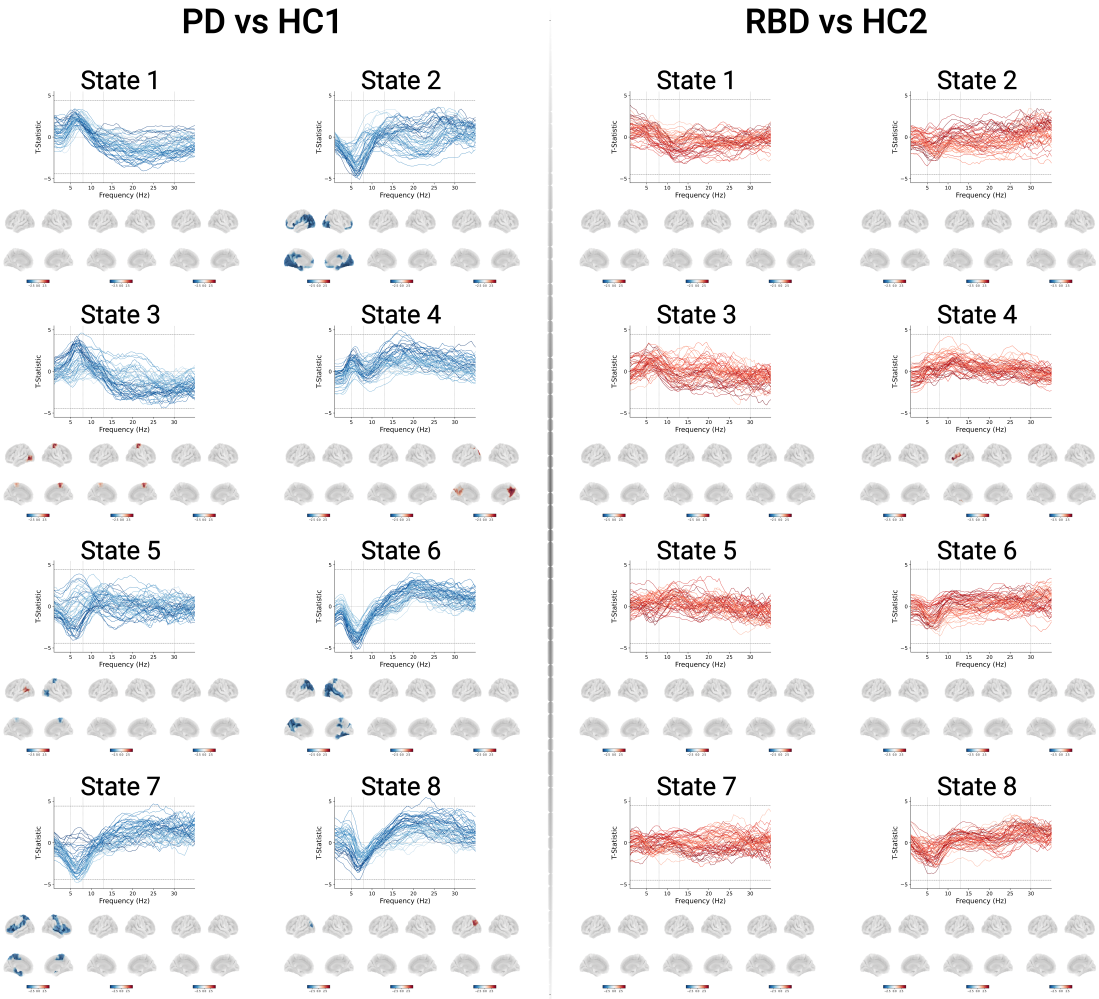


**Figure A3.4. State-specific power changes (after subtracting the mean across states) of various large-scale networks do not exhibit theta and beta-power alterations.** Each panel depicts group contrasts between state-specific spectral power of HCs and PD volunteers (left) or HCs and RBD volunteers (right) for one of the large-scale networks extracted with the TDE-HMM. At the top of each panel, t-statistics of state-specific frequency bin-wise group contrasts are presented. Each line represents t-statistics for a sperate parcel. Parcels with centre coordinates located in frontal brain regions are depicted in brighter shades, with colour intensity gradually darkening as parcel centres move

posteriorly. Horizontal dashed lines indicate significance thresholds obtained from maximum t-statistic permutation tests, pooling across frequency bins, parcels, and states. At the bottom of each panel, t-statistics of GLMs contrasting state-specific theta, alpha, and beta power, extracted from the respective state-specific power spectral changes, are depicted. T-statistic of parcels exhibiting significant group contrasts after correcting for multiple comparisons with maximum t-statistic permutation tests, pooling across parcels, frequency bands, and states, are plotted onto the brain surfaces.

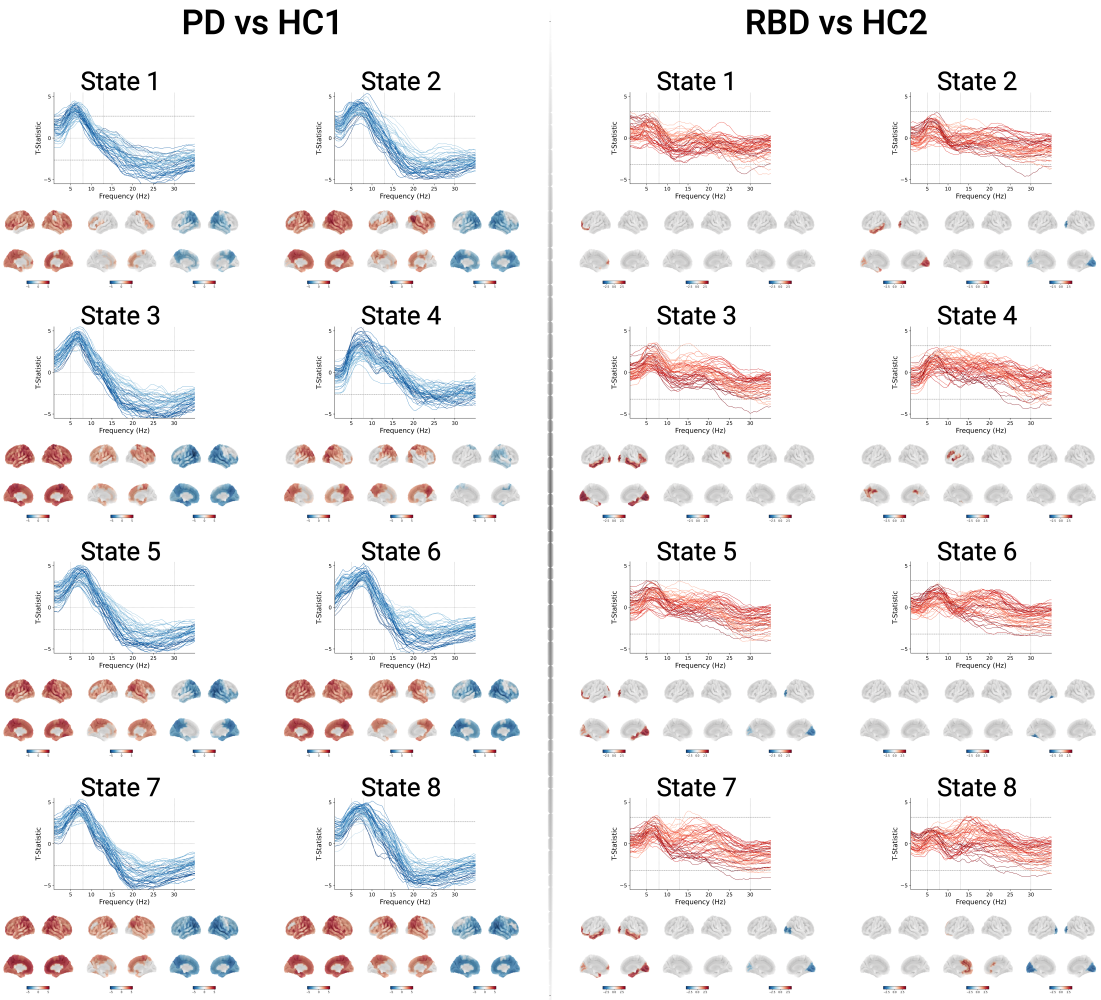


**Figure A3.5. State spectra (including the mean across states) of various large-scale networks demonstrate marked changes in theta and beta power, mimicking alterations observed in static power spectral analysis.** Each panel depicts group contrasts between state spectral power of HCs and PD volunteers (left) or HCs and RBD volunteers (right) for one of the large-scale networks extracted with the TDE-HMM. At the top of each panel, t-statistics of frequency bin-wise group contrasts are presented. Each line represents t-statistics for a sperate parcel. Parcels with centre coordinates located in frontal brain regions are depicted in brighter shades, with colour intensity gradually darkening as parcel centres move posteriorly. Horizontal dashed lines indicate significance

thresholds obtained from maximum t-statistic permutation tests, pooling across frequency bins, parcels, and states. At the bottom of each panel, t-statistics of GLMs contrasting theta, alpha, and beta power, extracted from the respective state power spectrum, are depicted. T-statistic of parcels exhibiting significant group contrasts after correcting for multiple comparisons with maximum t-statistic permutation tests, pooling across parcels, frequency bands, and states, are plotted onto the brain surfaces.

Large-scale networks extracted with TDE-HMM from only RBD data set

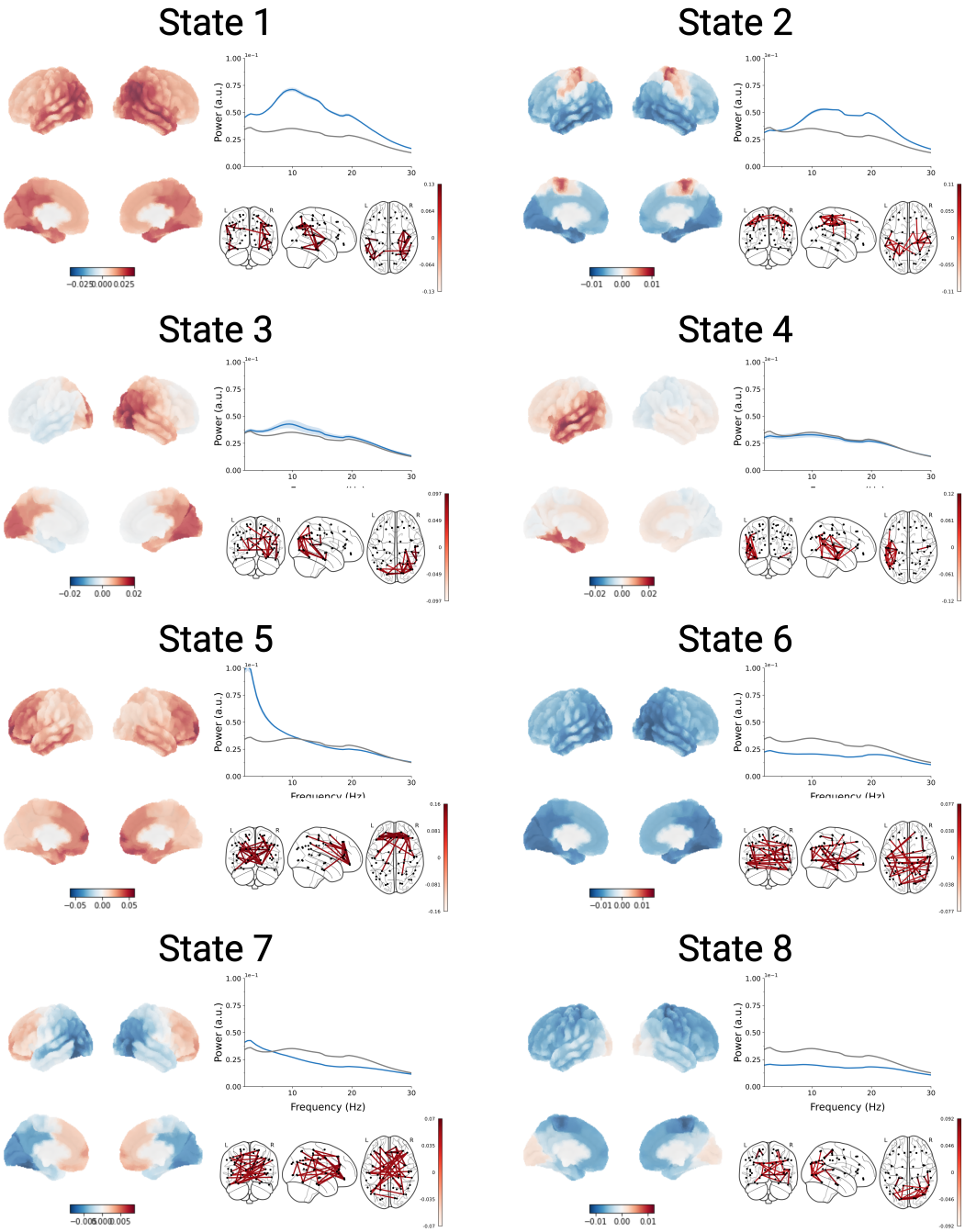


**Figure A3.6. Overview of dynamic-large scale networks extracted from the RBD dataset using a TDE-HMM.** Spectral properties of each state are described in 3 ways: 1) Wideband power of each parcel (relative to the average power across all states) is projected onto a cortical surface. 2) State-specific superior motor

cortical power spectra (blue) are displayed alongside superior motor cortical power spectra averaged across all state spectra (grey). 3) State-specific coherence networks averaged across frequency bins, as specified by the low-frequency spectral factor obtained from the NNMF (relative to the mean coherence across all states), are shown below the motor power spectra. States are sorted according to their state-specific beta power in the superior motor parcel.

# A4

## Chapter 4

# Effect of power spectra normalisation on beta power

## Motivation

A well-known limitation of MEG scans is the potential for variations in the overall power of the recorded signal due to differences in participants' seating positions and unique anatomical features, leading to varying distances between the signal sources and the sensors (Gross et al., 2013). To address this issue, standard practices involve standardizing time courses prior to power spectrum calculation (Chapters 1 to 3) or normalizing power spectra by dividing frequency bin power by the overall spectral power (Boon et al., 2023; Stoffers et al., 2007; Wiesman et al., 2023).

However, while addressing this confound is crucial, one must recognize that standardizing time courses or power spectra can introduce strong associations between beta-power values and peak frequency power. This could potentially complicate beta-power group comparisons between healthy controls and individuals with PD, particularly due to well-established co-occurring alterations in low-frequency power in PD (Boon et al., 2019, 2023; Bosboom et al., 2006; Soikkeli et al., 1991; Stoffers et al., 2007).

In the following, I will investigate the impact of normalising power spectra on the calculation of group contrasts between HCs and PD volunteers.

All analyses will be conducted on the pre-processed data previously analysed in Chapter 3. Additionally, I will replicate the presented analyses using resting-state data from "The Swedish National Facility for Magnetoencephalography Parkinson's disease dataset" (Vinding, Eriksson, et al., 2024).

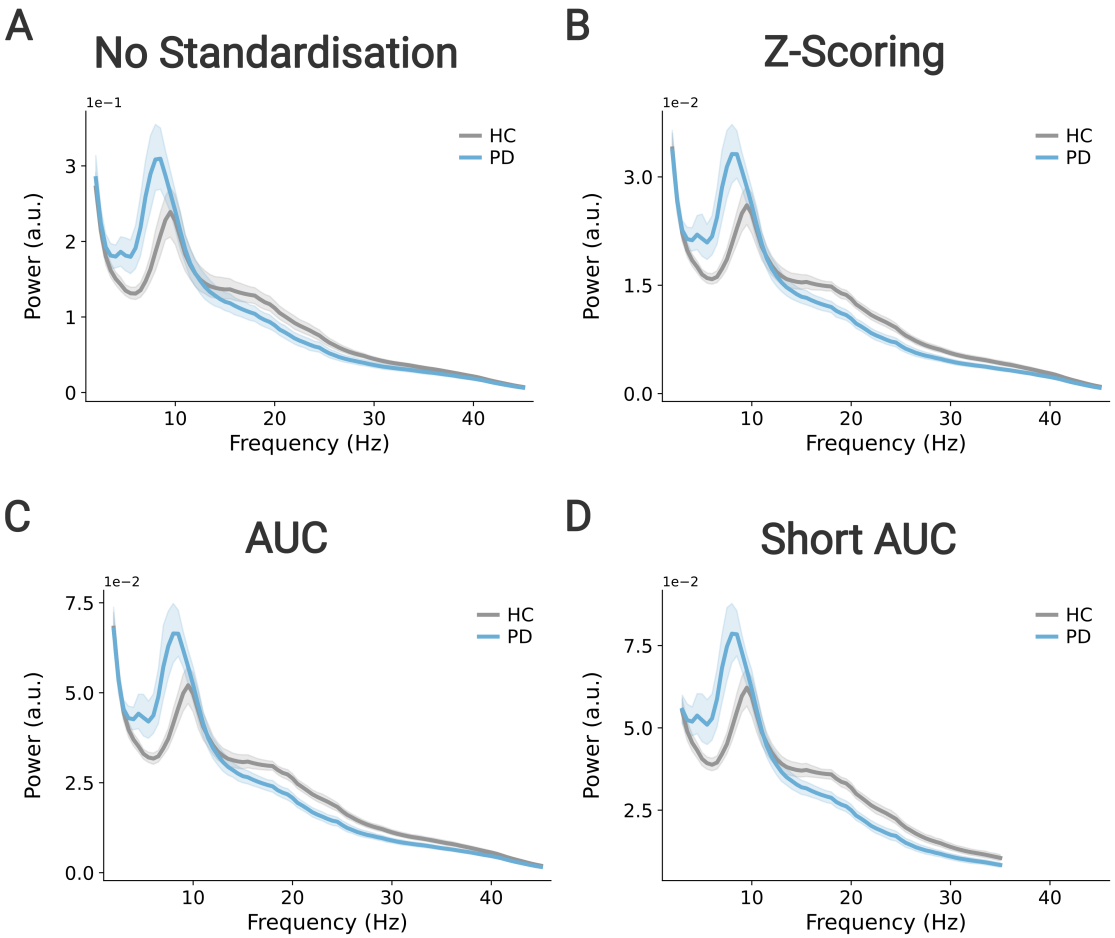


**Figure A4.1. HC and PD group power spectra calculated with varying normalisations. (A)** Power spectra calculated from unstandardised time courses, **(B)** power spectra calculated from z-scored time courses, **(C)** 1 to 45-Hz power spectra divided by the area under the curve, **(D)** 4 to 35-Hz power spectra divided by the area under the curve are presented. Qualitative observations suggest that beta-power group differences are larger in normalised spectra compared to unstandardised spectra.

Power spectra of HCs and PD volunteers were calculated with different normalisations for qualitative comparisons:

- **No Standardisation:**

  Calculate power spectra from unstandardised time-course signals.

- **Z-Scoring:**

  Calculate power spectra from z-scored time-course signals.

- **Area under the curve normalisation:**

  Calculate power spectra from unstandardised time-course signals and normalise 1 to 45-Hz power spectra relative to their area under the curve.

- **Area under the curve normalisation for narrow frequency range:**

  Repeat area-under-the-curve normalisation but for power spectra ranging from 2 to 35 Hz.

Qualitative comparisons of power spectra in the beta range suggest that group differences between HCs and PD volunteers may be larger in standardised spectra compare to the unstandardised spectrum.

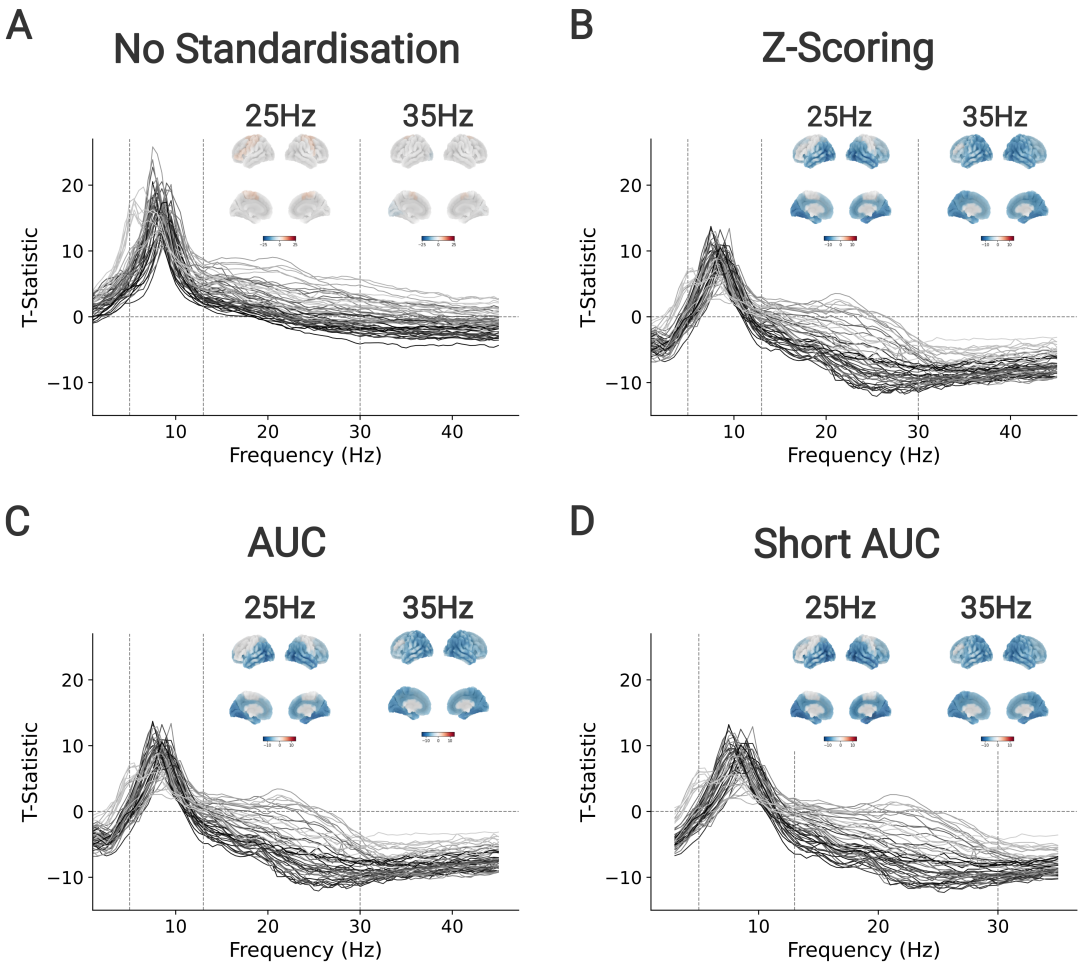


**Figure A4.2. Normalising power spectra introduces correlations between peak power and beta power, likely mixing peak power and beta-power group differences in comparisons of normalised power spectra. (A)** GLMs assessing frequency bin-wise associations between peak power and beta power in unstandardised power spectra. Each line represents t-statistics for a single parcel. Parcels with low peak frequency power are depicted in brighter shades, with colour intensity gradually darkening as parcel peak power increases. Surface plots depict t-statistics of parcels that yield significant associations after correcting for multiple comparisons with FDR correction across parcels and frequency bins. **(B)** Similarly, GLMs assessing frequency bin-wise associations between peak power in unstandardised power spectra and beta power in power

spectra calculated from z-standardised time courses are presented. **(C)** GLMs assessing frequency bin-wise associations between peak power in unstandardised power spectra and beta power in 1 to 45-Hz power spectra normalised by dividing frequency bin power values by area under the curve. **(D)** GLMs assessing frequency bin-wise associations between peak power in unstandardised power spectra and beta power in 4 to 35-Hz power spectra normalised by dividing frequency bin power values by area under the curve. Crucially, beta power in normalised spectra exhibits strong negative associations with unstandardised peak power (B, C, D), whereas beta power from unstandardised time courses does not (A). The colours of the lines indicate that negative associations are stronger in parcels with high unstandardised peak power.

I hypothesised that standardising power spectra introduces associations between beta-power values and peak frequency power, potentially complicating beta-power group comparisons between HCs and individuals with PD due to well-established alterations in low-frequency power in PD.

To assess whether associations between peak power and beta power differ between standardized and unstandardized power spectra, I employed Generalized Linear Models (GLMs). These models predicted power at each frequency bin based on a constant regressor and participants' peak power values. Peak power values were derived from unstandardized power spectra in all cases.

Results revealed that standardizing power spectra led to highly negative t-statistics in frequency bins within the beta and gamma range. These negative t-statistics indicate a strong negative association between unstandardized peak power and frequency bin

power, suggesting that participants with higher peak power demonstrated lower beta power. Importantly, these negative associations were not observed in the unstandardized power spectrum, suggesting that the strong associations between unstandardized peak power and beta/gamma power in standardized power spectra were due to the standardization process.

Furthermore, the lines in Figure A4.1. were coloured according to the respective parcels' unstandardized peak power. It was observed that darker lines exhibited more negative t-statistics in GLMs on standardized power spectra, indicating that parcels with higher peak power also displayed stronger associations between peak power and beta power.

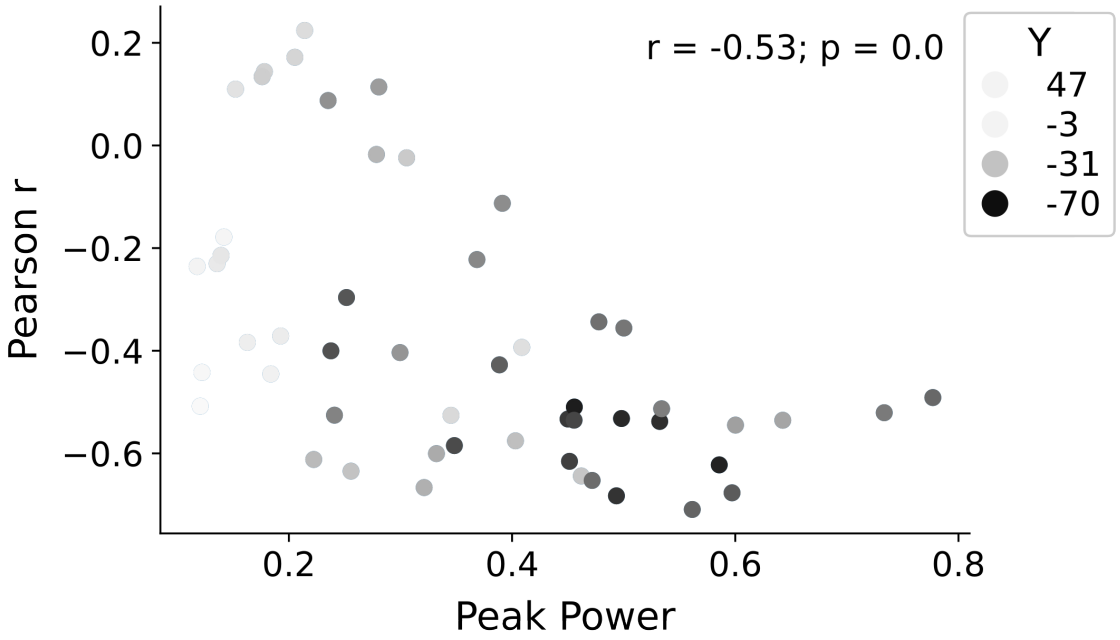


**Figure A4.3. Negative associations between unstandardised peak power and standardised beta power are more pronounced in parcels with high**

**unstandardised peak power.** Each dot represents a parcel. Brighter shades indicate more anterior positions of the parcel, whereas darker shades indicate more posterior positions. Pearson correlation coefficients were calculated as the association between unstandardised peak power and standardised beta power across participants for each parcel.

As described, parcels with higher unstandardized peak power displayed stronger associations between unstandardized peak power and standardized beta power. To quantify this association, the following steps were undertaken:

1. Peak power was extracted from unstandardized power spectra of all parcels across all participants.
2. Mean beta power was extracted from standardized power spectra (normalized by z-scoring of time course signals) of all parcels across all participants.
3. Correlation coefficients (Pearson r) were calculated between unstandardized peak power and standardized beta power across participants at each parcel.
4. The average unstandardized peak power across all participants was calculated at each parcel.
5. The obtained average peak power (Step 4) was correlated with the correlation coefficients (Step 3).

Importantly, the correlation between peak power and correlation coefficients revealed a significant negative association. This suggests that parcels with higher unstandardized peak power exhibited stronger correlations between unstandardized peak power and standardized beta power.

These analyses highlight that strong negative associations between peak power and beta/gamma power are evident in standardized power spectra but not in unstandardized power spectra. This indicates that standardizing power spectra introduces correlations between peak power and beta/gamma power.

This observation is particularly relevant in PD research because PD volunteers tend to exhibit significantly larger peak power values. Therefore, the introduction of such correlations through standardization may contaminate beta and gamma power comparisons between PD and control groups.

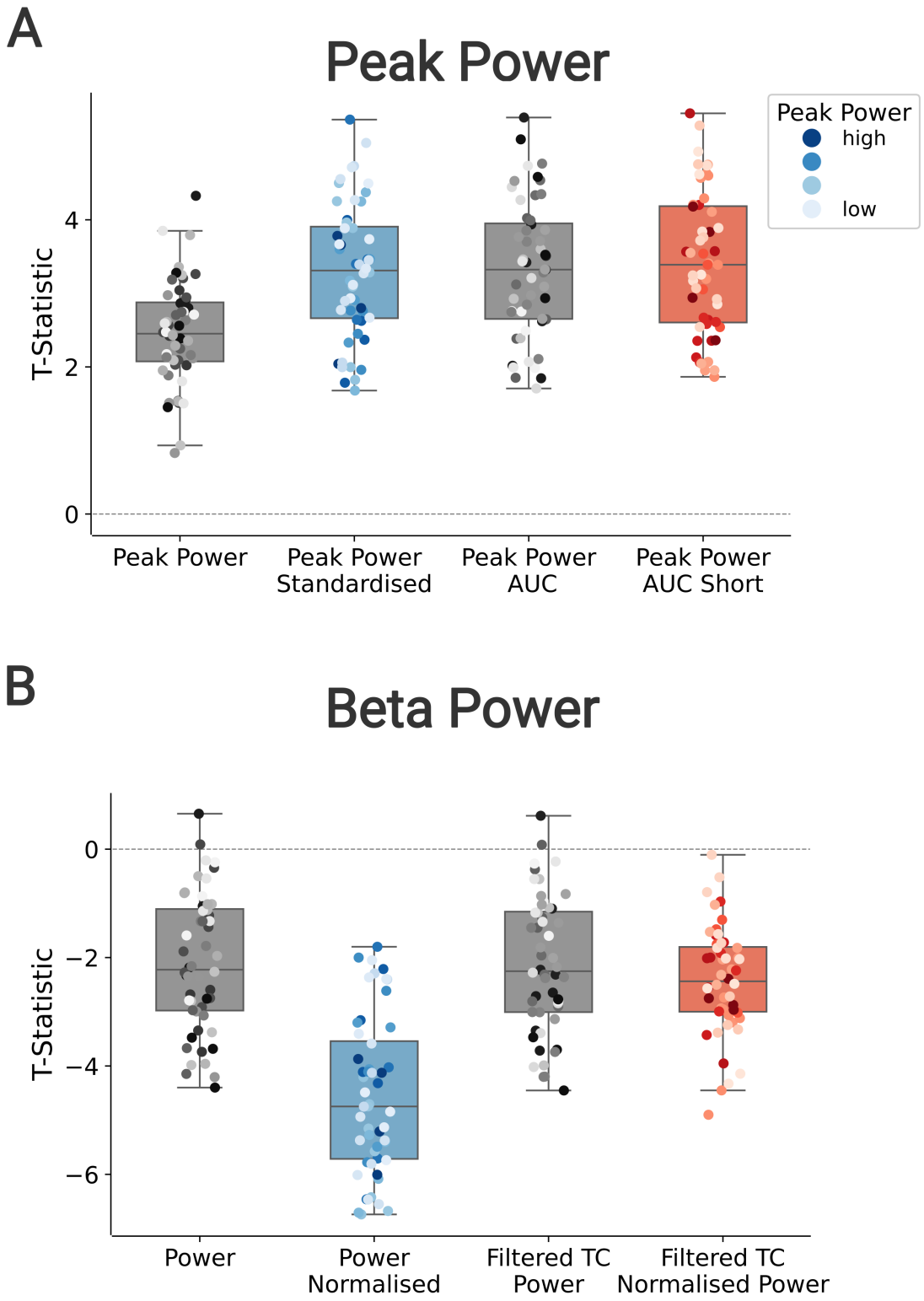


**Figure A4.4. Group differences between beta power of HCs and PD volunteers are larger for standardised beta power compared to unstandardised beta**

**power. (A)** Peak power group contrasts were calculated for all parcels for each of the different normalisation conditions. Each dot represents the t-statistic of the group contrast of a specific parcel. Brighter shades indicate higher unstandardised peak power. **(B)** Beta-power group contrasts were calculated at each parcel for unstandardised power spectra (grey), power spectra calculated from z-scored time courses (blue), power spectra calculated from 13 to 30-Hz filtered time courses (grey), and power spectra calculated from 13 to 30-Hz filtered and z-scored time courses (red).

Next, I tested whether standardising power spectra affects group comparisons between HCs and PD volunteers.

### *Peak Power*

To demonstrate that peak power is significantly larger in PD, I initially extracted peak power values for all parcels from each participant. These peak power values were then compared between the two groups using two-sided t-tests, resulting in one t-statistic value per parcel. This process was repeated for all normalization conditions. The t-statistics of the group contrast for peak power of all parcels under each normalization condition are displayed in the top panel. Importantly, the peak-power group contrasts revealed highly positive t-statistics across all parcels and under all conditions. This indicates a significant decrease in peak power throughout the entire brain in PD.

### *Beta*

Having established the significant increase in peak power in PD volunteers across the entire brain, I proceeded to investigate the systematic variation of beta-power group

differences between standardised and unstandardised power spectra. To achieve this, I replicated the aforementioned procedure for beta-power values, with a modification in the standardisation conditions:

1. Unstandardised power spectra:

   Power spectra that have not been subjected to any normalisation procedure.

2. Standardised Power spectra:

   Power spectra that have been normalised by z-scoring parcel time courses prior to power spectrum calculation.

3. Unstandardised beta power from 13 to 30Hz filtered time courses:

   Time courses were filtered to the 13 to 30Hz range prior to calculating power spectra and averaging across power in 13 to 30-Hz frequency bins.

4. Standardised beta power from 13 to 30Hz filtered time courses:

   Time courses were filtered to the 13 to 30Hz range and z-scored prior to calculating power spectra and averaging across power in 13 to 30-Hz frequency bins.

T-statistics of beta-power group contrasts are lowest for standardised beta-power values (blue). Given that t-statistics are clearly more negative in the standardised compared to all other conditions, this further suggests that beta-power differences may be enhanced by standardisation. Crucially, t-statistics of group comparisons for all other normalisation conditions were also negative, suggesting that standardising time courses enhances already present decreases in beta power of PD volunteers.

Due to the strong correlations between peak power and beta power in the standardised conditions and the strongly increased peak power values in PD, it seems

likely that the observed increases reflect a mixing between peak power and beta-power alterations in PD.

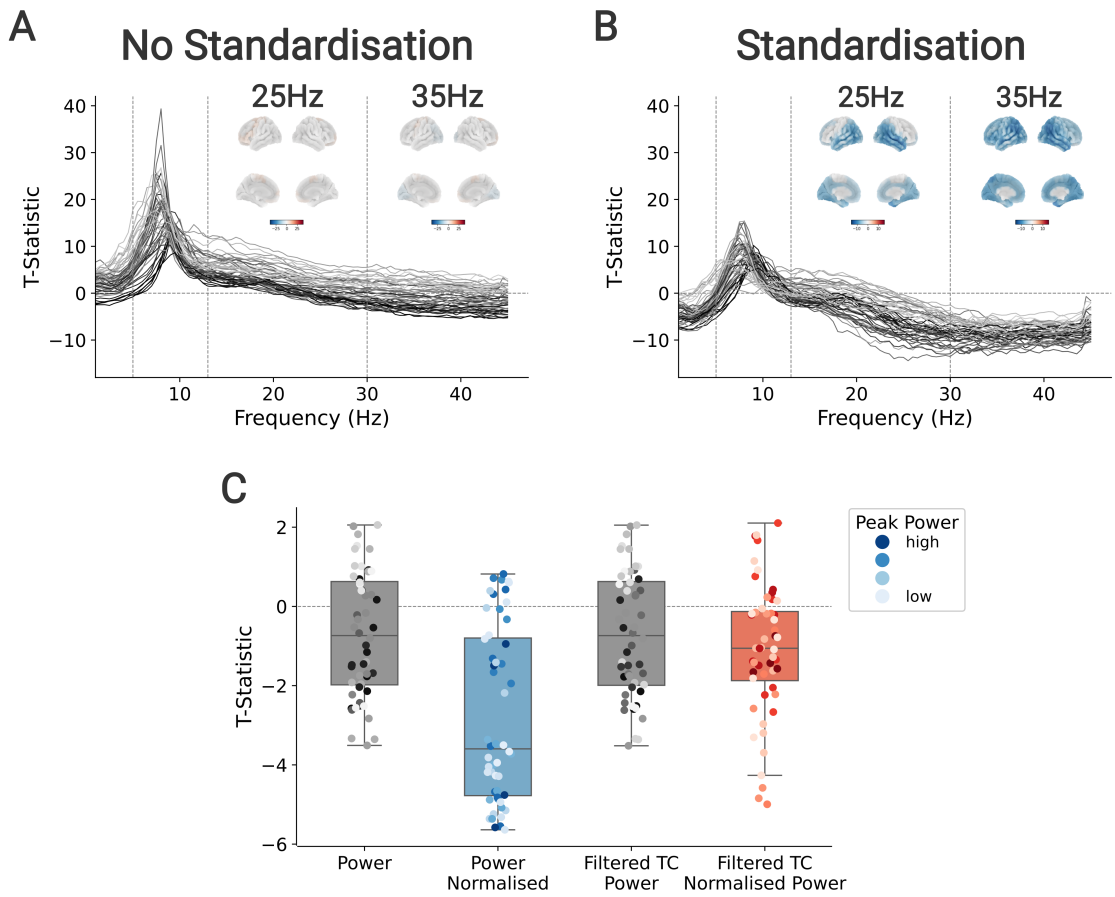


**Figure A4.5. Influence of normalisation of power spectra on associations between unstandardised peak power and beta power and beta-power group differences replicates in different PD data sets.** GLMs assessing associations between peak power and beta power calculated from unstandardised time courses **(A)** and peak power calculated from unstandardised time courses and beta power calculated from z-scored time courses **(B)**. **(C)** Group contrasts for different normalisation conditions. For a detailed description of the figures see figure descriptions of Figure D.1.

Lastly, I demonstrate that the above demonstrates findings are not specific to our PD sample but can be also observed in the resting-state data of "The Swedish National

Facility for Magnetoencephalography Parkinson's disease dataset" (Vinding, Eriksson, et al., 2024). Importantly, both the associations between unstandardised peak power and standardised beta power and the larger group differences for standardised beta power were replicated in the second dataset. Consequently, this effect is not specific to our PD sample but generalises to other PD datasets.

## Conclusion

See paragraph "Effects of normalising power spectra on beta power" of discussion in the main part of the thesis.